Gravitational anomaly and transport properties of topological semimetals

Baptiste Bermond

Thèse

en vue de l'obtention du grade de Docteur, délivré par

l'**École Normale Supérieure de Lyon**

École doctorale N°52

École doctorale de Physique et Astrophysique de Lyon

Discipline : Physique

soutenue publiquement le 09/11/2023 par

Baptiste BERMOND

Anomalie gravitationnelle et propriétés de transport des semi-métaux topologiques

Gravitational anomaly and transport properties of topological semimetals

---

devant le jury composé de

LANDSTEINER, Karl	Professeur,	*IFT-UAM/CSIC (Madrid)*	Rapporteur
PAVLOFF, Nicolas	Professeur de universités,	*LPTMS (Orsay)*	Rapporteur
GIAMARCHI, Thierry	Professeur,	*Université de genève*	Examinateur
GRUSHIN, Adolfo	Chargé de recherche,	*Institut Néel (Grenoble)*	Examinateur
ILAN, Roni	Professeure,	*Tel Aviv University*	Examinatrice
VOZMEDIANO, María	Professeure,	*ICMM (Madrid)*	Examinatrice
CARPENTIER, David	Directeur de Recherche,	*ENS de Lyon*	Directeur

Contents

Introduction **1**

1 From condensed matter to curved spacetime **5**
1.1 Curved spacetimes and black hole analogs in fluids in motion . . . 5
1.1.1 From classical hydrodynamic to curved spacetimes . . . 6
1.1.2 Scalar fields in curved-spacetime . . . 7
1.1.3 Curved spacetime from quantum fluids . . . 8
1.1.4 Black-holes in Bose-Einstein condensates: classical fluid interpretation . . . 13
1.2 Inhomogeneous 1D systems . . . 15
1.2.1 Flat spacetime Dirac Hamiltonian: From condensed matter to field theory 15
1.2.2 Dirac fermions: from flat to curved spacetimes . . . 17
1.2.3 Inhomogeneous 1+1 dimensional systems as curved spacetime Dirac Hamiltonians . . . 19
1.3 From thermal transport to curved spacetime: Luttinger's legacy . . . 23

2 Quantum field theory anomalies in curved spacetimes **25**
2.1 Anomalies in quantum field theory . . . 25
2.2 A historical example: chiral anomaly from field theory to condensed matter . . . 26
2.2.1 The historical diagrammatic derivation . . . 27
2.2.2 Anomalies, non-conserved currents, and effective actions . . . 29
2.2.3 Chiral anomaly as a Hilbert infinite hotel: from quantum field theory to experiments . . . 31
2.3 Gravitational anomalies . . . 37
2.3.1 Mixed axial-gravitational anomalies and condensed matter experiments . 38
2.3.2 Symmetries, conserved quantities and anomalies in curved spacetime . . 39
2.3.3 Gravitational anomalies as properties of the momentum-energy tensor in 1+1D . . . 43

3 Tolman-Ehrenfest equilibrium temperature in curved spacetimes **45**
3.1 Classical Tolman-Ehrenfest temperature and Luttinger equivalence . . . 46
3.1.1 From the Tolman-Ehrenfest temperature to the Luttinger's relation . . . 46
3.1.2 Classical Tolman-Ehrenfest temperature derivation . . . 47
3.1.3 Tolman-Ehrenfest temperature and momentum-energy tensor in 1+1 dimensions . . . 49
3.2 Gravitational anomalies and anomalous Tolman-Ehrenfest temperature . . . 51
3.2.1 Anomalies at play . . . 51
3.2.2 Anomalous Tolman-Ehrenfest temperature . . . 52
3.2.3 Temperature, thermodynamics, and trace anomalies . . . 54
3.3 Anomalous Luttinger equivalence and response theory . . . 55
3.3.1 Anomalous Luttinger relation . . . 55
3.3.2 Anomalous Luttinger response theory from perturbations . . . 59

4 Applications: From black holes to condensed matter and back 63
4.1 Quantum atmosphere of a black hole . . . 63
4.2 Far from equilibrium energy transport . . . 66
4.2.1 Anomalous Luttinger relation on a ring . . . 67
4.2.2 Temperature quench as a metric quench . . . 72
4.2.3 Spacetime periodic modulation: Floquet states . . . 74
4.3 Conditions of application . . . 76

5 Extension of the Luttinger's trick in the presence of two temperature profiles 79
5.1 From one to two temperature sources in black hole physics . . . 79
5.2 Luttinger extension to chiral temperature profiles . . . 84
5.2.1 Extended Luttinger equivalence: From one to two temperature profiles . 84
5.2.2 Bimetric theories: Definition, Hamiltonian and (non-)conservation equations . . . 86
5.2.3 Luttinger trick: From one to two temperature profiles . . . 89
5.2.4 From two temperature profile to two velocity profiles: tilted Dirac semimetals . . . 91
5.3 Conclusion and perspectives . . . 93

6 Remarks on purely dynamical metrics, the dynamical Casimir effect and anomalies 97
6.1 Dynamical gravitational anomalous correction: from expanding universes to condensed matter . . . 98
6.1.1 Dynamical curved spacetimes in condensed matter . . . 98
6.1.2 Momentum-energy tensor of purely dynamical systems . . . 100
6.1.3 Anomalous fluctuations and purely dynamical systems in condensed matter . . . 101
6.1.4 Limits and perspectives of this study . . . 106
6.2 A link with the dynamical Casimir effect . . . 107
6.2.1 Historical description . . . 107
6.2.2 Dynamical Casimir effect and trace anomaly . . . 108
6.2.3 Conclusion . . . 109

7 The consequences of anomalies for a historical dispute: Does the equilibrium temperature depend on gravity? 111
7.1 Loschmidt-Maxwell-Boltzmann dispute and the adiabatic temperature gradient . 111
7.1.1 Historical arguments . . . 111
7.1.2 The adiabatic temperature gradient . . . 112
7.2 Thermodynamic consequences of the anomaly . . . 114
7.2.1 Tolmann-Ehrenfest's temperature and thermal machine . . . 114
7.2.2 Anomalous Tolman-Ehrenfest's temperature and thermal machine . . . 115
7.3 Conclusion and discussions . . . 116

8 Magnetothermal transport in $ZrTe_5$ 119
8.1 Magnetothermal transport in $ZrTe_5$: motivations and measurements . . . 121
8.2 Thermal transport along the magnetic field as a 1+1 dimensional thermal transport 124
8.2.1 From a 3+1 dimensional band structure to 1+1 dimensional Landau levels in $ZrTe_5$ . . . 124
8.2.2 Thermal conduction and Landauer formula in a ballistic sample . . . 127
8.2.3 Scattering corrections to the magnetothermal conductivity properties . . . 130
8.3 From orthogonal energy transport to a new transport phase . . . 133

8.3.1 Evidence for a phonon-mediated transport . . . 133
8.3.2 Discussion . . . 136

Conclusion & future directions **137**

A Introduction to curved spacetimes and their coupling with spinor fields **141**
A.1 Introduction to Riemann-Cartan spaces . . . 141
A.2 Fermions in curved spacetime with torsion . . . 144

B Continuity and metric quenches **147**
B.1 Continuity equations during a metric quench . . . 147
B.2 Time evolution and spacetime quenches . . . 147
B.3 Floquet stroboscopic evolution . . . 148

C Killing vectors and conserved quantities in general relativity **151**

Bibliography **155**

Introduction

In 1915, Albert Einstein published a book presenting his theory of gravity, known as the theory of "general relativity". In this book, A. Einstein proposed an equation describing how the geometry of spacetime and its curvature are influenced by either matter or radiation. In the following years, these revolutionary ideas were verified on several occasions. For example, Einstein proved that his theory explained the anomalous perihelion advance of the planet Mercury without any arbitrary parameters. At the same time, in 1919, an expedition led by Eddington confirmed general relativity's prediction for the deflection of starlight by the Sun during the total solar eclipse of 29 May 1919. These general relativity field equations are nonlinear and, in consequence, hard to solve. Therefore, A. Einstein used approximation methods to derive the results used to test for the validity of his theory. The first non-trivial solution to Einstein's field equations was discovered in 1916 by the astrophysicist Karl Schwarschild [1]. This solution corresponds to the spherically symmetric, stationary spacetime in the vicinity of a massive object and is known as the Schwarzschild black hole metric. Although quite simple due to its symmetry constraints, this metric captures a lot of general relativity's weirdness. Indeed, on the one hand, the Schwarzscild black hole is so massive that even light cannot escape its gravitational attraction. On the other hand, Stephen Hawking proved in 1974 that black holes constantly radiate thermal radiations in their surrounding at a fixed temperature called the Hawking temperature [2].

The richness of curved spacetime physics and its mathematical beauty attracted the attention of many scientists and much popular fascination. It seems, however, following Einstein's ideas, that such curved spacetime is a specificity of gravity and general relativity. However, physicists realized that in other contexts, such as optics, the wave equations obeyed by light rays share some similarities with relativistic equations in a curved spacetime [3]. This thesis will focus on the manifestation of curved spacetime physical properties beyond gravity in condensed matter systems. Even though the analogy between curved spacetime physics and condensed matter is not new, the idea that one could build a tabletop experiment to explore the specifics of curved spacetime physics is more recent and attributed to William Unruh. Indeed, in 1981, W. Unruh demonstrated that in an irrotational, inviscid, and barotropic fluid, the propagation of sound waves is captured by a curved spacetime relativistic equation whose metric depends on the specifics of the fluid mean flow [4]. The groundbreaking idea that one could design in the laboratory an experiment probing the details of curved spacetime physics gave birth to the domain of physics known as analog gravity. The motivation for looking at an analog model is to reproduce in the laboratory various gravitational effects whose existence, while proven theoretically, surpasses our present observational capabilities. While originally, analog models were considered in classical fluid experiments [4], the search for exotic phenomena, such as Hawking radiation, only appearing in the low-energy regime of the analog systems, triggered the seacrh for analog gravity in quantum fluids, such as in Bose-Einstein condensate experiments [5, 6].

In another context, in 1930, Richard Tolman and Paul Ehrefest were studying black body radiation at thermal equilibrium in the presence of curved spacetime [7, 8]. They realized that contrary to the flat spacetime result, in the presence of a curved spacetime, the equilibrium temperature is not homogeneous but depends on the underlying spacetime. Later on, while studying thermal transport in solids, Joaquin Luttinger built on their study to relate the energy current observed in the presence of an inhomogeneous temperature profile to that induced by curved spacetimes [9]. This analogy between a temperature profile and a curved spacetime illustrates how one can use our knowledge of curved spacetime physics to determine results in condensed matter experiments. This underlines the two-sided interest of such a relation. On the one hand, one can use the knowledge of quantum fluids to build tabletop experiments to test for exotic gravitational phenomena. On the other hand, one can use the knowledge of field theory in curved spacetime to understand the transport properties of materials. The main objective of the present thesis lies exactly in between these two points of view. In this thesis, our objective is to relate analog gravity experiments and the thermal transport properties of semimetals. To establish such a connection between two seemingly distinct topics, we will resort to the concept of quantum fluctuations and anomalies.

Symmetries are a cornerstone of physics, common to quantum fields theory in curved spacetimes and condensed matter. Indeed, following the Noether theorem, it is possible to relate any continuous symmetry of a Hamiltonian to a conserved current. For example, time translation symmetry leads to energy conservation, while translation symmetry is associated with the conservation of momentum. In rare cases, a system is described by a Hamiltonian possessing a symmetry that does not translate in a conserved quantity. The field theory, describing in particular the quantum fluctuation of the system, does not possess the symmetry of the Hamiltonian. Such symmetries, referred to as anomalous symmetries, translate into non-conservation equations for the corresponding currents. Of specific interest in this thesis, the anomalous symmetries whose violation is induced by the presence of non-zero spacetime curvature are referred to as gravitational anomalies. Historically, the trace anomaly, a specific type of gravitational anomaly, was considered by Steven Christensen and Stephen Fulling in 1977 [10] to explain the physics of 1+1 dimensional Hawking radiation. At the same time, Sean Robinson and Frank Wilczek later related another type of gravitational anomaly known as the Einstein anomaly to the same physical phenomenon [11].
More recently and building on the relationship between electric transport and chiral anomaly established by Holger Nielsen and Masao Ninomiya [12], several papers look, both theoretically and experimentally, into the possible relationships between thermal transport and gravitational anomalies [13–16].

In this thesis, we explore the relationship between analog gravity and thermal transport in semimetals. In the process, we resort to a field theory in curved spacetime and, more precisely, to the notions of vacuum fluctuations and gravitational anomalies in the presence of a non-zero spacetime curvature. The manuscript is organized as follows. Chapter 1 describes briefly how curved spacetime physics emerges in condensed matter, whether in fluids, in one-dimensional conductors, or when studying thermal transport. In chapter 2, we introduce the concept of anomalies. Considering the historical example of the chiral anomaly, we introduce several methods of calculation of the chiral anomaly and the corresponding interpretations. We then conclude this chapter by introducing the gravitational anomalies at the heart of this thesis. In chapter 3, we introduce the historical derivation of the Tolmann-Ehrenfest temperature and its relationship with the Luttinger trick. This derivation is then reconsidered by taking into account gravitational anomalies and exploring how such anomalies modify the equivalence,

introducing the concept of anomalous Tolman-Ehrenfest temperature. This concept is afterward generalized to other physical systems in chapters 4, 5 and 6. In chapter 4, after showing how the concept of anomalous Tolman-Ehrenfest temperature naturally applies to the historical example of black holes, we extend this description to strongly out-of-equilibrium condensed matter systems either following a thermal quench or resulting from a periodic drive. In chapter 5 and 6, we consider systems with a dynamical metric and with different chirality of fermions coupled to different metrics. In chapter 7, we discuss our results through the prism of the historical dispute between Boltzmann, Maxwell, and Loschmidt concerning the presence of a thermal gradient at equilibrium in curved spacetime. We finally conclude this work with an analysis of a collaboration with an experimental group, which, while initially designed to test for gravitational anomaly consequences, reveals a much richer phenomenology induced by a strong coupling between phonons and electrons.

Chapter 1

From condensed matter to curved spacetime

This thesis is concerned with the study of the interplay between curved spacetime and condensed matter physics. The purpose of such a study is twofold: On the one hand, such a study can be used to understand and describe some "curved spacetime-like" phenomena arising in condensed matter setups. On the other hand, this study can also be used to design tabletop experiments to test for the manifestations of gravity, from simple wavepacket dynamics to the most exotic phenomena, such as quantum gravity or Hawking radiation induced by black holes. Therefore, a natural question is: how can we engineer curved spacetimes in the laboratory? There exist several strategies to do so. A first natural strategy is to observe that such curvature can, in principle, come from deformations applied to the material hosting the excitations we consider [17–19]; however, as we will try to convince you in the following, such curvature can also arise in many other contexts, from the simple study of heat conductivity to the hydrodynamics of fluid in motion in inhomogeneous backgrounds.

In this chapter, we will encounter several examples in which emergent curved spacetimes arise in condensed matter systems. First, we will treat the historical example, initially considered by W. Unruh, of a classical fluid in motion and its extension to quantum fluids. Then, we will try to convince you that, in the presence of inhomogeneities, the physics of 1+1 dimensional systems can be identified with the physics of fermions in curved spacetime. Finally, we will show that the idea of curved spacetime in condensed matter is rather natural since it constitutes a standard tool in the study of response theory in the presence of temperature gradients.

1.1 Curved spacetimes and black hole analogs in fluids in motion

The idea of using classical and quantum systems to unveil some curved spacetime properties dates back to the work of W. Gordon in 1923, who was studying inhomogeneous optics systems [3]. At the time, W. Gordon's objective was to determine an effective metric to describe his sample, or in other words, to use curved spacetime physics to mimic the dielectric properties of an optical setup. This strategy is opposite to the one exemplified in the book "The Classical Theory of Fields" by L. Landau and E. Lifshitz [20], where the objective of the problem "Equations of electrodynamics in the presence of a gravitational field" is to mimic gravity with optics. This simple example from optics exemplifies the twofold nature of curved spacetime in condensed matter used either to solve a problem of condensed matter using gravity or to mimic gravity in the laboratory. Several other works employed similar analogies between acoustics and curved spacetime wave equations to study the stability and the conservation laws obeyed

by shockwaves close to some celestial objects [21]. Another family of experimental works based on such analogies emerged later, focusing on the analogy between shallow water equations and gravity to build gravity analogs in the laboratory [22–25].

However, the paper usually considered as giving birth to the contemporary realm of analog gravity is the one by W. Unruh in 1981 [4]. This paper proposed to use a hydrodynamic system to mimic the physics behind black hole evaporation or Hawking radiation. In this section, we will rederive the analogy between hydrodynamics and curved spacetime equations for both a classical and a quantum fluid and draw an analogy between the obtained metric and one specific to the exotic example of Schwarzschild black holes.

1.1.1 From classical hydrodynamic to curved spacetimes

First, let us review how curved spacetime equations emerge from the hydrodynamics equation of a classical fluid. In his 1981 seminal paper [4], W. Unruh proved that if a classical fluid is both inviscid, irrotational, and barotropic, its equations of motion are equivalent to d'Alembertian equations, the equations obeyed by a massless scalar in curved spacetime.

The equations capturing the dynamic of an inviscid irrotational classical fluid are

$$\partial_t \rho + \vec{\nabla} \cdot (\rho\, \vec{v}\,) = 0\,, \qquad \text{(Continuity equation)} \tag{1.1}$$

$$\partial_t (\vec{v}\,) + \frac{1}{2}\vec{\nabla}(\vec{v}\cdot\vec{v}\,) + \frac{1}{\rho}\vec{\nabla} p + \vec{\nabla}\phi = \vec{0}\,, \qquad \text{(Euler irrotational equations)} \tag{1.2}$$

with ϕ an external potential, leading to the force $\vec{F} = -\vec{\nabla}\phi$.
Since the fluid is irrotational, one can locally define a field $\psi(\vec{x})$ satisfying $\vec{v} = -\vec{\nabla}\psi$. Moreover, in a barotropic fluid, the density solely depends on the pressure, such that one can define an enthalpy field

$$h(p) = \int_0^p \frac{\mathrm{d}p'}{\rho(p')}\,, \tag{1.3}$$

which depends solely on the pressure p. Expressed in terms of h and $\psi(x)$, Euler equations (1.2) take the simplified form

$$-\partial_t\psi + \frac{1}{2}\left(\vec{\nabla}\psi\right)\cdot\left(\vec{\nabla}\psi\right) + h + \phi = 0\,. \tag{1.4}$$

Linearizing the equation around a given background (ρ_0, p_0, ψ_0) such that

$$\begin{cases} p = p_0 + \epsilon p_1 + o(\epsilon)\,, \\ \rho = \rho_0 + \epsilon\rho_1 + o(\epsilon)\,, \\ \psi = \psi_0 + \epsilon\psi_1 + o(\epsilon)\,, \end{cases} \tag{1.5}$$

leads to the equations of motion for the background fields

$$\begin{cases} \partial_t\psi_0 = \phi + h(p_0) + \frac{1}{2}\left(\vec{\nabla}\psi_0\right)\cdot\left(\vec{\nabla}\psi_0\right)\,, \\ \partial_t\rho_0 = \vec{\nabla}\cdot\left(\rho_0\vec{\nabla}\psi_0\right)\,. \end{cases} \tag{1.6}$$

The sound waves are described by the solution (ρ_1, p_1, ψ_1), that satisfy

$$\begin{cases} p_1 = \rho_0\left[\partial_t\psi_1 - \left(\vec{\nabla}\psi_0\right)\cdot\left(\vec{\nabla}\psi_1\right)\right]\,, \\ \partial_t\left[c^{-2}\,p_1\right] - \vec{\nabla}\cdot\left[\rho_0\vec{\nabla}\psi_1 + c^{-2}\,p_1\vec{\nabla}\psi_0\right] = 0\,, \end{cases} \tag{1.7}$$

with the squared inverse velocity $c^{-2} = \frac{\partial\rho}{\partial p}\Big|_{p_0}$. Inserting the definition of p_1 into the second equation leads to the equation of motion for ψ_1:

$$\partial_t \left[\rho_0 c^{-2} \left(\partial_t\psi_1 - \partial_j\psi_0\partial_j\psi_1\right)\right] - \partial_i \left[\rho_0\partial_i\psi_1 + \rho_0 c^{-2}\left(\partial_t\psi_1 - \partial_j\psi_0\partial_j\psi_1\right)\partial_i\psi_0\right] = 0\,, \tag{1.8}$$

where $\partial_i \equiv \frac{\partial}{\partial x_i}$, and a sum on repeated indices is assumed.

Assuming a constant background ($\psi_0 = Cst$) and a fixed velocity c, this equation of motion takes the simple form of a d'Alambertian equation in flat spacetime

$$\Box\psi = 0 \Leftrightarrow \frac{1}{c^2}\frac{\partial^2\psi_1}{\partial t^2} - \sum_i \frac{\partial^2\Psi_1}{\partial x_i^2} = 0\,. \tag{1.9}$$

Similarly, as we will see in section 1.1.2, in the general case, the equation (1.8) verified by ψ_1 is nothing but a d'Alambertian equation in curved spacetime or, in other words, the equation of motion for a massless free scalar field in a curved spacetime, where the background (ρ_0, p_0, ψ_0) fully determines the metric according to

$$\sqrt{-\det(g_{\rho\sigma})}g^{\mu\nu} = \frac{\rho_0}{c^2}\begin{pmatrix} 1 & -\partial_i\psi_0 \\ -\partial_i\psi_0 & -c^2\delta^{ij} + \partial_i\psi_0\partial_j\psi_0 \end{pmatrix}. \tag{1.10}$$

Shaping this metric amounts to carefully choosing the external forces $(-\partial_i\phi)$ applied to the system to set the background flow. Note, at this point, that even though W. Unruh's main objective was to design a black hole metric, this demonstration is more general. It allows one to design specific curved spacetime metrics in hydrodynamic systems by controlling the evolution of the mean flow.

1.1.2 Scalar fields in curved-spacetime

We now turn to the study of Klein-Gordon field equations in curved spacetime. In the previous section, we have seen that in the presence of a constant background ($\Psi_0 = Cst$), the equation for sound waves takes the form of a massless d'Alambertian equation (1.9). In order to identify a possible curved spacetime analog underlying the evolution of sound waves in an inhomogeneous system, in this section, we describe the Klein-Gordon equation in curved spacetime. Indeed, in a flat spacetime, the dynamic of a real scalar field is captured by the Klein-Gordon (also known as Klein-Gordon-Fock) action [26, 27], defined in $D+1$ dimensions as

$$\mathcal{S}_{KG} = \int \mathrm{d}t\,\mathrm{d}^D\vec{x}\left(\frac{\hbar^2}{2}\partial_\mu\phi\,\partial^\mu\phi - \frac{1}{2}m^2c^2\phi^2\right).r \tag{1.11}$$

The corresponding equations of motion are

$$\left[\partial_\mu\partial^\mu + \left(\frac{mc}{\hbar}\right)^2\right]\phi = \left[\Box + \left(\frac{mc}{\hbar}\right)^2\right]\phi = 0 \Leftrightarrow \frac{1}{c^2}\frac{\partial^2\phi}{\partial t^2} - \sum_i \frac{\partial^2\Phi}{\partial x_i^2} + \left(\frac{mc}{\hbar}\right)^2\phi = 0\,. \tag{1.12}$$

from which we recover (1.9) with $m = 0$.

The action (1.11) can be extended to curved spacetime with metric $g_{\mu\nu}$ using a minimal coupling procedure to gravity. Such a procedure consists of two steps:

- Generalizing the notion of scalar product to curved spacetimes thanks to the metric $g_{\mu\nu}$:

$$A_\mu B^\mu \equiv A_\mu\,\eta^{\mu\nu}B_\nu \to A_\mu\,g^{\mu\nu}B_\nu\,. \tag{1.13}$$

- Generalizing the measure of integration covariantly:

$$\mathrm{d}^{D+1}\boldsymbol{x} \equiv c\,\mathrm{d}t\,\mathrm{d}^{D}\vec{x} \to \mathrm{d}^{D+1}\boldsymbol{x}\,\sqrt{|\det(g_{\mu\nu})|} \equiv c\,\mathrm{d}t\,\mathrm{d}^{D}\vec{x}\,\sqrt{|\det(g_{\mu\nu})|}\,. \tag{1.14}$$

The Klein-Gordon action then takes the form

$$\mathcal{S}_{KG} = \int \mathrm{d}^{D+1}\boldsymbol{x}\,\sqrt{|\det(g_{\mu\nu})|}\left[\frac{\hbar^2}{2}g^{\mu\nu}\partial_\mu\phi\,\partial_\nu\phi - \frac{1}{2}m^2c^2\phi^2\right]. \tag{1.15}$$

The corresponding equation of motion, generalizing (1.12) to a curved spacetime, reads

$$\left[\Box_g + \left(\frac{mc}{\hbar}\right)^2\right]\phi \equiv \frac{1}{\sqrt{|\det(g_{\rho\sigma})|}}\partial_\mu\left[\sqrt{|\det(g_{\rho\sigma})|}\,g^{\mu\nu}\partial_\nu\phi\right] + \left(\frac{mc}{\hbar}\right)^2\phi = 0\,. \tag{1.16}$$

A comparison with equation (1.8) allows us to identify it with the evolution of a massless Klein-Gordon field in a curved spacetime whose metric is defined by (1.10).

1.1.3 Curved spacetime from quantum fluids

Coming back to classical fluids, it is possible to engineer the mean flow of (1.6) by carefully choosing the forces applied to it [28] such that sound excitations are effectively described by curved spacetime equations, with a metric fixed by (1.10). Nonetheless, in addition to their classical properties, curved spacetimes possess a very rich semiclassical and quantum phenomenology, as exemplified by Hawking's predictions [2]. For this reason, it is interesting to extend the previous analogy to quantum fluids. However, to probe such quantum phenomena, it is essential to consider systems with a low temperature and a large quantum coherence to reduce the thermal noise. Therefore, to study such analogs in the laboratory, it is natural to generalize Unruh's ideas to quantum fluids such as superconductors, superfluid ^{3}He [29–32] or Bose-Einstein condensates [5, 33]. Following these ideas, in what follows, we analyze the emergence of curved spacetimes in two different quantum systems. First in a Bose-Einstein condensate, recovering equations reminiscent of the one obtained in classical hydrodynamics and then in a superfluid or analogously in a p-wave superconductor.

Emergent curved spacetimes physics in Bose-Einstein condensates

Let us first review how curved spacetime physics arises in Bose-Einstein condensates, following the review of C. Barcelo, S. Liberati, and M. Visser [33]. In a quantum system of N interacting bosons, Bose-Einstein condensation corresponds to a configuration where a finite fraction of the bosons lie in the same single-particle quantum state. The observables of such a condensate can, in principle, be deduced from a second quantized Hamiltonian of the form

$$\begin{aligned}\mathcal{H} = &\int \mathrm{d}\vec{x}\,\hat{\Psi}^\dagger(\vec{x},t)\left[-\frac{\hbar^2}{2m}\vec{\nabla}^2 + V_{ext}(\vec{x})\right]\hat{\Psi}(\vec{x},t)\\ &+\frac{1}{2}\int \mathrm{d}\vec{x}\,\mathrm{d}\vec{y}\,\hat{\Psi}^\dagger(\vec{x},t)\hat{\Psi}^\dagger(\vec{y},t)V\left(\vec{x}-\vec{y}\right)\hat{\Psi}(\vec{y},t)\hat{\Psi}(\vec{x},t)\,,\end{aligned} \tag{1.17}$$

with $V_{ext}(\vec{x})$ an external trapping potential and $V(\vec{x}-\vec{y})$ the interatomic two-body interacting potential. However, when N is large, computing the spectrum of this Hamiltonian, solving for $\hat{\Psi}$ becomes impractical. N. Bogoliubov introduced in 1947 a natural mean-field ansatz of the form

$$\hat{\Psi}(\vec{x},t) = \psi(\vec{x},t) + \hat{\phi}(\vec{x},t)\,, \tag{1.18}$$

where $\psi(\vec{x},t) = \langle\hat{\Psi}(\vec{x},t)\rangle$ is referred to as the wave function of the condensate [34], while $\hat{\phi}$ denotes the excitation on top of the condensate.

Assuming that the number of particles that do not lie in the condensate wavefunction is small compared to N, a zeroth order approximation leads to the equation of motion of the condensate

$$i\hbar\partial_t\psi(\vec{x},t) = \left[-\frac{\hbar^2}{2m}\vec{\nabla}^2 + V_{ext}(\vec{x}) + \int \mathrm{d}\vec{y}\,\psi^\dagger(\vec{y},t)V(\vec{x}-\vec{y})\psi(\vec{y},t)\right]\psi(\vec{x},t)\,. \tag{1.19}$$

If we further assume the two-body interaction to be short range $V(\vec{x}) \approx \kappa\delta(\vec{x})$ with $\kappa = \frac{4\pi a\hbar^2}{m}$ where a represents the scattering length, the condensate wave function verifies the Gross-Pitaevskii (also known as the non-linear Shrödinger or time-dependent Landau-Ginzburg) equation

$$i\hbar\partial_t\psi = \left(-\frac{\hbar^2}{2m}\vec{\nabla}^2 + V_{ext}(\vec{x}) + \kappa\psi^\dagger\psi\right)\psi\,, \tag{1.20}$$

where for brevity we omitted the $(\vec{x},t)$ explicit dependence of the wave function.

Starting from equation (1.20), let us show that in a way similar to the classical hydrodynamic, the weak fluctuation of ψ around a background ψ_0 can be described by a curved spacetime Klein-Gordon equation. To do so, let us parametrize ψ using the so-called Madelung representation with a phase and a density such as $\psi = \sqrt{n}\exp(i\theta/\hbar)$. Developing ψ around a background $\psi_0 = \sqrt{n_0}\exp(i\theta_0/\hbar)$ can be done by writing

$$\begin{cases} n = n_0 + \delta n\,, \\ \theta = \theta_0 + \delta\theta\,. \end{cases} \tag{1.21}$$

Assuming the perturbation to be small, there is no backreaction of the fluctuation $\delta n, \delta\theta$ on the background whose equation of motion

$$\begin{cases} \partial_t n_0 + \frac{1}{m}\vec{\nabla}\cdot\left(n_0\vec{\nabla}\theta_0\right) = 0\,, \\ \partial_t\theta_0 + \frac{1}{2m}\left(\vec{\nabla}\theta_0\right)\cdot\left(\vec{\nabla}\theta_0\right) + V_{ext} + \kappa n_0 - \frac{\hbar^2}{2m}\frac{\vec{\nabla}^2\sqrt{n_0}}{\sqrt{n_0}} = 0\,, \end{cases} \tag{1.22}$$

are identical to Euler equations for a barotropic inviscid irrotational fluid (1.6) where $\psi_0 \Leftrightarrow \frac{\theta_0}{m}$ with a quantum potential term $V_{quant} = -\frac{\hbar^2}{2m}\frac{\vec{\nabla}^2\sqrt{n_0}}{\sqrt{n_0}}$. Similarly, the fluctuations verify an equation similar to the one obeyed by the sound waves in classical fluid (1.7),

$$\begin{cases} \partial_t\delta n + \frac{1}{m}\vec{\nabla}\cdot\left(\delta n\vec{\nabla}\theta + n\vec{\nabla}\delta\theta\right) = 0\,, \\ \partial_t\delta\theta + \frac{1}{m}\left(\vec{\nabla}\delta\theta\right)\cdot\left(\vec{\nabla}\theta\right) + \kappa\delta n - \frac{\hbar^2}{2m}D_2\left[\delta n\right] = 0\,, \end{cases} \tag{1.23}$$

with

$$D_2\left[\delta n\right] = \frac{\vec{\nabla}^2\delta n}{2n_0} - \frac{\vec{\nabla}^2 n_0}{2n_0}\delta n - \frac{\left(\vec{\nabla}\delta n\right)\cdot\left(\vec{\nabla}n_0\right)}{2n_0^2} + \frac{\left(\vec{\nabla}n_0\right)^2}{2n_0^3}\delta n\,. \tag{1.24}$$

Comparison with equation (1.7) shows that a quantum correction appears through the operator D_2. However, on wavelengths larger than the healing length $\frac{2\pi}{k} > \xi = \frac{\hbar}{\sqrt{m\kappa n}}$, this term becomes negligible such that (1.23) can be interpreted, similarly to the classical case, as the equation of motion for a massless scalar field in a curved spacetime (1.16) whose metric is given by

$$\sqrt{-\det(g_{\rho\sigma})}g^{\mu\nu} = \frac{n}{c_s^2}\begin{pmatrix} 1 & -v_i \\ -v_j & -c_s^2\delta^{ij} + v_iv_j \end{pmatrix}\,, \tag{1.25}$$

with $v_i = \frac{\partial_i \theta}{m}$ the fluid velocity, and $c_s^{-2} = \frac{m}{\kappa n}$ the sound velocity. For larger wavelengths, another approximation applies. This approximation, called the eikonal approximation, assumes a slow variation of the background amplitude compared to the fluctuation amplitude, such that $D_2[\delta n] \approx \frac{1}{2n_0}\vec{\nabla}^2 \delta n$. Under this approximation, the energy spectrum becomes

$$\omega = \vec{v}\cdot\vec{k} \pm c_s\left|\vec{k}\right| \rightarrow \omega = \vec{v}\cdot\vec{k} \pm \sqrt{c_s^2\vec{k}^2 + \left(\frac{\hbar}{2m}\vec{k}^2\right)}\,. \tag{1.26}$$

We recover a linear spectrum for large wavelengths ($2\pi/k > \xi$). Therefore, the dynamic of the corresponding particles is well described by the relativistic physics picture presented previously. For smaller wavelengths ($2\pi/k < \xi$), quantum corrections induce non-linearities, and the relativistic picture breaks down.

Emergent curved-spacetime physics in superfluids and p-wave superconductors

As we have seen in the previous paragraph, curved spacetime physics emerges naturally in Bose-Einstein condensates. In this paragraph, we will focus on a different quantum system: superfluids and p-wave superconductors, illustrating the emergent metrics with the specific example of vortices, following the review of G. Volovik [35].

Let us consider a specific spinless example of BCS Hamiltonian leading to pairing in a p-wave state

$$\mathcal{H} - \mu\mathcal{N} = \sum_{\vec{p}}\left(\frac{\vec{p}^2}{2m} - \mu\right)a^\dagger_{\vec{p}}a_{\vec{p}} - \frac{\lambda}{V}\left(\sum_{\vec{q}}\vec{q}\,a^\dagger_{-\vec{q}}a^\dagger_{\vec{q}}\right)\cdot\left(\sum_{\vec{p}}\vec{p}\,a_{-\vec{p}}a_{\vec{p}}\right)\,, \tag{1.27}$$

with V the size of the sample and λ the interaction strength.

In the superconducting or superfluid state, the quantity $\sum_{\vec{p}}\vec{p}\,a_{-\vec{p}}a_{\vec{p}}$ acquires a non-zero vacuum expectation value. As in the case of s-wave superconductivity, the two Fermi particles form a Bose quasiparticle with 0 total momentum. However, in the case of p-wave superconductivity, the order parameter is no longer a complex scalar but a complex vector

$$\frac{2\lambda}{V}\left\langle\sum_{\vec{p}}\vec{p}\,a_{-\vec{p}}a_{\vec{p}}\right\rangle = \vec{e}_1 + i\,\vec{e}_2\,, \tag{1.28}$$

with $\vec{e}_{1,2}$ real vectors, whose value is determined by minimizing the vacuum energy.
Symmetry considerations, however, show that two types of solutions are possible:

- In the first case, the two vectors are perpendicular to each other and of equal magnitude

$$\begin{cases}\vec{e}_1\cdot\vec{e}_2 = 0\,,\\ |\vec{e}_1| = |\vec{e}_2| = \frac{\Delta_0}{p_F}\end{cases} \tag{1.29}$$

  with Δ_0 the amplitude of the superconducting gap and $p_F = \sqrt{2\mu\, m}$. Such a case arises, for example, in the superfluid phases ^{3}He-A or ^{3}He-A_1, whose precise form depends on the specific spin structure which we do not consider here.

- In the second case, the two vectors are parallel to each other and can only differ by a phase factor

$$\vec{e}_1 + i\vec{e}_2 = \vec{e}\,e^{i\Phi} \tag{1.30}$$

  with $\vec{e}$ a real vector along the common direction. Such a situation naturally arises in spin-triplet superfluid and superconductors.

For now, let us ignore their precise value and consider the situation in the limit of weak interactions $\lambda \to 0$. In this limit, the quantum fluctuations of the order parameter are small. Neglecting the term quadratic in these fluctuations, one obtains the simplified Hamiltonian

$$\begin{aligned} \mathcal{H} - \mu\mathcal{N} &\approx \frac{V}{4\lambda}\left((\vec{e}_1)^2 + (\vec{e}_2)^2\right)\sum_{\vec{p}}\mathcal{H}_{\vec{p}}\,, \\ \mathcal{H}_{\vec{p}} &= \left(\frac{\vec{p}\cdot\vec{p}}{2m} - \mu\right)\frac{a^\dagger_{\vec{p}}a_{\vec{p}} + a^\dagger_{-\vec{p}}a_{-\vec{p}}}{2} + \vec{p}\cdot\frac{\vec{e}_1 - i\,\vec{e}_2}{2}a_{-\vec{p}}a_{\vec{p}} + \vec{p}\cdot\frac{\vec{e}_1 + i\,\vec{e}_2}{2}a_{-\vec{p}}a_{\vec{p}}\,. \end{aligned} \tag{1.31}$$

For each $\vec{p}$, this Hamiltonian can be diagonalized using the operators $\mathcal{L}_i$ defined as

$$\mathcal{L}_1 + i\,\mathcal{L}_2 = a_{\vec{p}}a_{-\vec{p}}\,, \quad \mathcal{L}_1 - i\,\mathcal{L}_2 = a^\dagger_{\vec{p}}a^\dagger_{-\vec{p}}\,, \quad \mathcal{L}_3 = \frac{1}{2}\left(a^\dagger_{\vec{p}}a_{\vec{p}} + a^\dagger_{-\vec{p}}a_{-\vec{p}} - 1\right)\,, \tag{1.32}$$

such that $[\mathcal{L}_i\,,\mathcal{L}_j] = i\epsilon_{ijk}\mathcal{L}_k$. The corresponding Hamiltonian reads

$$\begin{aligned} \mathcal{H}_{\vec{p}} &= \frac{1}{2}\left(\frac{\vec{p}\cdot\vec{p}}{2m} - \mu\right) + \frac{1}{2}E\left(\vec{p}\right)\left(\tilde{a}^\dagger_{\vec{p}}\tilde{a}_{\vec{p}} + \tilde{a}^\dagger_{-\vec{p}}\tilde{a}_{-\vec{p}} - 1\right)\,, \\ E\left(\vec{p}\right) &= \sqrt{\left(\frac{\vec{p}\cdot\vec{p}}{2m} - \mu\right) + \left(\vec{p}\cdot\vec{e}_1\right)^2 + \left(\vec{p}\cdot\vec{e}_2\right)^2}\,, \end{aligned} \tag{1.33}$$

with $\tilde{a}_{\vec{p}}/\tilde{a}^\dagger_{\vec{p}}$ the creation and annihilation operators corresponding to fermionic quasiparticles (the so-called Bogoliubov quasiparticles). The Hamiltonian (1.33) is that of fermionic quasiparticle excitations above a mean field vacuum

$$\mathcal{H} - \mu\mathcal{N} \approx \langle\mathcal{H} - \mu\mathcal{N}\rangle + \sum_{\vec{p}}E\left(\vec{p}\right)\,\tilde{a}^\dagger_{\vec{p}}\tilde{a}_{\vec{p}}\,. \tag{1.34}$$

For the rest of this section, let us focus on the first case (1.29) for which $\vec{e}_1 \wedge \vec{e}_2 \neq 0$. The quasiparticle energy vanishes at two points in momentum space

$$\vec{q}_{pm} = \pm p_F\,\vec{l}\,, \quad \vec{l} = \frac{\vec{e}_1 \wedge \vec{e}_2}{|\vec{e}_1 \wedge \vec{e}_2|}\,, \tag{1.35}$$

with p_F the Fermi momentum of the ideal Fermi gas $p_F = \sqrt{2\mu m}$. Close to these points, called "Fermi points" by analogy with free fermions, the quasiparticle energy spectrum becomes

$$E^2\left(\vec{q}_\pm + \vec{k}\right) = \left(\vec{e}_1\cdot\vec{k}\right)^2 + \left(\vec{e}_2\cdot\vec{k}\right)^2 + \left(\vec{e}_3\cdot\vec{k}\right)^2\,, \tag{1.36}$$

with $\vec{e}_3 = c_\parallel\vec{l}$, $c_\parallel = \frac{p_F}{m}$, which corresponds to the energy spectrum of two massless relativistic particles in curved spacetime, and more precisely a so-called Weyl Hamiltonian.
This spectrum (1.36) then defines the components of the metric in a comoving frame[1]

$$\begin{cases} g^{00} = 1\,, \\ g^{i0} = g^{0i} = 0\,, \\ g^{ij} = -\sum_{k=1}^3 e^i_k e^j_k = -c_\parallel^2 l^i l^j - c_\perp^2\left(\delta^{ij} - l^i l^j\right)\,, \quad (i,j) \in \{x,y,z\}^2\,, \end{cases} \tag{1.37}$$

with $c_\perp = |\vec{e}_1| = |\vec{e}_2|$.

[1]Note that in these cases, the space-space components of the metric have the dimension of an inverse squared velocity, while g^{00} has no dimension. One could recover the usual dimensionality introducing a velocity scale v_F, and rescaling $g^{ij} \to 1/v_F^2 g^{ij}$, $g^{0i} \to 1/v_F g^{0i}$ and $g^{i0} \to 1/v_F g^{i0}$ with $x_0 = v_F t$

However, in the laboratory frame, the fluid can possess a non-zero velocity v_s, defined by

$$\vec{v}_s = \frac{\hbar}{2m} m^i \vec{\nabla} n^i \,, \tag{1.38}$$

where $\vec{m} = \vec{e}_1/c_\perp$ and $\vec{n} = \vec{e}_2/c_\perp$. The energy of such a system can be obtained from the comoving energy (1.36), via a Doppler shift $E\left(\vec{q}_\pm + \vec{k}\right) \to E\left(\vec{q}_\pm + \vec{k}\right) + \vec{k}\cdot\vec{v}_s \pm p_F \vec{l}\cdot\vec{v}_s$, such that the metric reads

$$\begin{cases} g^{00} = 1 \,, \\ g^{i0} = g^{0i} = -v_s^i \,, \\ g^{ij} = -c_\parallel^2 l^i l^j - c_\perp^2 \left(\delta^{ij} - l^i l^j\right) + v_s^i v_s^j \,, \quad (i,j) \in \{x,y,z\}^2 \,, \end{cases} \tag{1.39}$$

which implies a "line element" of the form

$$\mathrm{d}\tau^2 = \mathrm{d}t^2 + g_{ij}\left(\mathrm{d}x^i - v_s^i \mathrm{d}t\right)\left(\mathrm{d}x^j - v_s^j \mathrm{d}t\right) \,, \tag{1.40}$$

with

$$g_{ij} = -\frac{1}{c_\parallel^2} l^i l^j - \frac{1}{c_\perp^2}\left(\delta^{ij} - l^i l^j\right) \,, \quad (i,j) \in \{x,y,z\}^2 \,. \tag{1.41}$$

Curved spacetimes physics, therefore, naturally emerges when studying p-wave superconductivity as well as superfluid ^{3}He.

Note that contrary to the hydrodynamic equations used in equations (1.2), and (1.20), these systems are not irrotational: by taking the rotational of the fluid velocity $\vec{v}_s$, one recovers the Mermin-Ho relation [36]:

$$\vec{\nabla} \wedge \vec{v}_s = \frac{\hbar}{4m} \epsilon_{ijk} l^i \left(\vec{\nabla} l^j\right) \wedge \left(\vec{\nabla} l^k\right) \,. \tag{1.42}$$

However, when the vector $\vec{l}$ is constant, e.g. along the vector $\vec{e}_z$, one can define the angle Φ as

$$\vec{m} + i\vec{n} = \left(\vec{e}_x + i\vec{e}_y\right) e^{i\Phi} \,, \tag{1.43}$$

such that the velocity

$$v_s = \frac{\hbar}{2m} \vec{\nabla}\Phi \,, \tag{1.44}$$

can be interpreted as the angular velocity at which the axes $\vec{e}_{1,2}$ rotate around the z-axis. In such cases, the velocity field is, by definition, irrotational except in the presence of topological defects of the vierbein field. These are the so-called quantized vortices, characterized by their quantized circulation

$$\oint \vec{v}_s \cdot \mathrm{d}\vec{x} = n_1 \kappa_0 \,, \tag{1.45}$$

with n_1 an integer and $\kappa_0 = \pi\hbar/m$
In the vicinity of a $n_1 = 1$ vortex, a simple ansatz characterizing the emergent metric is given by

$$\begin{cases} \vec{l} = \vec{e}_z \,, \\ \vec{e}_1 = c(r)\vec{e}_r \,, \\ \vec{e}_2 = c(r)\vec{e}_\phi \,, \end{cases} \tag{1.46}$$

with $c(r)$ the "speed of light" verifying $c(0) = 0$ and $c(+\infty) = c_\perp$, while the speed of the fluid is characterized by $\vec{v}_s(r) = v_s(r)\vec{e}_\phi = \kappa \frac{1}{2\pi r}\vec{e}_\phi$. Therefore, the line element reads

$$\mathrm{d}s^2 = \mathrm{d}t^2\left(1 - \frac{v_s^2}{c^2}\right) - 2\vec{v}_s \cdot \mathrm{d}\vec{r}\,\mathrm{d}t - \frac{1}{c_\parallel}\mathrm{d}z^2 + \frac{1}{c^2}\left(\mathrm{d}r^2 + r^2\mathrm{d}\phi^2\right) \,. \tag{1.47}$$

As we will see in the next section, this line element is reminiscent of that close to a 2+1 dimensional black hole whose interior matches the ergoregion of the vortex (see Fig. 1.1).

Curved spacetimes can, therefore, arise both in the study of classical and quantum systems. The corresponding metric can be directly related to the order parameter in superfluids and superconductors. The metric depends on the mean flow in classical fluids and Bose-Einstein condensates. It can be controlled by applied potential or forces, allowing the use of such systems as gravity analogs to simulate curved spacetime physics in the laboratory.

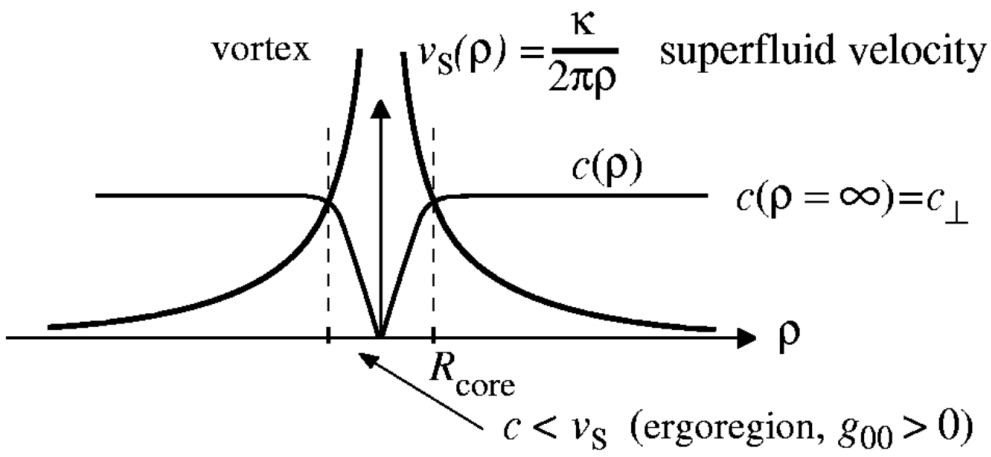

Figure 1.1: **Quantized vortex velocity profiles** Comparison between the radial velocity $c_\perp$ and the fluid velocity v_s defines the ergoregion, viewed as an analog black hole (extracted from [35]).

1.1.4 Black-holes in Bose-Einstein condensates: classical fluid interpretation

In 1974, S. Hawking predicted [2] that black holes are not entirely black; instead, they slowly evaporate, releasing an outgoing energy current called the Hawking radiation. Questions concerning entropy in the presence of black holes remain topical, such as the information paradox first established by S. Hawking in 1976 [37,38]. Designing a tabletop experiment whose metric identifies with that of a black hole is of particular interest. Given the form of the metric used to study sound waves (see (1.10), and (1.25)), can we describe exotic objects such as black holes, characterized by a Schwarzschild black-hole metric [1] in these setups? To answer this question, we will first review the notion of Gullstrand-Painlevé coordinates [39,40] before using them to relate our analog metrics to some intuitive description [41] of a black hole.

To do this, let us focus on the Schwarzschild metric, defined in spherical coordinates by the line element

$$\mathrm{d}s^2 = g_{\mu\nu}\mathrm{d}x^\mu \mathrm{d}x^\nu = \left(1 - \frac{r_H}{r}\right) c^2 \mathrm{d}t^2 - \left(1 - \frac{r_H}{r}\right)^{-1} \mathrm{d}r^2 - r^2 \mathrm{d}\Omega^2 \,, \tag{1.48}$$

where $\mathrm{d}\Omega^2$ is the angular line element (for example in 3+1 dimensions $\mathrm{d}\Omega^2 = \mathrm{d}\theta^2 + \sin^2(\theta)\mathrm{d}\phi^2$) while $r_H = \frac{2GM}{c^2}$ is the Schwarzschild radius. This metric contains two singularities at $r = 0$ and $r = r_H$. Such a metric describes a black hole if the radius of the physical object of mass M is smaller than r_H. However, despite its peculiar form, the singularity at $r = r_H$ is not a genuine physical singularity (contrary to the one at $r = 0$) but simply a singularity of the

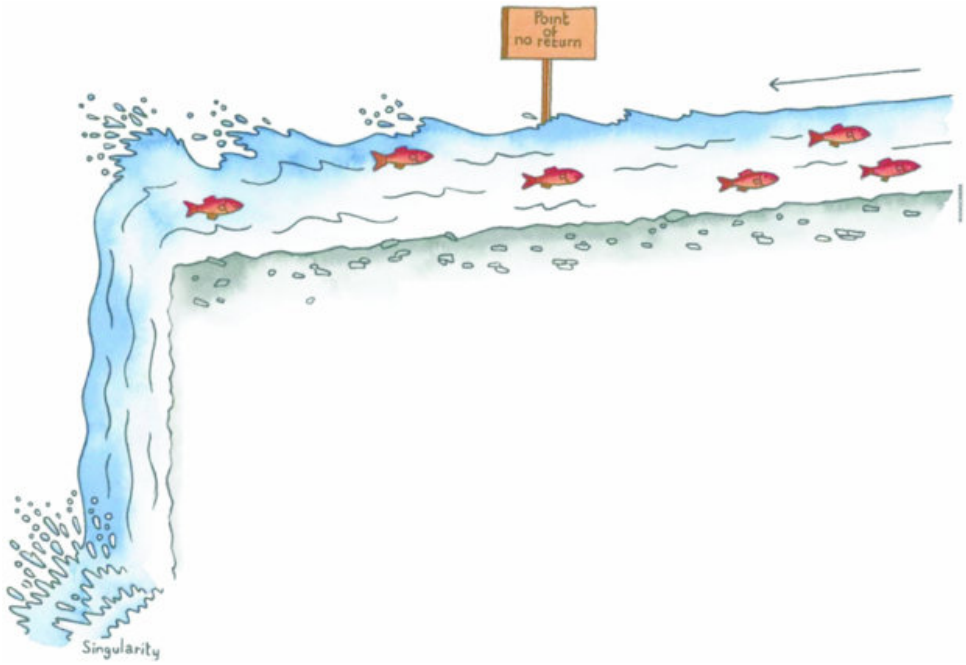

Figure 1.2: **Black holes as fish close to a waterfall** In this analogy, let us replace the space flowing into a Schwarzschild black hole with a river flowing towards a waterfall and photons (light rays) by fish swimming fiercely in the current. Outside the horizon, the fish swimming upstream can make way against the flow. Nevertheless, inside the horizon, beyond the point of no return, the river is flowing so fast towards the waterfall that it beats all fish doomed to fall into it (adapted from [43]).

coordinate system used to describe the black hole. This fact can be understood following A. Gullstrand [39], P. Painlevé [40] and G. Lemaître [42], by defining a new time coordinate $c\tau = ct + 2\sqrt{r r_H} + r_H \ln\left(\frac{\sqrt{\frac{r}{r_H}}-1}{\sqrt{\frac{r}{r_H}}+1}\right)$. The Schwarzschild metric then takes the simple form

$$\mathrm{d}s^2 = g_{\mu\nu}\mathrm{d}x^\mu \mathrm{d}x^\nu = c^2\mathrm{d}\tau^2 - \left(\mathrm{d}r + \sqrt{\frac{r_H}{r}}c\,\mathrm{d}\tau\right)^2 - r^2\mathrm{d}\Omega^2. \tag{1.49}$$

While the coordinate transformation is only defined for $r > r_H$, the metric (1.49) provides an extension of the metric (1.48) to the infinite future. Note that this metric no longer has any singularity at $r = r_H$. Since there exists a coordinate system presenting no singularity for $x = x_H$, we can deduce that $x = x_H$ is not a singularity of the metric but solely of the coordinate system.

Moreover, as noticed by A. Hamilton and J. Lisle in 2006 [41], looking at the light-like geodesics verifying $\mathrm{d}s^2 = 0 \Leftrightarrow \frac{\mathrm{d}r}{\mathrm{d}\tau} = -c\left(\sqrt{\frac{r_H}{r}} \pm 1\right)$ provides a relatively simple picture of the black hole, that we can extend to the hydrodynamic picture developed in the previous section: spaces itself flows radially towards $r = 0$ at a velocity $c\sqrt{\frac{r_H}{r}}$, and $r = r_H$ marks the horizon of the black hole: by analogy, in the case of the hydrodynamic metric, sound waves play the role of the excitation (photons) while the fluid with inhomogeneous velocity $\partial_i\theta$ plays the role of the spacetime. This analogy is often used to represent black holes using the image of fishes in a river (see Fig. 1.2).
While the description above is specific to Schwarzschild black holes, according to [41], this mental image of a black hole as a flowing river is far more general and can, for example, be applied to rotating black holes. Moreover, this common analogy underlies current laboratory studies of general analog black holes. A hydrodynamic metric with a characteristic line element

of the form

$$\mathrm{d}s^2 = g_{\mu\nu}\mathrm{d}x^\mu \mathrm{d}x^\nu = c_s^2 \mathrm{d}t^2 - \left(\mathrm{d}\vec{r} + \vec{V}(\vec{r})\mathrm{d}t\right)^2 , \tag{1.50}$$

will be analog to a black hole if we have both a sub-sonic($c_s < |\vec{V}|$) and a supersonic ($c_s > |\vec{V}|$) region, separated by an event horizon at which $c_s = |\vec{V}|$. For example, this correspondence enabled measuring correlations between inside and outside regions of such black holes, testing experimentally for Hawking radiation [44, 45].

1.2 Inhomogeneous 1D systems

As we have seen in the previous section, analogous curved spacetimes arise naturally when studying sound waves in both classical and quantum fluids. The tunability of these systems through the choice of the mean flow allows one to simulate several metrics and even the most exotic ones, such as black hole metrics. Analogy with curved spacetime physics also arises in the totally different context of the dynamics of fermions in inhomogeneous 1+1 dimensional systems. A significant difference in this context is the nature of the excitations since, as we will see in this section, instead of massless scalars in curved spacetimes, the excitations in such systems are described by fermionic fields in curved spacetime. This implies that their dynamics is now captured by a curved spacetime Dirac Hamiltonian instead of a curved spacetime Klein-Gordon Hamiltonian as in the previous section.

In this section, after reviewing how 1+1 dimensional Dirac Hamiltonians arise in condensed matter physics, we will introduce two strategies that can be used to create analog curved-spacetime Dirac Hamiltonians, modulating either the couplings or the trapping potentials of the homogeneous Hamiltonians. In other words, we will study to what extent the physics of these inhomogeneous Hamiltonians identify with the physics of curved spacetime fermions, introducing along the way the notion of curved-spacetime Dirac Hamiltonians.

1.2.1 Flat spacetime Dirac Hamiltonian: From condensed matter to field theory

From free electrons...

Let us start our presentation with the example of free, 1+1 dimensional fermions, whose Hamiltonian is given by

$$\mathcal{H} = \int_{-\infty}^{+\infty} \mathrm{d}x \; c^\dagger(x) \left[-\frac{\hbar^2}{2m}\partial_x^2 - \mu\right] c(x) \, . \tag{1.51}$$

This Hamiltonian describes the physics of free fermions, with a quadratic dispersion relation $\varepsilon(k) = \frac{\hbar^2}{2m}(k^2 - k_F^2)$, with $k_F = \frac{1}{\hbar}\sqrt{2m\mu}$ the Fermi momentum. Its large length scale (i.e., low energy $|\varepsilon - \mu| \ll \mu$) physics is obtained by linearizing the energy spectrum around the Fermi surface $k^\pm = \pm k_F$

$$\varepsilon(k^\pm + q) \approx \pm \hbar v_F q \, , \tag{1.52}$$

with $v_F = \frac{\hbar k_F}{m} = \sqrt{\frac{2\mu}{m}}$ the Fermi velocity.

This low-energy behavior can be shown formally to be described by a corresponding low-energy Hamiltonian,

$$\tilde{\mathcal{H}} = -\int_{-\infty}^{+\infty} \mathrm{d}x \; \frac{i\hbar v_F}{2}\left[\psi_R^\dagger \overset{\leftrightarrow}{\partial}_x \psi_R - \psi_L^\dagger \overset{\leftrightarrow}{\partial}_x \psi_L\right] . \tag{1.53}$$

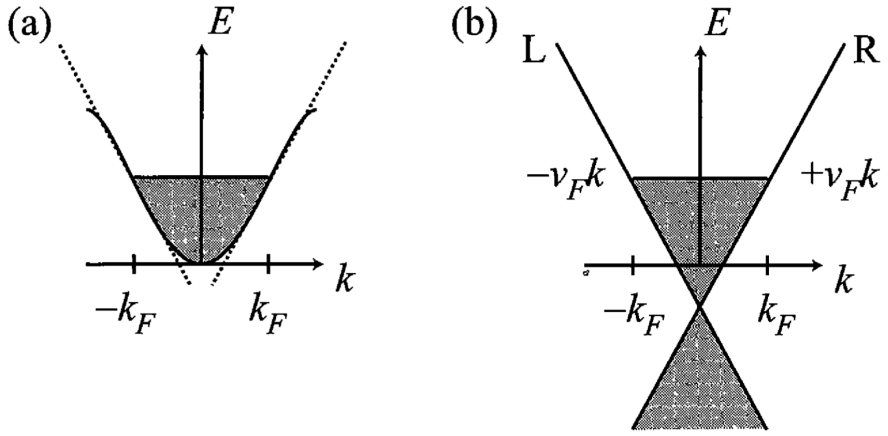

Figure 1.3: **From free to Dirac fermions** The original model of free fermions (a) is replaced by a model of Dirac fermions with a linear spectrum (b). This amounts to introduce two species of fermions (right(R) and left(L) moving fermions). The spectrum is now extended to all values of k, introducing an infinite number of negative energy states but describing low-energy physics properly. (Extracted from [46])

In this Hamiltonian, we introduce two species of fermions. ψ_R describes right-moving low energy excitation around $+k_F$ with a positive velocity $= v_F$ while ψ_L describes left-moving ones around $-k_F$ and with a negative velocity $-v_F$ (see Fig. 1.3). Such a Hamiltonian can alternatively be reformulated as a free, massless Dirac Hamiltonian

$$\tilde{\mathcal{H}} = -\frac{i\hbar v_F}{2}\int_{-\infty}^{+\infty} \mathrm{d}x\ \Psi^\dagger \gamma^0\gamma^1 \overset{\leftrightarrow}{\partial}_x \Psi, \tag{1.54}$$

where the Fermi velocity v_F replaces the speed of light c, the bispinor Ψ, stands for $\Psi \equiv \begin{pmatrix}\psi_R\\ \psi_L\end{pmatrix}$, while γ^0 and γ^1 are 2×2 matrices defined by

$$\gamma^0 = \sigma^x\,, \quad \gamma^1 = i\sigma^y\,. \tag{1.55}$$

In the absence of electron-electron interactions, generic 1+1 dimensional systems can be formally described by such a 1+1 dimensional Dirac Hamiltonian. The procedure can be understood as follows. After computing the energy spectrum of this model, one fills all energy states such as $\varepsilon < \mu$. Close to the crossing points $\varepsilon = \mu$ denoted k_n, one can linearize the energy spectrum as $\varepsilon(k_n + q) \approx \hbar v_n\, q$ for $|q| < \Lambda_n$ with v_n the corresponding Fermi velocity, and Λ_n a momentum cutoff. The large length (small wavelength) physics of the model is therefore captured by the generalized Dirac Hamiltonian

$$\tilde{\mathcal{H}} = -\sum_n \int_{-\infty}^{+\infty} \mathrm{d}x\ \frac{i\hbar v_n}{2}\psi_n^\dagger \overset{\leftrightarrow}{\partial}_x \psi_n\,, \tag{1.56}$$

where the field ψ_n describes the low energy excitations around $k = k_n$.

... to Luttinger liquids

However, free electrons are only an ideal limit in condensed matter, and one needs to consider electron-electron interactions. While in higher dimensions, it is possible to treat interaction perturbatively in a Fermi liquid approach introducing a notion of quasiparticle, in 1+1 dimensional systems, individual electrons cannot move without pushing surrounding electrons: effects

of interaction are exacerbated and only collective excitations exist [46]. The failure of perturbation theory and the emergence of these collective excitations are captured by the concepts of bosonization and Luttinger liquid theory [47–49], whose action is

$$S_{LL} = \frac{\hbar}{2\pi K} \int \mathrm{d}x\mathrm{d}t \, \left[\frac{1}{u} \left(\partial_t \phi\right)^2 - u \left(\partial_x \phi\right)^2 \right] , \tag{1.57}$$

where $\phi(x)$ is related to the density of particles $\rho(x)$ through $\rho(x) = -\frac{1}{\pi}\nabla\phi(x)$, while the parameters u and K depend on the interactions. In the absence of interactions, they equal $u = v_F$ and $K = 1$.

1.2.2 Dirac fermions: from flat to curved spacetimes

In order to modify the previous models to recover analog curved spacetimes, it is essential to remind ourselves how to generalize a Dirac Hamiltonian (1.54) to curved spacetimes. In this section, we will generalize the notion of Dirac Hamiltonians to curved spacetimes, as we have done for scalar in section 1.1.2. Then, we introduce the notion of momentum-energy tensor for Dirac fields, which will be useful throughout the rest of this thesis.

Minimal coupling for Dirac fermions: From flat to curved spacetimes

In flat spacetime, the dynamic of a spinor field is captured by the Dirac action [50], given in $1+1$ dimension by

$$\mathcal{S}_D = \frac{i\hbar v_F}{2} \int \mathrm{d}t \, \mathrm{d}x \, \left(\bar{\psi} \gamma^\mu \overset{\leftrightarrow}{\partial}_\mu \psi \right) , \tag{1.58}$$

and the corresponding equations of motion

$$\begin{cases} \gamma^\mu \overset{\rightarrow}{\partial}_\mu \psi = 0 \\ \bar{\psi} \overset{\leftarrow}{\partial}_\mu \gamma^\mu = 0 \end{cases} \tag{1.59}$$

with γ^μ the so-called gamma matrices verifying the flat spacetime Clifford algebra

$$\{\gamma^\mu \, , \gamma^\nu \} = \gamma^\mu \gamma^\nu + \gamma^\nu \gamma^\mu = 2\eta^{\mu\nu} \mathbb{1} \tag{1.60}$$

where $\eta^{\mu\nu} = \mathrm{diag}(1, -1)$. In 1+1 dimensions, a solution to these equations is provided by the Pauli matrices

$$\gamma^0 = \sigma^x \, , \quad \gamma^1 = i\sigma^y \, . \tag{1.61}$$

Generalizing the action (1.58) to a curved spacetime with a metric $g_{\mu\nu}$ is more subtle than in the case of scalar fields for two reasons: first, in curved spacetime, the Clifford algebra has to be modified following

$$\{\gamma^\mu \, , \gamma^\nu \} = \gamma^\mu \gamma^\nu + \gamma^\nu \gamma^\mu = 2g^{\mu\nu} \mathbb{1} \, . \tag{1.62}$$

Second, in special relativity, the action has to be invariant under the local Lorentz transform. Therefore, as one generalizes the covariant derivatives in the presence of an electromagnetic field to get a theory invariant under local U(1) transformations, one needs to generalize the partial derivatives ∂_μ such that $\partial_\mu \psi$ behaves as a spinor under local Lorentz transformation.

To solve these difficulties, one introduces a "square root" e^a_μ of the metric tensor called a tetrad, and its inverse, the cotetrad e^μ_a such as

$$\begin{cases} g_{\mu\nu} = e^a_\mu \eta_{ab} e^b_\nu \, , \\ e^\mu_a e^b_\mu = \delta^b_a \, , \\ e^\mu_a e^a_\nu = \delta^\mu_\nu \, . \end{cases} \tag{1.63}$$

The minimal coupling procedure can then be extended to fermions as follows:

- Generalizing the measure of integration covariantly:

$$\mathrm{d}^{D+1}\boldsymbol{x} \equiv c\,\mathrm{d}t\,\mathrm{d}^D\vec{x} \to \mathrm{d}^{D+1}\boldsymbol{x}\sqrt{|\det(g_{\mu\nu})|} \equiv c\,\mathrm{d}t\,\mathrm{d}^D\vec{x}\sqrt{|\det(g_{\mu\nu})|}\,, \tag{1.64}$$

- Generalizing the gamma matrices to curved spacetimes:

$$\gamma^\mu = e^\mu_a\gamma^a\,, \tag{1.65}$$

with γ^a the flat spacetime gamma matrices defined above,

- Replacing the partial derivatives by spinor derivative $\partial_\mu \to D_\mu = \partial_\mu + \omega_{ab\mu}\sigma^{ab}$ with $\sigma^{ab} = -\frac{i}{4}\left[\gamma^a\,,\gamma^b\right]$ the generator of Lorentz transformation and $\omega_{ab\mu}$ the spinor connection

$$\omega^a{}_{b\mu} = e^a_\nu\,\nabla_\mu e^\nu_b = e^a_\nu\left(\partial_\mu e^\nu_b + \begin{Bmatrix}\nu\\ \rho\mu\end{Bmatrix} e^\rho_b\right) \tag{1.66}$$

defined from the Levi-Civita affine connection $\begin{Bmatrix}\nu\\ \rho\mu\end{Bmatrix}$.

Following this minimal coupling procedure, the Dirac action (1.58) is generalized to curved space as

$$\mathcal{S}_D = \frac{i\hbar v_F}{2}\int \mathrm{d}x\,\mathrm{d}t\;\det\left(e^b_\nu\right)e^\mu_a\left(\bar\psi\gamma^a\overset{\leftrightarrow}{D}_\mu\psi\right)\,. \tag{1.67}$$

In 1+1 dimensions, this action can be simplified to

$$\mathcal{S}_D = \frac{i\hbar v_F}{2}\int \mathrm{d}x\,\mathrm{d}t\;\det\left(e^b_\nu\right)e^\mu_a\left(\bar\psi\gamma^a\overset{\leftrightarrow}{\partial}_\mu\psi\right)\,, \tag{1.68}$$

and it may seem pointless to introduce the notion of spinor derivatives. However, integrating by parts (1.68) leads to an equivalent action (up to a boundary term)

$$\tilde{\mathcal{S}}_D = i\hbar v_F\int \mathrm{d}x\,\mathrm{d}t\;\det\left(e^b_\nu\right)\bar\psi e^\mu_a\gamma^a D_\mu\psi\,, \tag{1.69}$$

which restores the dependence on the spinor connection.
From this action, we are now able to generalize the Dirac equation of motion (1.59) as

$$\begin{cases}\gamma^a e^\mu_a\,\vec{D}_\mu\psi = 0 \Leftrightarrow \gamma^a\left(e^\mu_a\vec{\partial}_\mu + \frac{1}{2\det(e)}\partial_\mu\left[\det(e)\,e^\mu_a\right]\right)\psi = 0\,,\\ \bar\psi\overleftarrow{D}_\mu\,e^\mu_a\,\gamma^a = 0 \Leftrightarrow \bar\psi\left(e^\mu_a\overleftarrow{\partial}_\mu + \frac{1}{2\det(e)}\partial_\mu\left[\det(e)\,e^\mu_a\right]\right)\gamma^a\,.\end{cases} \tag{1.70}$$

Hamiltonian and momentum-energy tensor

In the previous paragraph, we deduced the equations of motion of fermions in curved spacetime. However, contrary to the hydrodynamic approach in which we recognized a curved spacetime Klein-Gordon equation of motion (1.8), in section 1.2.1 the model is provided by a Hamiltonian instead of the equation of motion. Therefore, it is worth introducing the notion of Hamiltonian and momentum-energy tensor in the context of fermions in the curved spacetime.

By definition, the momentum conjugated to the fields ψ and $\psi^\dagger$ are

$$\pi^\dagger = \frac{\delta S}{\delta\partial_0\psi} = \frac{i\hbar v_F}{2}\det(e)\psi^\dagger\gamma^0\gamma^a e^0_a\,, \tag{1.71}$$

$$\pi = \frac{\delta S}{\delta\partial_0\psi^\dagger} = -\frac{i\hbar v_F}{2}\det(e)\gamma^0\gamma^a e^0_a\psi\,. \tag{1.72}$$

The Hamiltonian density is defined as the Legendre transform of the Lagrangian density

$$\begin{aligned}\mathcal{H}_D(x) &= \pi^\dagger \partial_0 \psi + \partial_0 \psi^\dagger \pi - \det(e)\mathcal{L}_g \\ &= -\det(e)\frac{i\hbar v_F}{2} e_a^x \left(\bar{\psi}\gamma^a \overset{\leftrightarrow}{\partial}_x \psi\right) ,\end{aligned} \tag{1.73a}$$

which can now be compared to the flat spacetime version:

$$\mathcal{H}_D(x) = -\frac{i\hbar v_F}{2}\left(\bar{\psi}\gamma^x \overset{\leftrightarrow}{\partial}_x \psi\right) . \tag{1.73b}$$

In curved spacetime, both the Hamiltonian and the momentum can be cast into the components of a single object called the momentum-energy tensor defined by

$$\mathcal{T}_{\mu\nu} = \frac{1}{2\det(e)}\left(\frac{\delta \mathcal{S}_D}{\delta e_a^\mu} e_{\nu a} + \mu \leftrightarrow \nu\right) , \tag{1.74}$$

or in other words, using the definition of Dirac's action in a curved spacetime (1.67), we obtain

$$\mathcal{T}_{\mu\nu} = \frac{i\hbar v_F}{4}\left[e_{\nu a}(x)\left(\bar{\psi}\gamma^a \overset{\leftrightarrow}{\partial}_\mu \psi\right) + \mu \leftrightarrow \nu\right] - g_{\mu\nu}\left[\frac{i\hbar v_F}{2} e_b^\rho(x)\left(\bar{\psi}\gamma^b \overset{\leftrightarrow}{\partial}_\rho \psi\right)\right] . \tag{1.75}$$

Alternatively, a non-symmetric version of this tensor is obtained by varying the action with respect to the tetrad while keeping the spinor connection fixed as

$$\begin{aligned}\mathcal{T}_{\ a}^{\mu} &= -\frac{1}{\det(e)}\frac{\delta \mathcal{S}_D}{\delta e_\mu^a} \\ &= \frac{i\hbar v_F}{2} e_a^\rho e_b^\mu \left[\bar{\psi}\gamma^b \overset{\leftrightarrow}{\partial}_\rho \psi\right] - e_a^\mu \left[\frac{i\hbar v_F}{2} e_b^\rho(x)\left(\bar{\psi}\gamma^b \overset{\leftrightarrow}{\partial}_\rho \psi\right)\right] .\end{aligned} \tag{1.76}$$

When working in curved space, it is often helpful to express the non-symmetric-version of the momentum-energy tensor with only curved spacetime indices corresponding to

$$\tilde{\mathcal{T}}_{\ \nu}^{\mu} = \mathcal{T}_{\ a}^{\mu} e_\nu^a , \tag{1.77}$$

from which we deduce the expressions of the densities and currents

$$\begin{cases} \varepsilon = \tilde{\mathcal{T}}_{\ 0}^{0} & \text{(Energy density)} \\ p = \tilde{\mathcal{T}}_{\ x}^{x} & \text{(Pressure)} \\ J_\varepsilon = v_F \det(e)\tilde{\mathcal{T}}^{x0} & \text{(Density of energy current)} . \\ \Pi = \frac{1}{v_F}\det(e)\tilde{\mathcal{T}}^{0x} & \text{(Momentum density)} \end{cases} \tag{1.78}$$

Note that the symmetrized version (1.74) can be recovered as

$$\mathcal{T}_{\mu\nu} = \tilde{\mathcal{T}}_{\mu\nu} + \tilde{\mathcal{T}}_{\nu\mu} . \tag{1.79}$$

1.2.3 Inhomogeneous 1+1 dimensional systems as curved spacetime Dirac Hamiltonians

Equipped with both the flat spacetime as well as the curved spacetime Dirac formalism, we are now ready to tackle the main question: Is it possible, similarly to the hydrodynamic case, to

relate the physics of inhomogeneous 1+1 dimensional systems to the one of curved spacetime field theory?

In this section, we will therefore introduce several basic examples of experimentally relevant inhomogeneous systems, studying to what extent these can be described as a field theory in curved spacetimes. We will afterward generalize these ideas to other inhomogeneous systems considered in other condensed matter contexts.

1+1 dimensional systems in inhomogeneous potentials

As a base example, and following the discussions of [51] and [52], let us consider a free fermionic system in an inhomogeneous external potential described by the Hamiltonian

$$\mathcal{H} = \int_{-\infty}^{+\infty} \mathrm{d}x \; c^\dagger(x) \left[-\frac{\hbar^2}{2m}\partial_x^2 - \mu + V_{ext}(x) \right] c(x) \,. \tag{1.80}$$

Such a Hamiltonian arises naturally as the continuum limit of an XX spin chain in an inhomogeneous magnetic field whose Hamiltonian is given by

$$\hat{\mathcal{H}} = -\frac{J}{2} \sum_n \left(\mathcal{S}_n^+ \mathcal{S}_{n+1}^- + \mathcal{S}_{n+1}^+ \mathcal{S}_n^- \right) - \sum_n h_n \, S_n^z \,. \tag{1.81}$$

Indeed, upon Jordan-Wigner transformation [53–55], this hamiltonian reduces to a lattice fermion model given by

$$\hat{\mathcal{H}} = -\frac{J}{2} \sum_n \left(c_{n-1}^\dagger c_n + c_n^\dagger c_{n-1} \right) - \sum_n h_n \, c_n^\dagger c_n \,. \tag{1.82}$$

From the spectrum of this Hamiltonian in the absence of magnetic field, $E = -J.\cos(k.a) - h$ with a the lattice spacing, we deduce that, for small wavelengths $k.a \ll 1$, the two models described, by Hamiltonians (1.81), and (1.80), are equivalent provided $m = \hbar^2/(J\,a^2)$ and $\mu - V_{ext}(n.a) = h_n$.

For simplicity, let us assume the potential $V(x)$ to be smaller than the chemical potential μ on a single interval, and let us define a local chemical potential on this interval defined by $\mu^{(\mathrm{loc})}(x) = \mu - V(x)$. By analogy with the system without any external potential studied in section 1.2.1, one would like to write an explicit and equivalent Dirac Hamiltonian to describe the low-energy physics properties of this system.
The corresponding approximation has been known for a long time in the literature as the so-called local density (or Thomas-Fermi) approximation. One obtains the ground state of such a system by filling all the negative energy eigenstates while letting all the positive ones empty. Several typical length scales control the dynamics of this problem:

- The size of the system L (interval on which $\mu > V(x)$),
- The average distance between two neighboring particles l_{cell} approximated as the inverse of the local density $n(x) = \langle c^\dagger(x) c(x) \rangle$,
- The typical length associated with the variation of the local potential $l_V = \frac{\mu^{(\mathrm{loc})}}{\partial_x \mu^{(\mathrm{loc})}}$,

If $l_{cell} \ll l_V$, an approximation valid in the thermodynamic limit, we can locally approximate the chemical potential as constant over a length l such that $l_{cell} < l < l_V$. Since we have a large

number of particles, we can interpret in these regions $\mu^{(\mathrm{loc})}$ as the local chemical potential and define a notion of local Fermi momentum $k_F^{(\mathrm{loc})}(x) = \frac{1}{\hbar}\sqrt{2m\,\mu^{(\mathrm{loc})}(x)}$. In this approximation, the Fermi gas behaves locally, in the low energy limit, as a free Fermi gas with a local Fermi momentum $k_F^{(\mathrm{loc})}(x)$ and hence a local Fermi velocity $v_F^{(\mathrm{loc})}(x) = \frac{\hbar k_F^{(\mathrm{loc})}}{m} = \sqrt{\frac{2(\mu - V(x))}{m}}$. The low-energy Hamiltonian reads

$$\tilde{\mathcal{H}}_V = -\frac{i\hbar}{2}\int_{-\infty}^{+\infty} \mathrm{d}x\, v_F^{(\mathrm{loc})}(x)\; \Psi^\dagger \gamma^0\gamma^1 \overset{\leftrightarrow}{\partial}_x \Psi\,, \tag{1.83}$$

which is nothing but a Dirac Hamiltonian in a curved spacetime (1.73a) whose line element is given by

$$\mathrm{d}s^2 = \left(v_F^{(\mathrm{loc})}(x)\,\mathrm{d}t\right)^2 - \mathrm{d}x^2\,. \tag{1.84}$$

We have shown in this section that free fermions in an inhomogeneous potential can be interpreted in a low-energy picture as massless Dirac fermions in curved spacetime. This statement, valid for free fermions, can be extended to several other types of excitations. It is possible, for example, to generalize it to interacting models such as inhomogeneous Luttinger liquids [51], or even to Tonks-Girardeau gases [52, 56].

While we used a local density approximation to identify these models with a specific fermionic model in curved spacetime, other strategies are available such as starting from the bosonized model, proving that, in a low energy limit, the height field defined by $\rho(x) = \frac{1}{2\pi}\partial_x h(x)$ verify a bosonic curved spacetime Hamiltonian [52, 56].

Another route towards curved spacetimes: inhomogeneous couplings

Starting from the homogeneous version of the lattice Hamiltonian (1.81,1.82), another logical and experimentally relevant strategy to induce inhomogeneities consists in considering inhomogeneous hoppings or, in other words, a position-dependent hopping J_n, in the presence of a constant magnetic field h along the z-axis. This construction leads to a Hamiltonian of the form

$$\hat{\mathcal{H}} = -\frac{1}{2}\sum_n J_n\left(\mathcal{S}_n^+\mathcal{S}_{n+1}^- + \mathcal{S}_{n+1}^+\mathcal{S}_n^-\right) - \sum_n h_n\, S_n^z\,., \tag{1.85}$$

where we introduce for simplicity the function $f(x)$ such as $J_n = J.\,f(n.a)$ with a the lattice spacing.

As we have seen previously, the low energy physics of such a Hamiltonian is obtained by linearizing the spectrum around the momenta $\pm k_F$. In this case, under the hypothesis that the perturbations are smooth enough, $k_F\frac{\partial_x f}{f} \ll 1$, as in the previous example, one can use a coarse-grained description of the system with local coupling $J(x) = J.\,f(x)$ that we can treat following the procedure developed in the homogeneous case. The total Hamiltonian can then be written in a low energy limit as

$$\tilde{\mathcal{H}}_V = -\frac{i\hbar}{2}\int_{-\infty}^{+\infty} \mathrm{d}x\, v_F^{(\mathrm{loc})}(x)\; \Psi^\dagger \gamma^0\gamma^1 \overset{\leftrightarrow}{\partial}_x \Psi\,, \tag{1.86}$$

where $v_F^{(\mathrm{loc})}(x) = v_F\sqrt{f(x)}$.

A third route: modulating the Hamiltonian density

Starting from a homogeneous lattice Dirac Hamiltonian

$$\hat{\mathcal{H}} = \sum_n \hat{h}_n \,, \tag{1.87}$$

with h_n local Hamiltonians (acting only on a finite number of sites and links), another strategy to realize an analogous curved spacetime Hamiltonian consists of modulating the whole Hamiltonian [52] such that

$$\hat{\mathcal{H}} = \sum_n f(n.a)\hat{h}_n \,. \tag{1.88}$$

This idea is actually motivated by the observation that, for a tetrad field of the form

$$e^a_\mu = \begin{pmatrix} f(x) & 0 \\ 0 & 1 \end{pmatrix} , \tag{1.89}$$

the curved spacetime Hamiltonian density $\hat{h}_c$ of a Dirac field (1.73a) is related to its flat spacetime couterpart (1.73b) $\hat{h}$ through

$$\hat{h}_c(x) = f(x)\,\hat{h}(x) \,. \tag{1.90}$$

Applying such a strategy to the XX spin chain (1.81) can be understood as a combination of both previous strategies since it implies a modulation of both the magnetic field $h \to f(x).\,h$ and the couplings $J \to f(x).\,J$.

Following the strategy discussed in the previous paragraphs, if the dynamic of the low-energy excitations in the original Hamiltonian is captured by a relativistic equation with a characteristic velocity v_F, obtained by linearizing the spectrum on a wavelength window of size δk, under the hypothesis that the modulation is smooth enough $\delta k \frac{\partial f}{f} \ll 1$, the same relativistic equation captures the dynamics of the low-energy excitations of the modulated Hamiltonian but now in curved spacetime with a space varying velocity $v_F^{\text{loc}}(x) = f(x).v_F$.

In the literature, such modulations of the Hamiltonian density and their curved spacetime interpretations were considered for several purposes:

- Initially, people considered the so-called spherical deformation characterized by the modulation function $f(x) = \sin^2\left(\frac{\pi x}{L}\right)$ with L the size of the system for numerical purposes [57–60]. Indeed, they realized that the fast decrease of the function f towards the end of the system reduces the dependence on the edge of the thermodynamic quantities. In particular, it was shown that the many-body ground state of a deformed open-ended system was identical to that of a periodic boundary system without any deformations [59].

- Similarly, the rainbow Hamiltonian, heavily studied for its specific entanglement properties [61–65], can be defined as such a deformed Hamiltonian (1.88) with $h_n = -\frac{J}{2}\left(c^\dagger_{n+1}c_n + c^\dagger_n c_{n+1}\right)$ and a deformation characterized by $f(x) = e^{-hm}$.

Therefore, curved spacetime field theory can describe the low-energy physics of inhomogeneous 1+1 dimensional systems. This claim, exemplified by the case of inhomogeneities induced either by an external potential or by varying the couplings, illustrates once again the importance of curved spacetimes in condensed matter physics, which was, in particular, used

to design Hamiltonians with specific spectra and entanglement properties.

Another possible type of inhomogeneity corresponds to space-dependant interaction strength, corresponding to a Luttinger liquid with an inhomogeneous parameter $K(x)$ following [66]. This, however, goes beyond the scope of this section.

1.3 From thermal transport to curved spacetime: Luttinger's legacy[2]

As we have seen in this chapter, curved spacetimes quantum physics arises naturally as effective theories of low-energy excitations in inhomogeneous systems. However, as we will see in this section, curved spacetimes also appear as a necessary tool when studying linear response theory in the presence of thermal gradients.

A system at equilibrium will respond to an external stimulus, leading to the appearance of local currents. When the strength of the perturbation is increased, the response of the system and the currents scale accordingly. For a weak enough perturbation, the current is proportional to the stimulus with a proportionality coefficient depending solely on the equilibrium property of the system. This is the essence of the linear response. For example, the electric conductivity tensor relates the charge current to an applied electric field $\vec{E}$ as

$$J_i = \sigma_{ij} E_j \,. \tag{1.91}$$

In condensed matter physics, common stimuli that one can apply to a system are an electric field $\vec{E}$ or a gradient of temperature $\vec{\nabla} T$. Linear response theory then predicts a response in the form of a particle and energy current expressed as [9, 15, 67, 68]

$$J_i = L_{ij}^{(1)} E_j + L_{ij}^{(2)} T \vec{\nabla}_j \frac{1}{T} \,, \tag{1.92a}$$

$$J_i^{\varepsilon} = L_{ij}^{(3)} E_j + L_{ij}^{(4)} T \vec{\nabla}_j \frac{1}{T} \,. \tag{1.92b}$$

In order to compute the coefficients $L_{ij}^{(k)}$, the usual strategy is to identify the relation between the response to an external field and the response to internal statistical forces. In the case of the electric field, at equilibrium, the external electric field is compensated by an internal gradient of electrochemical potential V such that $\vec{\nabla} V = -\vec{E}$. This relation, also known as Einstein's relation, allows one to relate the linear response to an electric field to that of a gradient of chemical potential. Linear response to an electric field can therefore be studied by considering the perturbation to the Hamiltonian in $D+1$ dimensions:

$$\delta \mathcal{H} = \int \mathrm{d}^D \vec{r}\, V(\vec{r}) \rho(\vec{r}) \,, \tag{1.93}$$

with $\rho(\vec{r})$ the charge density at position $\vec{r}$ and V the electrochemical potential such that $\vec{\nabla} V = -\vec{E}$.

When focusing on the response to a temperature gradient, a natural question arises: What is the corresponding thermal potential? Or, in other words, what is the relation analogous to the Einstein relation in the case of a thermal gradient, allowing one to compute the corresponding linear response? In 1964, J. Luttinger solved this issue in a seminal paper entitled "Theory of

[2] Yes, yes, the same Joaquin Luttinger

thermal transport coefficients" [9], demonstrating that the appropriate field is a gravitational potential Φ_g such that $\vec{\nabla}\Phi_g = -\frac{\vec{\nabla}T}{T}$. We can reformulate this as the fact that an external gravitational potential is compensated at equilibrium by an inhomogeneous temperature profile. Linear response theory to a temperature gradient can therefore be studied in this system by considering the perturbation

$$\delta\mathcal{H} = \int \mathrm{d}^D\vec{r}\,\Phi_g(\vec{r})h_0(\vec{r})\,, \tag{1.94}$$

with $h_0(\vec{r})$ the local Hamiltonian (energy) density[3] of the unperturbed Hamiltonian defined such that the unperturbed Hamiltonian reads

$$\mathcal{H}_0 = \int \mathrm{d}^D\vec{r}\,h_0(\vec{r}). \tag{1.95}$$

Therefore, the full Hamiltonian reads, at linear order in Φ_g,

$$\mathcal{H} = \mathcal{H}_0 + \delta\mathcal{H} = \int \mathrm{d}^D\vec{r}\,\left(1+\Phi_g(\vec{r})\right)h_0(\vec{r})\,, \tag{1.96}$$

which is nothing but the same Hamiltonian but now in a curved spacetime whose metric is given by $g_{\mu\nu} = \eta_{\mu\nu} + h_{\mu\nu}$, with $h_{\mu\nu}$ the linear perturbation.

Therefore, curved spacetime arises naturally in condensed matter whenever one studies a system with an inhomogeneous temperature profile. According to J. Luttinger, this equivalence between curved spacetime and temperature is so profound that he insisted in a footnote of his article [9] that

> "*In fact, if the gravitational field didn't exist, one could invent one for the purposes of this paper.*"

[3] This comes from the fact that in general relativity, a gravitational potential arises as a linear perturbation of the coefficient g_{00} of the flat metric $\eta_{\mu\nu} \to \eta_{\mu\nu} + 2\delta_{\mu 0}\delta_{\nu 0}\Phi_g$ and naturally couples to the momentum-energy tensor component $\mathcal{T}^{00}$, which is nothing but the Hamiltonian density whose expectation value is equal to the energy density.

Chapter 2

Quantum field theory anomalies in curved spacetimes

Symmetries simplify our understanding of the world. They underly both the classical and the quantum description of physical phenomena. However, surprisingly, a classical symmetry is sometimes lost in the quantization procedure. We will call such symmetry anomalous.

In this section, after introducing the notion of anomaly, we will, through the historical example of the chiral anomaly, see how to compute it and how it can manifest itself in condensed matter experiments. Then, coming back to the main focus of this thesis, quantum physics in curved spacetimes, we will identify anomalous symmetries while studying field theory in curved spacetimes, first in the general situation and then focusing on the specific case of 1+1 dimensional spacetimes.

2.1 Anomalies in quantum field theory

In classical field theory, following Noether's first theorem [69], one can associate a conserved current density to any continuous symmetry of the action. For example, time translation invariance implies energy density conservation. Similarly, space translation implies momentum conservation, and the $\mathbf{U}(1)$ symmetry implies electric current conservation.

If, at the quantum level, this invariance is no longer valid or, equivalently, if the classically conserved current is no longer conserved, the symmetry is then referred to as anomalous. There are different ways of computing anomalies (see, for example [70–76]), depending on the formalism employed, and leading to different interpretation. For example,

- In the **functional integral formalism**, the central object is the partition function of the theory defined as
$$\mathcal{Z}[A_\mu, ...] = \int \mathrm{D}\bar{\Psi}\mathrm{D}\Psi e^{\frac{i}{\hbar}\mathcal{S}\left[\bar{\Psi},\Psi,A_\mu,...\right]}, \tag{2.1}$$
with $\mathcal{S}\left[\bar{\Psi}, \Psi, A_\mu, ...\right]$ the action of the corresponding theory. In this formalism, invariances are captured by the so-called Ward-Identities.
A classical symmetry is related to an invariance of the action $\mathcal{S}$ under a symmetry operation. Assuming that this symmetry holds at the quantum level implies that the integration measure $(\mathrm{D}\bar{\Psi}\mathrm{D}\Psi)$ is also invariant under the same symmetry operations. If not, Ward-identities are violated by a term defined as the anomaly.

- Alternatively, in the **diagrammatic description**, a product of two operators is ill-defined; one, therefore, needs to introduce a proper regularization. There is, however, no guarantee that the regularized Green's function is still invariant under the symmetry; if they are not, there is an anomaly.

The first encounter of theorists with anomalies occurred in 1969, where the chiral anomaly explained the fast decay of the neutral pi-meson into two photons ($\pi^0 \to 2\gamma$) (see section 2.2 for a more detailed introduction). At first, it was thought to be an epiphenomenon. However, with the birth of QCD and string theory, anomalies became a fundamental property of quantum fields.

At this level, two kinds of anomalies need to be distinguished. On the one hand, if the symmetry we are studying corresponds to an external symmetry, for example, associated with a classical background metric or $\mathcal{U}(1)$ electromagnetic fields, anomalies lead to a physical violation of the conservation equations. On the other hand, if the symmetry is global, implying only internal degrees of freedom, anomalies inhibit a quantization of the theory together with the corresponding gauge field. This seems to be problematic. It is, however, quite the contrary. Imposing that anomalies must vanish constrains a quantum field theory. For example, they are essential for the study of string theory [77, 78] or for the standard model for which it provides crucial constraints on the particle content [75, 79–81].

In this thesis, we will mostly focus on symmetries and anomalies when coupling the system to a classical metric field. In the following section, we will come back to the historical example of the chiral anomaly and some of its consequences on transport in relativistic semimetals in condensed matter systems.

2.2 A historical example: chiral anomaly from field theory to condensed matter

The first occurrence of anomalies appeared in particle physics with the study of the decay of the neutral pi-meson into two photons ($\pi^0 \to 2\gamma$). Since the pi-meson π^0 is neutral, it cannot couple directly to any electromagnetic field. The first perturbative study of its decay rate by J. Steinberger in 1949, before the birth of QCD, used a coupling of pion with neutron doublet to obtain a result in perfect agreement with the experiments [82, 83]. However, it was realized by Y. Nambu that the nature of π^0, as a Nambu-Goldstone boson associated with the $\mathcal{SU}(2)_R \times \mathcal{SU}(2)_L$ symmetry, implies a coupling far smaller than first thought by a factor m_π^2/m_N^2 such that the amplitude computed initially was no longer in agreement with the decay (and even equal to 0 in the low-energy limit also known as soft π^0 limit [84]). This apparent issue was later solved in 1969, with the work of S. Adler [85] and J. Bell and R. Jackiw [86], proving that in the presence of an electromagnetic field, the $\mathcal{SU}(2)_R \times \mathcal{SU}(2)_L$ symmetry is violated by a mass independent term: the chiral anomaly.

In this section, we will review this historical example as an archetypical example of anomaly, studying two derivations of the anomalous term before turning to the emergence of this anomaly in condensed matter and some of its experimental consequences.

2.2.1 The historical diagrammatic derivation

The classical action and its symmetries

Even though the original calculations assumed 3+1 dimensions, for simplicity and following [76], let us focus on a 1+1 dimensional analog in this section. In a 1+1 dimensional flat spacetime, the Clifford algebra

$$\{\gamma^\mu, \gamma^\nu\} = \gamma^\mu\gamma^\nu + \gamma^\nu\gamma^\mu = 2\eta^{\mu\nu}\mathbb{1}_2, \quad \mu,\nu = 0,1\,, \tag{2.2}$$

with $\eta^{\mu\nu} = \mathrm{diag}(1,-1)$, is satisfied by the Pauli matrices

$$\gamma^0 = \sigma^x\,, \quad \gamma^1 = i\sigma^y\,. \tag{2.3}$$

Additionally, one defines a third gamma matrix, often referred to as γ^5, as

$$\gamma^5 = -\gamma^0\gamma^1 = \sigma^z\,, \quad \left\{\gamma^5, \gamma^\nu\right\} = 0\,, \mu = \{0,1\}\,. \tag{2.4}$$

If ψ is the Dirac spinor, with two components in 1+1 dimension, the free fermion action is given by

$$\mathcal{S} = \int \mathrm{d}x\mathrm{d}t\, \mathcal{L}_0 = i\hbar c \int \mathrm{d}x\mathrm{d}t\, \bar\psi\gamma^\mu\partial_\mu\psi\,, \tag{2.5}$$

with $\bar\psi = \psi^\dagger\gamma^0$.
This action (2.5) has two global symmetries:

- A $\mathcal{U}(1)$ symmetry associated with the transformations

$$\psi \to \psi' = e^{i\alpha}\psi\,, \quad \psi^\dagger \to (\psi')^\dagger = e^{-i\alpha}\psi^\dagger\,, \tag{2.6}$$

- A chiral or axial symmetry associated with the transformations

$$\psi \to \psi' = e^{i\alpha\gamma^5}\psi\,, \quad \psi^\dagger \to (\psi')^\dagger = \psi^\dagger e^{-i\alpha\gamma^5}\,. \tag{2.7}$$

When applying Noether's first theorem, these symmetries are respectively associated with the conservation of

- The charge or vector current

$$j^\mu_V = ec\bar\psi\gamma^\mu\psi\,, \tag{2.8}$$

- The axial current [1]

$$j^\mu_A = ec\bar\psi\gamma^\mu\gamma^5\psi\,. \tag{2.9}$$

Here, the conservation of these currents is expressed as

$$\partial_\mu j^\mu_\alpha = 0\,, \quad \alpha = V, A\,, \tag{2.10}$$

which can be verified using the equation of motions issued from (2.5):

$$\begin{cases} \gamma^\mu\overrightarrow{\partial}_\mu\psi = 0\,, \\ \bar\psi\gamma^\mu\overleftarrow{\partial}_\mu = 0\,. \end{cases} \tag{2.11}$$

Note that in 1+1 dimensions, since $\gamma^\mu\gamma^5 = -\epsilon^{\mu\nu}\gamma_\nu$, with $\epsilon^{01} = 1$, we can write

$$j^\mu_A = -\epsilon^{\mu\nu}\left(j_V\right)_\nu\,, \tag{2.12}$$

which will be useful in the following.

[1] Since the definition of the current involves a matrix γ^5 it is sometimes also denoted j^μ_5

Diagrammatic computation of the anomaly

When coupling the system to an external electromagnetic field with a minimal coupling Lagrangian density of the form

$$\mathcal{L}_{int} = j_V^\mu A_\mu \,, \tag{2.13}$$

both the $\mathcal{U}(1)$ (2.6) and the axial (2.7) symmetries are still present, and we would expect both currents to remain conserved. Our objective is, to compute $\langle j_V^\mu \rangle$ perturbatively in powers of A_μ, to deduce $\langle j_A^\mu \rangle$ using the relation (2.12).

In perturbation theory, the first non-zero contribution comes from the linear correction, which, given the form of the interaction (2.13), can be expressed as

$$\langle \delta j_V^\mu(x,t) \rangle = \frac{i}{\hbar} \int \mathrm{d}y \mathrm{d}t' \langle j_V^\mu(x,t) j_V^\nu(y,t') \rangle A_\nu(y) \,. \tag{2.14}$$

After a Fourier transform, this relation can be rewritten as

$$\langle \delta j_V^\mu(p) \rangle = \frac{i}{\hbar c} \Pi^{\mu\nu}(p) A_\nu(k) \delta^2(p+k) \,, \tag{2.15}$$

where $\Pi^{\mu\nu}$ is a linearly divergent integral given by

$$i\Pi^{\mu\nu}(p) = (-iec)^2 \int \frac{\mathrm{d}^2 q}{(2\pi)^2} \mathrm{tr} \left(\gamma^\mu \frac{i}{\not{p}} \gamma^\nu \frac{i}{\not{p} - \not{q}} \right) \,, \tag{2.16}$$

often represented as the Feynmann diagram shown in Fig. 2.1(a). After a proper regularization

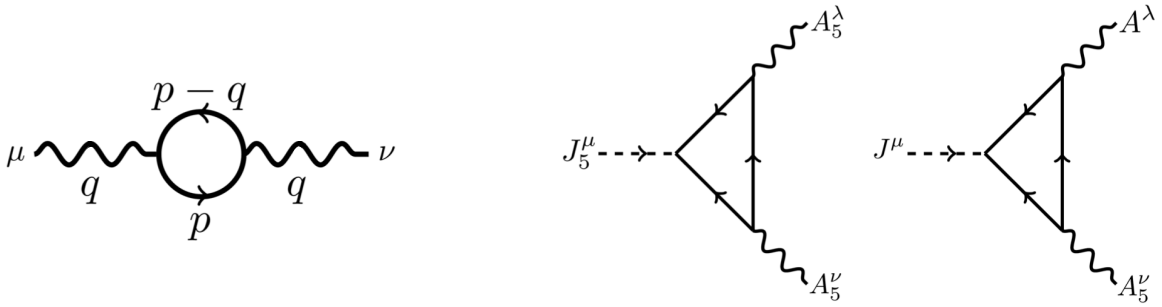

(a) Feynman diagram associated to the 1+1 dimensional chiral anomaly, corresponding to the integral (2.16) (extracted from [71]).

(b) Example of diagrams appearing in the computation of the 3+1 dimensional chiral anomaly (extracted from [71]).

Figure 2.1: **One loop Feynmann diagram involved in the computation of the chiral anomaly in dimensions 1+1 and 3+1**

of the linear divergence, we have

$$\Pi^{\mu\nu}(p) = \left(s\, \eta^{\mu\nu} p^2 - p^\mu p^\nu \right) \frac{1}{p^2} \frac{e^2 c^2}{\pi} \,, \tag{2.17}$$

with s a real number depending on the regularization procedure. This implies that the quantum regularized conservation equation for j_α^μ reads

$$\begin{cases} \partial_\mu j_V^\mu = (1-s) \frac{e^2 c}{\pi \hbar} \partial_\nu A^\nu \,, \\ \partial_\mu j_A^\mu = s \frac{e^2 c}{\pi \hbar} \epsilon^{\nu\rho} \partial_\nu A_\rho = s\, \frac{e^2 c}{2\pi\hbar} \epsilon^{\mu\nu} F_{\mu\nu} \,. \end{cases} \tag{2.18}$$

Since j_V^μ is a physical quantity related to the electric charge, we impose that it is conserved. Therefore, the only physical regularisation corresponds to $s = 1$, implying at the 1-loop order a chiral anomaly of the form

$$\partial_\mu j_A^\mu = \frac{e^2 c}{2\pi\hbar}\epsilon^{\mu\nu}F_{\mu\nu}\,. \tag{2.19}$$

Several remarks should be made at this point. First, the anomaly at 1-loop order is identical to the result obtained by summing higher perturbative orders. This surprising outcome is related to the fact, proven by S. Adler and W. Bardeen in 1969 [87] that the chiral anomaly is, in fact, 1-loop exact, or in other words, receives no correction from higher loop diagrams. The strategy used above can be generalized to any even dimension, where in $2n$ dimensions, the Feynman diagrams one needs to regularize are n+1-gons diagrams. For example, Fig. 2.1(b) shows two examples of the triangle (3-gons) diagrams used to compute the chiral anomaly in dimension 3+1. Finally, we realize that even though in the above arguments the anomalous current is the axial one, equations (2.18) only prove that the conservation of both currents is simultaneously impossible. The choice of the one we impose to conserve is motivated by physical arguments, a scenario quite recurrent in the study of anomalies.

2.2.2 Anomalies, non-conserved currents, and effective actions

In the previous section, we addressed the notion of chiral anomalies as an impossibility to regularize a theory after quantization. Here, we address it from an alternative point of view. Using the functional integral formalism, we will relate the chiral anomaly to a non-invariance of the measure of integration under the symmetry transformation.

In these calculations, it is convenient to work in a Euclidean formalism. Let us start with a reminder concerning the notion of Euclidean coordinates. These coordinates are defined by the correspondence

$$x^0 = c\,t \to -ix^4 = -ic\,\tau \tag{2.20}$$

where τ is considered as a real number. At the same time, the gamma matrix γ^0 is modified according to

$$\gamma^0 = -i\gamma^4\,. \tag{2.21}$$

The general contravariant vector V^μ is also replaced by $V^0 \to -iV^4$, and similarly $A_0 \to iA_4$, such that the contraction $v^\mu A_\mu$ stays unchanged in Euclidean theory. The metric however changes to $g^E_{\mu\nu} = -\delta_{\mu\nu}$.

Following these definitions, the Dirac operator in Euclidean theory is given by

$$\not{D}_E = \gamma^\mu\left(\partial_\mu - \frac{ie}{\hbar}A_\mu\right) \equiv \gamma^4\left(\partial_4 - \frac{ie}{\hbar}A_4\right) + \gamma^1\left(\partial_1 - \frac{ie}{\hbar}A_1\right)\,. \tag{2.22}$$

The partition function of the theory in the presence of an external electromagnetic field is now, in Euclidean signature, given by

$$\mathcal{Z}\left[A_\mu\right] = \int \mathrm{D}\bar{\psi}\mathrm{D}\psi\, e^{\frac{1}{\hbar}\mathcal{S}_E\left[\bar{\psi},\psi,A_\mu\right]}\,, \tag{2.23}$$

where the measure $\mathrm{D}\bar{\psi}\mathrm{D}\psi$ indicates an integration over all fields satisfying the proper boundary conditions while

$$\mathcal{S}_E\left[\bar{\psi},\psi,A_\mu\right] = i\hbar c\int \mathrm{d}x\mathrm{d}\tau\,\bar{\psi}\not{D}_E\psi\,. \tag{2.24}$$

Let us now reparametrize this action by introducing an infinitesimal chiral rotation of the spinors

$$\psi' = e^{ie\gamma^5\alpha}\psi\,,\quad \bar{\psi}' = \bar{\psi}e^{ie\gamma^5\alpha}\,. \tag{2.25}$$

Since this is a simple redefinition of the field, one can write

$$\begin{aligned}\mathcal{Z}\left[A_\mu\right] &= \int \mathrm{D}\bar{\psi}'\mathrm{D}\psi'\, e^{\frac{1}{\hbar}\mathcal{S}_E\left[\bar{\psi}',\psi',A_\mu\right]} \\ &= \int \mathrm{D}\bar{\psi}'\mathrm{D}\psi'\, e^{ic\int \mathrm{d}x\mathrm{d}\tau\, \bar{\psi}\gamma^\mu\left[\partial_\mu - \frac{ie}{\hbar}A_\mu + ie\,\partial_\mu\alpha\,\gamma^5\right]\psi} \\ &= \int \mathrm{D}\bar{\psi}'\mathrm{D}\psi'\, e^{\frac{1}{\hbar}\mathcal{S}_E\left[\bar{\psi},\psi,A_\mu\right] + \int \mathrm{d}x\mathrm{d}\tau\,\alpha\,\partial_\mu j_A^\mu}\,.\end{aligned} \tag{2.26}$$

Therefore, if one assumes that the measure of integration is invariant under the chiral rotation

$$\frac{\delta}{\delta\alpha(x)}\mathrm{D}\bar{\psi}'\mathrm{D}\psi' = 0\,, \tag{2.27}$$

then taking a functional derivative of (2.26) with respect to $\alpha(x)$, based on the definition of the average of an operator

$$\langle\mathcal{O}(x)\rangle = \frac{1}{\mathcal{Z}\left[A_\mu\right]}\int \mathrm{D}\bar{\psi}'\mathrm{D}\psi'\,\mathcal{O}(x)e^{\frac{1}{\hbar}\mathcal{S}_E\left[\bar{\psi}',\psi',A_\mu\right]}\,, \tag{2.28}$$

we recover the quantum version of the classical conservation equations (2.10)

$$\langle\partial_\mu j_A^\mu\rangle = 0\,. \tag{2.29}$$

However, additional care is required when looking at the measure of integration. As we will see in the following, the anomaly, in fact, hides in the fact that the measure of integration is not invariant under such a transformation. To see this, let us expand the spinors $\bar{\psi}$ and ψ in term of an orthonormal eigenbasis of the Dirac operator $\not{D}_E$ spanned by the spinors $\bar{\phi}_n$ and ϕ_m such that

$$\not{D}_E\,\phi_n = \lambda_n\phi_n\,, \tag{2.30}$$

and

$$\begin{cases}\bar{\psi} = \sum_n \bar{b}_n\bar{\phi}_n\,, \\ \psi = \sum_n a_n\phi_n\,,\end{cases} \tag{2.31}$$

with a_n and b_n being Grassman-value numbers.
The measure of integration can then be defined as

$$\mathrm{D}\bar{\psi}\mathrm{D}\psi = \prod_n \mathrm{d}a_n\mathrm{d}\bar{b}_n\,. \tag{2.32}$$

Let us now consider the effects of the chiral rotation $\psi \to \psi'$ on these Grassman variables, using the orthonormal properties of the eigenspinor basis. At first order in α, we get

$$\begin{aligned}a'_m &= \int \mathrm{d}^2x\,\bar{\phi}_m\left(1 + ie\alpha(x)\gamma^5\right)\sum_n a_n\phi_n \\ &= \delta_{mn} + \sum_n C_{mn}a_n\,,\end{aligned} \tag{2.33}$$

with

$$C_{mn} = ie\int \mathrm{d}^2x\,\alpha\bar{\phi}_m\gamma^5\phi_n\,. \tag{2.34}$$

The change of the measure of integration (2.32) is then given by the Jacobian of this transformation

$$\mathrm{D}\bar{\psi}'\mathrm{D}\psi' = \det\left(1+C\right)^{-2}\mathrm{D}\bar{\psi}\mathrm{D}\psi \approx e^{-2ie\,\mathrm{tr}\left(\sum_n\int \mathrm{d}^2x\,\alpha\bar{\phi}_n\gamma^5\phi_n\right)}\mathrm{D}\bar{\psi}\mathrm{D}\psi\,. \tag{2.35}$$

In order to compute the value of this Jacobian, it is important to pay attention to the divergences. Indeed, in this Jacobian, we have the product of an infinite number of terms with an operator whose trace vanishes. A proper way to regularize this issue was introduced by K. Fujikawa in 1979 [88] (see [89] for an overall review of the method). It consists in using the relation

$$\mathrm{tr}\left(\sum_n \bar{\phi}_n \gamma^5 \phi_n\right) = \lim_{\Lambda\to\infty} \mathrm{tr}\left[\sum_n \bar{\phi}_n \gamma^5 e^{-\left(\frac{\lambda_n}{\Lambda}\right)^2} \phi_n\right] . \tag{2.36}$$

Inserting a resolution of the identity and using the definition (2.30) of λ_n, one can rewrite this as

$$\begin{aligned}\mathrm{tr}\left(\sum_n \bar{\phi}_n \gamma^5 \phi_n\right) &= \lim_{\Lambda\to\infty} \left\langle x \left| \mathrm{tr}\left(\gamma^5 e^{-\left(\frac{\gamma^\mu\left(\partial_\mu - \frac{ie}{\hbar}A_\mu\right)}{\Lambda}\right)^2}\right) \right| x \right\rangle \\ &= \lim_{\Lambda\to\infty} \left\langle x \left| \mathrm{tr}\left(\gamma^5 e^{\frac{1}{\Lambda^2}\left[\partial_\mu - \frac{ie}{\hbar}A_\mu\right]^2 + \frac{ie}{\hbar\Lambda^2}\gamma^\mu\gamma^\rho\partial_\mu A_\rho}\right) \right| x \right\rangle .\end{aligned} \tag{2.37}$$

Expanded on a plane wave basis, this reduces to

$$\mathrm{tr}\left(\sum_n \bar{\phi}_n \gamma^5 \phi_n\right) = \lim_{\Lambda\to\infty} \Lambda^2 \int \frac{\mathrm{d}^2 q}{(2\pi)^2} \mathrm{tr}\left(\gamma^5 e^{-\left[q_\mu - \frac{eA_\mu}{\hbar\Lambda}\right]^2 + \frac{ie}{\hbar\Lambda^2}\gamma^\mu\gamma^\rho\partial_\mu A_\rho}\right) . \tag{2.38}$$

Expanding the exponential in powers of Λ, the only non-zero contribution turns out to be finite and given by

$$-2ie \int \mathrm{d}^2 x\, \alpha(x)\, \mathrm{tr}\left(\sum_n \bar{\phi}_n \gamma^5 \phi_n\right) = -\frac{e^2 c}{2\pi\hbar} \int \mathrm{d}x\mathrm{d}t\, \alpha(x)\, \epsilon^{\mu\nu} F_{\mu\nu} . \tag{2.39}$$

One calls it the (Euclidean) effective action.

Returning to the conservation equation, taking the derivative of (2.26) with respect to α ,with the proper definition of the measure of integration including (2.39), one gets

$$\langle \partial_\mu j_A^\mu \rangle = i \frac{e^2 c}{2\pi\hbar} \epsilon^{\mu\nu} F_{\mu\nu} . \tag{2.40}$$

Going back to Minkovski space, we recover the expression of the chiral anomaly

$$\langle \partial_\mu j_A^\mu \rangle = \frac{e^2 c}{2\pi\hbar} \epsilon^{\mu\nu} F_{\mu\nu} . \tag{2.41}$$

Therefore, in the path integral formalism, the anomaly hides in the non-invariance of the measure of integration and, more precisely, the Jacobian of the associated transformation, leading to the effective action. This strategy can be generalized to any even dimension. In particular, it was applied in 3+1 dimensions in Fujikawa's original work [88] to determine the 3+1 dimensional chiral anomaly

$$\langle \partial_\mu j_A^\mu \rangle = \frac{e^3 c}{16\pi^2\hbar^2} \epsilon^{\mu\nu\rho\sigma} F_{\mu\nu} F_{\rho\sigma} . \tag{2.42}$$

2.2.3 Chiral anomaly as a Hilbert infinite hotel: from quantum field theory to experiments

In the previous two sections, we have seen that the chiral anomaly can be described either as an impossibility to regularize a theory in section 2.2.1 or as a modification of the measure of

integration in a path integral approach in section 2.2.2. However, in condensed matter theory, the linear band description is only an approximation. One cannot choose the regularization procedure at will since the band structure naturally provides it. Therefore, we can wonder if, in such a case, the chiral anomaly still emerges in low-energy physics.

Here, we will show how the chiral anomaly emerges in condensed matter systems, first in 1+1 dimension, before generalizing our approach to 3+1 dimensional systems. Then, we will use these descriptions to describe a particular, experimentally observed consequence of the chiral anomaly: the negative magnetoresistance in Weyl semimetals.

The anomaly in 1+1D as particle-hole production from a Dirac sea

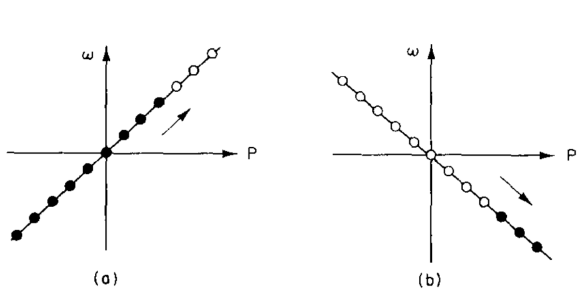

(a) Dispersion relation for a positive (a) and a negative (b) chirality crossing point. The black and white points denote the filled and empty states, while the arrow indicates the direction of movement of the particle when an electric field is turned on (taken from [12]).

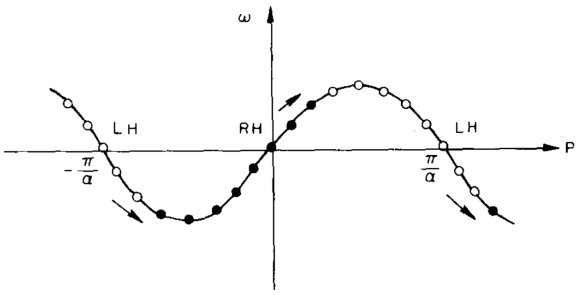

(b) Example of a 1+1 dimensional dispersion relation. The black and white points denote the filled and empty states, while the arrows indicate the direction of movement of the particle when an electric field is turned on (Note that the boundary of the Brillouin zone $P = \pm\frac{\pi}{a}$ are identified) (taken from [12]).

Figure 2.2: **Chiral anomaly in condensed matter in both low- and high-energy descriptions**

In 1983, H. Nielsen and M. Ninomiya generalized the high energy physics chiral anomaly to condensed matter systems [12]. Let us consider a 1+1 dimensional metallic band dispersion relation. By definition, a metal possesses points in momentum space whose energy equals the chemical potential μ. As described in section 1.2.1 and represented in Fig. 1.3, around these points, denoted k_n, one can linearize the energy spectrum as

$$\epsilon(k_n + \delta k) = \mu + \hbar v_n \delta k \,, \tag{2.43}$$

with $v_n = \partial_k \epsilon|_{k_n}$, and define a "chirality" for these modes as $\chi_n = \text{sign}(v_n)$; The low energy model close to k_n is then equivalent to a Dirac fermion with chirality χ_n. In condensed matter, to quantify such a theory, we define the vacuum or Dirac sea as the physical state with all states with energies smaller than μ occupied. This prescription then allows one to define ρ_n the particle density close to each one of the crossing points by comparing any state to this reference state.
Now, in 1+1 dimensions, a $\mathcal{U}(1)$ gauge symmetry allows to use a temporal gauge, such that a uniform electric field is captured by the gauge field $A_\mu = (0, A(t))$ with $E(t) = \frac{1}{c}\partial_t A(t)$. In a uniform electric field, in the low-energy picture, the dynamics of the particle close to these crossing points are given by

$$i\hbar\partial_t \psi_n = \left(-i\hbar v_n \partial_x - eA(t)\right)\psi_n \,. \tag{2.44}$$

Treating each of the ρ_n as independent from each other, one would naively expect, from symmetry considerations, each of these densities ρ_n to be conserved. However, in the presence of an electric field, the semi-classical equations of motion for electrons close to k_n are given by

$$\begin{cases} \partial_t x = v_n \,, \\ \partial_t p = eE \,, \end{cases} \tag{2.45}$$

implying, since the particle density verifies $\mathrm{d}\rho_n = \frac{\chi_n}{2\pi}\mathrm{d}k$ (see Fig. 2.2(a)),

$$\partial_t \rho_n = \chi_n \frac{eE}{2\pi\hbar} \,, \tag{2.46}$$

or in other words, written in a gauge invariant form

$$\partial_\mu j_n^\mu = \chi_n \frac{e^2 E}{2\pi\hbar} = \chi_n \frac{e^2 c}{4\pi\hbar} \epsilon^{\mu\nu} F_{\mu\nu} \,, \tag{2.47}$$

with $j_n^\mu = \begin{pmatrix} e v_n \rho_n \\ j_n \end{pmatrix}$. This is the chiral anomaly for a single chirality.

From this study, based on one of the crossings, we can deduce the total anomaly expression,

$$\begin{cases} \partial_\mu j_V^\mu = \partial_\mu \sum_n j_n^\mu = \left(\sum_n \chi_n\right) \frac{e^2 c}{4\pi\hbar} \epsilon^{\mu\nu} \mathcal{F}_{\mu\nu} \,, \\ \partial_\mu j_A^\mu = \partial_\mu \sum_n \chi_n j_n^\mu = \left(\sum_n 1\right) \frac{e^2 c}{4\pi\hbar} \epsilon^{\mu\nu} \mathcal{F}_{\mu\nu} \,, \end{cases} \tag{2.48}$$

which is identical to (2.19) if we consider only two crossing, with $\chi_{\pm 1} = \pm 1$. This description of the chiral anomaly illustrated in Fig. 2.2 provides yet another interpretation. First, notice that the chiral anomaly equations (2.48) do not guarantee the charge to be conserved. It will only be conserved if the total chirality is equal to 0. This observation provides a constraint on condensed matter models and was formulated and proven as a theorem based on topological arguments, translation invariance, and locality by H. Nielsen and M. Ninomiya [90–92]. This description allows us to formulate the chiral anomaly in a low energy description as the creation or annihilation of states coming from the infinitely deep Dirac Sea represented (see Fig. 2.2(a)). It should not appear as a surprise since when looking at the system beyond the linear regime approximation, one realizes that the number of such states is not infinite; in fact, the different crossing points are related through the high energy modes. In this picture, the anomaly is captured by the transit of electrons from one crossing to another through high-energy modes beyond the linear regime (see Fig. 2.2(b)).

From 1+1 dimension to 3+1 dimensions through Landau levels

The discussion in the previous paragraph seems very specific to 1+1 dimensional systems, while, in solid states experiments, we typically deal with 3+1 dimensional systems. In this paragraph, we will show, using the notion of Landau levels, how the 1+1 dimensional argument can be straightforwardly extended to a 3+1 dimensional system in the presence of a magnetic field.

Before discussing this dimensional reduction strategy, it might be interesting to discuss in more detail the systems to which we would like to apply such a strategy. In dimensions larger than 1+1, condensed matter materials whose low energy description is captured by a massless Dirac equation are called relativistic semimetals. Such materials are

- Dirac semimetals in 2+1 dimensions such as graphene;

- Dirac, Weyl, and nodal line semimetals in 3+1 dimensions, such as Na_3Bi [93] and TaAs [94].

For more details on the physics of relativistic semimetals, the interested reader is referred to the review [95, 96] or to the theses [97, 98].

This paragraph will focus on semimetals with a well-defined notion of chirality: Weyl semimetals. By definition, a Weyl semimetal is a material whose low-energy electronic properties are captured by a Weyl Hamiltonian. Using the Weyl representation for the gamma matrices [99], every spinor can be decomposed into eigenvectors of the chirality operator γ^5, defining

$$\psi_{R/L} = \frac{1}{2}\left(\mathbb{1} \pm \gamma^5\right) . \tag{2.49}$$

The low energy Hamiltonian of a Weyl semimetal can then be decomposed into two chirality sectors, each one forming a Weyl cone or massless Dirac cone of chirality $\chi_{R/L} = \pm 1$. They are located at two separate points in momentum space, and their Hamiltonian is defined by

$$\mathcal{H}_\chi = \chi \hbar v_F \delta\vec{k}.\vec{\sigma} \,, \tag{2.50}$$

with σ^i, $i \in x, y, z$, the Pauli matrices. Without loss of generality, let us introduce a magnetic field along the z-axis via a minimal coupling procedure. In the symmetric gauge, this is equivalent to the replacement

$$\hbar k_\mu \to \hbar K_\mu = \hbar k_\mu + eA_\mu \quad A_\mu = \frac{B}{2}\begin{pmatrix} 0 \\ -y \\ x \\ 0 \end{pmatrix} . \tag{2.51}$$

The translation symmetry along the z-axis, the direction of $\vec{B}$, is preserved. Therefore, k_z is a conserved quantity. Since the commutator

$$\left[\hat{K_x}, \hat{K_y}\right] = -i\frac{eB}{\hbar} \tag{2.52}$$

resembles the canonical commutator $[\hat{x}, \hat{p}] = i\hbar$, in analogy with a quantum oscillator, we introduce the ladder operators

$$\begin{aligned} \hat{a} &= \sqrt{\frac{\hbar}{2e|B|}}(\hat{K_x} - i.\mathrm{sign}(B)\hat{K_y}), \\ \hat{a}^\dagger &= \sqrt{\frac{\hbar}{2e|B|}}(\hat{K_x} + i.\mathrm{sign}(B)\hat{K_y}), \end{aligned} \tag{2.53}$$

such that the Hamiltonian can be rewritten as

$$\mathcal{H}_\chi = \begin{cases} \chi v_F \begin{pmatrix} \hbar k_z & \sqrt{-2eB\hbar}\,\hat{a}^\dagger \\ \sqrt{-2eB\hbar}\,\hat{a} & -\hbar k_z \end{pmatrix} & \text{if } B < 0\,, \\ \chi v_F \begin{pmatrix} \hbar k_z & \sqrt{2eB\hbar}\,\hat{a} \\ \sqrt{2eB\hbar}\,\hat{a}^\dagger & -\hbar k_z \end{pmatrix} & \text{if } B > 0\,. \end{cases} \tag{2.54}$$

Introducing $|n\rangle\,, n \in \mathbb{N}$, the eigenvectors of $\hat{N} = \hat{a}^\dagger\hat{a}$, such that

$$\hat{a}|0\rangle = 0\,, \text{ and } \hat{a}|n\rangle = \sqrt{n}|n-1\rangle,\ n \in \mathbb{N}^\star\,, \tag{2.55}$$

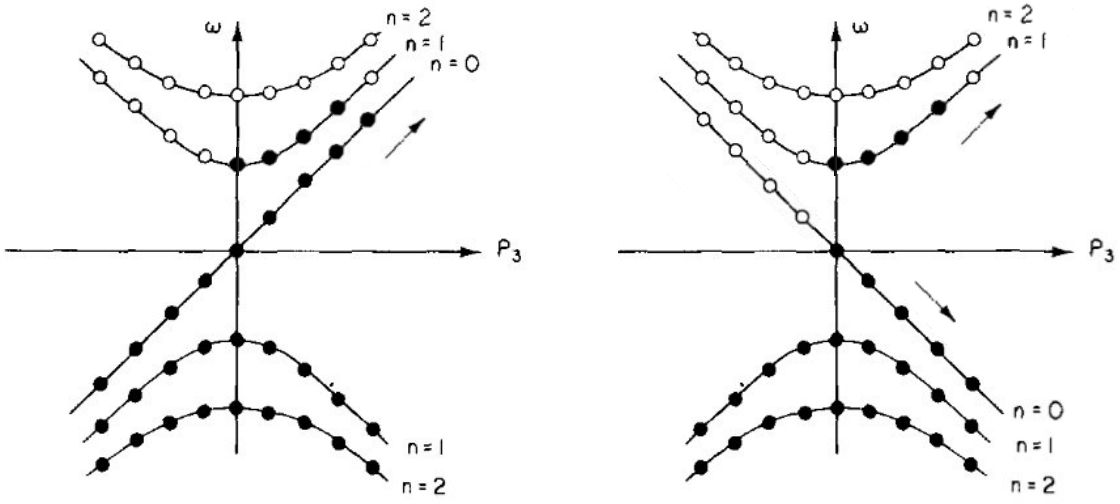

Figure 2.3: **Dispersion relation at the level of a positive (left) and negative (right) chirality Dirac cones** The black and white points denote the filled and empty states, while the arrow indicates the direction of motion of the particles when an electric field is turned on (adapted from [12]).

one identifies the eigenstates of $\mathcal{H}_\chi$ for $B > 0$ as $\begin{pmatrix} \alpha|n\rangle \\ \beta|n-1\rangle \end{pmatrix}$ if $n > 0$ and $\begin{pmatrix} 0 \\ |0\rangle \end{pmatrix}$ if $n = 0$, while for $B < 0$, these eigenstates are defined by $\begin{pmatrix} \alpha|n-1\rangle \\ \beta|n\rangle \end{pmatrix}$ if $n > 0$ and $\begin{pmatrix} |0\rangle \\ 0 \end{pmatrix}$ if $n = 0$. The associated spectrum of $\mathcal{H}_\chi$ is

$$\begin{aligned} \epsilon_n &= \pm v_F \sqrt{k_z^2 + 2ne|B|\hbar} \text{ for } n > 0\,, \\ \text{and } \epsilon_0 &= -\chi v_F \,\mathrm{sign}(B)\, k_z\,. \end{aligned} \tag{2.56}$$

These are the Landau levels with a degeneracy $g = \frac{e|B|}{2\pi\hbar}$.

For both Weyl cones one can define a charge density $\rho_\pm$ and a current density $\vec{j}_\pm$, that we can arrange as a four-vector

$$j_\pm^\mu = \begin{pmatrix} v_F \rho_\pm \\ \vec{j}_\pm \end{pmatrix}\,. \tag{2.57}$$

The vector or charge current corresponds to the total current, and the axial current to the difference between right and left currents:

$$j_V^\mu = j_+^\mu + j_-^\mu\,, \quad j_A^\mu = j_+^\mu - j_-^\mu\,. \tag{2.58}$$

The left and right Landau levels for $n \neq 0$ contribute equally to j_+^μ and j_-^μ. The only contribution to j_A^μ, therefore, originates from the $n = 0$ Landau level (defined following equation (2.56), see Fig. 2.3). Moreover, the transport in each Landau level is effectively 1+1 dimensional along the z-axis. From this point of view, one can then relate the 3+1D anomaly to a density $\frac{e|B|}{2\pi\hbar}$ of 1+1D chiral anomalies,

$$\partial_\mu j_A^\mu = \frac{e|B|}{2\pi\hbar}\frac{d\rho_A^{1D}}{dt} = \frac{e^3 \vec{E}\cdot\vec{B}}{2\pi^2\hbar^2} = \frac{e^3 c}{16\pi^2\hbar^2}\epsilon^{\mu\nu\rho\sigma}\mathcal{F}_{\mu\nu}\mathcal{F}_{\rho\sigma}\,. \tag{2.59}$$

This equation (2.59) encodes the 3+1 dimensional chiral anomaly.

A concrete consequence of the chiral anomaly in condensed matter: chiral magnetic effect and negative magnetoresistance

The previous paragraphs described the chiral anomaly as pumping electrons from one cone to another. However, one cannot pump electrons indefinitely in such a way. A relaxation process, transferring particles between the two Weyl cones with a characteristic time τ, is necessary to reach a steady state. If we assume that a fast relaxation inside of the cone is present or, in other words, that the intra-cone scattering time is far shorter than the inter-cone one (τ), then, in a homogeneous system, the chiral density ρ_5 follows a Boltzmann-like equation

$$\partial_\mu j^\mu_A = \frac{\partial \rho^{3D}_A}{\partial t} = \frac{e^3}{2\pi^2\hbar^2}\vec{E}\cdot\vec{B} - \frac{\rho_5}{\tau}\,, \tag{2.60}$$

such that, in the stationary regime, the charge imbalance is given by

$$\rho^{3D}_A = \tau\frac{e^3}{2\pi^2\hbar^2}\vec{E}\cdot\vec{B}\,. \tag{2.61}$$

Since the axial properties are entirely determined by the chiral, $n = 0$ Landau level, we can relate this density to a difference in chemical potential between the two cones

$$\rho^{3D}_A = \left(\frac{e|B|}{2\pi\hbar}\right)\frac{1}{2\pi\hbar}\frac{\mu_A}{|v_F|}\,. \tag{2.62}$$

Following Landauer's formula for a 1+1 dimensional system [100, 101], a chemical potential imbalance drives a 1+1 dimensional current density such as

$$j_{1D} = \frac{e^2}{2\pi\hbar}\frac{\mu_R - \mu_L}{-e} = \frac{e}{2\pi\hbar}\mu_A\,\mathrm{sign}(B)\,, \tag{2.63}$$

where $\mathrm{sign}(B)$ defines the chirality of the corresponding mode.

Applied to our 3+1 dimensional system, according to equation (2.62), the chiral anomaly induces an electric current such that

$$\vec{j}_{3D} = \left(\frac{e|B|}{2\pi\hbar}\right)j_{1D}\frac{\vec{B}}{\left|\vec{B}\right|} = \tau v_F\frac{e^3}{2\pi^2\hbar^2}\vec{E}.\vec{B}\frac{\vec{B}}{\left|\vec{B}\right|}\,, \tag{2.64}$$

which implies a conductivity tensor ($j^i = \sigma^{ij}E^j$) of the form

$$\sigma^{ij} = \tau v_F\frac{e^3}{2\pi^2\hbar^2}\frac{B^iB^j}{\sqrt{\vec{B}.\vec{B}}}\,. \tag{2.65}$$

This is the negative magnetoresistance.
Note, however, that we heavily used the Landau level's physics in this derivation. In this sense, it is only valid for a strong enough magnetic field. In weaker fields, using a semi-classical approximation, [102] and [103] proved that a similar effect also holds, but with a different scaling in B

$$\sigma^{ij} = \tau v_F\frac{3e^4v_F^2}{8\pi^2\hbar^2}\frac{B^iB^j}{\mu^2 + \pi^2k_B^2T^2}\,. \tag{2.66}$$

Despite spurious intrinsic effects, among which the most ubiquitous is current jetting (see Fig. 2.4), these theoretical predictions were verified experimentally in several compounds including $ZrTe_5$ [103, 104], TaAs [105] or NbP [16] (see Fig. 2.5).

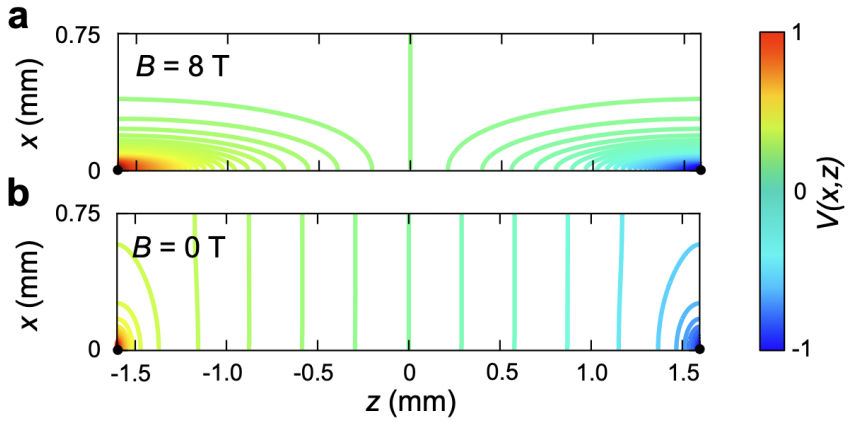

Figure 2.4: **Current jetting in TaP** The graphs compare the simulated potential distributions between 0 and 8 tesla for a magnetic field applied parallel to the contact ($\vec{B} \parallel \vec{e}_z$). The magnetic field drives a redistribution of the current density, leading to a focused current jet between the current contacts parallel to the magnetic field and strong bending of the equipotential lines, leading to a spurious measurement of intrinsic magneto-conductance known as current jetting. The black dots show the current source and drain contacts at $z = \pm 1.5$mm (taken from [106]).

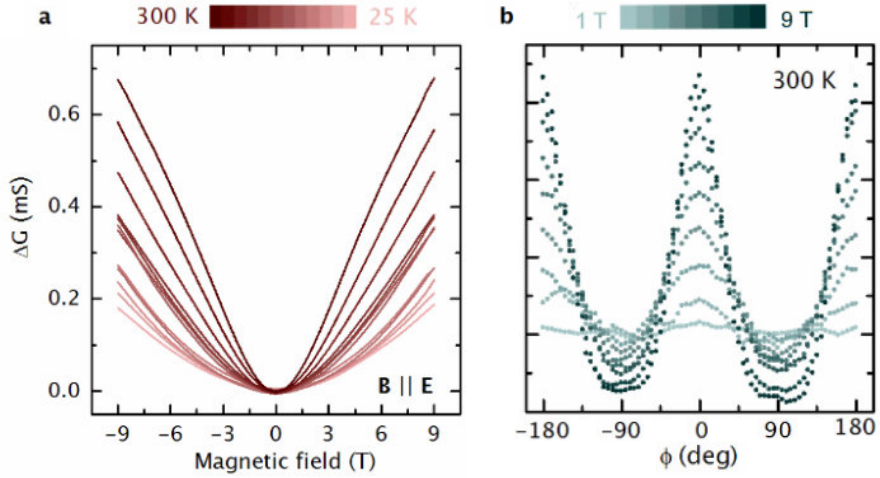

Figure 2.5: **Negative magnetoresistance in NbP** (a) Longitudinal magneto-conductance without zero-field contributions $\Delta G = \Delta\sigma^{zz}$ at selected temperatures. The transition from a quadratic dependence at low magnetic fields to a linear regime at high fields indicates a transition from the semi-classical regime (2.66) to the fully quantized regime, where only the lowest Landau levels are occupied (2.65). (b) Angular dependence of the longitudinal magnetoconductivity. At small magnetic fields ($|\vec{B}| < 3\mathcal{T}$), it is reasonably well described by a squared cosine function. However, the angular width at higher fields narrows considerably, indicating strong collimation (adapted from [16]).

2.3 Gravitational anomalies

In the previous section, we have seen that an electromagnetic field affects the axial current's conservation equations of relativistic particles in 1+1 dimensions. A natural question arises: Do other background fields have similar effects on these currents? And, are other current densities affected?

As we have seen in chapter 1, curved spacetimes naturally arise in condensed matter. It is, therefore, important to study the relationship between metric fields and anomalies. This question is also relevant from an experimental point of view. Indeed, following Luttinger theory 1.3, any thermal conductivity experiment is related to the response to a metric field. We can, therefore, wonder whether anomalies related to such a metric field may affect thermal conductivity experiments.

In this section, we will see that metric fields can affect the conservation properties of the chiral current. Then, we will review their effects on the currents associated with metric invariance through the momentum-energy tensor. We conclude with a more detailed discussion of the situation in dimension 1+1, of particular importance for the remainder of this thesis.

2.3.1 Mixed axial-gravitational anomalies and condensed matter experiments

Mixed axial-gravitational anomalies

Curved spacetimes are important in condensed matter since they emerge in several situations described in chapter 1. A natural question following our previous discussion on the chiral anomaly is, therefore: given a weakly curved spacetime described by $g_{\mu\nu} = \eta_{\mu\nu} + h_{\mu\nu}$ with $\eta_{\mu\nu}$ the flat space Minkowski metric and $h_{\mu\nu}$ a metric perturbation, is there any correction to the chiral current conservation equation, such that

$$\nabla_\mu j_A^\mu = f\left(h_{\mu\nu}\right) , \tag{2.67}$$

with $\nabla_\mu \mathcal{A}^\mu \equiv \frac{1}{\sqrt{-\det(g_{\alpha\beta})}}\partial_\mu\left(\sqrt{-\det(g_{\alpha\beta})}\mathcal{A}^\mu\right)$ the covariant derivative? The answer to this question was given only a few years after the discovery of the chiral anomaly by T. Kimura [107] and then rederived and generalized on several occasions [108–110]. The corresponding anomalous conservation equation is:

$$\nabla_\mu j_A^\mu = \frac{ec}{384\pi^2}\epsilon^{\mu\nu\rho\sigma}\mathcal{R}^\alpha_{\beta\mu\nu}\mathcal{R}^\beta_{\alpha\rho\sigma} , \tag{2.68}$$

with $\mathcal{R}^\alpha_{\beta\mu\nu}$ the curvature tensor (see Appendix. A), expressed up to first order in $h_{\mu\nu}$ as $\mathcal{R}_{\alpha\beta\mu\nu} = \frac{1}{2}\left[\partial_\beta\partial_\mu h_{\alpha\nu} + \partial_\alpha\partial_\nu h_{\beta\mu} - \partial_\alpha\partial_\mu h_{\beta\nu} - \partial_\beta\partial_\nu h_{\alpha\mu}\right]$. This is the mixed chiral-gravitational anomalies in 3+1 dimensions. Similar to the chiral anomaly, it can be rederived using either perturbation theory, considering the mixed chiral-gravitational triangle diagram (see Fig. 2.6), or by computing the effective action associated with the chiral rotation $\phi \to e^{ie\alpha(x)\gamma^5}\phi$ in the presence of curved spacetime. The resulting effective action is, in 3+1 dimensions,

$$\mathcal{S}_{eff}(h_{\mu\nu}) = \int \mathrm{d}^3\vec{x}\,\mathrm{d}t\,\sqrt{-\det(g_{\alpha\beta})}\,\frac{ec}{384\pi^2}\alpha(x)\epsilon^{\mu\nu\rho\sigma}\mathcal{R}^\alpha_{\beta\mu\nu}\mathcal{R}^\beta_{\alpha\rho\sigma} . \tag{2.69}$$

While such a term might seem like a straightforward application of the ideas introduced in the previous section, written as a contraction of tensor fields with the totally antisymmetric tensor $\epsilon^{\mu\nu\rho\sigma}$, there are at least two major differences between this anomalous contribution and the one presented previously. First, the usual chiral anomaly involves only two derivatives, while this term involves four derivatives. Then, one may note that such mixed anomalies were expressed above for a 3+1 dimensional field theory, while we previously presented results in 1+1 dimensional systems. Indeed, contrary to the chiral anomaly present in any even dimensional system [111,112], symmetry considerations imply that mixed anomalies can only exist in spacetime dimension such as $D+1 = 4k$, with k an integer [110,113,114]. Actually, in dimension $4k+2$, as we will see below, another kind of anomaly arises [81,108], the pure gravitational anomalies.

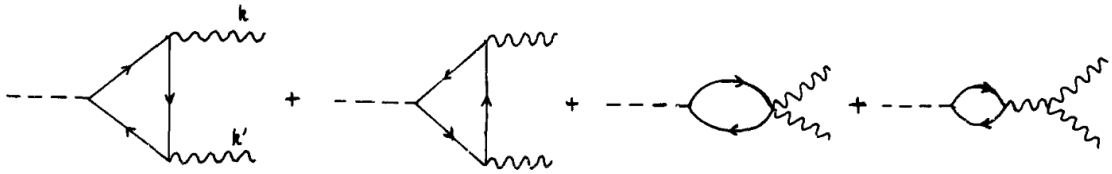

Figure 2.6: **One loop chiral-gravitational triangle diagramms** One loop fermion loop diagram contributing to the decay into two gravitons. The dashed lines correspond to the chiral current insertion, while the waves correspond to the gravitons ($h_{\mu\nu}$) (taken from [108]).

Mixed axial-gravitational anomalies and transport properties

Following the logic of the previous section, we can wonder if it is possible to relate the axial-gravitational anomaly to any transport properties similarly to the negative magnetoresistance manifestation of the chiral anomaly.

Following Luttinger, a natural way to introduce curvature in a system is via a thermal gradient. Hence, it seems rational to try to relate the mixed axial-gravitational anomaly to the thermo-electric transport properties of semimetals. K. Landsteiner *et al.* [14, 16, 115] pointed out that the mixed axial-gravitational anomaly coefficients d and b, occurring in the anomalous conservation equations

$$\nabla_\mu j_A^\mu = d\frac{e^3 c}{32\pi^2\hbar^2}\epsilon^{\mu\nu\rho\sigma}\mathcal{F}_{\mu\nu}\mathcal{F}_{\rho\sigma} + b\frac{ec}{768\pi^2}\epsilon^{\mu\nu\rho\sigma}\mathcal{R}^\alpha_{\beta\mu\nu}\mathcal{R}^\beta_{\alpha\rho\sigma}\,, \tag{2.70}$$

and deduced from the underlying Lie algebra, are identical to those present in the Kubo formula for single-cone magneto-electro-thermal response

$$\begin{cases} \vec{j} = d\frac{e^2}{4\pi^2\hbar^2}\mu\vec{B}\,, \\ \vec{J}_\epsilon = \left(d\frac{e}{8\pi^2\hbar^2}\mu^2 + b\frac{e}{24\hbar^2}\left(k_B T\right)^2\right)\vec{B}\,. \end{cases} \tag{2.71}$$

The same conclusion can be reached within a hydrodynamic approach as pointed out by S. Sachdev *et al.* [116] and K. Jensen *et al.* [117, 118]. Studying linear magnetotransport in the presence of thermal gradients and electric fields is, therefore, a natural testbench for the manifestation of these anomalies.
Experimental measurements in such setups, measuring the magneto-thermoelectric properties, were performed on NbP samples in 2020 (see Fig. 2.7) and displayed a good agreement with the theoretical computations [16, 119]. Another study of the magneto-thermal conductivity in $ZrTe_5$ was conducted more recently and will be the core focus of the chapter 8.

2.3.2 Symmetries, conserved quantities and anomalies in curved spacetime

As discussed above, in dimensions $4k+2$, a quantum field theory does not present any mixed chiral-gravitational anomaly. Instead, it presents a so-called pure gravitational anomaly described at the perturbative level by a Feynman diagram with all external legs representing gravitons. In order to understand the expression of these anomalies and those of the so-called weyl (or conformal or trace) anomalies, in this section, we will first review some additional symmetry properties of the fermionic action before studying how anomalies violate some of them.

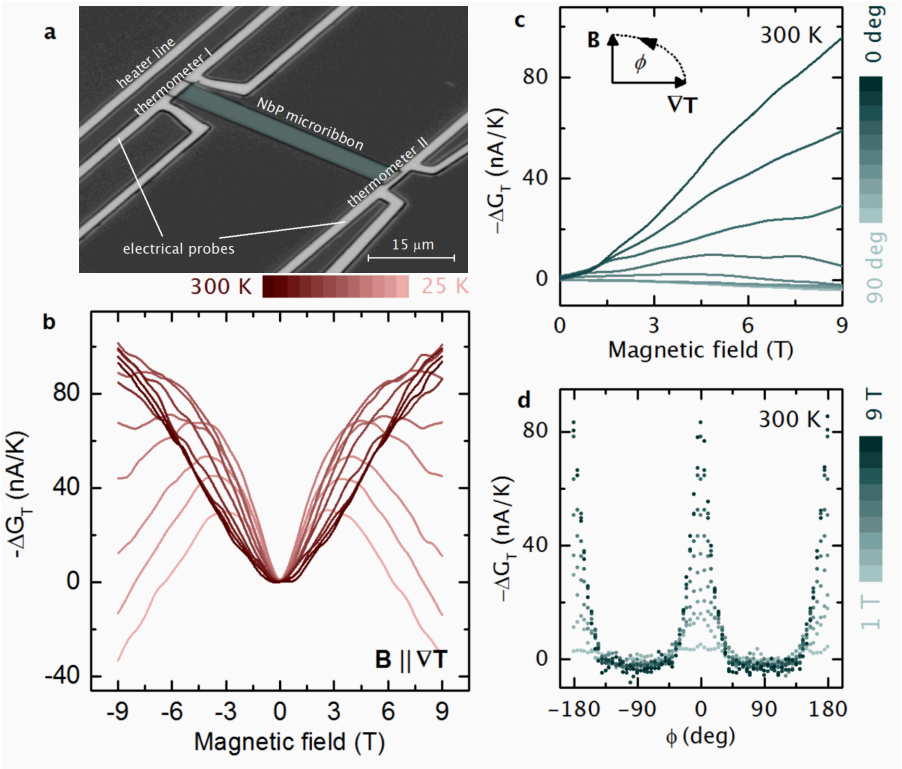

Figure 2.7: **Longitudinal magneto-thermoelectric conductivity in NbP** (a) Optical micrograph of a measured device. The NbP micro-ribbon is placed between two four-probe thermometers, which also serve as electrical probes. The electrically insulated heater line close to one end of the sample creates a temperature gradient along the length of the sample. (b) Negative longitudinal magneto-thermoelectric conductance without zero-field contributions $-\Delta G_T$ at selected temperatures (the minus sign accounts for the negative charge of the electrons). As expected from the theoretical prediction, the magneto-thermoelectric conductance exhibits a quadratic low-field dependence. At the same time, at higher fields, the formation of one-dimensional Weyl-Landau levels dispersing only along the magnetic field direction strongly suppresses G_T. (c) $-\Delta G_T$ versus $|\vec{B}|$ for different angles ϕ between the thermal gradient and the magnetic field. (d) Angular dependence of the axial current. Similar to the electrical conductance represented in Fig. 2.5, the magneto-thermoelectric conductance at all magnetic fields ($|\vec{B}| < 3T$) is reasonably well described by a squared cosine function. However, the angular width narrows considerably at higher fields, indicating strong collimation (adapted from [16]).

Symmetry properties

Let us first consider the fermionic action in curved spacetime in general dimension, given by

$$\mathcal{S}_\Psi = \frac{i\hbar}{2}\int \mathrm{d}^D x \det\left(e^b_\nu\right) e^\mu_a \bar{\Psi}\gamma^a \overleftrightarrow{D}_\mu \psi\,, \tag{2.72}$$

with e^a_μ the vielbein, and D_μ the spinor derivative (see Appendix A). The momentum-energy tensor of this theory can then be defined as

$$\mathcal{T}^\mu_{\ a} = -\frac{1}{\det(e^b{}_\nu)}\frac{\delta \mathcal{S}_\psi}{\delta e^b{}_\mu} = \frac{i\hbar c}{2} e_b{}^\mu e^\nu{}_a \bar{\Psi}\gamma^b \overleftrightarrow{D}_\nu \psi - i\hbar c\, e^\mu{}_a \bar{\Psi}\gamma^a \overleftrightarrow{D}_\mu \psi\,, \tag{2.73}$$

while its symmetric equivalent can be written as

$$\mathcal{T}^{\mu\nu} = \frac{1}{2}\left(e^{a\nu}\mathcal{T}^\mu_{\ a} + \mu \longleftrightarrow \nu\right). \tag{2.74}$$

This action possesses three interesting invariances:

- A Lorentz invariance corresponding to invariance under an infinitesimal local Lorentz transformation characterized by the antisymmetric matrix α_{ab}

$$\begin{cases} e^a{}_\mu \to e^a{}_\mu - \alpha^a{}_b e^b{}_\mu \,, \\ \psi \to \left(1 - \frac{1}{8}\alpha_{ab}\left[\gamma^a, \gamma^b\right]\right)\psi \,, \\ \bar{\psi} \to \bar{\psi}\left(1 + \frac{1}{8}\alpha_{ab}\left[\gamma^a, \gamma^b\right]\right) . \end{cases} \tag{2.75}$$

- An Einstein or diffeomorphism invariance corresponding to invariance under spacetime translations $x^\mu \to x^\mu - \xi^\mu$ leading to the variations

$$\begin{cases} e^a{}_\mu \to e^a{}_\mu + \xi^\nu \partial_\nu e^a{}_\mu + e^a{}_\nu \partial_\mu \xi^\nu \,, \\ \psi \to (1 + \xi^\nu \partial_\nu)\,\psi \,, \\ \bar{\psi} \to \bar{\psi}\left(1 + \overleftarrow{\partial_\nu}\right)\xi^\nu \,. \end{cases} \tag{2.76}$$

- A Weyl invariance corresponding to invariance under a Weyl rescaling $e^a{}_\mu \to e^{\sigma(x)} e^a{}_\mu$ written in an infinitesimal form as

$$\begin{cases} e^a{}_\mu \to (1+\sigma) e^a{}_\mu \,, \\ \psi \to \left(1 - \frac{D-1}{2}\sigma\right)\psi \,, \\ \bar{\psi} \to \bar{\psi}\left(1 - \frac{D-1}{2}\sigma\right) . \end{cases} \tag{2.77}$$

According to Noether's theorem, these give rise to the following properties of the momentum-energy tensor (equivalent to conservation equations), respectively

- The momentum-energy tensor can be made symmetric such as

$$\mathcal{T}^\mu{}_a e^{a\nu} = \mathcal{T}^\nu{}_a e^{a\mu} \,. \tag{2.78}$$

- The momentum-energy tensor is conserved

$$\nabla_\mu \mathcal{T}^\mu_\nu - \omega_{ab\nu}\mathcal{T}^{ab} = 0 \,, \tag{2.79}$$

  or, given the symmetry property of $\mathcal{T}^\mu_a$ (2.78), this implies

$$\nabla_\mu \mathcal{T}^\mu_\nu = 0 \,. \tag{2.80}$$

- The momentum-energy tensor can be made traceless

$$\mathcal{T}^\mu_\mu = 0 \,. \tag{2.81}$$

Chiral vs. conformal vs. Weyl invariance

A recurrent question occurs when looking at these symmetries and conservation laws. Indeed, in the literature, the tracelessness property of the momentum-energy tensor is, depending on the author, attached to either a Weyl invariance, a conformal symmetry, or a scaling symmetry. Therefore, one could wonder which symmetry is involved and what are the consequences of each one of them.

A scale symmetry corresponds to the symmetry under the global transformation

$$\begin{cases} x^\mu \to \lambda\, x^\mu \,, \\ \phi \to \lambda^{-\frac{D-1}{2}}\phi \,, \end{cases} \tag{2.82}$$

with λ a constant. Scale invariance leads to the conservation of the dilation current $j_D^\mu = x_\nu \mathcal{T}^{\nu\mu}$ whose conservation, together with the conservation of the momentum-energy tensor, leads to the tracelessness of the momentum-energy tensor.

Then, the conformal symmetry corresponds to the transformation under a change of coordinates $x^\mu \to f^\mu(x)$ that leaves the structure of the metric unchanged, up to a non-zero multiplicative function $g_{\mu\nu} \to \Omega(x) g_{\mu\nu}$. Notice that scale invariance is a specific case of conformal transformation with $\Omega = \lambda^2$

Finally, Weyl transformations correspond to a global rescaling of the metric without any change of coordinates. One might think that together with translation invariance, this implies the full conformal group; however, this is not true since a particular conformal transformation, the spacetime inversion $x^\mu \to \frac{x^\mu}{x^2}$ cannot be reduced to a composition of a Weyl and a translation transformation.

In conclusion, Weyl, conformal, and scaling transformations are different from one another. However, since each of them implies that the momentum-energy tensor is traceless, they are often mistaken for one another. In the realm of anomalies, since the end manifestation is similar ($\mathcal{T}^\mu_{\ \mu} \neq 0$), we consider Weyl, chiral, and scaling anomalies on the same footing, even though at the microscopic level, they are different (see [120] for a more complete discussion on this question).

Gravitational and trace anomalies

As in the case of the chiral anomaly, one might wonder whether these symmetries and conservation laws can be broken in curved spacetimes.

As in the case of the chiral anomaly, gravitational anomalies can be expressed as a breakdown of the conservation equations (2.78), (2.80) and (2.81).

- The **Lorentz anomaly** is equivalent to the existence of an antisymmetric part of the momentum-energy tensor
$$\mathcal{T}^{\mu\nu} - \mathcal{T}^{\nu\mu} \neq 0. \tag{2.83}$$
- The **Einstein anomaly** implies the non-conservation of the momentum-energy tensor [2]
$$\nabla_\mu \mathcal{T}^\mu_{\ \nu} = \omega_{ab\nu} \mathcal{T}^{ab} \neq 0. \tag{2.84}$$
- The **Weyl (trace, conformal or scale) anomaly** expresses the non tracelessness of the momentum-energy tensor
$$\mathcal{T}^\mu_{\ \mu} \neq 0. \tag{2.85}$$

However, we need to distinguish two cases [110]. On the one hand, we have the Lorentz and Einstein anomalies, which can only exist in dimensions $4k+2$ for symmetry reasons. For example, the two-dimensional case will be the focus of the next section 2.3.3.
On the other hand, trace anomalies can appear in any dimension, even though trace anomalies involving the spacetime curvature tensor $\mathcal{R}^\mu_{\nu\rho\sigma}$ can only be present in even dimensions. Once again, the two-dimensional case will be treated in the next section 2.3.3. In higher dimensions, since numerous Lorentz invariant quantities are built from the curvature tensor, determining

[2] The reverse is not true. A non-conservation of the momentum-energy tensor does not imply the presence of an Einstein anomaly since, according to (2.79), a Lorentz anomaly can lead to the same conclusion.

the precise form of the anomaly is more difficult. For example, in four dimensions, even though a first form was given by D. Capper and M. Duff almost 50 years ago [121–123], its precise form for several particles is, however, still debated [124, 125].

In generic interacting quantum field theories, scale anomalies can also arise when, through renormalization, quantum fluctuation affects the interaction coupling constants, irrespective of the dimension. For example, in four dimensions, in a background electromagnetic field, one gets the trace expression [75]

$$\mathcal{T}^{\mu}_{\ \mu} = \frac{\beta_e(e)}{2e}\mathcal{F}^{\mu\nu}\mathcal{F}_{\mu\nu}\,, \tag{2.86}$$

with β_e the beta-function associated to the electric charge, given at one loop order by

$$\beta_e(e) = \left.\frac{\mathrm{d}e(E)}{\mathrm{d}\,log(E)}\right|_{E=e} = \frac{e^3 c}{12\pi^2\hbar}\,. \tag{2.87}$$

However, contrary to all the previously mentioned anomalies, (2.87) is only true at the one-loop order and can receive corrections from every higher order of the perturbation theory.

2.3.3 Gravitational anomalies as properties of the momentum-energy tensor in 1+1D

Most of this thesis will be dedicated to 1+1 dimensional systems. Therefore, this section will focus on gravitational anomalies in 1+1 dimensional systems.
In two-dimensional systems, every metric is conformally flat. In other words, any metric can be, up to a change of variable, rewritten under the form

$$g_{\mu\nu} = e^{W(t',x')}\eta_{\mu\nu}\,, \tag{2.88}$$

where $\eta_{\mu\nu}$ is the Minkowski flat metric. Therefore, it is possible, in addition to all the techniques introduced in the previous section, to use this equivalence to our advantage by using all the machinery of flat spacetime two-dimensional conformal field theory before making a Weyl transform to compute the physical quantities. For example, in his textbook on string theory [78], D. Tong deduced the expression for the trace anomalies in 1+1 dimensions using a conformal field theory technique, the operator product expansion, proving that for a theory with central charge $\mathcal{C}$, the trace anomaly is given by

$$\mathcal{T}^{\alpha}_{\ \alpha} = \mathcal{C}\frac{\hbar v_F}{48\pi}\mathcal{R}\,, \tag{2.89}$$

with $\mathcal{R}$ the Ricci scalar (See Appendix. A).
Of course, it is still possible to use an effective action approach [110] or a perturbative one [70, 126] to determine the expression of the covariant gravitational anomalies for a theory with particles of chirality χ_i and central charge c_i

$$\begin{cases} \mathcal{T}^{\mu}_{\ \mu} = \mathcal{C}_w\frac{\hbar v_F}{48\pi}\mathcal{R}\,, \\ \nabla_\mu\mathcal{T}^{\mu\nu} = \mathcal{C}_g\frac{\hbar v_F}{96\pi}\bar{\epsilon}^{\nu\mu}\nabla_\mu\mathcal{R}\,, \\ \mathcal{T}^{\mu\nu} - \mathcal{T}^{\nu\mu} = 0\,, \end{cases} \tag{2.90}$$

with $\mathcal{C}_w = \sum_i c_i$, $\mathcal{C}_g = \sum_i \chi_i c_i$ and $\bar{\epsilon}^{\mu\nu} = \epsilon^{\mu\nu}/\det(e^a_{\ \rho})$. As we can see, the anomaly breaks both the Weyl and the diffeomorphism invariance under this form but keeps the Lorentz invariance intact. By a careful inspection of these relations, one realizes that it is equally possible to

redefine the momentum-energy tensor to make it covariantly conserved [127], breaking the Lorentz invariance

$$\begin{cases} \tilde{\mathcal{T}}^{\mu}_{\ \mu} = \mathcal{C}_w \frac{\hbar v_F}{48\pi}\mathcal{R} \\ \nabla_\mu \tilde{\mathcal{T}}^{\mu\nu} = 0\,, \\ \tilde{\mathcal{T}}^{\mu\nu} - \tilde{\mathcal{T}}^{\nu\mu} = \mathcal{C}_g \frac{\hbar v_F}{48\pi}\bar{\epsilon}^{\mu\nu}\mathcal{R}\,, \end{cases} \tag{2.91}$$

by defining

$$\tilde{\mathcal{T}}^{\mu\nu} = \mathcal{T}^{\mu\nu} + \mathcal{C}_g \frac{\hbar v_F}{96\pi}\bar{\epsilon}^{\mu\nu}\mathcal{R}\,. \tag{2.92}$$

One may note at this stage that $\tilde{\mathcal{T}}^{\mu\nu}$ breaks all of the previously defined invariances (2.78, 2.79, 2.81), since, due to its antisymmetric part $\tilde{\mathcal{T}}^{\mu\nu}$ does not fulfill the conservation equation (2.79).

Alternatively, one could have chosen another definition of $\mathcal{T}^{\mu\nu}$ in order to break the Lorentz invariance but not the diffeomorphism one

$$\begin{cases} \tilde{\mathcal{T}}^{\mu}_{\ \mu} = \mathcal{C}_w \frac{\hbar v_F}{48\pi}\mathcal{R} + \mathcal{C}_g \frac{\hbar v_F}{96\pi}\epsilon^{ab}\nabla_\mu \omega_{ab}{}^{\mu}\,, \\ \mathcal{T}^{\mu\nu} - \mathcal{T}^{\nu\mu} = \mathcal{C}_g \frac{\hbar v_F}{96\pi}\bar{\epsilon}^{\mu\nu}\mathcal{R}\,, \\ \nabla_\mu \mathcal{T}^{\mu}_{\ \nu} = \omega_{ab\nu}\mathcal{T}^{ab} = \mathcal{C}_g \frac{\hbar v_F}{192\pi}\epsilon^{ab}\omega_{ab\nu}\mathcal{R}\,. \end{cases} \tag{2.93}$$

Indeed, J. Bardeen and D. Zumino have shown in 1984 [128] that, in any dimension, it is possible to shift from a pure Einstein to a pure Lorentz anomaly (see also [70] 12.6.3 for a more careful review of this question).

Previously mentioned demonstrations of the gravitational anomalies seem disconnected from condensed matter physics, or at least difficult to relate to the condensed matter notions of particles, holes, and Dirac sea. However, similarly to how H. Nielsen and M. Ninomiya related the chiral anomaly to particle-antiparticle production from the Dirac sea 2.2.3, Y. Habara, H. Nielsen, and M. Ninomiya [129] showed that we could recover the trace anomaly from a careful study of the Dirac sea. In fact, they demonstrated that the Dirac sea in a curved spacetime corresponds to a continuum of particle-antiparticle pair creation applied to a flat spacetime Dirac sea through a generalized Bogoliubov transformation.

The following sections of this thesis will focus on studying the consequences of these gravitational anomalies in condensed matter systems, from analog spacetime to thermal transport and thermal heat engines.

Chapter 3

Tolman-Ehrenfest equilibrium temperature in curved spacetimes

As discussed in section 1.3, J.Luttinger suggested in 1963 that if a gravitational field did not exist in nature, one could have invented it for the purposes of calculating thermal responses [9]. This idea can be traced back to the work of R. Tolman and P. Ehrenfest in the advent of general relativity, who noticed that in a time-independent curved spacetime, the temperature of black-body radiation is not spatially uniform even in thermal equilibrium [7, 8]. Such a space-dependent temperature profile is known as the Tolman-Ehrenfest temperature. The insight of J. Luttinger was to suggest that thermal transport, thought of as a linear response of matter to a thermal gradient, can be derived by considering a counter-balancing weak gravitational field to restore equilibrium [9]. The Luttinger relation follows from the Tolman-Ehrenfest temperature and is the groundbreaking idea that established the gravitational field as a key concept in the study of heat transport in materials [130–132].

A central idea behind Luttinger's and Tolman-Ehrenfest's relations is that heat has weight. Therefore, heat contributes to energy density, adding up to the energy density due to the rest-mass of a massive particle [133]. The consequences are particularly remarkable for relativistic massless particles which lack any intrinsic energy density scale. The only relevant energy density scale is set by the temperature, whose variations follow those of spacetime.

However, new energy density scales absent in Luttinger's and Tolman-Ehrenfest's relations appear in strongly curved spacetimes. They manifest the anomalous thermodynamic behavior of quantum fluctuations induced by spacetime curvature. This interplay between geometry and vacuum fluctuations is analogous to the Casimir effect, induced by geometrical confinement instead of curvature [134, 135]. The fluctuations break the symmetries of the classical equation of motion, a phenomenon known as gravitational anomalies and discussed in section 2.3 of this thesis. The appearance of these anomalous energy density scales challenges us to understand their role in the equivalence relations between temperature and gravitational potential and their observable consequences for energy transport. This is the question we address in this chapter. Chapter 4 is dedicated to the consequences of these new energy scales in black-hole physics and condensed matter beyond linear response theory.

In this chapter, we quantitatively evaluate the quantum corrections to the Tolman-Ehrenfest temperature 1+1 dimensional systems, raising the question of how to define a temperature in such a system. We then show that this modified Tolman-Ehrenfest temperature implies that the Luttinger equivalence has to be corrected. This correction will be shown to be sizable when

the curvature of spacetime is significant or, equivalently, when the local spatial variation of temperature is sizable.

This chapter is based on original work published in the article Ariv:2206.08784 [136]

3.1 Classical Tolman-Ehrenfest temperature and Luttinger equivalence

In this section, we begin by recalling the Tolman-Ehrenfest temperature definition before showing how it can be related to Luttinger's ideas. Then, to understand the possible effects of anomalies, we will follow the historical derivation in generic D+1 dimensional systems before discussing the case of 1+1 dimensional conductors more carefully.

3.1.1 From the Tolman-Ehrenfest temperature to the Luttinger's relation

We begin by recalling the derivation of Luttinger's relation [9] from Tolman-Ehrenfest's work [7, 133].

R. Tolman and P. Ehrenfest realized that in curved spacetime, the temperature of blackbody radiation, and more generally of relativistic massless particles, is not spatially uniform even in thermal equilibrium. In essence, thermal equilibrium in the presence of a gravitational field requires a non-uniform temperature profile to compensate for the redshift experienced by radiation as it moves in the gravitational field [137] (See also Chapter. 7). They showed that the equilibrium temperature T_{TE} can be inferred from a reference temperature T_0, as

$$T_{\text{TE}}(\mathbf{r})\sqrt{\xi^\mu(\mathbf{r})g_{\mu\nu}(\mathbf{r})\xi^\nu(\mathbf{r})} = T_0\,, \tag{3.1}$$

where $g_{\mu\nu}$ is the stationary background metric which depends on spatial coordinates $\mathbf{r}$, and ξ^μ is the time-like Killing vector (see Appendix C). The constant T_0 is a reference temperature which has to be set, *e.g.* by boundary conditions.
Note that in this formulation of the Tolman-Ehrenfest temperature definition, one does not need the metric to be explicitly time-independent (static); instead, it has to possess a time-like Killing vector ξ^μ (see Appendix C), or in other words, to be stationary. For example, in 1+1 dimensions, a metric given by

$$g_{\mu\nu} = \begin{pmatrix} v^2(t) & 0 \\ 0 & -1 \end{pmatrix} \tag{3.2}$$

is stationary since it possesses a time-like Killing vector $\xi_\mu = \begin{pmatrix} v(t) \\ 0 \end{pmatrix}$ but it isn't static. The same can be said about the hydrodynamic metric (1.25) presented in section 1.1. However, similarly to R. Tolman and P. Ehrenfest in most of our derivations, we will focus on static metrics, whose line element can be written as

$$\mathrm{d}s^2 = g_{00}(\vec{x})v_F^2\mathrm{d}t^2 - \sum_{i,j=1}^{d} g_{ij}(\vec{x})\mathrm{d}x^i\mathrm{d}x^j\,. \tag{3.3}$$

In this case, (3.1) simplifies to

$$T_{\text{TE}}(\vec{x})g_{00}(\vec{x}) = Cst\,. \tag{3.4}$$

The Luttinger relation between temperature and gravitational potential

$$\vec{\nabla}\phi = -\frac{\vec{\nabla}T}{T}\,, \tag{3.5}$$

can be obtained from Eq. (3.4) as follows. Let us consider a time-independent metric

$$\mathrm{d}s^2 = e^{2\phi(\vec{x})}\, v_F^2 \mathrm{d}t^2 - \mathrm{d}\vec{x}^2. \tag{3.6}$$

parametrized by a small dimensionless gravitational factor $\phi \equiv \Psi/c^2 \ll 1$, expressed, in a weak-field limit, in terms of a static gravitational potential Ψ and the speed of light c. By substituting Eq. (3.6) into Eq. (3.4), we obtain the corresponding Tolman-Ehrenfest temperature (also called Luttinger temperature: see Section 27 of [138]):

$$T_{\mathrm{TE}}^2(\vec{x}) e^{2\phi(\vec{x})} = T_0^2\,. \tag{3.7}$$

Upon spatial differentiating we recover the Luttinger relation (3.5).

Therefore, Tolman and Ehrenfest proved that a system with a temperature gradient and a gravitational potential can be at equilibrium. Luttinger's insight is that such a system can be decomposed as a "sum" of two systems out of equilibrium. One sets out of equilibrium by a gradient of temperature and one by the gravitational potential. Therefore, each of these two systems possesses a non-zero energy current, but since their sum is at equilibrium, they must compensate each other. This paves the way towards the correspondence within the linear response framework between a perturbative parameter $\nabla\phi$ and the perturbative parameter $\nabla T/T$.

3.1.2 Classical Tolman-Ehrenfest temperature derivation

In order to understand the consequences of anomalies on the Tolman-Ehrenfest formula, it is interesting to reconsider R. Tolman and P. Ehrenfest original derivation of the equilibrium temperature profile in a curved spacetime [7]. Let us consider the thermodynamics of a D+1 dimensional relativistic gas in the background of a static gravitational potential with metric

$$g_{\mu\nu}(t,x) = \begin{pmatrix} g_{00}(\vec{x}) & 0 \\ 0 & g_{ij}(\vec{x}) \end{pmatrix}\,. \tag{3.8}$$

For a relativistic massless gas, the components of the momentum-energy tensor are related to the local energy density ε and pressure p as follows

$$\mathcal{T}^{\mu\nu} = (\varepsilon + p)u^\mu u^\nu - p g^{\mu\nu}\,, \tag{3.9}$$

where u^μ is the local $(D+1)$-velocity vector with $u^\mu u_\mu = +1$. Since these particles are massless, they propagate with the speed of light c. The temperature is then defined in the local frame where the spatial particle flow vanishes, $u^\mu = (1/\sqrt{g_{00}}, 0)$ such as the momentum-energy tensor (3.9) is diagonal

$$\mathcal{T}^\mu_{\ \nu} = \begin{pmatrix} \varepsilon & 0 \\ 0 & -p\ \mathbb{1}_D \end{pmatrix}\,. \tag{3.10}$$

In such a metric, momentum-energy tensor conservation can be rewritten as

$$\nabla_\nu \mathcal{T}^\nu_{\ \mu} \equiv \frac{1}{\sqrt{-g}}\frac{\partial}{\partial x^\nu}\left(\mathcal{T}^\nu_{\ \mu}\sqrt{-g}\right) - \frac{1}{2}\frac{\partial g_{\alpha\beta}}{\partial x^\mu}\mathcal{T}^{\alpha\beta} - \frac{1}{2}\frac{\partial g_{\mu\alpha}}{\partial x^\nu}\left[\mathcal{T}^{\nu\alpha} - \mathcal{T}^{\alpha\nu}\right] = 0. \tag{3.11}$$

Energy conservation, given by (3.11) with the index $\mu = 0$, is automatically fulfilled in the stationnary limit ($\partial_t \varepsilon = \partial_t p = 0$) for the static metric (3.8), while momentum conservation ($\mu \in [1, D]$) gives, in the notation of (3.10), a nontrivial relation [7]:

$$g_{00} \frac{\partial p}{\partial x_i} = -\frac{\varepsilon + p}{2} \frac{\partial g_{00}}{\partial x_i} \,. \tag{3.12}$$

For the relativistic gas of classical massless particles, the conformal anomaly is absent, and the scale symmetry implies a vanishing trace of the momentum-energy tensor and the following conformal equation of state in D+1 dimensions

$$\varepsilon = D.p \,. \tag{3.13}$$

This equation allows us to rewrite the conservation law (3.12) in terms of pressure only as

$$(g_{00})^{\frac{D+1}{2}} \; p = Cst \,. \tag{3.14}$$

Let us now deduce the temperature from this expression of the pressure. From the thermodynamic relation $dE = TdS - pdV$, we deduce the relation between densities

$$\varepsilon = \left.\frac{dE}{dV}\right|_T = T \left.\frac{dS}{dV}\right|_V - p \;\Rightarrow\; \varepsilon + p = T \left.\frac{dS}{dV}\right|_T = T \left.\frac{dp}{dT}\right|_V \,. \tag{3.15}$$

Combining this relation with (3.13), we get

$$(d+1)p = T \left.\frac{dp}{dT}\right|_V \,. \tag{3.16}$$

By integration of the above equation, we get the expression of the pressure and the energy density as a function of the temperature

$$p = \lambda \; T^{d+1} \tag{3.17}$$

$$\varepsilon = \lambda d \; T^{d+1} \tag{3.18}$$

with λ a constant. For example, considering a photon gas, in 3+1 dimension, we recover the Stefan-Boltzmann law $\epsilon = \sigma T^4$ with $\sigma = 3\lambda = \frac{\pi^2 k_B^4}{60 c^3 \hbar^3}$ [139–141].

Together with (3.14), these relations between pressure and temperature lead to the expression of the Tolman-Ehrenfest temperature:

$$T_{\text{TE}}^2 . g_{00} = Cst \tag{3.19}$$

Neither Luttinger's nor Tolman-Ehrenfest's relations account for possible quantum anomalies. The goal of this section is to show how these relations, widely used to identify the energy density and energy current of matter fields [130–132,142–145], are modified in the presence of anomalies.

Since anomalies strongly depend on the problem's dimensionality, we will restrict ourselves to the 1+1 dimensional case in the following discussions. Such discussions will naturally apply to the effective dynamics in reduced 1+1 dimension of quantum wires but also of rotationally invariant systems such as isotropic black holes, edge states of 2+1 dimensional topological gapped states of matter, or higher-dimensional systems in a strong magnetic field.

3.1.3 Tolman-Ehrenfest temperature and momentum-energy tensor in 1+1 dimensions

Since in the following sections our discussions are mainly dedicated to 1+1 dimensional systems, here we will discuss in greater detail the links between Tolman-Ehrenfest temperature and momentum-energy tensor, generalizing the previous discussion to chiral particles. Let us consider a $1+1$ dimensional space with coordinates $x^\mu = (x^0, x^1) \equiv (v_F t, x)$ and a general metric[1],

$$ds^2 \equiv g_{\mu\nu} dx^\mu dx^\nu = f_1(x) v_F^2 dt^2 - f_2(x)\, dx^2, \tag{3.20}$$

defined in terms of two time-independent, real, and positive-valued functions $f_{1,2}(x)$ of the one-dimensional spatial coordinate. For convenience, we included the Fermi velocity v_F of massless particles in the definition of the metric (3.20). In particular, the Luttinger metric (3.6) is recovered by considering the metric in the Fermi coordinate system:

$$f_1 \equiv g_{00} = e^{2\phi} \;;\; f_2 \equiv -g_{xx} = 1\,. \tag{3.21}$$

This choice corresponds to a general relativistic generalization of an inertial coordinate frame [146]. Note that a black-hole metric defined in section 1.1.4 can also be captured by (3.20) by setting $f_1 = 1/f_2 = f$ with f vanishing linearly at the horizon.

We consider massless relativistic particles propagating with velocity v_F in the curved 1+1 dimensional spacetime with metric (3.20). Energy and momentum densities of these particles and their associated current densities are encoded in the momentum-energy tensor $\mathcal{T}_{\mu\nu}$. As discussed in section 2.3, the scale invariance of the theory implies that its trace vanishes:

$$\mathcal{T}^\mu_{\ \mu} = 0. \tag{3.22}$$

The diagonal components of this momentum-energy tensor are the energy density $\varepsilon = \mathcal{T}^0_{\ 0}$ and the pressure $p = -\mathcal{T}^x_{\ x}$. Hence, scale invariance implies the equality

$$p = \varepsilon \tag{3.23}$$

The Lorentz invariance implies the symmetry of the momentum-energy tensor:

$$\mathcal{T}^{\mu\nu} = \mathcal{T}^{\nu\mu}, \tag{3.24a}$$

manifesting that the density of the energy current $J_\varepsilon = v_F \sqrt{-g}\mathcal{T}^{x0}$ is proportional to the momentum density $\Pi = \frac{1}{v_F}\sqrt{-g}\mathcal{T}^{0x}$:

$$J_\varepsilon = v_F^2 \Pi\,. \tag{3.24b}$$

Finally, spacetime translation invariance implies the conservation of this tensor at the classical level:

$$\nabla_\nu \mathcal{T}^\nu_{\ \mu} \equiv \frac{1}{\sqrt{-g}} \frac{\partial}{\partial x^\nu} \left(\mathcal{T}^\nu_{\ \mu} \sqrt{-g} \right) - \frac{1}{2} \frac{\partial g_{\alpha\beta}}{\partial x^\mu} \mathcal{T}^{\alpha\beta} - \frac{1}{2} \frac{\partial g_{\mu\alpha}}{\partial x^\nu} \left[\mathcal{T}^{\nu\alpha} - \mathcal{T}^{\alpha\nu} \right] = 0\,, \tag{3.24c}$$

or in other words, written in terms of ε, p, J_ε and Π:

$$\begin{cases} \partial_t \left(\sqrt{f_1 f_2}\, \varepsilon \right) + \partial_x \left(f_1\, J_\varepsilon \right) + \frac{1}{2} \left(v_F^2\, \Pi - J_\varepsilon \right) \partial_x f_1 = 0\,, & \text{(Energy conservation)} \\ \partial_t \left(\sqrt{f_1 f_2}\, \Pi \right) + \partial_x \left(f_1\, p \right) + \frac{1}{2} \left(\varepsilon - p \right) \partial_x f_1 = 0\,. & \text{(Momentum conservation)} \end{cases} \tag{3.24d}$$

[1] Even though, as described in our previous chapter, every 1+1 dimensional stationary metric is equivalent, up to a change of variable, to a conformally flat spacetime with metric $g_{\mu\nu} = e^{W(x)}\eta_{\mu\nu}$, here, I make the choice of keeping the original, "physical" coordinates (t, x) since it will help in the understanding of the thermodynamic quantities.

A general stationary solution of equations (3.24) is given by

$$[\mathcal{T}(x)]^{\mu}{}_{\nu} = \begin{pmatrix} \frac{C_0}{f_1} & \frac{C_1}{\sqrt{f_1 f_2}} \\ -\frac{f_2}{f_1}\frac{C_1}{\sqrt{f_1 f_2}} & -\frac{C_0}{f_1} \end{pmatrix}, \tag{3.25}$$

where C_0, C_1 are two constants. If we restrict ourselves to massless particles at equilibrium with a single local temperature, the only scale of energy density or pressure is set by this equilibrium temperature through the extended Stefan-Boltzmann law [147–150]: The energy density ε is obtained by summing the independent contributions $\varepsilon_\pm$ of left and right moving particles with respective central charges $\mathcal{C}_\pm$

$$\varepsilon = \varepsilon_+ + \varepsilon_-\,, \quad \varepsilon_\pm = \frac{1}{2}\mathcal{C}_\pm \gamma T^2\,, \quad \gamma = \frac{\pi k_B^2}{6\hbar v_F}\,. \tag{3.26}$$

Comparison with the diagonal terms of (3.25) leads to the relation

$$\frac{C_0}{f_1(x)} = \mathcal{T}^0_{\ 0} \equiv \varepsilon = -\mathcal{T}^x_{\ x} \equiv p\,. \tag{3.27}$$

The solution of equations (3.26,3.27) satisfies

$$T^2_{\text{TE}}(x) f_1(x) = \frac{2C_0}{\gamma(\mathcal{C}_+ + \mathcal{C}_-)} \tag{3.28}$$

which is independent of x. This turns out to be exactly the definition by Tolman and Ehrenfest of the equilibrium temperature. (3.7):

$$T_{\text{TE}} = T_0 \sqrt{\frac{f_1(x_0)}{f_1(x)}}, \tag{3.29}$$

where $T_0 = T(x_0)$ is an arbitrary reference temperature, conveniently chosen at the position where the metric is locally flat with $f_1(x_0) = 1$.

Alternatively, we can obtain this relation from the off-diagonal components of equation (3.25):

$$J_\varepsilon \equiv v_F \sqrt{-g}\mathcal{T}^{x0} = v_F \frac{C_1}{f_1} \quad \text{and} \quad \Pi \equiv \frac{1}{v_F}\sqrt{-g}\mathcal{T}^{0x} = \frac{1}{v_F}\frac{C_1}{f_1}\,. \tag{3.30}$$

During their ballistic evolution, right and left-moving particles do not exchange energies with each other. Each chiral species allows us to define the local temperature through its local equilibrium chiral currents $J_{\varepsilon,\pm} = \pm v_F\, \varepsilon_\pm$. Combining this definition with equations (3.26) and (3.30), we again recover the Tolman-Ehrenfest relation (3.29). The net equilibrium current vanishes unless $\mathcal{C}_+ \neq \mathcal{C}_-$, for which we obtain a density of energy current

$$J_\varepsilon = (\mathcal{C}_+ - \mathcal{C}_-)\frac{\gamma v_F}{2} T^2 = (\mathcal{C}_+ - \mathcal{C}_-)\frac{\pi}{12\hbar}(k_B T)^2\,, \tag{3.31}$$

and, following (3.24a), a momentum density

$$\Pi = v_F^2 J_\varepsilon = \frac{\mathcal{C}_+ - \mathcal{C}_-}{2}\frac{\gamma}{v_F} T^2 = (\mathcal{C}_+ - \mathcal{C}_-)\frac{\pi}{12\hbar v_F^2}(k_B T)^2\,. \tag{3.32}$$

As a result, the equilibrium form of the classical momentum-energy tensor (3.25) is expressed as follows:

$$[\mathcal{T}_{\text{cl}}(x)]^{\mu}{}_{\nu} = \begin{pmatrix} \mathcal{C}_w & \mathcal{C}_g\sqrt{\frac{f_1}{f_2}} \\ -\mathcal{C}_g\sqrt{\frac{f_2}{f_1}} & -\mathcal{C}_w \end{pmatrix} \times \frac{\gamma}{2} T^2_{\text{TE}}(x) \tag{3.33}$$

where we denoted

$$\mathcal{C}_w = \mathcal{C}_+ + \mathcal{C}_-\,, \qquad \mathcal{C}_g = \mathcal{C}_+ - \mathcal{C}_-\,. \tag{3.34}$$

3.2 Gravitational anomalies and anomalous Tolman-Ehrenfest temperature

We realize that previous computations of the Tolman-Ehrenfest temperature heavily rely on the concept of symmetry (see (3.24)). However, as we have seen in the previous chapter, in the presence of spacetime curvature, it is impossible to regularize the theory in a way that keeps all three symmetries conserved. It is, therefore, logical to look for a generalization of Tolman-Ehrenfest in the presence of such anomalies.

3.2.1 Anomalies at play

In the previous section, we discussed the anomalies present in 1+1 dimensional systems 2.3.3. Here, we will quickly review them in the specific case of the metric of Eq. (3.20), in terms of the thermodynamics quantities. Since gravitational anomalies can equivalently be written for Lorentz-breaking, Einstein-breaking, and covariantly conserved momentum-energy tensors, in this section, we will choose to present all computations for the Lorentz-breaking case, sometimes providing their expressions in the case of a covariantly conserved tensor.

The (non-)conservation equations satisfied by our momentum-energy tensor are, therefore:

- The Lorentz symmetry
$$\mathcal{T}^{\mu\nu} = \mathcal{T}^{\nu\mu} \tag{3.35a}$$
- The Einstein anomaly
$$\nabla_\mu \mathcal{T}^{\mu\nu} = \frac{\hbar v_F}{96\pi} \frac{\mathcal{C}_g}{\sqrt{-\det\left(g_{\rho\sigma}\right)}} \varepsilon^{\nu\mu} \nabla_\mu \mathcal{R}\,, \tag{3.35b}$$
with $\varepsilon^{0x} = 1$.
- The trace anomaly
$$\mathcal{T}^{\mu}_{\ \mu} = \mathcal{C}_w \frac{\hbar v_F}{48\pi} \mathcal{R}\,. \tag{3.35c}$$

where $\mathcal{R}$ stands for the Ricci scalar, which for the metric (3.20) simplifies to

$$\mathcal{R} = \frac{\partial_x^2 f_1}{f_1 f_2} - \frac{1}{2}\frac{\partial_x f_1}{f_1 f_2}\left[\frac{\partial_x f_1}{f_1} + \frac{\partial_x f_2}{f_2}\right]. \tag{3.36}$$

In terms of the thermodynamic quantities, these equations simplify to

$$\begin{cases} v_F^2 \Pi = J_\varepsilon\,, \\ \varepsilon - p = \mathcal{C}_w \frac{\hbar v_F}{48\pi}\mathcal{R}\,, \\ \partial_t\left(\sqrt{f_1 f_2}\,\varepsilon\right) + \partial_x\left(f_1\, J_\varepsilon\right) = \mathcal{C}_g \frac{\hbar v_F^2}{96\pi} f_1 \partial_x \mathcal{R}\,, \\ \partial_t\left(\sqrt{f_1 f_2}\,\Pi\right) + \partial_x\left(f_1\, p\right) = -\mathcal{C}_w \frac{\hbar v_F}{96\pi}\mathcal{R}\partial_x f_1\,. \end{cases} \tag{3.37}$$

Similarly, in the case of the covariantly conserved momentum-energy tensor, the (non-)conservation equations take the form

$$\begin{cases} v_F^2 \tilde{\Pi} - \tilde{J}_\varepsilon = \mathcal{C}_g \frac{\hbar v_F^2}{48\pi}\mathcal{R}\,, \\ \tilde{\varepsilon} - \tilde{p} = \mathcal{C}_w \frac{\hbar v_F}{48\pi}\mathcal{R}\,, \\ \partial_t\left(\sqrt{f_1 f_2}\,\tilde{\varepsilon}\right) + \partial_x\left(f_1\, \tilde{J}_\varepsilon\right) = -\mathcal{C}_g \frac{\hbar v_F^2}{96\pi}\mathcal{R}\partial_x f_1\,, \\ \partial_t\left(\sqrt{f_1 f_2}\,\tilde{\Pi}\right) + \partial_x\left(f_1\, \tilde{p}\right) = -\mathcal{C}_w \frac{\hbar v_F}{96\pi}\mathcal{R}\partial_x f_1\,. \end{cases} \tag{3.38}$$

3.2.2 Anomalous Tolman-Ehrenfest temperature

As shown in section 3.1.3, the equilibrium temperature for massless matter in curved spacetime can be consistently defined in two different ways. (i) It can be defined using thermodynamic quantities, the energy density (ε), and pressure (p), provided by the diagonal components of the momentum-energy tensor. (ii) It can be defined from kinematic quantities, the density of energy current (J_ε) and momentum (Π) of left and right movers, given by the off-diagonal components of the momentum-energy tensor. At the quantum level, in the stationary limit, diagonal and off-diagonal components get independently corrected by the scale anomaly and the Einstein - Lorentz anomalies, respectively. This immediately raises the question of whether a revised Tolman-Ehrenfest temperature can be defined by incorporating the effects of quantum fluctuations. Quite remarkably, in this section, we show that all three gravitational anomalies, while of different technical origins, concur to redefine the equilibrium temperature coherently, leading to an extended notion of Tolman-Ehrenfest temperature.

Anomalous symmetric momentum-energy tensor.

Solving equations (3.35) or equivalently (3.37) for a symmetric, stationary tensor, we obtain

$$\mathcal{T} = \mathcal{T}_{\rm cl} + \mathcal{T}_{\rm q}\,, \tag{3.39}$$

where $\mathcal{T}_{\rm cl}$ is the classical momentum-energy tensor given by Eq. (3.33) and the quantum correction components are

$$[\mathcal{T}_{\rm q}(x)]^{\mu}_{\ \nu} = \begin{pmatrix} \frac{\mathcal{C}_w}{2}\left(\varepsilon_q^{(1)} + \varepsilon_q^{(2)}\right) & \frac{\mathcal{C}_g}{2}\sqrt{\frac{f_1}{f_2}}\varepsilon_q^{(2)} \\ -\frac{\mathcal{C}_g}{2}\sqrt{\frac{f_2}{f_1}}\varepsilon_q^{(2)} & \frac{\mathcal{C}_w}{2}\left(\varepsilon_q^{(1)} - \varepsilon_q^{(2)}\right) \end{pmatrix}, \tag{3.40}$$

where $\varepsilon_q^{(1)}$ and $\varepsilon_q^{(2)}$ are the two new scales of energy density set by the quantum anomalies:

$$\varepsilon_q^{(1)} = \frac{\hbar v_F}{48\pi}\mathcal{R}\ ; \qquad \varepsilon_q^{(2)} = \frac{\hbar v_F}{48\pi}(\mathcal{R} - 2\bar{\mathcal{R}})\ , \tag{3.41}$$

with

$$\bar{\mathcal{R}} = \frac{1}{2f_1(x)}\int_{x_0}^{x} \mathrm{d}y\ \mathcal{R}(y)\partial_y f_1(y)\,. \tag{3.42}$$

With the help of the expression (3.36) for the curvature $\mathcal{R}$, we obtain

$$\bar{\mathcal{R}} = \frac{1}{4f_2}\left(\frac{\partial_x f_1}{f_1}\right)^2\,, \tag{3.43}$$

or in other words

$$\mathcal{R} - 2\bar{\mathcal{R}} = \frac{\partial_x^2 f_1}{f_1 f_2} - \frac{\partial_x f_1}{f_1 f_2}\left(\frac{\partial_x f_1}{f_1} + \frac{1}{2}\frac{\partial_x f_2}{f_2}\right)\,. \tag{3.44}$$

Anomalous temperature

Let us now focus on the explicit expression of the momentum-energy tensor corrected by the gravitational anomalies $\mathcal{T} = \mathcal{T}_{\rm cl} + \mathcal{T}_{\rm q}$ with both components given in equations (3.33) and (3.40)). Using the definition of the thermodynamic quantities (3.27) and currents (3.30) in

terms of the momentum-energy tensor, we obtain the expression for the density of energy, pressure, momentum, and energy current:

$$\varepsilon = \frac{1}{2}\mathcal{C}_w \left(\gamma T^2(x) + \varepsilon_q^{(1)}\right) \ , \tag{3.45a}$$

$$p = \frac{1}{2}\mathcal{C}_w \left(\gamma T^2(x) - \varepsilon_q^{(1)}\right) \ , \tag{3.45b}$$

$$J_\varepsilon = v_F^2 \Pi = \mathcal{C}_g \gamma \, v_F \, k_B^2 T^2(x) \ . \tag{3.45c}$$

with

$$\gamma T^2(x) = \gamma T_{\text{TE}}^2 + \varepsilon_q^{(2)} \, , \tag{3.46}$$

Remarkably, only two scales of energy set these values: the anomalous temperature $T(x)$, which incorporates $\varepsilon_q^{(2)}$ as we will see below in equation (3.49), and a quantum scale $\varepsilon_q^{(1)}$ defined in equation (3.41). The new scale $\varepsilon_q^{(1)}$ signals that in the presence of gravitational anomalies, the Stefan-Boltzmann law (3.26) is modified. The additive correction in (3.45a) signals a correction to the vacuum energy density at $T = 0$. This energy shift of pure geometrical origin is set by the local spacetime curvature $\mathcal{R}$. This local energy shift looks akin to the Casimir effect set by confinement [135], for which, at low temperatures in flat spacetime, we get

$$\varepsilon = \frac{1}{2}\mathcal{C}_w \left(\gamma T^2 - \varepsilon_L\right) \ , \tag{3.47a}$$

$$p = \frac{1}{2}\mathcal{C}_w \left(\gamma T^2 - \varepsilon_L\right) \ , \tag{3.47b}$$

with

$$\varepsilon_L = \frac{\pi \hbar v_F}{24 L^2} \, , \tag{3.48}$$

the Casimir energy density set by the confinement length L. However, as opposed to the Casimir effect (3.47), the geometrical effect (3.45) renormalizes pressure p and energy density ε with opposite magnitudes.

The temperature $T(x)$ is now set by the sum $\varepsilon + p = T.s = C_w \gamma \, T^2$, where s denotes the entropy density. Equivalently, for each chiral branch of particles, this temperature can be deduced from the off-diagonal components of the momentum-energy tensor, the energy current, and momentum in Eq. (3.45c). While the diagonal components of $\mathcal{T}$ including $\varepsilon + p$ are corrected by the trace anomaly, the off-diagonal components J_ε and Π are corrected by the Einstein anomaly. Yet, the same temperature is defined consistently from both diagonal and off-diagonal quantities. Both the trace and Einstein anomalies contribute coherently to correct the Tolman-Ehrenfest temperature into a generalized equilibrium temperature

$$\gamma T^2(x) = \gamma T_{\text{TE}}^2 + \varepsilon_q^{(2)} \, , \tag{3.49}$$

where the additive quantum correction $\varepsilon_q^{(2)}$ is defined in equation (3.41).
Note that in defining this temperature, we restricted ourselves to the natural case where the entropy density s is positive, which warrants that the right-hand side of Eq. (3.49) is positive, and hence the temperature is well defined.

Anomalous covariantly conserved momentum-energy tensor.

As we discussed in both section 3.2.1 and 2.3.3, the pure Einstein anomaly and its symmetric momentum-energy tensor can be traded for a theory breaking both Einstein and Lorentz anomaly but defining a covariantly conserved momentum-energy tensor, at the expense of a

transformation (2.92) of the momentum-energy tensor [127]. The corresponding quantum correction to the momentum-energy tensor is now expressed as

$$[\tilde{\mathcal{T}}_{\rm q}(x)]^{\mu}{}_{\nu} = \begin{pmatrix} \frac{\mathcal{C}_w}{2}\left(\varepsilon_q^{(1)}+\varepsilon_q^{(2)}\right) & \frac{\mathcal{C}_g}{2}\sqrt{\frac{f_1}{f_2}}\left(\varepsilon_q^{(2)}-\varepsilon_q^{(1)}\right) \\ -\frac{\mathcal{C}_g}{2}\sqrt{\frac{f_2}{f_1}}\left(\varepsilon_q^{(1)}+\varepsilon_q^{(2)}\right) & \frac{\mathcal{C}_w}{2}\left(\varepsilon_q^{(1)}-\varepsilon_q^{(2)}\right) \end{pmatrix} . \tag{3.50}$$

In this case, the momentum-energy tensor is no longer symmetric. Consequently, the momentum density Π and the density of energy current J_ε are now distinct quantities. The chiral currents and momenta satisfy $J_{\varepsilon,\pm} = \pm v_F\ p_\pm$ and $\Pi_\pm = \pm\frac{1}{v_F}\ \varepsilon_\pm$ corresponding to the expressions

$$\varepsilon = \frac{1}{2}\mathcal{C}_w\left(\gamma T^2(x) + \varepsilon_q^{(1)}\right) , \tag{3.51a}$$

$$p = \frac{1}{2}\mathcal{C}_w\left(\gamma T^2(x) - \varepsilon_q^{(1)}\right) , \tag{3.51b}$$

$$v_F^{-1} J_\varepsilon = \frac{1}{2}\mathcal{C}_g\left(\gamma T^2(x) - \varepsilon_q^{(1)}\right) , \tag{3.51c}$$

$$v_F \Pi = \frac{1}{2}\mathcal{C}_g\left(\gamma T^2(x) + \varepsilon_q^{(1)}\right) . \tag{3.51d}$$

3.2.3 Temperature, thermodynamics, and trace anomalies

At this level, even though both diagonal and off-diagonal components of the momentum-energy tensor point toward a same definition of temperature (3.49), a natural question is whether this definition is coherent with the thermodynamic notion of temperature.
To address this question, let us reconsider the derivation of the relationship between energy density ε, pressure p, and temperature from section 3.1.2 but now in the presence of a non-zero trace. From the thermodynamic relation $dE = TdS - pdV$, we deduce the relation between densities

$$\varepsilon = \left.\frac{dE}{dV}\right|_T = T\left.\frac{dS}{dV}\right|_V - p \ \Rightarrow\ \varepsilon + p = T\left.\frac{dS}{dV}\right|_T = T\left.\frac{dp}{dT}\right|_V . \tag{3.52}$$

In $D+1$ dimensions, the trace of the momentum-energy tensor $\mathcal{T}^\mu{}_\mu$ is expressed in terms of the energy density ε and pressure p as $\varepsilon = D\ p + \mathcal{T}^\mu{}_\mu$. In $1+1$ dimension, this trace is defined in (3.35c) in terms of an energy density $\varepsilon_q^{(1)}$ of (3.41) as $\mathcal{T}^\mu{}_\mu = C_w\varepsilon_q^{(1)}$. Combining this relation with (3.52), we get

$$(D+1)p + \mathcal{T}^\mu{}_\mu = T\left.\frac{dp}{dT}\right|_V . \tag{3.53}$$

Given that $\mathcal{T}^\mu{}_\mu$ is independent of the temperature, by integration of the above equation, we get

$$p = \lambda\ T^{D+1} - \frac{1}{D+1}\mathcal{T}^\mu{}_\mu \tag{3.54}$$

$$\varepsilon = \lambda D\ T^{D+1} + \frac{1}{D+1}\mathcal{T}^\mu{}_\mu \tag{3.55}$$

These relations identify with the equations (3.45) for $D = 1$.

Let us now consider the entropy density of the system, defined as $s = (E+F)/(TV) = (\varepsilon + p)/T$. From equations (3.54), and (3.55) we get

$$s = \lambda(D+1)T^D \tag{3.56}$$

$$= \lambda(D+1)\left(\frac{\varepsilon}{\lambda D} - \frac{1}{\lambda D(D+1)}\mathcal{T}^\mu{}_\mu\right)^{\frac{D}{D+1}} \tag{3.57}$$

Temperature and entropy are related through the relation $T^{-1} = ds/d\varepsilon$. Indeed, we check that the temperature entering the relations (3.54,3.55) satisfy this equality:

$$\frac{ds}{d\varepsilon} = \left(\frac{\varepsilon}{\lambda D} - \frac{1}{\lambda D(D+1)} \mathcal{T}^{\mu}_{\ \mu} \right)^{-\frac{1}{D+1}} = \frac{1}{T} \, . \tag{3.58}$$

Specifying these relations to $D = 1$, from the equations (3.45a,3.45b), the entropy reads $s = (\varepsilon + p)/T = 2\gamma T = 2\sqrt{\gamma(\varepsilon - \varepsilon_q^{(1)})}$. From this, we check that $ds/d\varepsilon = \sqrt{\gamma/(\varepsilon - \varepsilon_q^{(1)})} = 1/T$. This shows that whenever a temperature can be defined through the relations (3.17,3.18), it can be associated with standard thermodynamics with a positive entropy[2].

3.3 Anomalous Luttinger equivalence and response theory

As discussed earlier in this chapter, the notion of Luttinger's trick is directly related to the notion of Tolman-Ehrenfest temperature. Since this notion evolves in the presence of anomalies, it is logical to study the corrections that such anomalies bring to Luttinger's equivalence. This study will be two-fold. First, we will deduce the anomalous Luttinger relation from the anomalous Tolmann-Ehrenfest temperature (3.49) before showing how one could have deduced it straightforwardly from response theory.

3.3.1 Anomalous Luttinger relation

Anomalous Luttinger relation

By inserting the Luttinger metric, defined as $f_1 = e^{2\phi}$ and $f_2 = 1$, in equation (3.41), anomalous energy scales turn out to be

$$\varepsilon_q^{(1)} = \frac{\hbar v_F}{24\pi} \left[\partial_x^2 \phi + (\partial_x \phi)^2 \right] \; ; \quad \varepsilon_q^{(2)} = \frac{\hbar v_F}{24\pi} \partial_x^2 \phi, \tag{3.59}$$

such that the corresponding Tolman-Ehrenfest temperature is corrected by a second derivative of the gravitational potential ϕ:

$$\frac{T^2(x)}{T_0^2} = e^{-2\phi(x)} + \lambda_{T_0}^2 \partial_x^2 \phi \, , \qquad \lambda_T = \frac{\hbar v_F}{2\pi k_B T} \, , \tag{3.60}$$

where T_0 is the reference temperature introduced in equation (3.1) and (3.29), chosen as $T_0 = T(x_0)$ at a point x_0 such that $\phi(x_0) = \partial_x^2 \phi(x_0) = 0$.

Multiplying equation (3.60) by $T_0^2 e^{2\phi}$ and then differentiating with x we obtain a correction to the original Luttinger relation (3.5) by an additional term induced by quantum anomalies:

$$\underbrace{\frac{\partial_x T}{T} = -\partial_x \phi}_{\text{Original relation}} + \underbrace{\lambda_T^2(x) \left[(\partial_x \phi) \, \partial_x^2 \phi + \frac{1}{2} \partial_x^3 \phi \right]}_{\text{Quantum correction}} \, . \tag{3.61}$$

Notice that since the equilibrium temperature $T(x)$ is inhomogeneous, the thermal length λ_T is a coordinate-dependent quantity.

[2] In this thesis, following the relation (3.49), having a positive entropy corresponds to following the condition $\gamma T_{\mathrm{TE}}^2 - \varepsilon_q^{(2)} > 0$. The fate of a system escaping this condition goes beyond the scope of our study.

Luttinger's momentum-energy tensors

The energy density, pressure, energy currents, and momentum are provided by equations. (3.45) and (3.51). By using the explicit expression (3.59) for the corrections, we get

$$\varepsilon = \frac{\mathcal{C}_w}{2}\left[\gamma T_0^2 e^{-2\phi(x)} + \frac{\hbar v_F}{12\pi}\,\partial_x^2\phi + \frac{\hbar v_F}{24\pi}(\partial_x\phi)^2\right]\,, \tag{3.62a}$$

$$p = \frac{\mathcal{C}_w}{2}\left[\gamma T_0^2 e^{-2\phi(x)} - \frac{\hbar v_F}{24\pi}(\partial_x\phi)^2\right]\,, \tag{3.62b}$$

$$J_\varepsilon = v_F^2\Pi = \mathcal{C}_g\,\left[\frac{\pi}{12\hbar}(k_B T_0)^2 e^{-2\phi(x)} + \frac{\hbar v_F^2}{48\pi}\partial_x^2\phi\right]\,, \tag{3.62c}$$

when Lorentz invariance (symmetry) is enforced.

Alternatively, if we relax Lorentz invariance while imposing the covariant conservation of the momentum-energy tensor, the thermal current and momentum no longer identify with each other and are expressed as

$$J_\varepsilon = \mathcal{C}_g\,\left[\frac{\pi}{12\hbar}(k_B T_0)^2 e^{-2\phi(x)} - \frac{\hbar v_F^2}{48\pi}(\partial_x\phi)^2\right], \tag{3.63a}$$

$$v_F^2\Pi = \mathcal{C}_g\,\left[\frac{\pi}{12\hbar}(k_B T_0)^2 e^{-2\phi(x)} + \frac{\hbar v_F^2}{48\pi}\left(2\partial_x^2\phi + (\partial_x\phi)^2\right)\right]\,. \tag{3.63b}$$

Luttinger's relations for a constant temperature profile

Because of the nonlinearity of the anomalous Luttinger relation (3.60) and (3.61) between temperature and gravitational potential ϕ, a fixed temperature profile $T(x)$ corresponds to a continuum of fields $\phi(x)$, contrarily to the case of the standard Luttinger relation (3.7) or (3.5). This leads to additional freedom in the choice of ϕ for a given profile, typically imposed by additional boundary conditions. It is, therefore, natural to analyze these equations and their solution for different temperature profiles.

A first natural analysis concerns the case of a constant temperature profile. The standard Luttinger relation (3.7) imposes a coordinate-independent gravitational potential $\phi = Cst$. In contrast, the anomalous relation (3.61) allows a constant temperature to be realized in a weak field limit ($|\phi| \ll 1$) by a class of dilation fields of the form:

$$\phi(x) = \phi_0 + \phi_+ e^{\sqrt{2}x/\lambda_{T_0}} + \phi_- e^{-\sqrt{2}x/\lambda_{T_0}}\,, \tag{3.64}$$

valid provided the anomalous corrections to equation (3.64) are small, subjected to the condition $|x| \ll \lambda_{T_0}$. The arbitrary coefficients $\phi_\pm$ highlight the degeneracy of the gravitational "zero modes" (3.64), which parametrizes the anomalous isothermal surfaces in the metric space. Note that in the case of a finite system with periodic boundary conditions, imposing the smoothness of the gravitational potential allows to recover a unique gravitational potential $\phi(x) = \phi_0 = Cst$.

Relaxing the weak field limit, the anomaly-corrected Luttinger relation (3.61) translates into a nonlinear differential equation for the gravitational "zero modes" or equivalently for a constant temperature profile:

$$\partial_\xi^3\phi + 2\partial_\xi\phi\;\partial_\xi^2\phi - 2\partial_\xi\phi = 0\,, \tag{3.65}$$

where we introduced the rescaled coordinate $\xi = x/\lambda_{T_0}$. This third-order differential equation (3.65) on ϕ possesses one trivial degeneracy corresponding to a global coordinate-independent shift of the gravitational potential $\phi \to \phi + \phi_0$. On top of this trivial degeneracy, this equation possesses two physically meaningful degeneracies labeling the space of possible zero modes, each one labeled by the value of the first and second derivatives of the field ϕ at a spatial reference point x_0. Hence, a unique choice of field $\phi(x)$ for a given profile $T(x)$ requires fixing these higher derivatives with boundary conditions, such as periodic boundary conditions on smooth fields.

Perturbative solution for Luttinger's relations in the case of a constant temperature gradient

For experimental purposes, it is interesting to solve Luttinger's relation for a system weakly out of equilibrium, i.e., characterized by a temperature profile

$$T(x) = T_0(1 + a\ \tau(x)). \tag{3.66}$$

with $a \ll 1$.

We consider a region of size L in the bulk of a thermal conductor away from boundaries. Setting $\tau(\pm L/2) = \pm 1/2$, we get $T_0 = (T_L + T_R)/2, a = 2(T_R - T_L)/(T_R + T_L)$ where $T_L = T(-L/2), T_R = T(+L/2)$. We wish to derive both the gravitational potential ϕ and the momentum-energy tensor components perturbatively in the parameter a. First, this amounts to identifying the gravitational potential ϕ equivalent to this temperature profile, which satisfies

$$\frac{T^2(x)}{T_0^2} = e^{-2\phi(x)} + \lambda_{T_0}^2 \partial_x^2 \phi(x)\,, \tag{3.67}$$

with a thermal lengthscale $\lambda_{T_0} = \frac{\hbar v_F}{2\pi k_B T_0}$.

A generic solution $\phi(x) = \sum_{n=0}^{\infty} a^n \phi^{(n)}(x)$ of eq. (3.67) satisfies

$$\begin{aligned}\phi^{(n)}(x) = a_n \sinh\left(\sqrt{2}\,\frac{x}{\lambda_{T_0}}\right) + b_n \cosh\left(\sqrt{2}\,\frac{x}{\lambda_{T_0}}\right) \\ + \frac{1}{\sqrt{2}\lambda_{T_0}} \int_0^x \sinh\left(\sqrt{2}\,\frac{x-x'}{\lambda_{T_0}}\right) \alpha^{(n)}(x') dx'\ .\end{aligned} \tag{3.68}$$

With $\alpha^{(n)}$ a source term which is set by $\tau(x)$ and the lower orders $\phi^{(m)}$ with $m < n$.
For practical reasons, let us focus on a linear temperature profile, for which $\tau(x) = x/L$, such as $a \equiv L\partial_x T/T_0$. From (3.68) we get

$$\phi^{(1)}(x) = \left(a_1 + \frac{\lambda_{T_0}}{\sqrt{2}L}\right) \sinh\left(\sqrt{2}\,\frac{x}{\lambda_{T_0}}\right) + b_1 \cosh\left(\sqrt{2}\,\frac{x}{\lambda_{T_0}}\right) - \frac{x}{L}\ . \tag{3.69}$$

Imposing a finite gravitational potential in the thermodynamic limit $L \gg \lambda_{T_0}$ sets $a_1 = -\lambda_{T_0}/(\sqrt{2}L)$ and $b_1 = 0$, leading to $\phi^{(1)}(x) = -\,x/L$. Recursively, we get

$$\phi^{(1)}(x) = -\frac{x}{L}\,, \tag{3.70}$$

$$\phi^{(2)}(x) = \frac{1}{2L^2}\left(x^2 + \lambda_{T_0}^2\right)\,, \tag{3.71}$$

$$\phi^{(3)}(x) = \frac{1}{L^3}\left(-\frac{1}{3}x^3 - 2x\lambda_{T_0}^2\right)\,, \tag{3.72}$$

$$\phi^{(4)}(x) = \frac{1}{4L^4}\left(x^4 + 20x^2\lambda_{T_0}^2 + 21\lambda_{T_0}^4\right)\,, \tag{3.73}$$

which corresponds to $\phi(x) = \phi_{\text{Lutt}} + \delta\phi$ where $\phi_{\text{Lutt}} = -\ \ln(T_0/T(x))$ is the potential deduced from the standard Luttinger equivalence, and $\delta\phi$ encodes the modifications of this potential induced by the gravitational anomalies, corresponding to the last term on eq. (3.67):

$$\delta\phi = \frac{a^2}{2L^2}\lambda_{T_0}^2 - 2\frac{a^3}{L^2}x\lambda_{T_0}^2 + \frac{a^4}{4L^4}\left[20x^2\lambda_{T_0}^2 + 21\lambda_{T_0}^4\right] + \mathcal{O}(a^5)\ . \tag{3.74}$$

We now express the components of the momentum-energy tensor in the temperature profile (3.66) using the expression (3.74) of the equivalent gravitational potential. From equations (3.62,3.63), these components identify, in a Lorentz invariant situation, with

$$\varepsilon^+/\varepsilon_0 = T^2/T_0^2 + \varepsilon_q^{(1)}/(\gamma T_0^2)\,, \tag{3.75a}$$
$$p^+/\varepsilon_0 = T^2/T_0^2 - \varepsilon_q^{(1)}/(\gamma T_0^2)\,, \tag{3.75b}$$
$$J_\varepsilon^+/\varepsilon_0 = v_F^2\Pi^+/\varepsilon_0 = T^2/T_0^2 \tag{3.75c}$$

with

$$\varepsilon_0 = \gamma T_0^2/2\,. \tag{3.76}$$

The quantum anomaly corrections are encoded solely in $\varepsilon_q^{(1)} = \frac{\hbar v_F}{24\pi}\left[\partial_x^2\phi + (\partial_x\phi)^2\right]$, which induces a modification of the momentum-energy tensor components at non-linear order in the temperature gradient $a = L\partial_x T/T_0$. At this stage, we realize that $\delta\phi$ of equation (3.74) leads to a $\varepsilon_q^{(1)}$ at least of order $(a/L)^4$. Hence, to second order in the temperature gradient, we can neglect the modification of this gravitational potential due to the anomalous Luttinger relation. Inserting the bare Luttinger potential ϕ_{Lutt} in the expression (3.59) of $\varepsilon_q^{(1)}$, we obtain the following expression for the momentum-energy tensor components

$$\frac{\varepsilon^+}{\varepsilon_0} = 1 + 2x\ \frac{\partial_x T}{T_0} + \left[x^2 - 4\lambda_{T_0}^2\right]\left(\frac{\partial_x T}{T_0}\right)^2 + \mathcal{O}\left(\frac{\partial_x T}{T_0}\right)^3\ , \tag{3.77a}$$

$$\frac{p^+}{\varepsilon_0} = 1 + 2x\ \frac{\partial_x T}{T_0} + \left[x^2 + 4\lambda_{T_0}^2\right]\left(\frac{\partial_x T}{T_0}\right)^2 + \mathcal{O}\left(\frac{\partial_x T}{T_0}\right)^3\ , \tag{3.77b}$$

$$\frac{J_\varepsilon^+}{v_F\varepsilon_0} = \frac{v_F\Pi^+}{\varepsilon_0} = 1 + 2x\ \frac{\partial_x T}{T_0} + x^2\left(\frac{\partial_x T}{T_0}\right)^2\ , \tag{3.77c}$$

with a thermal lengthscale λ_{T_0} defined in (3.60) at the reference temperature T_0.

We note at this stage that the anomaly-related corrections to the thermodynamic corrections appear at nonlinear order in the temperature gradient $\partial_x T/T_0$.

Alternatively, in the case of a covariantly conserved momentum-energy tensor, the anomalous correction can be shown to be equal to $v_F\Pi^+/\varepsilon_0 = \varepsilon^+/\varepsilon_0 = T^2/T_0^2 + \varepsilon_q^{(1)}/(\gamma T_0^2)$; and $J_\varepsilon^+/(v_F\varepsilon_0)p^+/\varepsilon_0 = T^2/T_0^2 - \varepsilon_q^{(1)}/(\gamma T_0^2)$; or in other words, perturbatively in the thermal gradient,

$$\frac{v_F\Pi^+}{\varepsilon_0} = \frac{\varepsilon^+}{\varepsilon_0} = 1 + 2x\ \frac{\partial_x T}{T_0} + \left[x^2 - 4\lambda_{T_0}^2\right]\left(\frac{\partial_x T}{T_0}\right)^2 + \mathcal{O}\left(\frac{\partial_x T}{T_0}\right)^3\ , \tag{3.78a}$$

$$\frac{J_\varepsilon^+}{v_F\varepsilon_0} = \frac{p^+}{\varepsilon_0} = 1 + 2x\ \frac{\partial_x T}{T_0} + \left[x^2 + 4\lambda_{T_0}^2\right]\left(\frac{\partial_x T}{T_0}\right)^2 + \mathcal{O}\left(\frac{\partial_x T}{T_0}\right)^3\ . \tag{3.78b}$$

These expressions encode the effects of the gravitational anomaly within a regime of small thermal gradients. Note that it is nonlinear in thermal gradient $\nabla T/T_0$, although it originates from an expression linear in ϕ and its derivative. This illustrates that linear response theory in the gravitational potential ϕ can apply beyond the regime linear in $\partial_x T/T_0$.

3.3.2 Anomalous Luttinger response theory from perturbations

Since the correction arising in anomalous Luttinger currents (3.78) are linear in the gravitational potential, it is interesting to see how such corrections appear from response theory linear in the gravitational potential ϕ.
Hence, we consider a $D = 1 + 1$ chiral Dirac Hamiltonian in curved spacetime given by

$$\mathcal{H} = \int \mathrm{d}x \; e^{\phi(x)} \; \hat{h}_+(x), \tag{3.79}$$

where, in terms of second quantized fields $\Psi_+(x), \Psi_+^\dagger(x)$, the Hamiltonian density operator is

$$\hat{h}_+(x) = -\frac{i\hbar v_F}{2} \; \Psi_+^\dagger(x) \overset{\leftrightarrow}{\partial}_x \Psi_+(x). \tag{3.80}$$

where $\overset{\leftrightarrow}{\partial}_x = \overrightarrow{\partial_x} - \overleftarrow{\partial_x}$. We learned from Eqs. (3.63) that the energy density and momentum operators must be treated separately when accounting for quantum fluctuations. Indeed, the momentum

$$\Pi_+ = -\frac{i\hbar}{2} \langle \Psi_+^\dagger \overset{\leftrightarrow}{\partial}_x \Psi_+ \rangle = \frac{1}{v_F} \varepsilon_+ \tag{3.81}$$

identifies with the energy current

$$J_{\varepsilon,+} = \frac{i\hbar v_F}{2} e^{-\phi(x)} \langle \Psi_+^\dagger \overset{\leftrightarrow}{\partial}_t \Psi_+ \rangle = v_F p_+ \tag{3.82}$$

only for classical fields satisfying the equation of motion.

For simplicity, we focus here on the momentum density, which only involves the equal time Green's function:

$$\Pi_+(x) = \int \frac{\mathrm{d}k\mathrm{d}q}{(2\pi)^2} \; e^{iqx} \left\langle \Psi^\dagger_{+,k-\frac{q}{2}} \hbar \, k \Psi_{+,k+\frac{q}{2}} \right\rangle = -i \int \frac{\mathrm{d}k\mathrm{d}q}{(2\pi)^2} \frac{\mathrm{d}\omega}{2\pi} e^{iqx} \hbar \, k \, G^<_{k+\frac{q}{2},k-\frac{q}{2}}(\omega) \tag{3.83}$$

where the lesser green functions $G^<$ is defined by

$$G^<_{k,k'}(\omega) = i \int_0^\infty \mathrm{d}t \; e^{i\omega t} \langle \Psi^\dagger_{+,k}(0) \Psi_{+,k'}(t) \rangle. \tag{3.84}$$

Working in perturbation theory at first order in the gravitational potential $\phi(x)$, we expand the Green's function using the Dyson equation written schematically for a perturbation $H = H_0 + V$

$$G = G_0 + G_0 V G \, . \tag{3.85}$$

Since, in our case, $\hat{V}(x) = \hat{h}_+(x)\phi(x)$, we expand the Green's function

$$G^<_{k',k}(\omega) = (G_0^<)_{k',k} + \int \mathrm{d}x \; e^{i(k-k')x} \phi(x) \left(\left(G_0^R\right)_{k',k'} \hat{h}_{k',k} \, (G_0^<)_{k,k} + (G_0^<)_{k',k'} \, \hat{h}_{k',k} \left(G_0^A\right)_{k,k} \right) , \tag{3.86}$$

expressed in terms of the retarded Green's functions in flat spacetime

$$G^R_{k,k'}(\omega) = -i \int_0^\infty \mathrm{d}t \; e^{i\omega t} \langle \{ \Psi_k^\dagger(0), \Psi_{k'}(t) \} \rangle \, , \tag{3.87}$$

the advanced Green's function $G^A_{k,k'}(\omega) = (G^R_{k,k'}(\omega))^*$ and the lesser Green's function (3.84). Note that the dependence on the fixed frequency index ω has been omitted for clarity in the right-hand side of the equation.

In the absence of perturbation,

$$(G_0^{R/A})_{k,k'}(\omega) = \delta_{k,k'}[\omega - \hat{h}_{k,k} \pm i0^+]^{-1}, \tag{3.88}$$
$$(G_0^{<})_{k,k'}(\omega) = 2i\pi\delta_{k,k'} f(\omega)\delta(\omega - h_{k,k}). \tag{3.89}$$

with

$$f(\omega) = \frac{1}{1 + e^{\frac{\omega}{k_B T}}} \ . \tag{3.90}$$

By using the Dyson expansion of the Green's function (3.86) into the expression (3.83) we obtain the perturbative expansion in ϕ of the momentum density. At temperatures $k_B T_0 \neq 0$ small compared to the energy range over which the system is well described by the Dirac linear Hamiltonian, we can develop the Fermi-Dirac distribution as

$$f(\omega) = \Theta(-\omega) - \frac{\pi^2}{6} k_B^2 T_0^2 \ \partial_\omega \delta(\omega) + \mathcal{O}\left((k_B T_0)^4\right). \tag{3.91}$$

The equilibrium energy current density corresponds to the 0^{th} order term and can therefore be written as

$$\begin{aligned}\Pi^{(0)}(x) &= -i \int \frac{\mathrm{d}k}{2\pi} \frac{\mathrm{d}\omega}{2\pi} \ \hat{\Pi}_{k,k} f(\omega) \left[\frac{1}{\omega - \hat{h}_{k,k} - i0^+} - \frac{1}{\omega - \hat{h}_{k,k} + i0^+} \right] \\ &= \overline{\Pi} + \frac{\mathrm{sign}(v_F)}{v_F^2} \frac{\pi}{12\hbar} k_B^2 T_0^2 + O\left((k_B T_0)^4\right), \end{aligned} \tag{3.92}$$

where $\overline{\Pi}$ is the Fermi sea contribution to the momentum density. The contribution to first order in ϕ is then given by

$$\begin{aligned}\Pi^{(1)}(x) = -i \int \frac{\mathrm{d}k\mathrm{d}q}{(2\pi)^2} \frac{\mathrm{d}\omega}{2\pi} \mathrm{d}y \ \hat{\Pi}_{k-\frac{q}{2},k+\frac{q}{2}} e^{iq(x-y)} \phi(y) \Big\{ \left(G_0^R\right)_{k+\frac{q}{2},k+\frac{q}{2}} \hat{h}_{k+\frac{q}{2},k-\frac{q}{2}} \left(G_0^{<}\right)_{k-\frac{q}{2},k-\frac{q}{2}} \\ + \left(G_0^{<}\right)_{k+\frac{q}{2},k+\frac{q}{2}} \hat{h}_{k+\frac{q}{2},k-\frac{q}{2}} \left(G_0^A\right)_{k-\frac{q}{2},k-\frac{q}{2}} \Big\} \\ = -2 \int \frac{\mathrm{d}k\mathrm{d}q}{(2\pi)^2} \frac{\mathrm{d}\omega}{2\pi} \mathrm{d}y \phi(y) f(\omega) \ \mathrm{Im} \left[e^{iq(x-y)} \frac{\hat{\Pi}_{k-\frac{q}{2},k+\frac{q}{2}} \hat{h}_{k+\frac{q}{2},k-\frac{q}{2}}}{\left(\omega - \hat{h}_{k+\frac{q}{2},k+\frac{q}{2}} + i0^+\right)\left(\omega - \hat{h}_{k-\frac{q}{2},k-\frac{q}{2}} + i0^+\right)} \right]. \end{aligned} \tag{3.93}$$

The long-range physics dominating the linear response theory is given by the first orders in the development of

$$\begin{aligned}\frac{\hat{\Pi}_{k-\frac{q}{2},k+\frac{q}{2}} \hat{h}_{k+\frac{q}{2},k-\frac{q}{2}}}{\left(\omega - \hat{h}_{k+\frac{q}{2},k+\frac{q}{2}} + i0^+\right)\left(\omega - \hat{h}_{k-\frac{q}{2},k-\frac{q}{2}} + i0^+\right)} &= \frac{v_F \left(\hbar k\right)^2}{\left(\omega - v_F \hbar k + i0^+\right)^2} \\ &+ \frac{v_F \left(\hbar k\right)^2}{\left(\omega - v_F \hbar k + i0^+\right)^4} \frac{\left(v_F \hbar q\right)^2}{4} + \mathcal{O}\left((\hbar q)^4\right). \end{aligned} \tag{3.94}$$

The gradient expansion of the regularized current can, therefore, be written after integration

by parts on the variable y,

$$\begin{aligned}\Pi^{(1)}(x) \approx & -2\int \frac{\mathrm{d}k\mathrm{d}q}{(2\pi)^2}\frac{\mathrm{d}\omega}{2\pi}\mathrm{d}y\phi(y)f(\omega) \\ & \mathrm{Im}\left[\frac{v_F\left(\hbar k\right)^2}{\left(w-v_F\hbar k+i0^+\right)^2}e^{iq(x-y)}-\frac{\hbar^2v_F^2}{4}\frac{v_F\left(\hbar k\right)^2}{\left(w-v_F\hbar k+i0^+\right)^4}\partial_y^2\left(e^{iq(x-y)}\right)\right] \\ \approx & -2\int \frac{\mathrm{d}k\mathrm{d}q}{(2\pi)^2}\frac{\mathrm{d}\omega}{2\pi}\mathrm{d}yf(\omega) \\ & \mathrm{Im}\left[e^{iq(x-y)}\left\{\frac{v_F\left(\hbar k\right)^2}{\left(w-v_F\hbar k+i0^+\right)^2}\phi(y)-\frac{\hbar^2v_F^2}{4}\frac{v_F\left(\hbar k\right)^2}{\left(w-v_F\hbar k+i0^+\right)^4}\partial_y^2\left(\phi(y)\right)\right\}\right] \\ \approx & -2\int \frac{\mathrm{d}k}{2\pi}\frac{\mathrm{d}\omega}{2\pi}f(\omega)\ \mathrm{Im}\left[\frac{v_F\left(\hbar k\right)^2}{\left(w-v_F\hbar k+i0^+\right)^2}\phi(x)-\frac{\hbar^2v_F^2}{4}\frac{v_F\left(\hbar k\right)^2}{\left(w-v_F\hbar k+i0^+\right)^4}\partial_x^2\left(\phi(x)\right)\right].\end{aligned}$$

By using

$$\mathrm{Im}\left(\frac{(-1)^n n!}{(\omega-x\pm i0^+)^{n+1}}\right)=\mp\pi\partial_\omega^n\left[\delta\left(\omega-x\right)\right], \tag{3.95}$$

we can express this momentum density as

$$\begin{aligned}\Pi^{(1)}(x) \approx & -\int \frac{\mathrm{d}k}{2\pi}\mathrm{d}\omega\left\{\Theta(-\omega)-\frac{\pi^2}{6}k_B^2T_0^2\partial_\omega\delta(\omega)\right\}\left[v_F\left(\hbar k\right)^2\partial_\omega\delta\left(\omega-h_{k,k}\right)\phi(x)\right. \\ & \left.-\frac{\hbar^2}{24}\partial_x^2\phi(x)v_F^3\left(\hbar k\right)^2\partial_\omega^3\delta\left(\omega-h_{k,k}\right)\right] \\ \approx & -\int \frac{\mathrm{d}k}{2\pi}\mathrm{d}\omega\ \delta\left(\omega\right)\left[v_F\left(\hbar k\right)^2\delta(\omega-h_{k,k})\phi(x)-\frac{\hbar^2v_F^2}{24}\partial_x^2\phi(x)\ v_F\left(\hbar k\right)^2\partial_\omega^2\delta\left(\omega-h_{k,k}\right)\right] \\ & -\frac{\pi^2}{6}k_B^2T_0^2\int \frac{\mathrm{d}k}{2\pi}\mathrm{d}\omega\ \delta\left(\omega\right)\left[v_F\left(\hbar k\right)^2\partial_\omega^2\delta\left(\omega-h_{k,k}\right)\phi(x)\right. \\ & \left.-\frac{\hbar^2v_F^2}{24}\partial_x^2\phi(x)\ v_F\left(\hbar k\right)^2\partial_\omega^4\delta\left(\omega-h_{k,k}\right)\right].\end{aligned} \tag{3.96}$$

Using the replacement $\partial_\omega\delta(\omega-h_{k,k})=-\frac{1}{\hbar v_F}\partial_k\delta(\omega-h_{k,k})$, we can integrate on ω to get

$$\begin{aligned}\Pi^{(1)}(x) \approx & -\int \frac{\mathrm{d}k}{2\pi}\left[v_F\left(\hbar k\right)^2\delta(h_{k,k})\phi(x)-\frac{\hbar^2v_F^2}{24}\partial_x^2\phi(x)v_F\left(\hbar k\right)^2\left(\frac{-1}{\hbar v_F}\right)^2\partial_k^2\delta\left(h_{k,k}\right)\right] \\ & -\frac{\pi^2}{6}k_B^2T_0^2\int \frac{\mathrm{d}k}{2\pi}\left[v_F\left(\hbar k\right)^2\left(\frac{-1}{\hbar v_F}\right)^2\partial_k^2\delta\left(h_{k,k}\right)\phi(x)\right. \\ & \left.-\frac{\hbar^2v_F^2}{24}\partial_x^2\phi(x)\ v_F\left(\hbar k\right)^2\left(\frac{-1}{\hbar v_F}\right)^4\partial_k^4\delta\left(h_{k,k}\right)\right] \\ \approx & -\int \frac{\mathrm{d}k}{2\pi}\left[v_F\left(\hbar k\right)^2\phi(x)-\frac{1}{12}\partial_x^2\phi(x)v_F\hbar^2\right]\delta(h_{k,k})-\frac{\pi^2}{6v_F^2}k_B^2T_0^2\int \frac{\mathrm{d}k}{2\pi}2v_F\phi(x)\delta(h_{k,k}) \\ \approx & \ \mathrm{sign}\left(v_F\right)\left\{\frac{\hbar}{24\pi}\partial_x^2\phi(x)-\frac{\pi}{6\hbar v_F^2}k_B^2T_0^2\phi(x)\right\}.\end{aligned} \tag{3.97}$$

Gathering the different terms, we obtain, at linear order in the gravitational field $\phi(x)$, the momentum density

$$\Pi(x)=\bar{\Pi}+\mathrm{sign}(v_F)\left[\frac{\pi}{12\hbar v_F^2}k_B^2T_0^2\Big(1-2\phi(x)\Big)+\frac{\hbar}{24\pi}\partial_x^2\phi(x)\right], \tag{3.98}$$

which is identical to the first order in ϕ of the full result (3.63b).
Direct Kubo calculation provides a result in agreement with the gravitational anomaly prediction. Indeed, the strategy here applied for a specific metric field is, in fact, close to the diagrammatic strategy used to determine the gravitational anomalies.

In this chapter, we generalized the notion of Tolman-Ehrenfest to 1+1 dimensional spacetimes in the presence of gravitational anomalies before using it to correct the Luttinger trick when taking the gravitational anomalies into account. While this is a direct application of the modified Tolman-Ehrenfest relation, we will focus on discovering other consequences of this modification in the next chapter.

It is important to stress that the original work from R. Tolman and P. Ehrenfest is not specific to 1+1 dimensional systems [7]. An anomalous Tolman-Ehrenfest temperature can then be defined in any dimension. However, the case 1+1 dimensions is particular, as gravitational anomalies alone specify the momentum-energy tensor. In higher dimensions, gravitational anomalies do not sufficiently constrain the momentum-energy tensor. Additional requirements from *e.g.*, symmetries of the problem, have to be analyzed on a case-to-case basis [151] and deserve separate studies.

Chapter 4

Applications: From black holes to condensed matter and back

As we have seen in the previous chapter 3, in curved spacetimes, the notion of temperature has to be updated to take into account the effects of gravitational anomalies. Since the notion of temperature in curved spacetime is at the heart of Luttinger's trick, these deviations implied a modification of Luttinger's relation, leading to corrections in response theory.

In this chapter, the objective will be to identify physical situations in which these corrections to the Tolman-Ehrenfest temperature matter beyond the historical justifications of equilibrium temperature in curved spacetime and response theory. First, we reconsider the case of black holes. Historically, Black holes Hawking's radiation and anomalous fluctuations were described using either the trace [10] of the Einstein anomaly [11]. Therefore, our objective will be to reconcile both points of view by studying how gravitational anomalies modifiy the notion of temperature in the vicinity of a black hole. Then, coming back to condensed matter, we consider strongly out-of-equilibrium systems. We show that the local energy density fluctuations as well as the propagating heat waves resulting from a quench and recently identified within conformal field theory [152–155] are a manifestation of the anomalous thermodynamics relation identified in the previous chapter. Finally, we focus on a periodic sequence of quench applied to relativistic fermions. This procedure induces a Floquet state recently considered within conformal field theory [156–162]. Here, we show that the energy landscape, similar to the one observed close to black holes, is strongly modified due to the presence of gravitational anomalies.

This chapter is based on original work published in the article Ariv:2206.08784 [136].

4.1 Quantum atmosphere of a black hole

We start our discussion of the physical consequences of the anomalous Tolman-Ehrenfest relation (3.49) by revisiting the Hawking radiation from a black hole. This corresponds to the generic situation of a spacetime background with a large curvature $\mathcal{R}$, which induces significant anomalous quantum corrections $\varepsilon_q^{(1)}$ and $\varepsilon_q^{(2)}$, that are even comparable with the classical Tolmann-Ehrenfest temperature. For this purpose, we consider a generic black hole characterized by a metric of the form (3.20) with $f_1 = 1/f_2 = f$. Such a metric encompasses both Schwarzschild black holes [1] for $f(x) = 1 - x_H/x$, with x_H the black hole horizon, as well as evanescent Callan–Giddings–Harvey–Strominger (CGHS) black holes [163], initially introduced in the context of string theory [164], for $f(x) = 1 - \exp[-\alpha(x - x_H)]$. Generically, we consider a metric $f(x)$ which is asymptotically flat $\lim_{x\to\infty} f(x) = 1$ and vanishes linearly as x approaches

the event horizon x_H: $f(x \to x_H^+) \approx 2\kappa c^{-2}(x - x_H)$ where κ is its surface gravity.

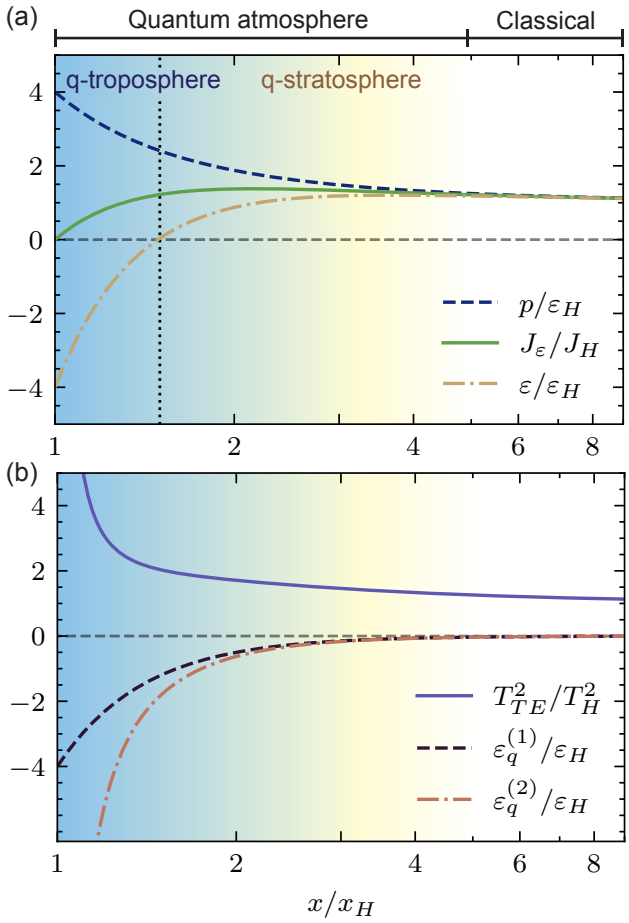

Figure 4.1: **Quantum atmosphere of a $1+1$ dimensional Schwarzschild black hole** (a) The dimensionless energy density ε, pressure p and energy current J_ε, rescaled by their asymptotic values $\varepsilon_H = \frac{1}{2}\gamma T_H^2$ and $J_H = (\pi/12\hbar)k_B^2 T_H^2$ where T_H is the Hawking temperature, are represented as a function of the distance x to the core of the black-hole (central singularity) rescaled by its radius x_H. Far from the horizon, all three quantities are proportional to $T^2_{\rm TE}(x)$, where $T_{\rm TE}(x)$ is the classical Tolman-Ehrenfest equilibrium temperature. Close to the horizon, quantum fluctuations strongly affect this classical behavior: an anomalous equilibrium temperature $T^2(x)$ is set by both $\varepsilon + p$ and J_ε. (b) The difference between the anomalous $T^2(x)$ and the classical $T^2_{\rm TE}(x)$ is set by a quantum scale $\varepsilon_q^{(2)}$. The divergence of $T^2_{\rm TE}$ at the horizon is counterbalanced by a diverging correction $\varepsilon_q^{(2)}$, leading to a vanishing $T^2(x)$. Simultaneously, the difference $\varepsilon_q^{(1)}$ between ε and p sets an independent quantum scale which remains finite at the horizon. These results illustrate the generation by a large spacetime curvature $\mathcal{R}$ of a finite energy density and asymptotic energy currents captured by the trace and gravitational anomaly corrections to the thermodynamic quantities. In (a) and (b), the region where $T^2(x) \neq T^2_{\rm TE}(x)$ defines the quantum atmosphere. Within it, we defined the quantum stratosphere, where $\varepsilon_q^{(1)} \approx \varepsilon_q^{(2)}$, and the quantum troposphere, where $\varepsilon_q^{(1)} \neq \varepsilon_q^{(2)}$, color coding the smooth crossover between them. The vertical dotted line in (a) indicates where $\varepsilon = 0$.

Anomalous fluctuations and Hawking radiation.

We focus on the outgoing chiral flux of particles of velocity $v_F = c$. Their momentum-energy tensor is given by equations (3.25, 3.40) with $\mathcal{C}_w = \mathcal{C}_g = 1$ (or in other words, $\mathcal{C}_+$=1 and $\mathcal{C}_- = 0$).

The two anomalous scales are deduced from equations (3.36, 3.41, 3.42):

$$\varepsilon_q^{(1)} = \frac{\hbar c}{48\pi}\partial_x^2 f \; ; \; \varepsilon_q^{(2)} = \frac{\hbar c}{48\pi}\left(\partial_x^2 f - \frac{(\partial_x f)^2}{2f}\right) . \tag{4.1}$$

The corresponding thermal current, identical to the momentum density, is deduced from equations (3.45c, 3.49), with a temperature $T(x)$ satisfying

$$k_B^2 T^2(x) = \frac{k_B^2 T_H^2}{f} + \frac{6\hbar c}{\pi}\,\varepsilon_q^{(2)} \; , \tag{4.2}$$

where we deduced $T_{\rm TE}^2 = T_H^2/f(x)$ from equation (3.29), with T_H the asymptotic temperature at $x \to \infty$, where $f(x \to \infty) = 1$.

In both the Israel-Hartle-Hawking and Unruh vacua, the momentum tensor for the outgoing particles is regular at the horizon $x = x_H$ [165]. Therefore the divergence of J_ε or $T^2(x)$ at the horizon, induced by the vanishing of $f(x \to x_H)$, has to be cancelled. The classical temperature $k_B^2 T_H^2/f$ always diverges at the horizon. On the other hand, the temperature (4.2) corrected by anomalous fluctuations remains finite at the horizon, provided we counterbalance the diverging classical temperature with the second contribution $\varepsilon_q^{(2)}$ in equation (4.2). This amounts to imposing the condition

$$k_B T_H = \frac{\hbar}{2\pi c}\kappa \; . \tag{4.3}$$

This is precisely the expression of the Hawking temperature [2, 11, 166, 167].

The above reasoning demonstrates that anomalous fluctuations are essential close to the horizon, given that the associated energy $\varepsilon_q^{(2)}$ corrects the spurious classical temperature divergence. Moreover, this subtle interplay between classical thermal and quantum fluctuations is at the origin of the asymptotic value of the temperature and energy variation. Quite remarkably, this implies that this asymptotic radiation originates from these anomalous quantum fluctuations close to the horizon. Indeed, plugging (4.3) into equation (4.2), we find that $T(x)$ and thus $J_{\varepsilon,+}$ vanish at the horizon [168], irrespective of the specific form of $f(x)$. No thermal current exits from inside the horizon. The asymptotic Hawking radiation

$$J_H = \frac{\pi}{12\hbar}k_B^2 T_H^2 = \frac{\hbar\kappa^2}{48\pi c^2} \tag{4.4}$$

originates from a region *outside* of the black hole's horizon, its quantum atmosphere [169].

Let us now focus more closely on this region of strong anomalous fluctuations outside of the black hole.

Quantum troposphere and stratosphere.

In Fig. 4.1(a), we illustrate the behavior of the energy density, pressure, and energy current around the quantum atmosphere of a Schwarzschild black hole by choosing the metric $f(x) = 1 - x_H/x$. The thermodynamic quantities are rescaled by their asymptotic values $\varepsilon_H = \frac{1}{2}\gamma T_H^2$ and $J_H = c\,\varepsilon_H$ for $x \to \infty$. Between the horizon $x = x_H$ and $x \simeq 4x_H$, the effects of quantum fluctuations lead to a sizable departure of ε, p, J_ε and, Π from their classical values. This is the quantum atmosphere of the black hole, which hosts strong quantum fluctuations. Its extension depends on the specific black hole, corresponding to a choice of metric $f(x)$.

In the outer part of this atmosphere, the amplitude of the anomalous corrections decreases, and the classical values dominate: in particular, the energy density ε remains positive. We denote this region as the quantum stratosphere. Close to the horizon, irrespective of the choice of metric $f(x)$, the energy density $\varepsilon(x)$ always becomes negative. Indeed, from the decay of the gravity with x, we deduce that $\partial_x^2 f(x) < 0$, corresponding to a negative curvature $\mathcal{R}$ in (3.41) and thus a negative scale $\varepsilon_q^{(1)}$ in (4.1). Given that $T(x)$ vanishes at the horizon, the energy density (3.45a) is negative close enough to the black hole. Its asymptotic value satisfies $\varepsilon = -p = (\hbar c/96\pi)\partial_x^2 f(x_H) < 0$. This negative energy density is a hallmark of a region dominated by anomalous quantum fluctuations: classical fluctuations satisfy a Stefan-Boltzmann law (3.26) with an energy density always larger than that of the vacuum in flat spacetime $\varepsilon > 0$. We denote the region of $\varepsilon < 0$, where thermodynamic quantities are dominated by anomalous quantum fluctuations, the quantum troposphere.

Our analysis shows that the quantum atmosphere can be interpreted as the cradle of strong anomalous quantum fluctuations. In the quantum troposphere, gravitational anomalies even dominate thermodynamics. Signatures of such dominant quantum fluctuations are a negative energy density and large relative $\varepsilon - p$ compared to the average $\varepsilon + p$. In practice, the amplitude of the Hawking temperature is of the order of a few 10^{-8}K for the smallest (i.e., the hottest) observed black holes [170], rendering the direct detection of these anomalous quantum phenomena elusive in real black holes.

Before focusing on other physical places where the anomaly might play a role, let us briefly comment on historical references of the description of these anomalous quantum fluctuations. The relation between the Hawking radiation and quantum anomalies in $1+1$ dimensions was pioneered by S. Christensen and S. Fulling, who focused on the trace anomaly [10]. S. Robinson and F. Wilczek followed an alternative route by considering the consequences of the Einstein anomaly on an effective chiral theory [11, 171, 172]. The associated modified equilibrium temperature (3.49) was first derived in [173] while its relation to ballistic energy current (3.45c) through the Einstein anomaly was unnoticed. As we showed in section 3.2.2, both anomalies should be treated on the same footing when considering the effects of quantum fluctuations for a generic theory. The notion of quantum atmosphere of a black hole, beyond its horizon, and at the origin of the Hawking radiation was recently discussed by S. Giddings [169] on CGHS black holes using conformal field theory techniques within the tortoise coordinates representation of the momentum-energy tensor. This analysis was complemented in [174] by a general analysis of the Stefan-Boltzmann law accounting for the anomalous Tolman-Ehrenfest temperature.

4.2 Far from equilibrium energy transport

A quench procedure, in which external parameters controlling an equilibrium system are suddenly changed, allows us to explore the dynamics of quantum systems beyond the realm of linear response theory. The rich possibilities offered by experiments using ultra-cold atoms have triggered a recent interest in such an out-of-equilibrium dynamics [175].

In this section, we focus on the situation of a finite-size quantum system connected to a thermal bath, whose temperature is varied rapidly. In a standard partition procedure, such as the one studied in [155], two halves of the conductor are maintained at different temperatures $T_{R/L} = T_0 \pm \Delta T/2$, see Fig. 4.2(a). The corresponding external temperature profile $T(x)$ maintains the conductor in an out-of-equilibrium state. The temperature profile is then later released at some time $t = 0$. Local heat currents appear in the equilibration process between different regions of the conductor. Remarkably, an oscillating heat wave was observed

in a pioneering numerical study on spin chains [155], later described analytically within either perturbation theory [154] or conformal field theory [152].

In this section, we demonstrate that these oscillations and an associated pressure discontinuity at time $t = 0$ can be recovered within a curved spacetime approach as measurable signatures of the gravitational anomalies. They originate from the energy density characterizing the steady out-of-equilibrium state at time $t < 0$, which we describe first. In a later refinement of this quench physics, we compare this thermal quench procedure with a quench obtained by suddenly changing the local velocity. Finally, building on this protocol, we consider Floquet states generated by periodically changing the local velocity profile, a procedure that can be shown to be equivalent to imposing and releasing an external temperature profile.

4.2.1 Anomalous Luttinger relation on a ring

From generalized Gibbs measure to curved spacetime

We consider a generic interacting gas on a ring of size L, described in a low-energy limit by a relativistic Luttinger liquid [46–48, 176, 177]. For time $t < 0$, this system is spatially modulated either by a variation of the local Fermi velocity or by an external temperature. In the resulting inhomogeneous out-of-equilibrium steady state, physical observables $\langle \mathcal{O} \rangle$ are assumed to be described by statistical averages with a generalized Gibbs measure

$$\langle \mathcal{O} \rangle = \frac{\mathrm{Tr}\ \mathcal{O}\, e^{-\mathcal{G}}}{\mathrm{Tr}\ e^{-\mathcal{G}}}\ ; \quad \mathcal{G} = \int_0^L dx\ \frac{1}{k_B T_0\, \xi(x)} h(x)\,, \tag{4.5}$$

where $\mathcal{H}(x)$ is the Hamiltonian density and $\xi(x)$ the parameter of the spatial modulation.

It is natural to expect that the local equilibrium temperature of the wire is set by $T_{\mathrm{Gibbs}}(x) = \xi(x)\, T_0$. However, we show below that this is not the case. To engineer a given temperature profile, gravitational anomalies corrections have to be accounted for to determine the equivalent profile $\xi(x)$. Besides, our results demonstrate that equivalence between modulating the velocity or the inverse temperature of relativistic excitations requires some particular care, as we will see in a following paragraph 4.2.1.

To identify the local equilibrium temperature corresponding to the generalized Gibbs measure (4.5), we start by interpreting it as a Gibbs measure at constant temperature T_0 but in a curved spacetime whose metric tensor verifies

$$\mathrm{d}s^2 = g_{\mu\nu}\mathrm{d}x^\mu \mathrm{d}x^\nu = \frac{v_F^2}{\xi^2(x)}\mathrm{d}t^2 - \mathrm{d}x^2\,. \tag{4.6}$$

It is associated with the Luttinger gravitational potential $\phi_{\mathrm{Lutt}}(x) = -\ln \xi(x)$, since it can be rewritten under the form (1.73a),

$$\mathcal{G} = \frac{1}{k_B T_0} \int_0^L dx \sqrt{f_1} h(x)\,, \tag{4.7}$$

with $f_1 = 1/\xi^2$.

We can now use our results of chapter 3. The equilibrium temperature $T(x)$ in this curved spacetime does not directly identify with the standard Tolman-Ehrenfest temperature $T_{\mathrm{TE}}(x) = T_{\mathrm{Gibbs}}(x)$, the difference is actually a direct measure of the amplitude of the corrections

due to the trace and gravitational anomalies.

More precisely, let us recall the relation (3.49) between the anomalous Tolman-Ehrenfest and the Gibbs temperatures: $\gamma T^2(x) = \gamma T^2_{\rm Gibbs} + \varepsilon_q^{(2)}$ where the quantum energy scale

$$\varepsilon_q^{(2)} = \frac{\hbar v_F}{24\pi}\left[-\frac{\partial_x^2\xi}{\xi} + \left(\frac{\partial_x\xi}{\xi}\right)^2\right] = \frac{\hbar v_F}{24\pi\ell_T^2} \tag{4.8}$$

depends on the length ℓ_T which encodes the local variation of the metric:

$$\ell_T^{-2}(x) = \partial_x^2 \ln\xi(x)\,. \tag{4.9}$$

The relative correction to the temperature is thus set by a ratio of lengths :

$$\frac{T^2(x)}{T^2_{\rm Gibbs}(x)} = 1 + \left(\frac{\lambda_T(x)}{\ell_T(x)}\right)^2. \tag{4.10}$$

with the de Broglie relativistic thermal length

$$\lambda_T = \frac{\hbar v_F}{2\pi k_B T_{\rm Gibbs}(x)}\,. \tag{4.11}$$

From equations (3.62) we obtain the energy density and pressure

$$\varepsilon = \frac{1}{2}(\mathcal{C}_+ + \mathcal{C}_-)\left(\gamma T^2 + \varepsilon_q^{(1)} + \varepsilon_C\right), \tag{4.12}$$

$$p = \frac{1}{2}(\mathcal{C}_+ + \mathcal{C}_-)\left(\gamma T^2 - \varepsilon_q^{(1)} + \varepsilon_C\right). \tag{4.13}$$

The homogeneous Casimir energy correction ε_C induced by the finite size of the system [178]

$$\varepsilon_C = -\frac{\pi\hbar v_F}{24L^2}\,, \tag{4.14}$$

is locally corrected by the anomalous quantum scale $\varepsilon_q^{(1)}$

$$\varepsilon_q^{(1)} = \frac{\hbar v_F}{24\pi}\left[-\frac{\partial_x^2\xi}{\xi} + 2\left(\frac{\partial_x\xi}{\xi}\right)^2\right] = \frac{\hbar v_F}{24\pi}\left[\ell_T^{-2} + \tilde{\ell}_T^{-2}\right], \tag{4.15}$$

whose amplitude is set by both the length ℓ_T from Eq. (4.9) and a second length scale parametrizing the variations of the inhomogeneity parameter $\xi(x)$:

$$\tilde{\ell}_T(x) = \left|\frac{\xi}{\partial_x\xi}\right|. \tag{4.16}$$

Similarly, the energy current and momentum densities read

$$\begin{aligned} J_{\varepsilon,\pm} &= \pm\mathcal{C}_\pm\left[\frac{\pi}{12\hbar}(k_BT)^2 + v_F\,\varepsilon_q^{(1)}\right] \\ &= \pm\mathcal{C}_\pm\left[\frac{\pi}{12\hbar}(k_BT_0)^2\xi^2 - \frac{\hbar v_F^2}{48\pi}\left(\frac{\partial_x\xi}{\xi}\right)^2\right], \end{aligned} \tag{4.17}$$

$$\begin{aligned} \Pi_\pm &= \pm\mathcal{C}_\pm\left[\frac{\pi}{12\hbar v_F^2}(k_BT)^2 - \frac{1}{v_F}\varepsilon_q^{(1)}\right] \\ &= \pm\mathcal{C}_\pm\left[\frac{\pi}{12\hbar v_F^2}(k_BT_0)^2\xi^2 + \frac{\hbar}{48\pi}\left(3\left(\frac{\partial_x\xi}{\xi}\right)^2 - 2\frac{\partial_x^2\xi}{\xi}\right)\right]. \end{aligned} \tag{4.18}$$

In the following, we consider Gibbs' states associated to two different situations. First, we consider a system set out of equilibrium by an inhomogeneous temperature profile $T(x)$. Then, we compare these results with those for a system whose inhomogeneities come from an inhomogeneous velocity profile.

Inhomogeneous temperature

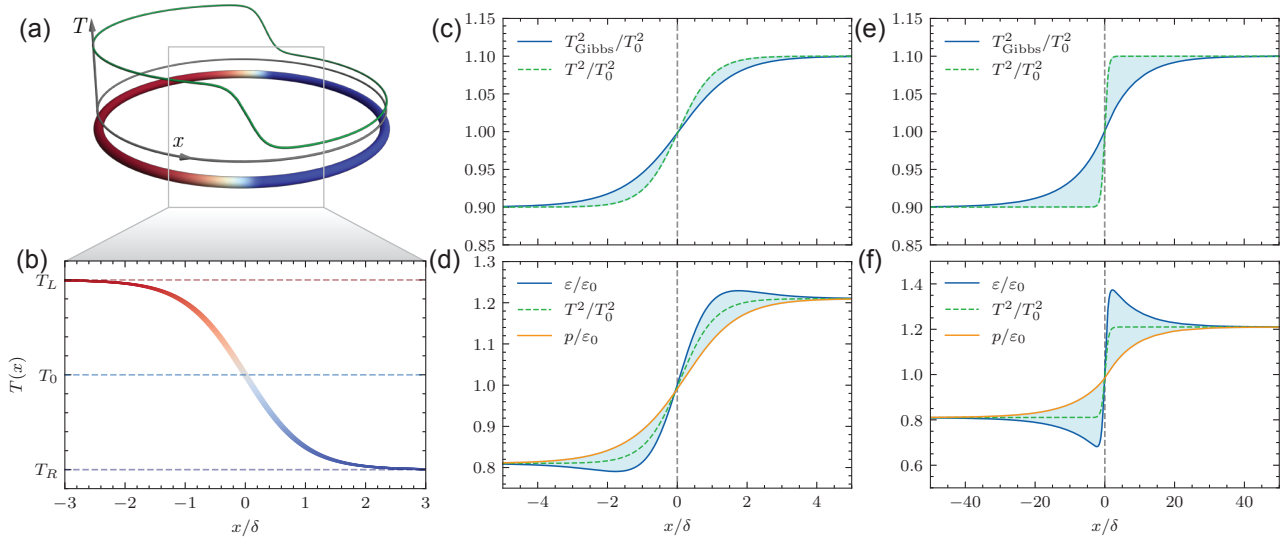

Figure 4.2: **Quantum corrections to the out-of-equilibrium steady state imposed by a temperature jump.** (a) Two halves of a close ring of non-interacting particles ($\mathcal{C}_+ = \mathcal{C}_- = 1$) are set at two temperatures $T_{R/L} = T_0 \pm \Delta T/2$. (b) At the two contacts, the temperature smoothly varies over a region of size δ. We consider a Fermi velocity $v_F = 10^6 \mathrm{m{\cdot}s^{-1}}$ typical for relativistic materials, a cryogenic temperature $T_0 = 100$ mK and a small relative temperature jump $\Delta T/T_0 = 0.2$. (c) and (d) for a size of the contact region $\delta = 10$ μm, we observe small deviation of T_{Gibbs} compared to the applied temperature. As a consequence, the energy density $\varepsilon(x)$ and the pressure p depart from the classical law $\varepsilon = P = \gamma T^2$: the amplitude of the corresponding correction, represented by the shaded area, is set by a single quantum energy scale $\varepsilon_q^{(1)}$. This energy scale originates from quantum fluctuations, at the origin of scale and gravitational anomalies, of similar origin that in the black hole's atmosphere. In the present case, the curvature $\mathcal{R}$ of spacetime is set by the imposed temperature through the Luttinger equivalence relation. (e) and (f) for a smaller size $\delta = 1$ μm, We observe an important deviation of T_{Gibbs} compared to the applied temperature, T_{Gibbs} appear to be much smoother than the applied temperature. The difference, represented by the shaded area, is set by the single quantum energy scale $\varepsilon_q^{(2)}$. As before, the energy density $\varepsilon(x)$ and the pressure p depart from the classical law $\varepsilon = P = \gamma T^2$, with a correction encoded by the quantum energy scale $\varepsilon_q^{(1)}$.

Let us evaluate the amplitude of the corrections by quantum fluctuations encoded in the trace and gravitational anomalies by considering a non-chiral wire $\mathcal{C}_+ = \mathcal{C}_- = \mathcal{C}$, maintained in an out-of-equilibrium steady state by a temperature profile $T(x)$. Let us then consider a temperature profile that is constant in two regions with values $T_{L/R} = T_0 \pm \Delta T/2$, and smoothly interpolates over a length δ between them, at positions $x = 0, L/2$ as displayed in Fig. 4.2(a). Although our approach applies to a generic temperature profile, for the sake of clarity, we choose a profile such that

$$T(x) = T_0 - \frac{\Delta T}{2} \tanh\left[\frac{L}{2\pi\delta}\sin\left(2\pi\frac{x}{L}\right)\right] . \tag{4.19}$$

Given this temperature profile, we identify the equivalent parameter of the spatial modulation $\xi(x)$ by inverting numerically the relation (4.10). This function $\xi(x)$ is then used to calculate the amplitudes of the quantum corrections $\varepsilon_q^{(1)}$ and the corresponding densities and currents. The results are shown on Fig. 4.2. We expect the gravitational anomalies to alter the classical properties of the steady state in regions where $\varepsilon_q^{(1)}$ become sizable, or in other

words, where $\xi(x)$ varies a lot, *i.e.* close to the temperature jumps for a strong enough relative variation of this temperature. Therefore we focus, in the following, on the temperature jump around $x = L/2$ of the temperature profile (4.19), as shown in Fig. 4.2(b). For a steady state, J_ε and Π vanish.

The parameters of Fig. 4.2 are motivated by relativistic electronic conductors. In graphene [179], Carbon nanotubes [180] and Dirac and Weyl semimetals [96], the Fermi velocity of Dirac particles is of the order $v_F \sim 10^6$ ms^{-1}, yielding a thermal length $\lambda_{T_0} \times T_0 \simeq 1.22 \times 10^{-5}$ m for a dilution refrigerator temperature of $T_0 = 100$ mK. We choose a relative temperature jump $\Delta\xi = 0.2$. For smooth temperature jump over a length $\delta = 10\mu$m, we obtain from (4.10) that $\tilde{\ell}_T(x)$ is very large and $\ell_T(x) \ll \tilde{\ell}_T(x)$. A single length scale $\ell_T(x) \simeq |\xi/\partial_x^2\xi|^{1/2}$, set by the Ricci scalar R, characterizes the anomalous fluctuations. Correspondingly, gravitational anomaly corrections, characterized both by the departure of T from T_{Gibbs} and by the difference between ε and γT^2 involve a single quantum energy scale $\varepsilon_q^{(1)} \approx \varepsilon_q^{(2)} \approx -\mathcal{C}\hbar v_F/(24\pi\ell_T^2)$. Both the pressure and the energy density display small departures from the classical law $\varepsilon = p = \mathcal{C}\gamma T^2$, as shown in Fig. 4.2(d). The amplitude of this correction, symmetric around the temperature jump, corresponding to the shaded area, is a direct measure of the quantum correction $\varepsilon_q^{(1)}$ set by the anomalies, ε_C being negligible here. For sharper temperature jump over $\delta = 1\mu$m, we observe that the corresponding Gibbs or Tolman-Ehrenfest temperature $T_{\rm Gibbs}(x) = T_{\rm TE}(x)$ is much smoother, as shown in Fig. 4.2(e). This illustrates that an inhomogeneous temperature induces analog gravitational potentials that are smoother than those induced by velocity variations, *e.g.* by varying the couplings. Remarkably, the energy density displays some deeps and spikes around the temperature jump, represented in Fig. 4.2(e), which are signatures of the gravitational anomaly corrections. In that situation, the two lengthscales $\ell_{T_{\rm ext}}(x)$ and $\tilde{\ell}_{T_{\rm ext}}(x)$ slightly differ, corresponding to two different quantum energy scales $\varepsilon_q^{(1)}$ and $\varepsilon_q^{(2)}$. However, in practice, only $\varepsilon_q^{(1)}$ leads to experimentally measurable corrections through the difference $\varepsilon - p = 2\mathcal{C}(\varepsilon_q^{(1)} + \varepsilon_C)$.

Inhomogeneous Couplings

For the sake of comparison, let us evaluate the amplitude of the corrections induced by an inhomogeneous velocity profile $v(x)$. Although our approach applies to a generic velocity profile, we choose a velocity profile of the form

$$v(x) = \frac{v_F}{1 - \frac{\Delta T}{2T_0} \tanh \frac{L}{2\pi\delta} \sin 2\pi \frac{x}{L}} \,. \tag{4.20}$$

Classically, a system maintained out-of-equilibrium by a velocity profile of the form (4.20) at a homogeneous temperature T_0 and a system at an inhomogeneous temperature set out of equilibrium by a temperature profile of the form (4.19) are both described by the same generalized Gibbs ensemble with a spatial modulation induced by the parameter

$$\xi(x) = 1 - \frac{\Delta T}{2T_0} \tanh \frac{L}{2\pi\delta} \sin 2\pi \frac{x}{L} \,. \tag{4.21}$$

One could expect the momentum-energy tensor of both systems to be identical. However, as we have seen in the previous paragraph, in the case of a thermal origin of the inhomogeneities, the "correct" parameter ξ is determined by solving numerically equation (4.10). Therefore, the experimentally relevant corrections, given by $\varepsilon - \mathcal{C}\gamma T^2$ and by $p - \mathcal{C}\gamma T^2$ are both equal to $\mathcal{C}\varepsilon_q^{(1)}$.

In contrary, for a system set out of equilibrium by inhomogeneous couplings, since the experimentally imposed quantity is the velocity profile, the experimentally relevant quantities are

both $\varepsilon - \mathcal{C}\gamma T_{\text{Gibbs}}^2$ and $p - \mathcal{C}\gamma T_{\text{Gibbs}}^2$ expressed respectively, in terms of the anomalous energy scales as $\mathcal{C}\left(\varepsilon_q^{(1)} + \varepsilon_q^{(2)}\right)$ and $\mathcal{C}\left(\varepsilon_q^{(2)} - \varepsilon_q^{(1)}\right)$[1]. In this case, two different situations can arise depending on the value of $\Delta T/T_0$, as displayed in Fig. 4.3.

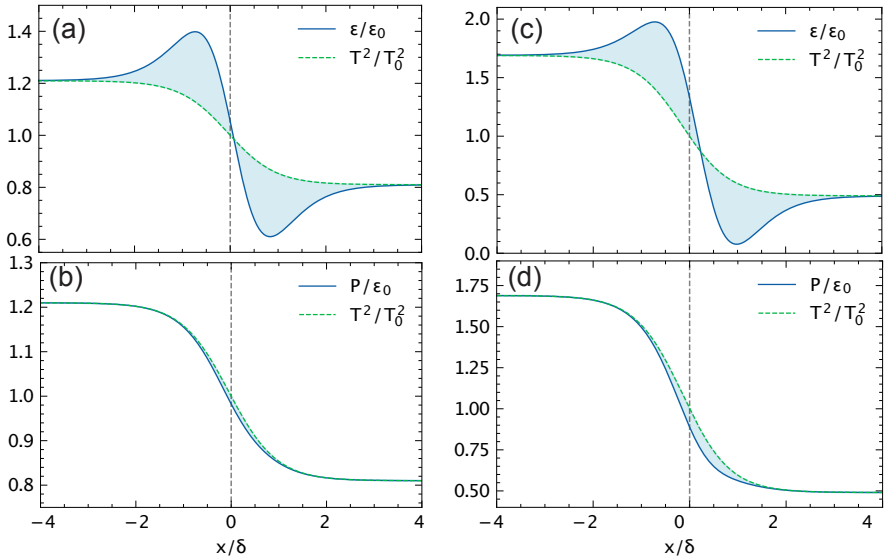

Figure 4.3: **Quantum corrections to the out-of-equilibrium steady state imposed by an inhomogeneous velocity profile.** (a) and (b) For a small difference of velocity $\Delta v/v_F \approx 0.2$, the pressure, shown relative to its means value $\varepsilon_0 = \gamma T_0^2$, follows the classical law $P \approx \gamma T^2$. On the other hand, the energy density $\varepsilon(x)$ departs from this classical law: the amplitude of the corresponding corrections, represented by the shaded area, is set by the quantum energy scale $\varepsilon_q^{(1)}$. This energy scale originates from quantum fluctuations at the origin of the gravitational anomalies of a similar origin that in the black hole's atmosphere. In the present case, the curvature $\mathcal{R}$ of spacetime is set by ξ the parameter of the spatial variations through the anomalous Tolman-Ehrenfest law (3.49). (c) and (d) for larger relative velocity variations $\Delta v/v_F \approx 0.6$, two quantum energy scales $\varepsilon_q^{(1)}$ and $\varepsilon_q^{(2)}$ have to be distinguished. While $(\varepsilon_q^{(1)} + \varepsilon_q^{(2)})/2$ still appears as the amplitude of the oscillating corrections to ε, the difference $\varepsilon_q^{(1)} - \varepsilon_q^{(2)}$ manifests itself both in the asymmetry of these corrections around the temperature jump, and a departure of the pressure from the classical law.

For small relative velocity variations $\Delta v/v_F$, $\tilde{\ell}_T(x)$ is very large and $\ell_T(x) \lesssim \lambda_T(x) \ll \tilde{\ell}_T(x)$. A single length scale $\ell_T(x) \simeq |1/\partial_x^2 \xi|^{1/2}$, set by the Ricci scalar $\mathcal{R}$, characterizes the anomalous fluctuations. Correspondingly, gravitational anomaly corrections involve a single quantum energy scale $\varepsilon_q^{(1)} \approx \varepsilon_q^{(2)} \approx -\mathcal{C}\hbar v_F/(24\pi \ell_T^2)$. While the pressure follows the classical amplitude $p = \mathcal{C}\left(\gamma T_{\text{Gibbs}}^2 - \varepsilon_C\right)$, the energy density $\varepsilon = \mathcal{C}\left(\gamma T_{\text{Gibbs}}^2 + 2\varepsilon_q^{(1)} + \varepsilon_C\right)$ displays an oscillation around the temperature jump, as shown in Figs. 4.3(a) and 4.3(b). The amplitude of this oscillation, symmetric around the temperature jump, corresponding to the shaded area, is a direct measure of the quantum correction $\varepsilon_q^{(1)}$ set by the anomalies.

For larger velocity variations $\Delta v/v_F$ for which $\ell_T(x) \lesssim \tilde{\ell}_T(x) \lesssim \lambda_T(x)$ the two quantum energy scales $\varepsilon_q^{(1)}$ and $\varepsilon_q^{(2)}$ are no longer approximately equal. The difference $\varepsilon_q^{(2)} - \varepsilon_q^{(1)}$ manifests

[1]Note that in the previous expressions, the parameters ε and p corresponds to the one measured with respect the flat spacetime hamiltonian density $h(x)$ and not those measured with respect to the inhomogeneous hamiltonian $h(x)/\xi(x)$

itself in two ways. First, as a departure of the pressure from the classical behavior, as shown in Fig. 4.3(d). Second, as the asymmetry around the temperature jump at $x = 0$ of the shaded areas at $x > 0$ and $x < 0$ of the energy density ε as shown in Fig. 4.3(c).

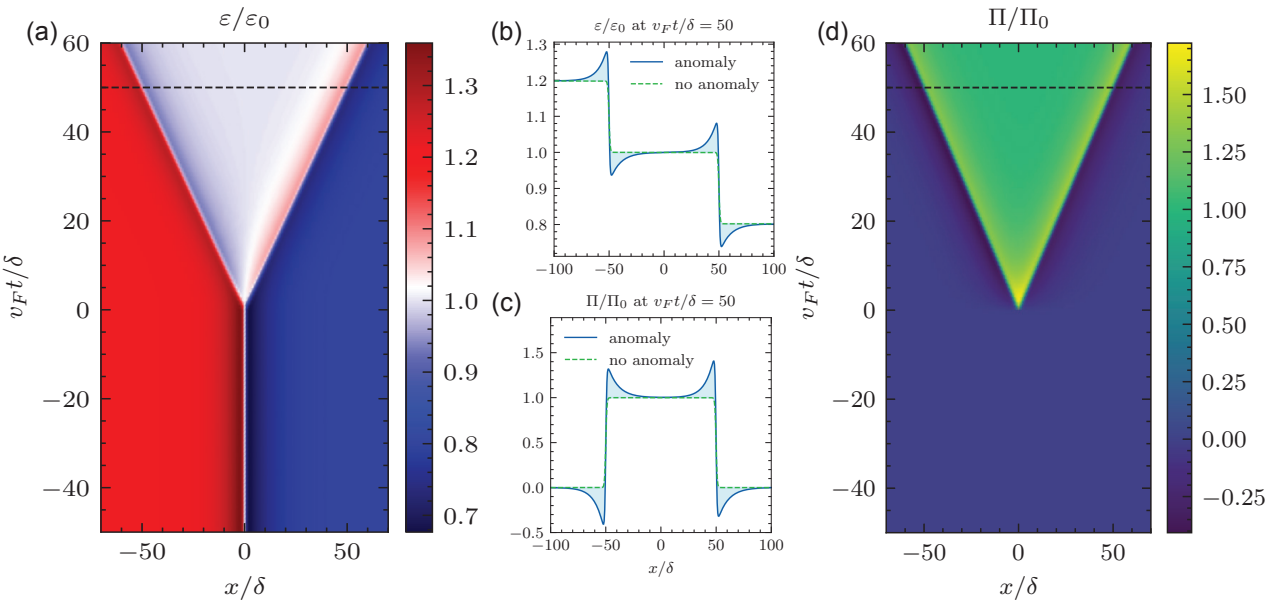

Figure 4.4: **Quantum corrections to energy traveling waves imposed by a temperature quench** (a) Two halves of a wire of non-interacting particles ($\mathcal{C}_+ = \mathcal{C}_- = 1$) with Fermi velocity of $v_F = 10^6$ ms^{-1} are set at two temperatures $T_{R/L} = T_0 \mp \Delta T/2$ following the same protocol as in Fig. 4.2. The average temperature is $T_0 = 100$mK, and the ramp of temperature of amplitude $\Delta T = 20$mK is imposed over a length $\delta = 1\mu$m. At time $t = 0$, this external temperature difference is released. Following this quench, two traveling waves of energy appear. (b) The non-monotonous behavior of the density of energy profile is a manifestation of the anomaly corrections originating from quantum fluctuations of similar nature than close to a black hole. The amplitude of the corrections, represented by the shaded area, is a direct measure of the new quantum scale of energy $\varepsilon_q^{(1)} \simeq \varepsilon_q^{(2)}$ set by gravitational anomalies. In between the two waves appears a region of homogeneous density of energy $\bar{\varepsilon} = \frac{1}{2}\gamma(T_L^2 + T_R^2) + 2\varepsilon_C = \gamma(T_0^2 + \Delta T^2/4) + 2\varepsilon_C$. (c) and (d) This intermediate region is not in equilibrium: it is crossed by right-moving particles at temperature T_L and left moving particles at temperature T_R, leading to a steady current $\bar{J}_\varepsilon = \frac{1}{2}\gamma v_F(T_L^2 - T_R^2) = 2\gamma v_F T_0 \Delta T$ and momentum $\bar{\Pi} = v_F^{-2}\bar{J}_\varepsilon$. The oscillating corrections to the momentum or energy current close to the interface between the three regions, shown in (b) and (c) as shaded areas, are also an accessible manifestation of corrections due to quantum fluctuations due to the trace and gravitational anomalies, similarly to those at the vicinity of a black hole. In the present case, they originate from the local strong curvature of the effective spacetime accounting, following Luttinger equivalence, for the temperature variation.

4.2.2 Temperature quench as a metric quench

In practice, maintaining a conductor in an out-of-equilibrium steady state is difficult and not practical: it is often easier to study the dynamics following a corresponding quench. As we show below, the dynamics reflects the quantum corrections to the initial steady state. Thus we consider a situation where the temperature profile (4.19) is imposed up to time $t = 0$, and released afterwards.

The out-of-equilibrium dynamics occurs in a closed system, but a ballistic evolution forbids the exchange of energy between left and right movers. Given that the equilibrium temperature of such a system is uniform, the Tolman-Ehrenfest equivalence implies that this dynamics occurs in a flat spacetime, with vanishing curvatures $\mathcal{R} = 0$ and $\overline{\mathcal{R}} = 0$. In this flat spacetime, $\varepsilon = p$ and $v_F^2 \Pi = J_\varepsilon$.

Following the extended Luttinger correspondence that we developed in chapter 3, the out-of-equilibrium dynamics at time $t > 0$ can be viewed as resulting from a quench of the spacetime metric at time $t = 0$ from the Luttinger metric (4.6) to a flat metric. Continuity conditions on the momentum-energy tensor, derived in Appendix B, imply that both the energy density ε as well as the momentum Π are continuous during this quench of metric: $\varepsilon(t = 0^+) = \varepsilon(t = 0^-)$ and $\Pi_\pm(t = 0^+) = \Pi_\pm(t = 0^-)$. On the other hand, the energy current density and the pressure are discontinuous, with $J^\varepsilon_\pm(t = 0^+) - J^\varepsilon_\pm(t = 0^-) = \mathcal{C}_\pm v_F \, \varepsilon_q^{(1)}$ and $p(t = 0^+) - p(t = 0^-) = (\mathcal{C}_+ + \mathcal{C}_-)\varepsilon_q^{(1)}$, where $\varepsilon_q^{(1)}$ is set by (4.15).

Given that low-energy excitations of our system evolve ballistically, we obtain for time $t > 0$

$$J^\varepsilon_\pm(x, t) = v_F^2 \Pi_\pm(x, t) = v_F^2 \Pi_\pm(x \mp v_F t, 0^+) \tag{4.22}$$

where the momenta at $t = 0^+$ are defined in (4.18). The resulting energy density and momentum are represented in Fig. 4.4 for the same parameters than Figs. 4.2(e) and 4.2(f). The quantum corrections characterizing the energy density and pressure of the steady state at $t < 0$ now manifest themselves as traveling waves of energy after the quench, as shown in Figs. 4.4(a) and 4.4(b). In between the two traveling waves emerges a region of homogeneous density of energy

$$\bar{\varepsilon} = \frac{1}{2}\gamma \left(\mathcal{C}_+ T_L^2 + \mathcal{C}_- T_R^2 \right) + (\mathcal{C}_+ + \mathcal{C}_-)\varepsilon_C \, , \tag{4.23}$$

where the average temperature T_0 is defined in Fig. 4.2(b). In this region, right-moving particles carry an energy density $\frac{1}{2}\mathcal{C}_+(\gamma T_L^2 + \varepsilon_C)$ while left-moving particles carry an energy density $\frac{1}{2}\mathcal{C}_-(\gamma T_R^2 + \varepsilon_C)$, resulting in a steady-state value of the current $\bar{J}_\varepsilon = \frac{1}{2}\gamma v_F(\mathcal{C}_+ T_L^2 - \mathcal{C}_- T_R^2)$ and momentum $\bar{\Pi} = v_F^{-2} \bar{J}_\varepsilon$. This expression agrees with the pioneering study on interacting chains [155] and [150] as well as a Landauer-Büttiker approach for non-interacting fermions [181].

The traveling waves of energy, shown in Figs. 4.4(a) and 4.4(b), reflect as traveling waves of momentum shown in Figs. 4.4(c) and 4.4(d). The amplitudes of the quantum corrections, represented as the shaded area, are equal to that of the energy density before the quench, shown in Fig. 4.2: it is set by $\varepsilon_q^{(1)}$, a quantum scale defined in (4.15).

These results, which we derived for a temperature quench from gravitational anomaly corrections in a curved spacetime as well as continuity conditions following a metric quench, can easily be extended to a quench of Gibbs temperature, where the quenched quantity is directly $\xi(x)$. Results for such a quench of the Gibbs temperature were previously derived using series expansions and conformal field theory techniques in [152, 154]. The presence of a Schwarzian derivative in the expression for the density of energy and energy current can indeed be traced back to a manifestation of the trace anomaly identified in the present paper. Through the (extended) Luttinger equivalence, a thermal quench can be treated as a quench of metric, which appears seemingly identical to a quench imposed by the release of an external confining potential considered in [51]. In both cases, anomalies capture the quantum corrections induced by large spacetime curvatures.

4.2.3 Spacetime periodic modulation: Floquet states

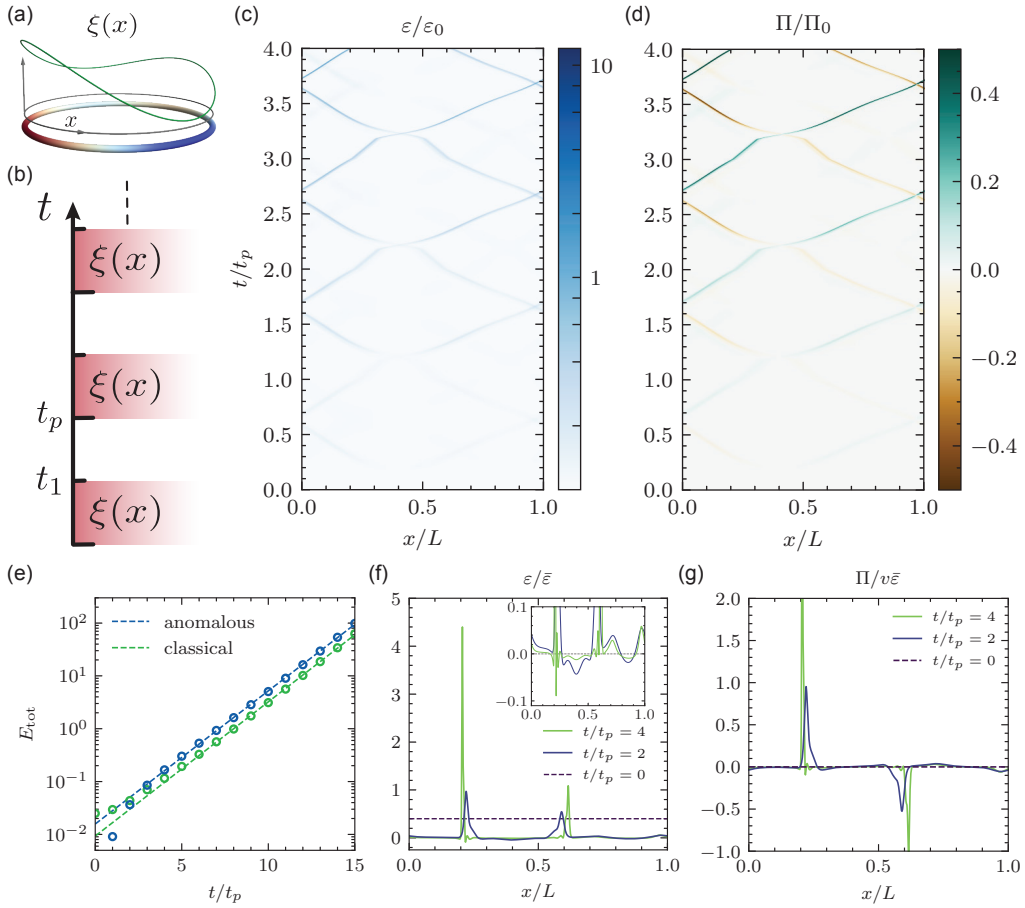

Figure 4.5: **Floquet heating state.** (a) and (b) We consider a ring of free relativistic fermions with a spatially modulated velocity $\xi(x)v_F(x) = 1$. The modulation $\xi(x)$ is periodic in time with a period $t_p = t_1 + t_2$, such that (i) during time t_1 set to the smooth profile shown in (a), and (ii) during time t_2 no modulation is applied and $\xi(x) = 1$. The two times $Lt_1/v_F = 0.1$ and $Lt_2/v_F = 0.45$, are chosen such that the period coincides approximately with the time of flight of particles around the ring: $L \approx v_F t_1 + \tilde{v}_F t_2$ where $\tilde{v}_F$ is the averaged effective velocity over the profile $\xi(x)$.(c) and (d) As a function of time, both the energy density ε and the momentum Π become highly inhomogeneous, and concentrate on a few trajectories. They are represented rescaled by the classical values $\varepsilon_0 = v_F\Pi_0 = \gamma T_0^2$. The energy and momentum profiles are represented after two and four periods in panels (f) and (g), illustrating the localization mechanism. (e) Besides being focused spatially, the net energy of the ring $E_{\rm tot} = \int_0^L \varepsilon\, dx = L\bar{\varepsilon}$ increases: the Floquet state is heating. This is represented by monitoring the stroboscopic dynamics at times $t_n = nt_p$ of the ring for which $E_{\rm tot}$ increases exponentially. Remarkably the rate of increase of this energy is not classical: quantum fluctuations, responsible for the trace and gravitational anomaly corrections, have a growing energy. The two focusing trajectories behave as heating black holes: in their neighborhood, the energy density becomes negative, as shown in the inset of panel (f). This is an additional manifestation of the effects of quantum fluctuations induced by a local large curvature similar to those in a black-hole atmosphere.

In this section, building on the above study of a single thermal quench, we explore how anomalous quantum fluctuations appear following a periodic sequences of quantum quenches. While periodic thermal quenches realize the same physics, for technical reasons we follow the

protocol recently proposed in [158–161] by implementing directly a quench of coupling $\xi(x)$, see Eq. (4.5). This choice allows to bypass the numerical determination of a metric equivalent to a thermal profile as done in section 4.2.1. By interpreting time-periodic, or Floquet, change in the spatial dependence of the system's parameters as metric quench (Fig. 4.5(a)), we highlight the role that gravitational and trace anomalies play in the phenomenology of the resulting Floquet conformal field theories [156, 157].

The peculiarity of Floquet conformal field theories relies on the striking, but analytic, thermalization properties [158–161] occurring when periodically modulating the system between two inhomogeneous states. This two-step periodic drive is obtained when the dynamics of particles on a circle of size L is alternatively described by a uniform and an inhomogeneous Hamiltonian:

$$H = \int_0^L dx \, \frac{1}{\xi(x,t)} h_0(x), \tag{4.24}$$

where

$$\xi(x,t) = \begin{cases} \xi(x) & \text{for } t \in [0, t_1] \\ 1 & \text{for } t \in [t_1, t_1 + t_2 \equiv t_p], \end{cases} \tag{4.25}$$

where t_p is the period. While initially $\xi(x)$ was chosen to be an inverse sine squared deformation $\xi^{-1}(x) = 2\sin^2(\pi x/L)$ [156, 157], we consider more general profiles in the following [160, 161]. For concreteness the results of Fig. 4.5 are obtained for a profile deduced from a simple metric proposed in [160]:

$$\xi(x) = 1 + \frac{1}{3}\sin\left(\frac{4\pi x}{L}\right) + \frac{1}{3}\cos\left(\frac{2\pi x}{L}\right), \tag{4.26}$$

represented in Figs. 4.5(a) and 4.5(b). Note that such a profile is slowly varying, and does not yield abrupt changes of metric: we do not expect the type of anomalous corrections due to quantum fluctuations discussed in the previous section after a single quench. Yet, we will see that the succession of such quenches leads to manifestations of the gravitational anomaly.

For a period t_p comparable with the time of flight for particles across the system, two distinct dynamical phases are reached at long-time depending on the relative magnitudes t_2/t_1 [158, 159]. A heating and non-heating phases are characterized by the evolution of the total energy $E_{\text{tot}} = L\bar{\varepsilon}$ of the closed system, which either grows exponentially or oscillates. Furthermore, in the heating phase, the energy density becomes highly inhomogeneous, localizing exponentially around a few spatial fixed points [158, 159].

First, following the discussion in section 4.2.1, we realize that the periodic modulation of energy density of Eq. (4.25) can be realized by a periodic sequence of thermal quenches, with a profile $T(x)$ obtained by solving Eq. (4.10), provided this profile is always positive. Let us now notice that the Floquet drive Eq. (4.25) enforces a time-periodic quenches of a metric (3.20) with $f_2(x,t) = 1$ and

$$f_1(x,t) = \begin{cases} 1 & \text{for } t \in 0 < t < t_1 \\ 1/\xi^2(x) & \text{for } t \in t_1 < t < t_p \end{cases} \tag{4.27}$$

Proceeding as in the single quench of the previous section, we solve the time-evolution of the momentum-energy tensor stepwise and apply suitable continuity equations determined in appendix B. In doing so, we access the energy and momentum density which are plotted in Figs 4.5(c) and 4.5(d), respectively, up to $t = 4t_p$. Three stroboscopic times are shown in Figs. 4.5(f) and 4.5(g). In these plots, the Hamiltonian H_0 was chosen as that of free Dirac fermions, with the duration of the two steps of metric chosen such that $Lt_1/v_F = 0.1$ and $Lt_2/v_F = 0.45$. Note that during step 2, the average velocity $\bar{v}_F$ is defined as $1/\bar{v}_F =$

$\int_0^L dx/v(x) = \frac{1}{v_F}\int_0^L dx/\xi(x)$ such that the time of flight across the circle of the particles is approximatively one period: $L \approx v_F t_1 + \bar{v}_F t_2$, corresponding to the conditions to realise a heating phase [158, 160].

Focusing on the heating phase, we show that several of its features are manifestations of quantum fluctuations and can be traced back to gravitational anomalies. Indeed the gravitational anomaly modifies the rate of the exponential growth of the average energy density. To show this we plot the total energy density $E_{\rm tot} = \bar{\varepsilon} L$ at stroboscopic times in Fig. 4.5(e), extracted from Fig. 4.5(c). Plotted in Log-scale, it shows a clear linear trend as a function of time. To highlight the contribution of the gravitational anomaly, in Fig. 4.5(e) we have separated two contributions: that arising from the classical Tolman-Ehrenfest temperature, and that directly linked to the gravitational anomaly. We observe that both have the same order of magnitude at large times and grow exponentially.

A second signature of the gravitational anomaly is apparent in the spatial profile of the energy density, shown in Fig. 4.5(f) for stroboscopic times. The inset shows that the energy density can be locally negative while satisfying that the total energy is always positive (Fig. 4.5(e)). Without quantum effects, the classical Tolman-Ehrenfest contribution $\varepsilon > 0$ for all x. This can be seen by noting that without the anomalous contribution $\varepsilon_q^{(1)}$ to (3.45a) the energy density is always positive for all x. However, in Fig. 4.5(f), we see that this is not the case, a clear manifestation of the Einstein and scale anomaly, reminiscent of the negative energy density close to the horizon of a black hole, as shown in Fig. 4.1.

We expect this relation between the quantum properties of black holes and Floquet heating states to be generic. Indeed, the authors of [159] noted the connection between the effective metric of a sine-squared Floquet CFT and that of two black holes at the accumulation points. This is in agreement with the manifestation of the trace and gravitational anomalies that we identified, in particular with the negative density of energy close to these accumulation points, reminiscent of the black hole atmosphere.

4.3 Conditions of application

Before discussing these results in detail, let us start by commenting on the conditions of application of our approach. Crucially, the notion of local temperature $T(x)$ requires some local energy relaxation on scales smaller than the characteristic scales of variations of $T(x)$. While close to the black hole, only the outgoing flux of Hawking's radiation needs to be locally equilibrated. In the strongly out-of-equilibrium condensed matter examples discussed above, we have assumed a single local temperature $T(x)$ common to left and right moving excitations 4.2.1, while still describing their motion as ballistic. This corresponds to a situation where the forward inelastic scattering occurs on scales much smaller than the backscattering between left and right movers, which is effectively neglected in this chapter. This imposes a condition on the scattering potential, whose $2k_F$ components should be negligible compared to the $q \simeq 0$ components.

In more detail, denoting by ℓ_f and ℓ_b the forward and backscattering lengths, a sufficient condition for the excitations to be at a local thermal equilibrium amounts to consider a small enough thermal gradient satisfying $\ell_f \ll \tilde{l}_T \ll \ell_b$ in terms of the length $\tilde{l}_T$ defined in (4.16). In practice, in a system with a fixed velocity v_F, average temperature T, scattering time τ, and size L, our theory will apply if the temperature difference between both ends of the system

satisfies $\frac{\Delta T}{\bar{T}} \ll \frac{L}{v_F \tau_{intra}}$.

Situations where left and right movers are equilibrated at two different temperatures require more care and will be the focus of the next chapter 5.

In this chapter, we have discussed observable imprints on the thermal current and energy densities of anomalous quantum fluctuations at the origin of gravitational anomalies in field theory. These imprints manifest naturally in curved spacetime, such as the neighborhood of black holes. However, extending Luttinger's correspondence beyond the realm of perturbative response theory, we have shown how they emerge, as naturally, in a flat spacetime when subjected to a single or periodic temperature quenches. The reason is that the equilibrium temperature profile in all the above situations can be phrased as an anomalous Tolman-Ehrenfest temperature, an equilibrium temperature profile that upgrades the classical result by R. Tolman and P. Ehrenfest by incorporating the quantum energy scales originating from gravitational anomalies.

Chapter 5

Extension of the Luttinger's trick in the presence of two temperature profiles

In chapters 3 and 4, we discussed the corrections brought by gravitational anomalies to the concept of Tolman-Ehrenfest temperature. Furthermore, we introduced several physical setups in which these corrections were both relevant and sizable. However, as discussed in section 4.3, these analyses are restricted to situations in which the temperatures of both chiral species are identical. As a conclusion, we observed that in their steady states, non-chiral conductors, defined by $\mathcal{C}_g = 0$, present no energy current.

This behavior is, however, not general to every setup. For example, in ballistic materials, left and right-moving electrons do not interact, and hence, each species has an independent temperature fixed by their boundary condition. In this chapter, we will extend the notion of Tollman-Ehrenfest temperature and Luttinger's trick to systems in which left and right movers have independent temperature profiles, or in other words, in the presence of two local temperature profiles. First, we will see how such independent temperature profiles can arise from a single metric tensor with several boundary conditions, considering both in and out-going radiation close to a black hole. Then, introducing a condensed matter system displaying independent temperature profiles for left and right-moving electrons, we will see that the original Luttinger's strategy is not sufficient. Extending Luttinger's trick to such a setup requires introducing one metric tensor per chirality, a strategy also known as bimetric gravity. Then, we will discuss another possible application of this strategy to tilted semimetals. Finally, we will conclude this chapter with a discussion of the advantage of such setups to observe signatures of gravitational anomalies.

The results of this chapter are new and currently unpublished.

5.1 From one to two temperature sources in black hole physics

In section 4.1, we proved, based on gravitational anomalies, that black holes induce in their vicinity out-going thermal energy currents (radiation) at a temperature fixed by their surface gravity, following Hawking's relations. In that demonstration, we focused on out-going energy fluxes, fixing the boundary condition at the horizon of the black holes and completely disregarding the incoming energy flux.

In this section, building on this example, we wish to consider a system with two local temperature profiles. In analogy with a conductor connecting two temperature sources, and as proposed but not studied by M. Stone and J. Kim in [182], a natural setup to study such radiations consists in considering the thermodynamics of a region in between two black holes.

Let us study a single metric describing the physics induced by two distant black holes, whose centers are respectively at $x = 0$ and $x = 2L$ with respective radius x_L and x_R (with $x_{L/R} < L$). Even though such a metric is not a solution of Einstein's general relativity equations [183–185], it captures the phenomenology of two distant Schwarzschild black holes. It is defined by the line element

$$\mathrm{d}s^2 = f(x)\mathrm{d}t^2 - \frac{1}{f(x)}\mathrm{d}x^2, \tag{5.1}$$

with

$$f(x) = \left(1 - \frac{x_L}{x}\right)\left(1 - \frac{x_R}{2L - x}\right). \tag{5.2}$$

Classically, following Hawking's calculations, one would expect both black holes to radiate at a temperature $T_{L/R} \propto \frac{1}{x_{R/L}}$, and hence an energy current in the middle of the sample given by

$$J_\varepsilon = \frac{\pi k_B^2}{12\hbar}\left(T_L^2 - T_R^2\right), \tag{5.3}$$

consistent with Landauer's formula for a ballistic conductor with heat sources at temperatures T_R and T_L [186, 187].

We can then wonder if the strategy based on anomalies used in section 4.1 can be used to explain such a result and what corrections might arise due to gravitational anomalies. If we apply directly the strategy, developed in section 3.2.2 to the double black hole metric (5.1), one finds a single anomalous temperature given by

$$k_B^2 T_{an}^2 = \frac{k_B^2 T_0^2}{f(x)} + \frac{\hbar^2 c^2}{8\pi^2}\left(\partial_x^2 f(x) - \frac{1}{2}\frac{\left(\partial_x f(x)\right)^2}{f(x)}\right), \tag{5.4}$$

with T_0 a constant to be fixed. Following the single black hole study of section 4.1, we would like to fix this constant by requiring the temperature profile to be regular everywhere. However, such a requirement is, in the case of the metric (5.1), impossible to fulfill whenever the two Hawking's temperatures differ, i.e., when $x_R \neq x_L$, since the regularity condition imposes

- On the left side: $k_B T_0 = k_B T_L = \frac{\hbar \kappa_L}{2\pi c}$, with $\kappa_L \equiv c^2 \left.\frac{|\partial_x f|}{2}\right|_{x_L} = \frac{c^2}{2x_L}\left(1 - \frac{x_R}{2L - x_L}\right)$ the left black hole's surface gravity
- On the right side: $k_B T_0 = k_B T_R = \frac{\hbar \kappa_R}{2\pi c}$, with $\kappa_R \equiv c^2 \left.\frac{|\partial_x f|}{2}\right|_{2L - x_R} = \frac{c^2}{2x_R}\left(1 - \frac{x_L}{2L - x_R}\right)$ the right black hole's surface gravity

The choice of a single constant T_0 is then too restrictive to fit both boundary conditions.

A natural strategy to solve this question consists in considering separately left-going and right-going radiations instead of the total radiations. The right-going radiation will be required to be well-defined close to the left black hole, and similarly for the left-going radiation close to the right black hole, defining one temperature profile per chirality. To do so, let us define a new variable y such as $\mathrm{d}y = \frac{\mathrm{d}x}{f(x)}$, and the corresponding chiral variables $y^\pm = \frac{1}{2}(ct \pm y)$. In the basis (t, y), the metric tensor can be expressed as

$$g_{\mu\nu} = f\left(x\left(y\right)\right)\begin{pmatrix} 1 & 0 \\ 0 & -1 \end{pmatrix}, \tag{5.5}$$

or, in the chiral variable language (y^+, y^-),

$$g_{\mu\nu} = 2f\left(y^+ - y^-\right)\begin{pmatrix}0 & 1\\ 1 & 0\end{pmatrix} \tag{5.6}$$

such as the only non-zero affine connection coefficients are

$$\left\{\begin{matrix}+\\ ++\end{matrix}\right\} = -\left\{\begin{matrix}-\\ --\end{matrix}\right\} = \frac{\partial_y f}{f(x)} = \partial_x f\,. \tag{5.7}$$

In this basis, the (non-)conservation equations (3.35)

$$\begin{cases}\mathcal{T}^{\mu}_{\ \mu} = \frac{\hbar c}{48\pi}\mathcal{C}_w\mathcal{R}\,,\\ \mathcal{T}^{\mu\nu} = \mathcal{T}^{\nu\mu}\,,\\ \nabla_\mu\mathcal{T}^{\mu\nu} = \frac{\hbar c}{96\pi}\mathcal{C}_g\frac{\epsilon^{\nu\mu}}{\sqrt{-g}}\nabla_\mu\mathcal{R}\,,\end{cases} \tag{5.8}$$

can be written as

$$\begin{cases}2f\left(\mathcal{T}^{+-} + \mathcal{T}^{-+}\right) = \frac{\hbar c}{48\pi}\mathcal{C}_w\mathcal{R}\,,\\ \mathcal{T}^{+-} = \mathcal{T}^{-+}\,,\\ f\partial_-\left(f\mathcal{T}^{-+}\right) + \partial_+\left(f^2\mathcal{T}^{++}\right) = \mathcal{C}_g\frac{\hbar c}{192\pi}f\partial_+\mathcal{R}\,,\\ f\partial_+\left(f\mathcal{T}^{+-}\right) + \partial_-\left(f^2\mathcal{T}^{--}\right) = -\mathcal{C}_g\frac{\hbar c}{192\pi}f\partial_-\mathcal{R}\,,\end{cases} \tag{5.9}$$

which can be solved as

$$\begin{cases}\mathcal{T}^{+-} = \mathcal{T}^{-+} = \frac{\hbar c}{192\pi}\frac{\mathcal{C}_w}{f}\mathcal{R}\,,\\ \mathcal{T}^{++} = \frac{\alpha\left(y^-\right)}{f^2(y^+-y^-)} + \frac{\hbar c}{192\pi}\frac{\mathcal{C}_g+\mathcal{C}_w}{f^2(y^+-y^-)}\int f\partial_y\mathcal{R} \quad \text{(Right going current)}\\ \mathcal{T}^{--} = \frac{\beta\left(y^+\right)}{f^2(y^+-y^-)} + \frac{\hbar c}{192\pi}\frac{-\mathcal{C}_g+\mathcal{C}_w}{f^2(y^+-y^-)}\int f\partial_y\mathcal{R} \quad \text{(Left going current)}\end{cases} \tag{5.10}$$

with α and β, two unknown functions that we need to fix using the boundary conditions.

Stationarity implies that both α and β are constants that we will fix by imposing vanishing out-going current boundary conditions at x_L and $2L - x_R$:

- Nothing coming out of the left black hole implies that $\mathcal{T}^{++}(y(x_L)) = 0$, or in other words,

$$\alpha = \mathcal{C}_+\frac{\gamma T_L^2}{2} = \frac{\mathcal{C}_g + \mathcal{C}_w}{4}\gamma T_L^2\,, \tag{5.11}$$

- Nothing coming out of the right black hole implies that $\mathcal{T}^{--}(y(2L - x_R)) = 0$, or in other words,

$$\beta = \mathcal{C}_-\frac{\gamma T_R^2}{2} = \frac{-\mathcal{C}_g + \mathcal{C}_w}{4}\gamma T_R^2\,, \tag{5.12}$$

Restoring the original coordinate system (t, x), we can express the different thermodynamic quantities as

$$\begin{cases}\varepsilon \equiv \varepsilon^+ + \varepsilon^- = \frac{\alpha+\beta}{f(x)} + \frac{\mathcal{C}_w}{2}\left(\varepsilon_q^{(1)} + \varepsilon_q^{(2)}\right)\,,\\ p \equiv p^+ + p^- = \frac{\alpha+\beta}{f(x)} + \frac{\mathcal{C}_w}{2}\left(\varepsilon_q^{(2)} - \varepsilon_q^{(1)}\right)\,,\\ v_F^2\,\Pi = J_\varepsilon \equiv J_\varepsilon^+ + J_\varepsilon^- = \frac{\alpha-\beta}{f(x)} + \frac{\mathcal{C}_g}{2}\varepsilon_q^{(2)}\,,\end{cases} \tag{5.13}$$

with

$$\begin{cases}\varepsilon_q^{(1)} = \frac{\hbar c}{48\pi}\partial_x^2 f\,,\\ \varepsilon_q^{(2)} = \frac{\hbar c}{48\pi}\left(\partial_x^2 f - \frac{(\partial_x f)^2}{2f}\right)\,.\end{cases} \tag{5.14}$$

We define, similarly to chapter 3, an anomalous temperature for each chirality as

$$\left(k_B T_{an}^{\pm}\right)^2 = \frac{k_B^2 T_{R/L}^2}{f(x)} + \frac{\hbar^2 c^2}{8\pi^2}\left(\partial_x^2 f(x) - \frac{1}{2}\frac{\left(\partial_x f(x)\right)^2}{f(x)}\right) , \tag{5.15}$$

such that the chiral components of the momentum-energy tensor verify

$$\begin{cases} \varepsilon^{\pm} = \frac{\mathcal{C}^{\pm}}{2}\left[\gamma\left(T_{an}^{\pm}\right)^2 + \varepsilon_q^{(1)}\right] , \\ p \equiv p^{\pm} = \frac{\mathcal{C}^{\pm}}{2}\left[\gamma\left(T_{an}^{\pm}\right)^2 - \varepsilon_q^{(1)}\right] , \\ c^2\,\Pi^{\pm} = J_{\varepsilon}^{\pm} = \frac{\mathcal{C}^{\pm}}{2}\gamma c\left(T_{an}^{\pm}\right)^2 . \end{cases} \tag{5.16}$$

Considering a non-chiral conductor, such that $\mathcal{C}_+ = \mathcal{C}_- = \mathcal{C}$, the total momentum-energy tensor (5.13) take the simplified form

$$\begin{cases} \varepsilon = \mathcal{C}\frac{\gamma}{2}\frac{T_L^2+T_R^2}{f(x)} + \mathcal{C}\left(\varepsilon_q^{(1)} + \varepsilon_q^{(2)}\right) , \\ p = \mathcal{C}\frac{\gamma}{2}\frac{T_L^2+T_R^2}{f(x)} + \mathcal{C}\left(\varepsilon_q^{(2)} - \varepsilon_q^{(1)}\right) , \\ c^2\,\Pi \equiv J_{\varepsilon} = \mathcal{C}\frac{\gamma c}{2}\frac{T_L^2-T_R^2}{f(x)} . \end{cases} \tag{5.17}$$

Considering the two black holes to be far apart ($2L \gg x_R + x_L$), let us now analyze these thermodynamic quantities (5.17), also represented in Fig. 5.1. Focusing on the right-moving particles, corresponding to the blue curve in Fig. 5.1(a), we observe, as in section 4.1, that the temperature vanishes close to the left horizon. This illustrates the fact that nothing can escape the black holes. Therefore, the right-going Hawking radiations, propagating towards the right black hole, are produced in the quantum atmosphere of the left black hole. Close to the right black hole, since the right black hole is cooler than the left one ($x_R^{-2} < x_L^{-2}$), its quantum fluctuations are not sufficient to compensate for the gravitational redshift, inducing a divergence of the right-going Tolmann-Ehrenfest temperature. On the contrary, close to the left black holes, these anomalous fluctuations dominate the physics, and the Hawking radiation produced close to the right black hole has a non-physical negative temperature, as observe in orange in Fig. 5.1(a). In the middle of the sample, anomalous fluctuations are negligible, and we recover the classical results

$$\varepsilon = p = \mathcal{C}\frac{\gamma}{2}\left(T_R^2 + T_L^2\right) . \tag{5.18}$$

For the currents in non-chiral conductors, the anomalous contributions from both left and right-moving radiation exactly compensate each other. As a consequence, the energy current, displayed in red in Fig. 5.1(b), is proportional to the value deduced from the classical Tolman-Ehrenfest formula and

$$J_{\varepsilon} = c^2\Pi = \frac{T_L^2 - T_R^2}{f(x)} \tag{5.19}$$

Since we assumed the black holes to be distant from each other, the energy current in the middle of the sample is given by the difference of Hawking's temperature of these two black holes: $v_F^2\,\Pi = J_{\varepsilon} = \mathcal{C}\frac{\gamma v_F}{2}\left(T_L^2 - T_R^2\right)$, as expected for a ballistic system situated in between two heat baths, and in agreement with M. Stone and J. Kim proposal [182].

While the expressions of the momentum-energy tensors defined in this section (5.13) look similar to the one considered in chapter 3 and 4, there exists, however, a major difference. While in chapter 3, and 4, we were defining a single temperature profile, fixing $\alpha^+ = \alpha^-$, in this section, we are considering an out-of-equilibrium situation in which left and right currents are defined with respect to different temperature profiles

$$\gamma T_{\pm}^2 = \frac{\alpha^{\pm}}{f_1} + \epsilon_q^{(2)} . \tag{5.20}$$

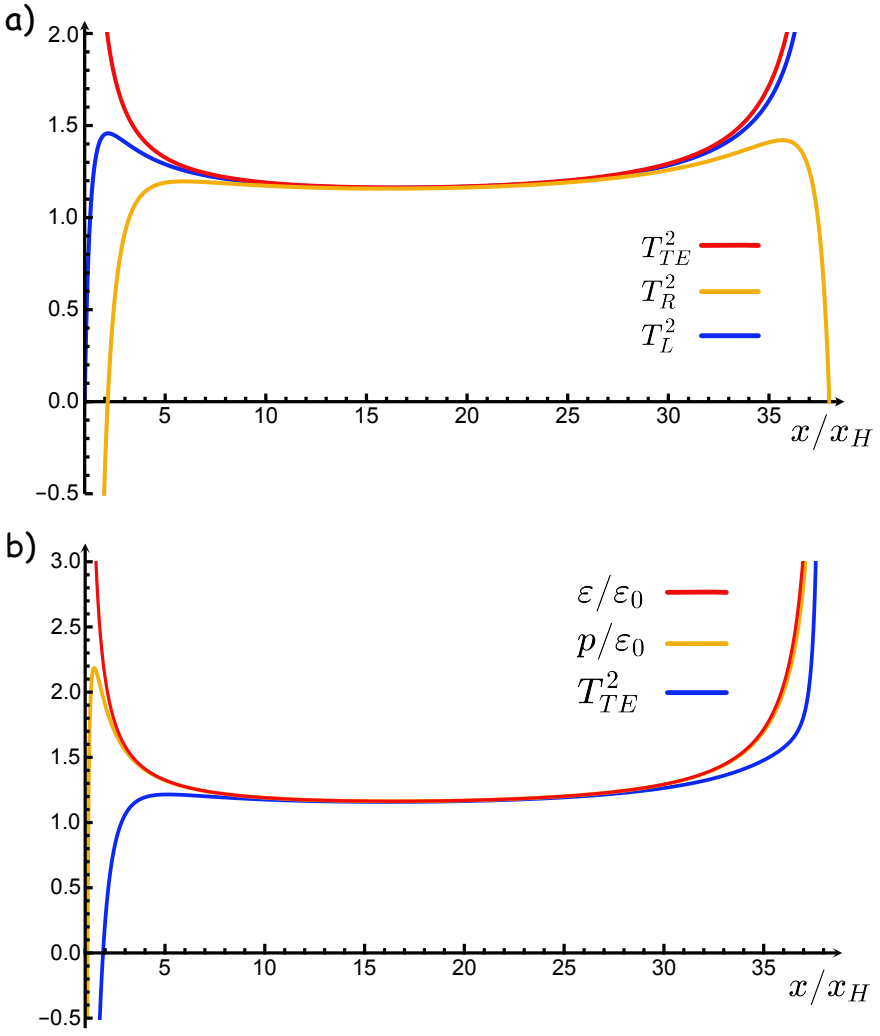

Figure 5.1: **Two temperature models in two black hole metrics** Thermodynamic quantities as a function of the position expressed as a function of x_H, the radius of the left black hole. The radius of the right black hole is chosen such that $x_L = 2x_H$, while we considered distant black holes $L = 20x_H$ (a) Represented in red is the solution corresponding to a common Tolmann-Ehrenfest temperature to both chiral particles, divergent close to the horizon of both black holes. The anomalous equilibrium temperatures are unique to each chiral species, in blue for the right movers and orange for the left movers. The anomalous temperature profile for the right movers is chosen to be vanishing close to the left black hole. However, close to the right black holes, anomalous quantum corrections of the cooler black holes are not sufficient to compensate for the divergence of the temperature profile. Similarly, the anomalous left-going temperature profile is well defined in $x = x_R$. However, it diverges and becomes negative close to the left black holes due to large quantum fluctuations engendered by the hottest black hole. (b) The thermodynamic quantities in between the two black holes can then be defined from both these chiral temperatures and the quantum energy scale $\varepsilon_q^{(1)}$, leading to the thermal current $J^\varepsilon/J_0^\varepsilon$ in red, the energy density $\varepsilon/\varepsilon_0$ in blue and the pressure p/ε_0 in orange, where $J_0^\varepsilon = 1/2c\gamma(T_L^2 - T_R^2)$ and $\varepsilon_0 = 1/2\gamma(T_L^2 - T_R^2)$

Even though they are based on the same metric tensor, they differ due to their corresponding boundary conditions.

In this section, we considered a metric with two black holes to underline that a single metric tensor might give rise to two local temperature profiles based on the choice of boundary conditions. However, the choice of the metric tensor leads to an unphysical result since gravitational anomalies induce a temperature profile such as $T_{\text{An}}^2 < 0$, close to the hottest black hole.
These results are closely related to those presented in section 4.1 and reveal the surprising fact that since both chiral species interact with the same background metric, the anomalous contributions to the energy currents simplify out in a non-chiral system. In the following section, we will see that such a strategy based on a single metric with two boundaries is not always sufficient. Indeed, extending Luttinger's trick to a generic conductor with independent temperature profiles for left and right movers requires the introduction of one metric per chiral species, a strategy known as bimetric theory.

5.2 Luttinger extension to chiral temperature profiles

In the previous section 5.1, we have seen that depending on the boundary conditions, a single metric tensor can lead to different temperature profiles for each chirality. This non-equilibrium situation leads to a non-vanishing heat current even in non-chiral systems. In the literature, M. Stone and J. Kim proposed in [182] that such a system can be used to understand the relationship between thermal transport and gravitational anomalies.

In this section, to explore this relationship between gravity and thermal transport in more detail, we would like to extend the discussion of Luttinger's trick from chapter 3 to conductors in which the temperature for left and right-moving electrons can differ. After motivating this extension by unveiling conductors presenting two temperature profiles, we will see that in the generic case and opposite to the two black holes systems, applying Luttinger's trick imposes going beyond general gravity, considering systems in which both chiralities couple to different metrics, an extension of general relativity known as bimetric gravity. After reviewing this formalism, we will use it to extend Luttinger's trick before proposing an extension of such a formalism to tilted semimetals.

5.2.1 Extended Luttinger equivalence: From one to two temperature profiles

In condensed matter physics, the temperature profiles in a sample in contact with two heat reservoirs can differ for left and right-moving particles, depending on how they interact with each other. In this paragraph, after introducing a system in which such chiral temperature profiles can arise, we will identify the curved spacetime equivalent as Luttinger did in the presence of a single temperature profile.

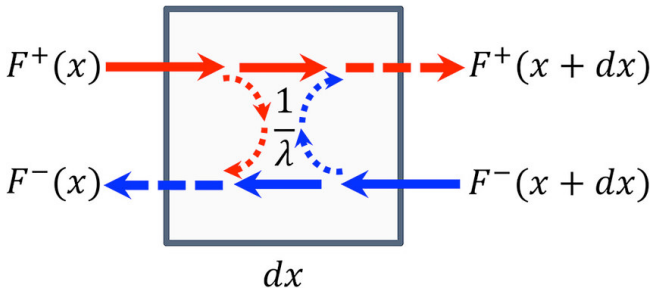

Figure 5.2: **Scheme of the scattering process considered**

In order to model the energy current profile in a conductor between two heat baths at respective temperatures T_R and T_L, one can follow the simple formalism used by J.P. Mc Kelvey *et al.* [188] and W. Shockley [189], allowing to describe both ballistic and diffusive regime as well as the regime interpolating in between these. Taking into account a single linear band ($E = \pm v\hbar k$) in the absence of electron-phonon scattering, the Mc Kelvey-Shockley equations can be rewritten as [190, 191]

$$\begin{cases} \frac{\partial F^+(E,x)}{\partial x} &= \frac{1}{\lambda(E)}\left(F^-(E,x) - F^+(E,x)\right) \\ \frac{\partial F^-(E,x)}{\partial x} &= \frac{1}{\lambda(E)}\left(F^-(E,x) - F^+(E,x)\right) \end{cases} \tag{5.21}$$

with

- $\lambda(E)$ the mean free path for particles with energy E
- $F^{\pm}$ the forward (+) and backward (-) energy fluxes with particles at energy E

Assuming that λ does not depend on E, these equations can be solved as

$$\begin{cases} F^+(E,x) &= F_0^L(E) - \left(F_0^L(E) - F_0^R(E)\right)\frac{x}{L+\lambda} \\ F^-(E,x) &= \frac{L\,F_0^L(E)+\lambda F_0^R(E)}{\lambda+L} - \left(F_0^L(E) - F_0^R(E)\right)\frac{x}{L+\lambda} \end{cases} \tag{5.22}$$

where

$$F_0^{R/L} = \frac{E.v}{1 + e^{\frac{E}{k_B T_{R/L}}}} \tag{5.23}$$

are the thermal distribution of the baths at $x = 0/L$ that fix thermal boundary conditions. While the space-dependent distributions $F^{\pm}(E,x)$ are not strictly thermal for $\lambda \neq 0$, in the presence of a redistribution of the energy density mediated by forward-scattering, these distributions tend locally towards a thermal distribution. Assuming an energy redistribution without any energy loss, the local energy density is conserved, and the local temperature associated with these energy fluxes can be defined as

$$\frac{\pi}{12\hbar}k_B^2 T_{\pm}^2(x) = \int \mathrm{d}E\, F^{\pm}(E,x)\,, \tag{5.24}$$

or in other words

$$\begin{cases} T_+^2(x) &= T_L^2 - \frac{T_L^2 - T_R^2}{L+\lambda}x\,, \\ T_-^2(x) &= \frac{L\,T_L^2+\lambda T_R^2}{\lambda+L} - \frac{T_L^2-T_R^2}{L+\lambda}x\,. \end{cases} \tag{5.25}$$

As long as $\lambda/L \neq 0$, each chirality presents a different, well-defined temperature profile. One can, therefore, wonder if it is possible, similarly to what J. Luttinger did in 1964 [9], to define a gravitational analog of this model, and if so, what are the variables conjugated with the gravitational fields.

However, as we have seen in section 3.1, in the absence of anomalies, for a gravitational potential ϕ, inducing a metric tensor of the form

$$g_{\mu\nu} := \begin{pmatrix} e^{2\phi} & 0 \\ 0 & -1 \end{pmatrix}. \tag{5.26}$$

The corresponding equilibrium temperature profiles must verify Eq. (3.5):

$$\vec{\nabla}\phi = -\frac{\vec{\nabla}T}{T}\,, \tag{5.27}$$

However, as long as $T_L \neq T_R$ and away from the ballistic ($\lambda/L \to \infty$) and diffusive ($\lambda/L \to 0$) cases[1], we have

$$\frac{T_R^2 - T_L^2}{T_L^2\,(L+\lambda-x) + T_R^2\,x} \neq \frac{T_R^2 - T_L^2}{T_L^2\,(L-x) + T_R^2\,(\lambda+x)} \Leftrightarrow \frac{\vec{\nabla} T_+}{T_+} \neq \frac{\vec{\nabla} T_-}{T-}\,. \tag{5.28}$$

Therefore, in the generic case, it is impossible for both temperature profiles to be at equilibrium with a single gravitational potential, similarly to the case of the two black holes metric discussed in the previous section 5.1. As a consequence, in order to generalize the Luttinger trick to systems in the presence of two temperature profiles, it is necessary to consider one gravitational potential for each temperature profile, or in other words, one metric per chiral component. In the following part 5.2.2, we will thus introduce this strategy, known as bimetric theory or metric axial tensor theory, before applying it to generalize the Luttinger trick, both in the presence and in the absence of anomalous corrections.

5.2.2 Bimetric theories: Definition, Hamiltonian and (non-)conservation equations

Historically, a bimetric theory was first considered in 3+1 dimension as a possible high-energy extension of general relativity able to solve the expansion problem [192–194]. Its history with gravitational anomalies is more recent. Bimetric theories were considered in a series of papers by L. Bonora and M. Cvitan as a tool to determine the coefficients of the trace anomaly for Weyl fermions in general relativity for 3+1 dimensional systems. The main idea of the authors was to consider general relativity as a limiting case of bimetric theory, generalizing to the trace anomaly the strategy initially proposed by W.A. Bardeen to compute the $\mathcal{U}(1)$ axial anomaly [124, 125, 195]. However, as mentioned earlier in this section, bimetric formalism can find applications in condensed matter physics to generalize Luttinger's trick to theory with two temperature profiles. Therefore, in the following paragraphs, I introduce a bimetric theory, its coupling to fermions, and the corresponding gravitational anomalies. These will then be applied in section 5.2.3 to extend the Luttinger's trick applicability and in section 5.2.4 to tilted semimetals.

Definition and notation

Depending on the problem, two different sets of notations can be used to describe a problem within bimetric formalism:

- A first strategy, similar to the one used in [124, 195], consists in considering a generalized metric operator and its inverse, defined by

$$\begin{cases} \widehat{G}_{\mu\nu} &= g_{\mu\nu} + \widehat{\gamma}^5 f_{\mu\nu}\,, \\ \widehat{G}^{\mu\nu} &= g^{\mu\nu} + \widehat{\gamma}^5 f^{\mu\nu}\,, \end{cases} \tag{5.29}$$

  with

$$\widehat{G}_{\mu\nu}\widehat{G}^{\nu\rho} = \delta_\mu^\rho \Longleftrightarrow \begin{cases} g_{\mu\nu}g^{\nu\rho} + f_{\mu\nu}f^{\nu\rho} = \delta_\mu^\rho \\ g_{\mu\nu}f^{\nu\rho} + f_{\mu\nu}g^{\nu\rho} = 0 \end{cases}\,, \tag{5.30}$$

  and $\widehat{\gamma}^5$ being the chirality operator defined for example in 1+1 dimensions as $\widehat{\gamma}^5 = -\widehat{\gamma}^0\widehat{\gamma}^1 \equiv \widehat{\sigma}^z$.

[1] In the diffusive case, the two temperature profile are identical. We recover the limit considered in chapter 3 that can be treated within the standard Luttinger's trick, resorting to a single gravitational potential.

Note that while $g+f$ and $g-f$ are well-defined metric tensors, f and g are not necessarily well-defined metrics (invertible and with a proper signature) since, for example, general relativity is recovered in the limit $f \to 0$. Moreover, one should pay attention to the fact that whenever f is non-zero, $g^{\mu\nu}$ is no longer the inverse of $g_{\mu\nu}$, see (5.30).
From this operatorial definition of the metric, any given quantity based on the metric, such as the Levi-Civita affine connection $\left\{ \begin{matrix} \mu \\ \nu\rho \end{matrix} \right\}$, the curvature tensor $\mathcal{R}^{\mu}{}_{\nu\rho\sigma}$ or even the momentum-energy tensor $\mathcal{T}^{\mu}_{\nu}$, can be defined, in a similar way, as operators depending on the chiral operator $\widehat{\gamma}^5$. For example, one gets

$$\widehat{\left\{ \begin{matrix} \mu \\ \nu\rho \end{matrix} \right\}} \equiv \left\{ \begin{matrix} \mu \\ \nu\rho \end{matrix} \right\} + \widehat{\gamma}^5 \left\{ \begin{matrix} \mu \\ \nu\rho \end{matrix} \right\}_5 = \frac{1}{2} \widehat{G}^{\mu\epsilon} \left(\partial_\nu \widehat{G}_{\epsilon\rho} + \partial_\rho \widehat{G}_{\nu\epsilon} - \partial_\epsilon \widehat{G}_{\nu\rho} \right) \tag{5.31}$$

or in other words,

$$\begin{aligned} \left\{ \begin{matrix} \left\{ \begin{matrix} \mu \\ \nu\rho \end{matrix} \right\} \\ \left\{ \begin{matrix} \mu \\ \nu\rho \end{matrix} \right\}_5 \end{matrix} \right. &= \tfrac{1}{2} g^{\mu\epsilon} \left(\partial_\nu g_{\epsilon\rho} + \partial_\rho g_{\nu\epsilon} - \partial_\epsilon g_{\nu\rho} \right) + \tfrac{1}{2} f^{\mu\epsilon} \left(\partial_\nu f_{\epsilon\rho} + \partial_\rho f_{\nu\epsilon} - \partial_\epsilon f_{\nu\rho} \right) \\ &= \tfrac{1}{2} g^{\mu\epsilon} \left(\partial_\nu f_{\epsilon\rho} + \partial_\rho f_{\nu\epsilon} - \partial_\epsilon f_{\nu\rho} \right) + \tfrac{1}{2} f^{\mu\epsilon} \left(\partial_\nu g_{\epsilon\rho} + \partial_\rho g_{\nu\epsilon} - \partial_\epsilon g_{\nu\rho} \right) \end{aligned} \tag{5.32}$$

- Alternatively, another strategy consists in decomposing all the quantities into left and right-moving components. Then one defines one metric for left-moving particles $g^{-}_{\mu\nu}$ and one for right-moving particles $g^{+}_{\mu\nu}$. All the metric-dependent quantities can afterward be defined in each chiral sector $+/-$ following the usual route and ignoring entirely the other chirality since left and right-going particles do not interact.

Actually, these two strategies are entirely equivalent, and it is always possible to switch between these conventions, decomposing each quantity as

$$\begin{aligned} \alpha &= \frac{\alpha^+ + \alpha^-}{2} \,, \\ \alpha_5 &= \frac{\alpha^+ - \alpha^-}{2} \,. \end{aligned} \tag{5.33}$$

For example, in terms of the chiral notation, the component of the bi-metric tensor can be written as

$$\begin{aligned} g_{\mu\nu} &= \frac{1}{2} \left(g^{+}_{\mu\nu} + g^{-}_{\mu\nu} \right) \,, \\ f_{\mu\nu} &= \frac{1}{2} \left(g^{+}_{\mu\nu} - g^{-}_{\mu\nu} \right) \,. \end{aligned} \tag{5.34}$$

Now, since in most of our discussion, we decomposed all the thermodynamic quantities into their chiral constituents, for example, as (3.26): $\varepsilon = \varepsilon^+ + \varepsilon^-$, it seems logical for our purpose, to use in the following the second description, defining a metric tensor for each chirality: $g^{\pm}_{\mu\nu}$.

Action, Hamiltonian and momentum-energy tensor

In these chiral notations, the action, the Hamiltonian, and the momentum-energy tensor are split into their left and right-moving components. The total action is then simply the sum of its chiral constituents

$$\mathcal{S} = \mathcal{S}_+ + \mathcal{S}_- \,, \tag{5.35}$$

with

$$\mathcal{S}_\pm = \int \mathrm{d}x^2 \det\left(e^\pm\right) \mathcal{L}_\pm \,, \quad \mathcal{L}_\pm = \frac{i\hbar v_F}{2} \left(e^\pm\right)^{\mu}_{a} \left[\bar{\psi}_\pm \gamma^a \overset{\leftrightarrow}{\partial}_\mu \psi_\pm \right] \,, \tag{5.36}$$

with $(e^{\pm})^{b}_{\ \nu}$ the zweibein associated with the left and right metrics and the chiral fields

$$\psi_{\pm} = \left(1 \pm \gamma^5\right)\psi\,. \tag{5.37}$$

Similarly, one can define one Hamiltonian per chirality as the Legendre transform of the corresponding chiral Lagrangian density

$$\det\left(e^{\pm}\right)\mathcal{H}_{\pm} = \frac{\delta S_{\pm}}{\delta\partial_0\psi}\partial_0\psi + \partial_0\bar{\psi}\frac{\delta S_{\pm}}{\delta\partial_0\bar{\psi}} - \det\left(e^{\pm}\right)\mathcal{L}_{\pm}\,, \tag{5.38}$$

such as

$$\mathcal{H}_{\pm} = \frac{-i\hbar v_F}{2}\left(e^{\pm}\right)^{x}_{a}\left[\bar{\psi}_{\pm}\gamma^a\overset{\leftrightarrow}{\partial}_x\psi_{\pm}\right] \tag{5.39}$$

as well as the corresponding momentum-energy tensor

$$(\mathcal{T}_{\pm})^{\mu}_{\ a} = -\frac{1}{\det(e^{\pm})}\frac{\delta\mathcal{S}_{\pm}}{\delta e^{a}_{\mu}}\,. \tag{5.40}$$

At this level, one could be tempted to deduce an expression for the total momentum-energy tensor from these expressions. However, this is not possible since the indices of each one of the chiral components are raised or lowered using the corresponding chiral metrics. The operatorial form of the metric can solve this issue; however, with our convention, we will always work with each component separately, computing the total contribution solely when measuring the average value of an observable in the laboratory frame.

Anomalies and anomalous momentum-energy tensor in the bimetric formalism

From the gravitational anomalies expressions in the presence of a single metric involving $\mathcal{C}_w = \mathcal{C}_+ + \mathcal{C}_-$ and $\mathcal{C}_g = \mathcal{C}_+ - \mathcal{C}_-$ (2.91), one realizes that these anomalies can be split into two contributions: one for left-going particles and their momentum-energy tensor and one for right-going particles

$$\begin{cases} (\mathcal{T}_+)^{\mu}_{\ \mu} = \mathcal{C}_+\frac{\hbar v_F}{48\pi}\mathcal{R}\,, \\ \nabla_\mu\,(\mathcal{T}_+)^{\mu\nu} = 0\,, \\ (\mathcal{T}_+)^{\mu\nu} - (\mathcal{T}_+)^{\nu\mu} = \mathcal{C}_+\frac{\hbar v_F}{48\pi}\bar{\epsilon}^{\mu\nu}\mathcal{R}\,, \end{cases} \quad \text{and} \quad \begin{cases} (\mathcal{T}_-)^{\mu}_{\ \mu} = \mathcal{C}_-\frac{\hbar v_F}{48\pi}\mathcal{R}\,, \\ \nabla_\mu\,(\mathcal{T}_-)^{\mu\nu} = 0\,, \\ (\mathcal{T}_-)^{\mu\nu} - (\mathcal{T}_-)^{\nu\mu} = -\mathcal{C}_-\frac{\hbar v_F}{48\pi}\bar{\epsilon}^{\mu\nu}\mathcal{R}\,, \end{cases} \tag{5.41}$$

where

$$\mathcal{T}^{\mu\nu} = (\mathcal{T}_+)^{\mu\nu} + (\mathcal{T}_-)^{\mu\nu}\,. \tag{5.42}$$

These equations can, therefore, be generalized within the bimetric formalism modifying the (non-)conservation equation of each chirality by using the corresponding metric to define the curvature, $\mathcal{R}_\pm$, the covariant derivatives $\nabla^{\pm}_{\mu}$ as well as to raise or lower the greek indices. The (non-)conservation equations read[2]

$$\begin{cases} (\mathcal{T}_\pm)^{\mu}_{\ \mu} = \mathcal{C}_\pm\frac{\hbar v_F}{48\pi}\mathcal{R}_\pm\,, \\ \nabla^{\pm}_{\mu}\,(\mathcal{T}_+)^{\mu\nu} = 0\,, \\ (\mathcal{T}_\pm)^{\mu\nu} - (\mathcal{T}_\pm)^{\nu\mu} = \pm\mathcal{C}_\pm\frac{\hbar v_F}{48\pi}\bar{\epsilon}^{\mu\nu}_{\pm}\mathcal{R}_\pm\,. \end{cases} \tag{5.43}$$

[2]In this section of the thesis, we chose to consider the mixed anomaly (conserved but non-symmetric momentum-energy tensor). The purpose is two-fold. First, we explicitly chose to break the chiral symmetry since $\mathcal{H}_R \neq \mathcal{H}_L$, which makes it logical to break this symmetry in (5.43). Second, such a choice is important such that both anomalies only alter the corresponding chiral currents

They can be solved for metrics of the form

$$\mathrm{d}s_{\pm}^2 = f_{1\pm}(x)\mathrm{d}t^2 - f_{2\pm}(x)\mathrm{d}x^2\,, \tag{5.44}$$

in the stationary limit, as

$$\begin{aligned}(\mathcal{T}_{\pm})^{\mu}{}_{\nu} = &\frac{1}{2}\mathcal{C}_{\pm}\begin{pmatrix} 1 & \pm\sqrt{\frac{f_{1\pm}}{f_{2\pm}}} \\ \mp\sqrt{\frac{f_{2\pm}}{f_{1\pm}}} & -1 \end{pmatrix}\gamma\left(T_{\mathrm{TE}}^{\pm}\right)^2 \\ &+\frac{1}{2}\mathcal{C}_{\pm}\begin{pmatrix} \varepsilon_{q\pm}^{(1)}+\varepsilon_{q\pm}^{(2)} & \pm\sqrt{\frac{f_{1\pm}}{f_{2\pm}}}\left(\varepsilon_{q\pm}^{(2)}-\varepsilon_{q\pm}^{(1)}\right) \\ \mp\sqrt{\frac{f_{2\pm}}{f_{1\pm}}}\left(\varepsilon_{q\pm}^{(1)}+\varepsilon_{q\pm}^{(2)}\right) & \varepsilon_{q\pm}^{(1)}-\varepsilon_{q\pm}^{(2)} \end{pmatrix},\end{aligned} \tag{5.45}$$

with the chiral Tolman-Ehrenfest temperatures

$$\gamma\left(T_{\mathrm{TE}}^{\pm}\right)^2 = \frac{\alpha^{\pm}}{f_{1\pm}}\,, \tag{5.46}$$

where $\alpha^{\pm}$ are two constants defined by the boundary conditions. The new chiral quantum energy scales are

$$\varepsilon_{q\pm}^{(1)} = \frac{\hbar v_F}{48\pi}\mathcal{R}_{\pm}\;; \qquad \varepsilon_{q\pm}^{(2)} = \frac{\hbar v_F}{48\pi}\left(\mathcal{R}_{\pm}-2\bar{\mathcal{R}}_{\pm}\right)\,, \tag{5.47}$$

where

$$2\bar{\mathcal{R}}_{\pm} = \frac{1}{f_{1\pm}(x)}\int_{x_0}^{x}\mathrm{d}y\;\mathcal{R}_{\pm}(y)\partial_y f_{1\pm}(y)\,. \tag{5.48}$$

From these definitions, one can deduce the corresponding chiral anomalous Tolman-Ehrenfest temperatures

$$\gamma T_{\pm}^2 = \gamma T_{\mathrm{TE}}^2 + \varepsilon_{q\pm}^{(2)}\,, \tag{5.49}$$

such as the chiral momentum-energy tensors simplify as

$$(\mathcal{T}_{\pm})^{\mu}{}_{\nu} = \begin{pmatrix} 1 & \pm\sqrt{\frac{f_{1\pm}}{f_{2\pm}}} \\ \mp\sqrt{\frac{f_{2\pm}}{f_{1\pm}}} & -1 \end{pmatrix}\mathcal{C}_{\pm}\frac{\gamma}{2}T_{\pm}^2 + \frac{1}{2}\mathcal{C}_{\pm}\begin{pmatrix} \varepsilon_{q\pm}^{(1)} & \mp\sqrt{\frac{f_{1\pm}}{f_{2\pm}}}\varepsilon_{q\pm}^{(1)} \\ \pm\sqrt{\frac{f_{2\pm}}{f_{1\pm}}}\varepsilon_{q\pm}^{(1)} & \varepsilon_{q\pm}^{(1)} \end{pmatrix}. \tag{5.50}$$

At this level, we note that the previous anomalous momentum-energy tensors are identical to those of chapter 3. This is natural since left and right-moving fermions do not interact. Therefore, a theory with a single chiral component, let us say the right moving ones, is equivalent to the result of chapter 3 with a single metric $g_{\mu\nu}^{R}$, and $\mathcal{C}_w = \mathcal{C}_R = \mathcal{C}_g$. Similarly, the left-moving one can be recovered using chapter 3 with a single metric $g_{\mu\nu}^{L}$, and $\mathcal{C}_w = \mathcal{C}_R = -\mathcal{C}_g$.

Equipped with this new formalism, let us then come back to the study of the extended Luttinger's equivalence.

5.2.3 Luttinger trick: From one to two temperature profiles

As we have seen in section 5.2.1, in conductors such that left and right-moving electrons have different temperature profiles, if the left and right temperature gradients are such that

$$\frac{\vec{\nabla}T_R}{T_R} \neq \frac{\vec{\nabla}T_L}{TL}\,, \tag{5.51}$$

it is impossible to directly apply the standard Luttinger's trick. In other words, it is impossible to define a single gravitational potential ϕ such as both T_+ and T_- are equilibrium temperature profile in a metric of the form

$$g_{\mu\nu} = \begin{pmatrix} e^{2\phi} & 0 \\ 0 & -1 \end{pmatrix} \tag{5.52}$$

Observing that in bimetric theory, the presence of chiral equilibrium temperature profiles is natural (5.46), it is logical to explore the possibility of extending the Luttinger trick to such two temperatures systems by resorting to such a bimetric formalism.

Following Luttinger, let us consider a bimetric theory such as left and right metrics are expressed in terms of chiral gravitational potential $\phi_{L/R}$ as

$$g^{\pm}_{\mu\nu} = \begin{pmatrix} e^{2\phi_\pm} & 0 \\ 0 & -1 \end{pmatrix} . \tag{5.53}$$

According to (5.39), the corresponding Hamiltonian reads

$$\mathcal{H} = -\frac{i\hbar v_F}{4} \int \mathrm{d}x \left(e^{\phi_+} + e^{\phi_-}\right) \bar{\psi}\gamma^x \partial_x \psi + \left(e^{\phi_+} - e^{\phi_-}\right) \bar{\psi}\gamma^x\gamma^5 \partial_x \psi \, . \tag{5.54}$$

Note that, by rewriting this Hamiltonian in terms of the flat spacetime energy density and momentum density operators (1.2.2)

$$\mathcal{H} = -\frac{1}{2} \int \mathrm{d}x \left(e^{\phi_+} + e^{\phi_-}\right) h + v_F \left(e^{\phi_+} - e^{\phi_-}\right) \Pi \, , \tag{5.55}$$

one identifies, at the perturbative level in terms of the gravitational fields $\phi_\pm = \phi \pm \phi_5$, ϕ as a field conjugate to the Hamiltonian density h. In contrast, ϕ_5 is conjugated with the chiral Hamiltonian density $h_5 = h_+ - h_-$, which identifies (up to the equation of motion) with the momentum density ($h_5 \equiv v_F \Pi$).

Now, following the previous section 5.2.2, classically (in the absence of anomalies), the equilibrium temperature in this system is given by

$$\begin{cases} \nabla\phi_+ = \frac{\nabla T_+}{T_+} \, , \\ \nabla\phi_- = \frac{\nabla T_-}{T_-} \, , \end{cases} \tag{5.56}$$

or in other words,

$$\begin{cases} \nabla\phi = \frac{\nabla\left[\bar{T}^2 - \Delta T^2\right]}{\bar{T}^2 - \Delta T^2} \\ \nabla\phi_5 = 2\frac{\bar{T}\nabla(\Delta T) - \Delta T \nabla \bar{T}}{\bar{T}^2 - \Delta T^2} \end{cases} \tag{5.57}$$

where $T_\pm = \bar{T} \pm \Delta T$. Classically, and as proposed by J. Luttinger, this implies that one can compute the response of a system set out of equilibrium by chiral temperature profiles by computing the finite homogeneous temperature response of a bimetric gravity system set out of equilibrium by a chiral gravitational potential $\phi_{R/L}$, as long as these gravitational potentials follow (5.56). Note, however, that contrary to what we may have expected, ϕ and ϕ_5 are not simply related to $\bar{T}$ and ΔT respectively, as T with ϕ in the simple metric case, but instead depends both on $\bar{T}$ and ΔT.

In the presence of anomalies, there still exists an equivalence between a system set out of equilibrium by the chiral temperature profiles $T_\pm$ and a system at a fixed non-zero temperature T_0 set out of equilibrium by bimetric gravity metrics of the form (5.53). However,

following (5.20), the classical relation (5.56) gets a quantum correction such that

$$\frac{T_\pm^2(x)}{T_0^2} = e^{-2\phi_\pm(x)} + \lambda_{T_0}^2 \partial_x^2 \phi_\pm(x)\,, \tag{5.58}$$

with $\lambda_{T_0} = \frac{\hbar v_F}{2\pi k_B T_0}$ the thermal length scale.

Therefore, bimetric theory appears as a necessary tool in response theory when considering chiral temperature profiles. It is indeed necessary to extend the notion of Luttinger's trick in conductors such as left and right movers do not have the same temperature profiles. However, as we have seen in chapter 4, the Luttinger trick and the equivalence between curved spacetime physics and condensed matter can be helpful beyond response theory. To illustrate this interest in the case of bimetric theory, in the following section 5.2.4, we will propose a strategy to use bimetric theory to our advantage to study the physics of tilted semimetals.

5.2.4 From two temperature profile to two velocity profiles: tilted Dirac semimetals

In chapter 4, when exploring the correspondence between curved spacetimes and condensed matter physics, we realized that analog curved spacetimes can be obtained in condensed matter by either varying the temperature or the coupling (local velocity). In section 5.2.1, we explored an extension of the Luttinger trick to the case of conductors in which left and right movers temperature differs, introducing the concept of bimetric theories. By analogy, in this section, we would like to consider systems in which left and right movers have different local velocity profiles, a phenomenology reminiscent of the so-called tilted velocity profiles.

In 3+1 dimensional semimetals known as tilted Weyl semimetals such as WP_2 [196] or $Co_3Sn_2S_2$ [197, 198], such dispersion relations naturally arise. They also appear as an effective low-energy theory in semimetals subjected to external stress/deformations such as deformed graphene-like materials [199, 200], or 3D materials such as $NiTe_2$ [201], but also can also be chemically engineered as presented in [202].

In this section, to stick to the strategy developed in the previous section, we focus on 1+1 dimensional systems with chiral velocity profiles $v_{R/L}$ (See Fig. 5.3). To differentiate the magnitude of the velocity from the tilt angle, we use the notations

$$v_{R/L} = v\,(1 \pm \Xi)\ , \tag{5.59}$$

with v the space-dependent Fermi velocity, and Ξ the tilt parameter.
To simplify our approach, in this paragraph, we will make two additional assumptions: first, we will consider either a constant Ξ or a constant v; then, we consider systems such that both v_R and v_L stay positive ($|\Xi| < 1$), opposite to the dramatic case of analog black and white holes often considered in such systems, with a sonic horizon defined by $|\Xi| = 1$ (See Fig. 5.3).

Our objective in this section is to compute the value of observables in the laboratory frame to extend the analysis of the previous chapter to bimetric theory and to underline that despite the absence of analog black holes, such systems still display traces of gravitational anomalies. Let us then consider a bimetric theory defined by

$$\mathrm{d}s_\pm^2 = (1 \pm \Xi)^2 v^2 \mathrm{d}t^2 - \mathrm{d}x^2\,. \tag{5.60}$$

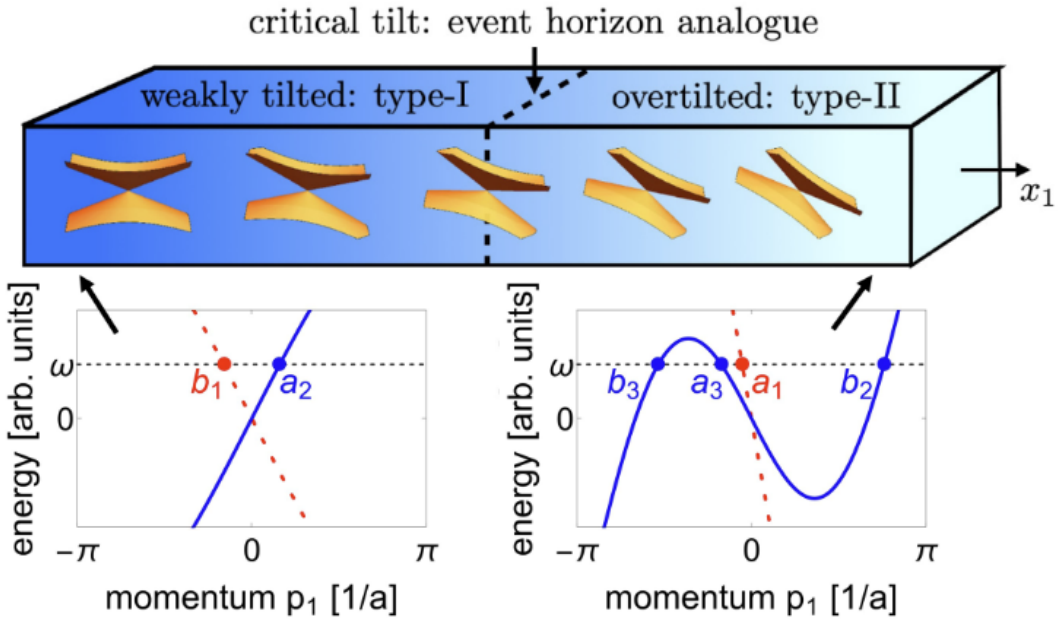

Figure 5.3: **Sketch of a Weyl semimetal with tilt varying along x_1 realizing a white hole analog**. In the region denoted as weakly tilted, the tilt angle is such that $\Xi > -1$, we still observe two chiral velocities with opposite signs. A sketch of the corresponding spectrum is shown in the bottom left corner. Passed the critical tilt $\Xi = -1$, both velocities are negatives, and the electrons propagate in the same direction, providing a white hole analog. A sketch of the corresponding spectrum is shown in the bottom right corner. Note that while we still observe an over-tilted cone around $p_1 = 0$, for symmetry reasons, two other modes labeled b_2 and b_3 appear on each side of the Weyl cone and are not directly captured by the tilted Weyl model. (Extracted from [203])

According to Eq. (5.45), the corresponding momentum-energy tensor reads

$$\begin{aligned}(\mathcal{T}_\pm)^\mu{}_\nu = &\frac{1}{2}\mathcal{C}_\pm \begin{pmatrix} 1 & \pm\frac{v}{v_F}(\Xi\pm 1) \\ \mp\frac{v_F}{v}(\Xi\pm 1)^{-1} & -1 \end{pmatrix} \gamma \left(T^\pm_{\mathrm{TE}}\right)^2 \\ &+ \frac{1}{2}\mathcal{C}_\pm \begin{pmatrix} \varepsilon^{(1)}_{q\pm} + \varepsilon^{(2)}_{q\pm} & \pm\frac{v}{v_F}(\Xi\pm 1)\left(\varepsilon^{(2)}_{q\pm} - \varepsilon^{(1)}_{q\pm}\right) \\ \mp\frac{v_F}{v}(\Xi\pm 1)^{-1}\left(\varepsilon^{(2)}_{q\pm} + \varepsilon^{(1)}_{q\pm}\right) & \varepsilon^{(1)}_{q\pm} - \varepsilon^{(2)}_{q\pm} \end{pmatrix},\end{aligned} \tag{5.61}$$

with $\gamma = \frac{\pi k_B^2}{6\hbar v_F}$ and

$$T^\pm_{\mathrm{TE}} = \frac{v_F}{v} T_0 \left(1\pm\Xi\right)^{-1}, \tag{5.62}$$

while

$$\begin{cases} \varepsilon^{(1)}_{q\pm} = \frac{\hbar v_F}{24\pi}\left[\frac{\partial_x^2 v}{v} \pm \frac{\partial_x^2\Xi}{1\pm\Xi} \pm 2\frac{\partial_x v}{v}\frac{\partial_x\Xi}{1\pm\Xi}\right], \\ \varepsilon^{(2)}_{q\pm} = \frac{\hbar v_F}{24\pi}\left[\frac{\partial_x^2 v}{v} - \left(\frac{\partial_x v}{v}\right)^2 \pm \frac{\partial_x^2\Xi}{1\pm\Xi} - \left(\frac{\partial_x\Xi}{1\pm\Xi}\right)^2\right], \end{cases} \tag{5.63}$$

where v_F defines a fixed velocity scale in the problem.

In such a system, in the laboratory frame, the chiral energy density $\varepsilon_\pm$ read

$$\begin{aligned}\varepsilon^\pm &= \left\langle -\frac{i\hbar v\left(1\pm\Xi\right)}{2}\left(e^\pm\right)^x_a\left[\bar\psi_\pm\gamma^a\overleftrightarrow{\partial}_x\psi_\pm\right]\right\rangle = \left\langle \det\left(e^\pm\right)\left(\mathcal{T}_\pm\right)^0{}_0\right\rangle \\ &= \frac{\mathcal{C}_\pm}{2}\left(\frac{\pi k_B^2 T_0^2}{6\hbar v\left(1\pm\Xi\right)} + \frac{\hbar v\left(1\pm\Xi\right)}{24\pi}\left[2\frac{\partial_x^2 v}{v} \pm 2\frac{\partial_x^2\Xi}{1\pm\Xi} - \left(\frac{\partial_x v}{v} \mp \frac{\partial_x\Xi}{1\pm\Xi}\right)^2\right]\right)\end{aligned} \tag{5.64}$$

while the energy current is expressed as

$$J_\varepsilon^\pm = \pm\frac{\mathcal{C}_\pm}{2}\left(\frac{\pi k_B^2 T_0^2}{6\hbar} + \frac{\hbar v^2\left(1\pm\Xi\right)^2}{24\pi}\left[-\left(\frac{\partial_x v}{v}\right)^2 - \left(\frac{\partial_x \Xi}{1\pm\Xi}\right)^2 \mp 2\frac{\partial_x v}{v}\frac{\partial_x \Xi}{1\pm\Xi}\right]\right). \tag{5.65}$$

Therefore, in the laboratory frame, for a non-chiral theory s($\mathcal{C}_+ = \mathcal{C}_- = \mathcal{C}$), the observables read

- For a fixed tilt parameter Ξ

$$\begin{cases} \varepsilon = \mathcal{C}\left(\frac{\pi k_B^2 T_0^2}{6\hbar v(1-\Xi^2)} + \frac{\hbar v}{12\pi}\left[\frac{\partial_x^2 v}{v} - \frac{1}{2}\left(\frac{\partial_x v}{v}\right)^2\right]\right) \\ J_\varepsilon = -\mathcal{C}\frac{\hbar}{12\pi}\Xi\left(\partial_x v\right)^2 \end{cases} \tag{5.66}$$

- For a fixed velocity v

$$\begin{cases} \varepsilon = \mathcal{C}\left(\frac{\pi k_B^2 T_0^2}{6\hbar v(1-\Xi^2)} - \frac{\hbar v}{24\pi}\frac{(\partial_x \Xi)^2}{1-\Xi^2}\right) \\ J_\varepsilon = 0 \end{cases} \tag{5.67}$$

  Note that $T_\Xi = \frac{\hbar v}{2\pi k_B}\partial_x \Xi$ plays a role of temperature in this system, since at low temperatures and for weak tilts

$$\epsilon \approx -\mathcal{C}\gamma T_\Xi^2\,. \tag{5.68}$$

Note that in these examples, inhomogeneous tilt gives rise to Hawking-like radiation without introducing effective horizons. Moreover, contrary to the example of section 4.2, we observe, thanks to the non-zero tilt, in the steady state of non-chiral conductors, a non-zero energy current.

5.3 Conclusion and perspectives

Historically, the strategy used to describe inhomogeneously tilted Weyl semimetals in section 5.2.4 within the gravity analogy consists in considering metrics with line elements of the form

$$\mathrm{d}s^2 = \alpha\left[c^2\mathrm{d}t^2 - \left(\vec{v}\mathrm{d}t - \mathrm{d}\vec{x}\right)^2\right] \tag{5.69}$$

with α a function depending on the system details. Such a choice of metric also enables us to treat such systems on the same footing as acoustic metrics systems described in section 1.1. Indeed, the 3+1 dimensional acoustic metrics discussed in section 1.1.1 are recovered setting $\alpha = \rho_0$.

A reason underlying this choice of metric is that, in 1+1 dimensions, solving for the light-ray equations

$$\mathrm{d}s^2 = 0\,, \tag{5.70}$$

we end up with two velocities

$$v_\pm = v \pm c\,. \tag{5.71}$$

It turns out that both these strategies, either based on a bimetric theory (5.60), described in the previous section 5.2.4 or on a dynamical acoustic metric (5.69) described above lead to the same action and Hamiltonian. The advantage of the bimetric theory lies in the fact that this strategy is based on equilibrium computations, while the sonic metric (5.69) is a dynamical

metric. An alternative argument, in favor of the acoustic strategy, is the possibility of considering such tilted systems in analogy with the fluids models defined in section 1.1.

This dual treatment of the tilted semimetals in 1+1 dimensions naturally leads to the question regarding the equivalence of these strategies. Indeed, we have seen in chapter 2 that after quantization, the action does not possess the entire information concerning the observables since the measure of integration also matters. It would then be interesting to complete this study by comparing term by term the momentum-energy tensors to check for their strict equivalence between these models. A natural question would then be to determine, in both models, the equilibrium temperature profiles. A complementary question regarding this equivalence concerns Luttinger's trick. We have seen in section 5.2.1 that a traditional treatment based on a single gravitational potential ϕ and the corresponding metric tensor (5.26) cannot account for generic two temperature profiles systems, no matter the corresponding boundary conditions. To extend this strategy, we proposed in section 5.2.3 to resort to a bimetric strategy. Based on this apparent equivalence, we can wonder if a treatment of the Luttinger trick based on a single dynamical metric tensor of the form (5.69).

In this section, extending the concept of Luttinger's trick to chiral temperature profiles, we noticed that while for the double black hole system, a single metric was sufficient to account for two temperature profiles to describe condensed matter conductors, a strategy consists in considering one metric per chirality, or in other words a bimetric theory. Besides, such a strategy raises the question regarding the possibility of considering bimetric theories in physics. This question was first discussed by J. Nissinen and G. Volovik in [204]. They noticed that bimetric theories are heavily constrained by the underlying physics system. There are three important cases:

- If gravity is the primary degree of freedom, there should be a single tetrad field e^{μ}_{a}, identical for both chiralities, which means that the two $SU(2)_{R/L}$ representations are complex conjugates and must have different signs for left and right fermions: This is, for example, the case of the black hole system considered in section 5.1.
- If the chiral left and right fields are the primary degrees of freedom as in the different condensed matter analogs presented in chapter 1, then two subcases can be considered:
  - If the gravity analog has a single spacetime geometry, then there is a constraint that both left and right tetrads should describe the same metric or, in other words,

$$g_{\mu\nu} = \left(e^{a}_{\mu}\right)_{+}\left(e^{b}_{\nu}\right)_{+}\eta_{ab} = \left(e^{a}_{\mu}\right)_{-}\left(e^{b}_{\nu}\right)_{-}\eta_{ab}\,. \tag{5.72}$$

    The possibility to choose them independently comes from the fact that there exists a whole family of tetrad verifying (5.72) since, by definition of a local Lorentz transform

$$\eta_{cd} = \Lambda^{a}{}_{c}(x,t)\eta_{ab}\Lambda^{b}{}_{d}(x,t)\,, \tag{5.73}$$

    one can go from one solution of the tetrad equation (5.72) to another via

$$e^{a}_{\mu}(x,t) \to \tilde{e}^{a}_{\mu}(x,t) = \Lambda^{a}{}_{b}(x,t)e^{b}_{\mu}(x,t)\,. \tag{5.74}$$

    This is, for example, the case of the hydrodynamic analogs presented in section 1.1, in which the mean flow entirely fixes the metric but not the tetrads.
  - If both left and right fermions can have different effective geometries, as described in section 5.2 of this thesis, then both tetrads are entirely independent of each other

since they obey different geometric constraints. This is, for example, the case in systems where left and right fermions interact weakly and possess different velocity or temperature profiles. For example, a platform to realize such a system is given by the inhomogeneous Hamiltonians described in section 1.2.

In this section, we considered several strategies used to describe physical setups in which left and right movers have different properties, either different temperatures or different velocities. First, considering a two-black hole system, we analyzed a natural strategy to introduce two independent temperature profiles based on a single metric tensor with separate boundary conditions. Then, to extend Luttinger's trick to systems with two temperature profiles, we introduced the notion of bimetric theories that we then extended to the study of tilted semimetals. Comparing this new strategy to the historical one, based on acoustic metrics, led us to question their strict equivalence as well as the possibility of using such acoustic metrics to extend Luttinger's trick to two temperature systems. Both of these questions constitute works in progress.

Chapter 6

Remarks on purely dynamical metrics, the dynamical Casimir effect and anomalies

In the examples studied in the last three chapters 3, 4 and, 5, we followed closely the works by R. Tolman and P. Ehrenfest, thus only considering stationary metrics. The notion of dynamics only appeared when considering quenches between two static spacetimes. Our objective was, indeed, to correct the definition of the Tolman-Ehrenfest temperature in the presence of gravitational anomalies and to show their role both in the context of general relativity and of inhomogeneous condensed matter systems.

However, in dynamical systems driven either by their own dynamics, as in cosmology, or by an exterior parameter, as in condensed matter experiments, the perturbation can depend on time. In this chapter, we wish to explore the effects of anomalous corrections in such spacetime. For simplicity, and by analogy with the work we have done in chapter 3 and 4, we will consider purely dynamical spacetimes whose line element read

$$\mathrm{d}s^2 = f_1(t)c^2\mathrm{d}t^2 - f_2(t)\mathrm{d}x^2\,. \tag{6.1}$$

Such spacetimes include for example the Friedmann-Lemaître-Robertson-Walker metric [205–212], introduced to capture the dynamic of the evolution of our universe, and given by

$$\mathrm{d}s^2 = c^2\mathrm{d}t^2 - a^2(t)\mathrm{d}x^2\,, \tag{6.2}$$

where $a(t)$, the scale factor, encodes the universe's evolution: $\partial_t a(t) > 0$ for an expanding universe and $\partial_t a(t) < 0$ for a contracting one.

Therefore, in this section, our objective is to consider such purely dynamical spacetimes and the associated momentum-energy tensors to determine the effects of anomalous fluctuations. After showing how such metrics can be obtained in experimental condensed matter setups, we will compute the associated momentum-energy tensor identifying, in these experiments the effect of anomalous fluctuations on the energy density, the pressure, and the energy currents. Ultimately, we will compare these anomalous gravitational corrections to those appearing in the dynamical Casimir effect. We will, in particular, show that despite their similarity, the anomalous corrections identified in this chapter are unrelated to such dynamical Casimir effects.

The results of this chapter are original and currently unpublished.

6.1 Dynamical gravitational anomalous correction: from expanding universes to condensed matter

In this section, our objective is twofold. First, we would like, analogously to what we have done in chapter 3, to determine and study the anomalous corrections of the momentum-energy tensor of a relativistic quantum field theory in the presence of a purely dynamic curved spacetime given by

$$\mathrm{d}s^2 = f_1(t)c^2\mathrm{d}t^2 - f_2(t)\mathrm{d}x^2\,. \tag{6.3}$$

Then, we would like to demonstrate the experimental relevance of such anomalous corrections. To do this, we will identify experimental platforms whose low energy physics is captured by a quantum field theory in a curved spacetime of the form (6.1). Then, computing the corresponding momentum-energy tensor, we will identify experimental setups in which such anomalous corrections could be observed.

6.1.1 Dynamical curved spacetimes in condensed matter

In chapter 1 and 4, of this thesis, motivated by the Tolmann-Ehrenfest equivalence, we stressed out how inhomogeneities in space could lead to analog curved spacetimes. In this section, in order to study dynamical spacetimes, we will reconsider examples from section 1.1 in the presence of an external drive to show that dynamical metrics of the form (6.1) can be obtained experimentally within several experimental setups.

From expanding Bose-Einstein condensate to expanding universes

A first experimental platform to realize a dynamical metric of the same form as the Friedmann-Lemaître-Robertson-walker metric (6.2) is to consider an expending Bose-Einstein condensate. To understand this parallel, let us follow the derivation used by S. Eckel *et al.* in [213].
As we have seen in section 1.1.2 of the first chapter of this thesis, sound waves in a 3+1 dimensional Bose-Einstein condensate satisfy a curved spacetime Klein-Gordon equation whose metric is given by

$$\mathrm{d}s^2 = \frac{n}{c_s}\left[c_s^2\mathrm{d}t^2 - (\vec{v}\mathrm{d}t - \mathrm{d}\vec{x})^2\right]\,. \tag{6.4}$$

Let us consider a Bose-Einstein condensate ring that we let expand freely with a time-dependent radius given by $R(t)$. The reduced dynamic of the azimuthal modes is captured by the two-dimensional spacetime metric

$$\mathrm{d}s^2 = c_s\left[c_s^2\mathrm{d}t^2 - R^2\mathrm{d}\theta^2\right]\,, \tag{6.5}$$

and the corresponding dynamic tensor

$$f^{\mu\nu} = \sqrt{-g}g^{\mu\nu} = \begin{pmatrix} R & 0 \\ 0 & \frac{-c_s^2}{R} \end{pmatrix}\,. \tag{6.6}$$

The equation of motion of the azimuthal modes ϕ is then captured by

$$\partial_\mu\left(f^{\mu\nu}\partial_\nu\phi\right) = 0\,, \tag{6.7}$$

which corresponds to the equation of motion of a massless Klein-Gordon field in a purely dynamical metric of the form (6.1), with $f_1 = c_s^3$ and $f_2 = c_s R^2$. Considering R_0, the radius at some time t_0, and assuming the sound velocity to be constant, this metric takes the form

$$\mathrm{d}s^2 = c_s^2\mathrm{d}t^2 - \left(\frac{R(t)}{R_0}\right)^2\mathrm{d}x^2\,, \tag{6.8}$$

with $x \equiv \theta R_0$, a metric identical to the expansion metric (6.2), with a scale factor $a(t) = R(t)/R_0$.

Another type of metric in Bose-Einstein condensates obtained by modulating the sound velocity

Following the work from P. Jain *et al.* in [214], another type of dynamical metric can be obtained in experimental setups based on Bose-Einstein condensates. The corresponding protocol is quite different since it involves a modulation of the scattering length, obtained in practice by using a Feshbach resonance [33, 215, 216], instead of modifying its shape as in the previous example. Focusing on a system in which the background flow vanishes $\vec{v} = \vec{0}$, the 3+1 dimensional acoustic metric (6.4) reduces to

$$\mathrm{d}s^2 = \frac{n}{mc_s}\left[c_s^2\mathrm{d}t^2 - \mathrm{d}\vec{x}^2\right] \tag{6.9}$$

with a time dependence solely contained in the sound velocity c_s, since by definition it is related to the scattering length $a(t)$ following

$$c_s^2(t) = \frac{n}{m}\frac{4\pi\hbar^2}{m^2}a(t)\,. \tag{6.10}$$

Note that this metric is 3+1 dimensional, while we are interested in 1+1 dimensional systems. However, by inducing a cigar-shaped trapping potential, the dynamics can be reduced to 1+1 dimensions. Denoting $a(t) = a_0 b(t)$ with a_0 a characteristic length scale, one realizes that modulating the scattering lengths in a cigar-shaped Bose-Einstein condensate realizes yet another example of a dynamical metric of the form (6.1) since the corresponding line element takes the form

$$\mathrm{d}s^2 = \frac{n_0}{c_0}\left[\sqrt{b(t)}c_0^2\mathrm{d}t^2 - \frac{1}{\sqrt{b(t)}}\mathrm{d}\vec{x}^2\right]\,. \tag{6.11}$$

Expanding universes in optical systems

Outside of Bose-Einstein condensates, it is possible to realize dynamical metrics of the form (6.1) in optical systems. Indeed, in optics, the standard length scale $\mathrm{d}x$ is replaced by a new length scale parameter $n(x,t)\mathrm{d}x$, called the optical length, with $n(x,t)$ the refraction index of the considered media. As presented by I. Martin in [217], if one considers the propagation of a polarized electric field in a cavity whose optical index is modulated in time, the equations of motion are given by

$$\frac{1}{c^2}\partial_t^2 E - \frac{1}{n^2(t)}\partial_x^2 E = 0\,. \tag{6.12}$$

This corresponds to a massless Klein-Gordon equation in curved spacetimes whose line element reads

$$\mathrm{d}s^2 = c^2\mathrm{d}t^2 - n^2(t)\mathrm{d}x^2\,, \tag{6.13}$$

reminiscent of an expending universe metric of the form (6.2), with a scale factor such that $a(t) = n(t)$.

Dynamical metrics are, therefore, present in several experimental platforms. Therefore, it is interesting to extend the study of chapter 3 to such spacetime, studying the momentum-energy tensor of such systems and the corresponding anomalous corrections.

6.1.2 Momentum-energy tensor of purely dynamical systems

By analogy with purely stationary metrics, in a purely dynamical metric, the non-zero affine connection components are

$$\begin{aligned} \begin{Bmatrix} 0 \\ 00 \end{Bmatrix} &= \frac{\partial_t f_1}{2f_1}\,, \\ \begin{Bmatrix} 1 \\ 01 \end{Bmatrix} = \begin{Bmatrix} 1 \\ 10 \end{Bmatrix} &= \frac{\partial_t f_2}{2f_2}\,, \\ \begin{Bmatrix} 0 \\ 11 \end{Bmatrix} &= \frac{\partial_t f_2}{2f_1}\,, \end{aligned} \tag{6.14}$$

implying a scalar curvature of the form

$$\mathcal{R} = \frac{1}{v_F^2}\left[-\frac{\partial_t^2 f_2}{f_1 f_2} + \frac{1}{2}\frac{\partial_t f_2}{f_1 f_2}\left(\frac{\partial_t f_2}{f_2} + \frac{\partial_t f_1}{f_1}\right)\right]. \tag{6.15}$$

The solution of the (non-)conservation equations

$$\begin{cases} \mathcal{T}^{\mu}_{\ \mu} = \frac{\hbar c}{48\pi}\mathcal{C}_w\mathcal{R}\,, \\ \mathcal{T}^{\mu\nu} = \mathcal{T}^{\nu\mu}\,, \\ \nabla_\mu \mathcal{T}^{\mu\nu} = \frac{\hbar c}{96\pi}\mathcal{C}_g\frac{\epsilon^{\nu\mu}}{\sqrt{-g}}\nabla_\mu\mathcal{R}\,, \end{cases} \tag{6.16}$$

therefore takes the form

$$\begin{aligned} \mathcal{T}^{\mu}_{\ \nu} = &\begin{pmatrix} u\left(v_F\tau - x\right) + v\left(v_F\tau + x\right) & \sqrt{\frac{f_1}{f_2}}\left[u\left(v_F\tau - x\right) - v\left(v_F\tau + x\right)\right] \\ \sqrt{\frac{f_2}{f_1}}\left[-u\left(v_F\tau - x\right) + v\left(v_F\tau + x\right)\right] & -u\left(v_F\tau - x\right) - v\left(v_F\tau + x\right) \end{pmatrix}\frac{1}{2f_2} \\ &+ \frac{\hbar v_F}{96\pi}\begin{pmatrix} \mathcal{C}_w\left(\varepsilon_q^{(a)} + \varepsilon_q^{(b)}\right) & \mathcal{C}_g\sqrt{\frac{f_1}{f_2}}\varepsilon_q^{(a)} \\ -\mathcal{C}_g\sqrt{\frac{f_2}{f_1}}\varepsilon_q^{(a)} & \mathcal{C}_w\left(\varepsilon_q^{(b)} - \varepsilon_q^{(a)}\right) \end{pmatrix}, \end{aligned} \tag{6.17}$$

with u and v two unknown functions fixed by the boundary condition and τ a new time coordinates defined by

$$\partial_t\tau = \sqrt{\frac{f_2}{f_1}}\,. \tag{6.18}$$

$\varepsilon_q^{(a)}$ and $\varepsilon_q^{(a)}$ are two new energy scales of the problem defined by

$$\varepsilon_q^{(a)} = \frac{\hbar v_F}{48\pi}\left[\frac{1}{f_2}\int \mathcal{R}\partial_t f_2 - \mathcal{R}\right], \quad \varepsilon_q^{(b)} = \frac{\hbar v_F}{48\pi}\mathcal{R}\,. \tag{6.19}$$

Starting from an initially homogeneous and stationary system, the system stays homogeneous in time, with a momentum-energy tensor

$$\mathcal{T}^{\mu}_{\ \nu} = \begin{pmatrix} \mathcal{C}_w & \sqrt{\frac{f_1}{f_2}}\mathcal{C}_g \\ -\sqrt{\frac{f_2}{f_1}}\mathcal{C}_g & -\mathcal{C}_w \end{pmatrix}\frac{\epsilon_0}{2f_2} + \frac{1}{2}\begin{pmatrix} \mathcal{C}_w\left(\varepsilon_q^{(a)} + \varepsilon_q^{(b)}\right) & \mathcal{C}_g\sqrt{\frac{f_1}{f_2}}\varepsilon_q^{(a)} \\ -\mathcal{C}_g\sqrt{\frac{f_2}{f_1}}\varepsilon_q^{(a)} & \mathcal{C}_w\left(\varepsilon_q^{(b)} - \varepsilon_q^{(a)}\right) \end{pmatrix}, \tag{6.20}$$

with $\varepsilon_0 = \varepsilon_T + \varepsilon_L$ the initial energy density defined in the limit of flat space as the sum of the thermal energy density $\varepsilon_T = \gamma T_0^2$ and the Casimir energy density defined for a system of finite size L by

$$\epsilon_L = -\frac{\pi\hbar v_F}{24L^2}\,. \tag{6.21}$$

It appears that analogously to purely stationary metrics, in spacetimes characterized by a metric of the form (6.1), the component of the classical momentum-energy tensor

$$\mathcal{T}^{\mu}_{\ \nu} = \begin{pmatrix} \mathcal{C}_w & \sqrt{\frac{f_1}{f_2}}\mathcal{C}_g \\ -\sqrt{\frac{f_2}{f_1}}\mathcal{C}_g & -\mathcal{C}_w \end{pmatrix} \tag{6.22}$$

receive a correction induced by two new energy scales $\varepsilon_q^{(a)}$ and $\varepsilon_q^{(b)}$. While similar to the energy scales $\varepsilon_q^{(1/2)}$, obtained in chapter 3, the signs of the different terms are different. Therefore, as we will see in the following, the corrections induced by such a dynamical metric are not identical to those obtained in the previous chapters for stationary metrics.

However, similarly to the results obtained in chapter 3, since Einstein anomaly is proportional to the chiral central charge $\mathcal{C}_g$, in non-chiral systems ($\mathcal{C}_g = 0$), the new energy scales $\varepsilon_q^{(a)}$ and $\varepsilon_q^{(b)}$ induced by the drive do not modify the energy currents but only the energy density and the pressure.

6.1.3 Anomalous fluctuations and purely dynamical systems in condensed matter

As we have seen in section 6.1.2, anomalous fluctuations induce in 1+1 dimensional systems two new energy scales that modify the expectation value of the momentum-energy tensor components. In section 6.1.1, we introduced different setups in which such dynamical spacetimes. In this section, our objective is for the two types of dynamical metric we introduced in Eq. (6.8) and (6.11), to discuss the corrections induced by these fluctuations as well as the possibility of observing them experimentally.

Anomalous corrections and analogous expanding universe

Let us start by reconsidering the case of expending universes, realized either in Bose-Einsten condensates or in optical setups. An expanding universe is captured by a metric tensor of the form

$$\mathrm{d}s^2 = c_s^2 \mathrm{d}t^2 - a^2(t)\mathrm{d}x^2\,, \tag{6.23}$$

where c_s, the sound velocity is assumed to be a constant. In such a metric, the new energy scales turn out to be defined as

$$\begin{cases} \varepsilon_q^{(a)} = \frac{\hbar}{24\pi c_s}\left[\frac{\partial_t^2 a}{a} - \left(\frac{\partial_t a}{a}\right)^2\right]\,, \\ \varepsilon_q^{(b)} = -\frac{\hbar}{24\pi c_s}\frac{\partial_t^2 a}{a}\,. \end{cases} \tag{6.24}$$

The energy density, pressure, and energy currents, therefore read

$$\begin{cases} \varepsilon = \frac{\mathcal{C}_w}{2}\left(\frac{\varepsilon_0}{a^2} - \frac{\hbar}{24\pi c_s}\left(\frac{\partial_t a}{a}\right)^2\right)\,, \\ p = \frac{\mathcal{C}_w}{2}\left(\frac{\varepsilon_0}{a^2} + \frac{\hbar}{24\pi c_s}\left[2\frac{\partial_t^2 a}{a} - \left(\frac{\partial_t a}{a}\right)^2\right]\right)\,, \\ J_\varepsilon = \frac{\mathcal{C}_g}{2}\left(c_s\frac{\varepsilon_0}{a^2} + \frac{\hbar}{24\pi}\left[\frac{\partial_t^2 a}{a} - \left(\frac{\partial_t a}{a}\right)^2\right]\right)\,. \end{cases} \tag{6.25}$$

Considering a zero temperature system such as the ground state energy is dominated by the Casimir effect contribution (6.21), over a size L, Eq. (6.25) simplify as

$$\begin{cases} \varepsilon = \frac{\mathcal{C}_w}{2}\left(-\frac{\pi\hbar c_s}{24L^2(t)} - \frac{\hbar}{24\pi c_s}\left(\frac{\partial_t a}{a}\right)^2\right)\,, \\ p = \frac{\mathcal{C}_w}{2}\left(-\frac{\pi\hbar c_s}{24L^2(t)} + \frac{\hbar}{24\pi c_s}\left[2\frac{\partial_t^2 a}{a} - \left(\frac{\partial_t a}{a}\right)^2\right]\right)\,, \\ J_\varepsilon = \frac{\mathcal{C}_g}{2}\left(-\frac{\pi\hbar c_s^2}{24L^2(t)} + \frac{\hbar}{24\pi}\left[\frac{\partial_t^2 a}{a} - \left(\frac{\partial_t a}{a}\right)^2\right]\right)\,. \end{cases} \tag{6.26}$$

with $L(t) = L.a(t)$. Similarly to the study we have performed for the thermal quenches in section 4.2.1, the importance of the anomalous corrections engendered by the gravitational anomalies can be inferred from a comparison of two anomalous time scales of this problem

$$\tau_1^{-1} = \frac{\partial_t a}{a} \text{ and, } \tau_2^{-2} = \partial_t^2 \log \frac{a}{a_0}\,, \tag{6.27}$$

with the natural time scale $L(t)/c_s$. From the anomalous thermodynamic relationship (6.26), we note that the the anomalous time scale τ_1 induces an anomalous corrections $\frac{\hbar}{24\pi v_F \tau_1^2}$ to the instantaneous Casimir energy density $-\frac{\pi\hbar c_s}{24L^2(t)}$. Similarly, the time scale τ_2 is related to the differences between the anomalous energy current and its classical counterpart $J^0_\varepsilon = v_F \frac{\varepsilon_0}{2}$.

In the case of the optical system, interpreting the scale factor $a \equiv n(t)$ as an inverse velocity $n(t) = c/c(t)$, the anomalous correction to the energy density $\Delta\varepsilon = \varepsilon - \frac{\mathcal{C}_w}{2}\frac{\varepsilon_0}{a^2}$ reads

$$\Delta\varepsilon = \mathcal{C}_w \frac{\hbar}{48\pi c}\left(\frac{\partial_t c(t)}{c(t)}\right)^2 . \tag{6.28}$$

This result is reminiscent of the Unruh effect [168,218,219] (also known as the Fulling-Davies-Unruh effect), defining an analog temperature in an accelerated frame. Note that in such a situation, the time scale τ_1 induces a decrease of the total energy of the system.

In the following, to underline the experimental relevance of these corrections, let us evaluate the amplitude of the corrections by considering the momentum-energy tensor of the azimuthal modes of an expanding Bose-Einstein condensate's ring. Let us then consider a fast expansion of the ring between the radius R_0 and R_1 over a time τ. Although our approach applies to a generic radius profile $R(t)$, for the sake of clarity, we choose a profile such that

$$R(t) = \frac{R_0 + R_1}{2} + \frac{R_1 - R_0}{2}\tanh\left(\frac{t}{\tau}\right) . \tag{6.29}$$

The parameters of Fig. 6.1 are motivated by the parameters observed in the experimental work of S. Eckel *et al.* on a ^{23}Na Bose-Einstein condensate described in [213]. We will then consider a sound velocity of the order $c_s \approx 4.10^{-3}\text{m}s^{-1}$, with a Bose-Einstein condensate of radius $R \approx 10\mu$m, and modulate the radius of this ring on a timescale τ such that $\tau \approx 5ms$.

For a small expansion of the condensate, corresponding to a relative ratio $R_0/R_1 = 1.5$, there is a single new timescale τ_2. Indeed, as observed in Fig. 6.1(b), the second timescale τ_1 is negligible compared to R/c_s. As a consequence, the corrected energy density is approximately equal to its classical value, the instantaneous Casimir energy

$$\varepsilon \approx \frac{\mathcal{C}_w}{2}\frac{\varepsilon_0}{a^2} = -\frac{\mathcal{C}_w}{2}\frac{\pi\hbar c_s}{24.(2\pi R(t))^2} . \tag{6.30}$$

For a larger relative ratio $R_0/R_1 = 2.3$, or in other words, a faster expansion of the ring, τ_1 become comparable to R/c_s. As a consequence, and as observed in Fig. 6.1(d), the energy correction becomes noticeable. Two independent timescales then have to be distinguished: τ_1 enters the correction to the energy density while $\tau_1 - \tau_2$ enters the correction to the local pressure. In the case of both large and small expansions, the correction to the classical pressure encoded in $\tau_1 - \tau_2$ is relevant. However, the appearance of the second timescale τ_1 for large expansion can also be observed on the pressure profile. Indeed, while for small expansions, in Fig. 6.1(c), the correction is symmetric with respect to $t = 0$, for larger correction, as

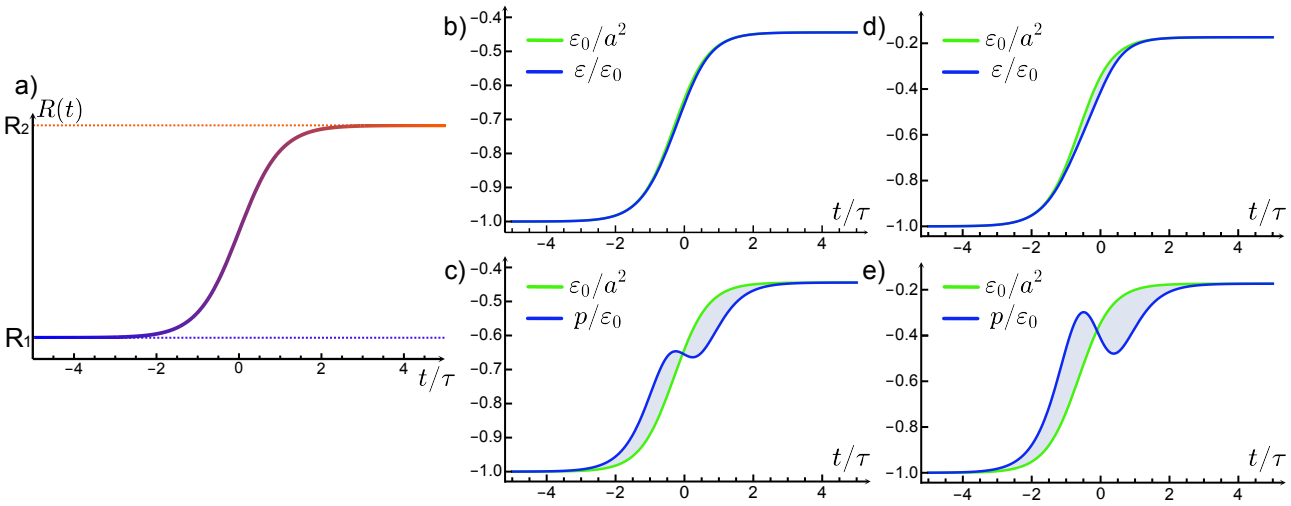

Figure 6.1: **Anomalous corrections to thermodynamics quantities in an expending Bose-Einstein condensate** a) A Bose-Einstein condensate prepared as a ring of radius R_0 undergoes a forced expansion over a time τ until reaching a radius R_1. We consider a time independent sound velocity of $c_s = 4.10^{-3}\mathrm{m}s^{-1}$, observed in a ^{23}Na condensate in [213]. Considering the model to be at zero temperature where the thermodynamics is dominated by the Casimir effect, the quantum corrected thermodynamic quantities are compared to the classical vacuum Casimir energy due to the confinement (6.21) $\varepsilon_0 = \frac{\hbar c_s}{96\pi R_0^2}$. (b) and (c) For a small expansion of the condensate $R_1/R_0 = 1.5$, the time scale τ_1 is neglectful. As a consequence, the energy density is well approximated by the instantaneous Casimir energy $\varepsilon = \frac{-\pi\hbar c_s}{24(2\pi R(t))^2}$, while the pressure is corrected by τ_2, the only relevant timescale. (d) and (e) for larger expansions of the condensate $R_1/R_0 = 2.5$, both τ_1 and τ_2 become relevant. The instantaneous Casimir energy is affected by a quantum correction encoded in τ_1, while the pressure is no longer symetric with respect to the time t=0, due to the timescale τ_1 correcting the symmetric contribution issued from τ_2.

represented in Fig. 6.1(e), due to the timescale τ_1, the pressure become asymmetric. These observations are opposed to the ones of section 4.2.1, for which the pressure was close to its classical value while the energy density was affected by strong quantum corrections.

Another important consequence of the anomalous correction, highlighted in Figs. 6.1(c) and 6.1(e), is that the pressure becomes non-monotonous in time, since it decreases at the middle of the expansion, when $\partial_t^2 a(t)$ cancels out. While in this section, we considered the forced expansion of a condensate, in the case of a freely expanding condensate as the one considered by S. Eckel *et al.* in [213] such a negative pressure would induce an instability. Actually, in the experiment, we do not observe a pure expansion, at late times, the radius of the condensate ring oscillates before reaching an equilibrium value. This observation, therefore, raises the question of whether these observed oscillations can be understood as consequences of the pressure variations induced by the gravitational anomalies that we have identified.

Anomalous corrections in a Bose-Einstein condensate with time-dependent interactions

As we have seen in section 6.1.1, another strategy used to induce a curve spacetime in a Bose-Einstein condensate consists in modulating the sound velocity, for example, by modulating the

scattering length using a Feshbach resonance. In this section, we will therefore analyze the anomalous corrections arising in such a context.

As we have seen in section 6.1.1, the metric tensor corresponding to a 3+1 dimensional condensate whose scattering length is varied is given by

$$\mathrm{d}s^2 = \sqrt{b(t)}c_0\mathrm{d}t^2 - \frac{1}{\sqrt{b(t)}}\mathrm{d}x^2\,. \tag{6.31}$$

where the dimensionless coefficient $b(t)$ encodes the variation of the scattering length $b(t) = a(t)/a_0$, and c_0 the sound velocity associated to the scattering length a_0.

In this context, the two new energy scales are given by

$$\begin{cases} \varepsilon_q^{(a)} = \frac{\hbar}{96\pi c_0\sqrt{b}}\left[\frac{\partial_t^2 b}{b} - \frac{3}{2}\left(\frac{\partial_t b}{b}\right)^2\right], \\ \varepsilon_q^{(b)} = \frac{\hbar}{96\pi v_F\sqrt{b}}\left[-\frac{\partial_t^2 b}{b} + \frac{5}{4}\left(\frac{\partial_t b}{b}\right)^2\right]. \end{cases} \tag{6.32}$$

where $c_0\sqrt{b}$ corresponds to the instantaneous sound velocity $c_s(t)$. The energy density, pressure, and energy currents, therefore read

$$\begin{cases} \varepsilon = \frac{\mathcal{C}_w}{2}\left[\sqrt{b}\varepsilon_0 - \frac{\hbar}{384\pi c_0\sqrt{b}}\left(\frac{\partial_t b}{b}\right)^2\right], \\ p = \frac{\mathcal{C}_w}{2}\left[\sqrt{b}\varepsilon_0 + \frac{\hbar}{48\pi c_0\sqrt{b}}\left[\frac{\partial_t^2 b}{b} - \frac{11}{8}\left(\frac{\partial_t f}{f^2}\right)^2\right]\right], \\ J_\varepsilon = \frac{\mathcal{C}_g}{2}\left[\sqrt{b}\varepsilon_0 + \frac{\hbar}{96\pi c_0\sqrt{b}}\left[\frac{\partial_t^2 b}{b} - \frac{3}{2}\left(\frac{\partial_t b}{b}\right)^2\right]\right]. \end{cases} \tag{6.33}$$

In the limit of zero temperature, the classical energy density is dominated by the Casimir energy density (6.21)

$$\varepsilon_0 = -\frac{\pi\hbar c_0}{24L^2}\,. \tag{6.34}$$

Restoring the instantaneous sound velocity $c_s(t)$, Eq. (6.33) simplify into

$$\begin{cases} \varepsilon = \frac{\mathcal{C}_w}{2}\left[-\frac{\pi\hbar c_s}{24L^2} - \frac{\hbar}{384\pi c_s}\left(\frac{\partial_t b}{b}\right)^2\right], \\ p = \frac{\mathcal{C}_w}{2}\left[-\frac{\pi\hbar c_s}{24L^2} + \frac{\hbar}{48\pi c_s}\left[\frac{\partial_t^2 b}{b} - \frac{11}{8}\left(\frac{\partial_t f}{f^2}\right)^2\right]\right], \\ J_\varepsilon = \frac{\mathcal{C}_g}{2}\left[-\frac{\pi\hbar c_s}{24L^2} + \frac{\hbar}{96\pi c_s}\left[\frac{\partial_t^2 b}{b} - \frac{3}{2}\left(\frac{\partial_t b}{b}\right)^2\right]\right], \end{cases} \tag{6.35}$$

with $-\frac{\pi\hbar c_s}{24L^2}$ the instantaneous Casimir energy. Written in this form, as in the case of an expanding condensate, we identify two anomalous energy scales

$$\tau_1^{-1} = \frac{\partial_t b}{b} \text{ and, } \tau_2^{-2} = \partial_t^2 \log b\,, \tag{6.36}$$

that, compared to the natural energy scale L/c_s, control the physics of the system.

Let us then evaluate the amplitude of the corrections for a ramping of the scattering length from its original value a_0 to a maximal value of a_1 over a time τ. While Eq. (6.35) gives us access to the anomalous correction for any ramp profile, in this section, for simplicity, we will consider a scattering length profile of the form

$$a(t) = \frac{a_0 + a_1}{2} + \frac{a_1 - a_0}{2}\tanh\left(\frac{t}{\tau}\right). \tag{6.37}$$

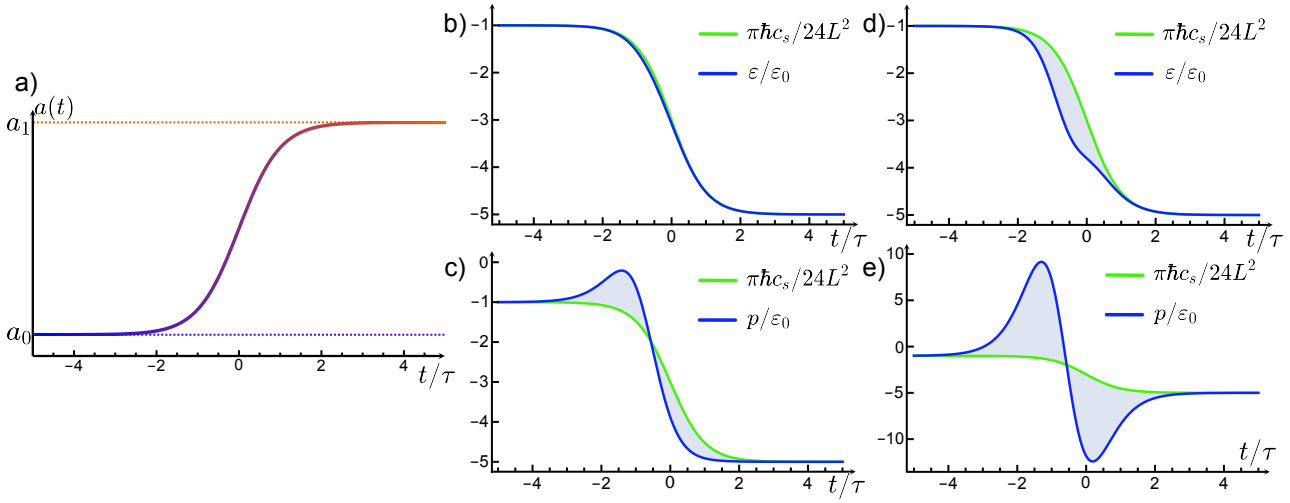

Figure 6.2: **Anomalous corrections to thermodynamics quantities while ramping the scattering lengths in a Bose-Einstein condensate** a) A Bose-Einstein condensate is prepared as a thin needle of length $L \approx 10\mu$m. Using a Feshbach resonance strategy one modulates the scattering length from an initial value a_0 to a final value of $a_1 = 5a_0$ over a time τ. We consider a sound velocity of $c_s = 4.10^{-3}\mathrm{m}s^{-1}$, observed in a ^{23}Na condensate in [213]. For simplicity of the treatment, we will consider the model to be at zero temperature such as the classical energy density is given by the instantaneous Casimir energy due to the confinement (6.21): $\varepsilon_L = -\frac{\pi\hbar c_s}{24L^2} - \frac{\hbar}{384\pi c_s}$, with $c_s = c_0\sqrt{\frac{a(t)}{a_0}}$ the time-dependent sound velocity. (b) and (c) For a slow ramp of the condensate scattering length, over a time $\tau = 5ms$, the time scale τ_1 is negligible compared to the natural timescale L/c_s. As a consequence, the energy density is well approximated by the instantaneous Casimir energy $\varepsilon = \frac{-\pi\hbar c_s(t)}{24L^2}$, while the pressure is corrected by τ_2, the only relevant anomalous timescale. A striking consequence of this new energy scale, common with the previous example, is that the pressure is non-monotonous (d) and (e) for faster ramps of the condensate scattering length, over a time $\tau = 1ms$, both τ_1 and τ_2 become relevant. The instantaneous Casimir energy is reduced by a quantum correction encoded in τ_1, while the pressure correction is increased.

The results are shown in Fig. 6.2. We expect the gravitational anomalies to alter the classical properties of the steady states in regions where τ_1 and τ_2 become sizable and of the same order of magnitude than L/c_s, or in other words, when the scattering length varies a lot. Therefore, we focus in the following on the effects of the gravitational anomalies in the vicinity of the ramp at $t = 0$.

The parameters of Fig. 6.2 are the same that those used for Fig. 6.1, motivated by the realization of a Bose-Einstein condensate in ^{23}Na by S. Eckel *et al.* described in [213]. For a slow ramp of the condensate scattering lengths, corresponding to a ramp over a time $\tau = 5ms$, there is a single anomalous timescale τ_2. Indeed, as observed in Fig. 6.2(b), the second timescale τ_1, correcting the local energy density, is negligible. As a consequence, the corrected energy density is approximately equal to its classical value, the instantaneous Casimir energy

$$\varepsilon \approx \frac{\mathcal{C}_w}{2}\frac{\varepsilon_0}{a^2} = -\frac{\mathcal{C}_w}{2}\frac{\pi\hbar c_s(t)}{24.L^2}\,. \tag{6.38}$$

For a faster ramp, over a time $\tau = 1ms$, as observed in Fig. 6.2(d), the timescale τ_1 becomes relevant and, as a consequence the energy density corrections become noticeable. Two independent timescales have to be distinguished, both τ_1 entering the correction to the energy density

and $\tau_1 - \tau_2$ entering the correction to the local pressure. For both large and small relative ratios, the correction to the classical pressure encoded in $\tau_1 - \tau_2$ is relevant. A particularly striking consequence of the corrected pressure, also observed in Figs. 6.1(c) and 6.1(e) is that due to these corrections, the pressure becomes non-monotonous over time.

6.1.4 Limits and perspectives of this study

In this section, we have seen that anomalous quantum fluctuations induced by the gravitational anomalies can induce corrections on the observables of Bose-Einstein condensates that are modulated in time. They notably correct the pressure and the energy density when the time variation of the metric is strong enough. However, as noticed in section 6.1.2, in non-chiral systems, the energy current is not affected by such anomalous corrections.

However, the previous study was done in an ideal limit. It is then interesting to reconsider these approximations to underline the limit of our approaches, which constitutes a possible extension of this work. First of all, this study was done in the ideal limit of a zero-temperature system. In the case of a non-zero temperature system, we can wonder if the thermal contribution to the energy density is low enough to observe the anomalous corrections we mentioned in section 6.1.3. Moreover, in this section, the computed thermodynamics quantities correspond to vacuum properties or, in other words, to the many-body ground state properties. Therefore, an underlying approximation of this chapter is that despite the external drive, the system stays in its ground state. This approximation, sometimes called the adiabatic approximation, implies that the drive must be slow enough to prevent populating higher energy states. A natural extension of this work would then be to study the consequences of non-adiabatic effects on the anomalous corrections discussed in this chapter. Finally, a major hypothesis in this section is that we considered all these examples as purely 1+1 dimensional systems. This constraint raises two major questions. First, in bosonic analog models, 1+1 dimensionality induces a strong constraint on the dynamical tensor defined by $f^{\mu\nu} = \sqrt{\det(g_{\alpha\beta})}g^{\mu\nu}$, where $g_{\mu\nu}$ is the metric tensor. Indeed, the determinant of $f^{\mu\nu}$ must be equal to -1, or at least have to be a constant to be absorbed in the constant of the problem. This explains why we had to consider the sound velocity as a constant in section 6.1.1. However, in the experiment, this constraint is not always satisfied, in [213], the authors noticed that the radial velocity depends on the Bose-Einstein condensate radius as $c_s \propto R^{-2/7}$. Therefore, one can wonder what consequences of the anomalous fluctuations deduced in this chapter remain relevant in the presence of this time-dependent sound velocity. Another related question is that, assuming the system to be completely 1+1 dimensional, we consider the orthogonal degree of freedom as frozen. One can legitimately wonder which conclusions of our 1+1 dimensional approach would remain relevant if these orthogonal degrees of freedom were not entirely frozen, exchanging energy with the longitudinal ones.

Both of the limits mentionned in the previous paragraph come from the fact that the system considered is bosonic and not purely 1+1 dimensional. An alternative strategy to observe the consequence of anomalous fluctuation would be to consider quantum Hall systems with expanding edges, as discussed recently in [220] since such systems are fermionic and purely 1+1 dimensional. The metric tensor in such systems, as well as the corresponding anomalous contribution, remains to be explored.

Besides these remarks concerning the range of applicability of our results, it is interesting to note that the density of energy current J_ε obtained in the analog expanding systems (6.25) is

similar to the one obtained by S. Fulling and P. Davies in the context of the dynamical Casimir effect [166]. In the next section, we will show that despite this similarity, the dynamical Casimir effect is in fact, disconnected from the anomalous correction we discussed in this section but is nonetheless related to the notion of trace anomaly.

6.2 A link with the dynamical Casimir effect

As we have seen in the previous section, in a time-dependent medium, the energy density, the pressure, and the energy current are modified by the anomalous fluctuations issued from the gravitational anomalies. Another correction to the momentum-energy tensor emerging in a 1+1 dimensional cavity modulated in time is the dynamical Casimir effect [221, 222]. Therefore, it is natural to wonder if it is possible to relate the correction induced by gravitational anomalies to the modified momentum-energy tensor observed in the context of the dynamical Casimir effect.

In this section, after introducing the dynamical Casimir effect, we will compare the results obtained in this context to the one obtained from the gravitational anomalies in the previous section before concluding the section on another way to relate trace anomalies to the dynamical Casimir effect.

6.2.1 Historical description

The dynamical Casimir effect in 1+1 dimensions characterizes the properties of systems in a 1+1 dimensional cavity with moving boundaries. An archetypical example is, therefore, that of a polarized electric field $\vec{E} = E(x,t)\vec{e}_z$ between two mirrors whose positions are given by $x = 0$ and $x = L(t)$. The corresponding equations of motion are given by

$$\partial_t^2 E = c^2 \partial_x^2 E \,, \tag{6.39}$$

with reflective (Dirichlet) boundary conditions

$$E(0,t) = E(t, L(t)) = 0 \,. \tag{6.40}$$

While, first considered for classical mechanics in 1921 by E. Nicolai for a mirror with a fixed velocity [221] ($L(t) = L_0(1 + \alpha t)$), the interests of such a setup raised in the 1960s with the invention of lasers. In quantum mechanics, this problem is also fascinating since it can be shown that, starting from the ground state of the cavity, the mirror's movement induces the creation of light quanta in the cavity [222].

A key technique to solve this problem was identified by G. Moore [222], who realized that it is possible to map the flat spacetime problem with time-dependent boundary conditions onto a curved spacetime problem with static boundary conditions. The corresponding trick works as follows. Let us introduce new coordinates s and y such as

$$\begin{cases} ct - x = f(c\tau - y) \,, \\ ct + x = g(c\tau + y) \,. \end{cases} \tag{6.41}$$

The equations of motion in the new coordinates system (τ, y) are identical to the one in (t, x),

$$\partial_\tau^2 E = c^2 \partial_y^2 E \,, \tag{6.42}$$

but the boundary conditions now depend on the choice of f and g. It is then possible to select a specific choice of coordinates in which the two mirrors stay fixed in time at position $y = 0$ and $y = l$ by imposing $f(x) = g(x) = R^{-1}(x)$ with

$$R\left(t + L(t)\right) - R\left(t - L(t)\right) = l\,. \tag{6.43}$$

This strategy to map a flat-spacetime problem with dynamic boundary conditions onto a curved-spacetime problem with fixed boundary conditions was later used by P. Davies and S. Fulling in 1976 [166] to define the renormalized momentum-energy tensor of the theory given in the flat spacetime coordinates by

$$\mathcal{T}_{\mu\nu} = \begin{pmatrix} -f(ct-x) - f(ct+x) & f(ct-x) - f(ct+x) \\ f(ct-x) - f(ct+x) & -f(ct-x) - f(ct+x) \end{pmatrix}, \tag{6.44}$$

with

$$f(x) = \frac{\pi\hbar c}{48 l^2}\left(\partial_x R\right)^2 + \frac{\hbar c}{24\pi}\left[\frac{\partial_x^3 R}{\partial_x R} - \frac{3}{2}\left(\frac{\partial_x^2 R}{\partial_x R}\right)\right]. \tag{6.45}$$

These results were afterward verified experimentally in several platforms such as Bose-Einstein condensates [223], Josephson junstions [224], and microwave cavities [225].

Comparing this expression of the momentum-energy tensor to the one obtained for the dynamical metric, one realizes that f looks identical to the expression obtained for the anomalous energy current obtained in the expanding universe model (6.25) at zero temperature for $a = 1/\partial_x R$. This raises the question of a possible link between the dynamical Casimir effect and the gravitational anomalies.

6.2.2 Dynamical Casimir effect and trace anomaly

In this section, our objective is to determine whether one can relate the dynamical Casimir effect to gravitational anomalies. Following the analysis of G. Moore [222], it is possible to relate the system with time-dependent boundaries with a system with static boundaries by changing the coordinates as

$$\begin{cases} R(ct-x) = c\tau - y\,, \\ R(ct+x) = c\tau + y\,. \end{cases} \tag{6.46}$$

Starting from a flat spacetime, $\mathrm{d}s^2 = c^2\mathrm{d}t^2 - \mathrm{d}x^2$, this implies that the new spacetime is curved with a metric given by

$$\mathrm{d}s^2 = \left(\mathrm{d}\tau^2 - \mathrm{d}y^2\right)\partial R^{-1}(c\tau - y)\cdot\partial R^{-1}(c\tau + y)\,. \tag{6.47}$$

However, this metric's scalar curvature $\mathcal{R}$ still vanishes. Therefore, the gravitational anomaly corrections to the momentum-energy tensor presented in the previous chapter of this thesis are absent. This led P. Davies and S. Fulling to state that

> "*The relation of that (conformal anomaly) effect, which involves a failure of the usual tracelessness of $\mathcal{T}_{\mu\nu}$, to the present work is unclear.*"

In fact, an indirect relation exists between the precise form of the momentum-energy tensor and the conformal anomaly that goes beyond the scope of the present thesis. Indeed, even though there is no scalar curvature ($\mathcal{R} = 0$), the effective action is not strictly equal to zero. As a consequence, the momentum-energy tensor no longer transforms under a conformal transform $x^\mu \to \tilde{x}^\mu$ as a tensor

$$\mathcal{T}_{\mu\nu} \to \tilde{\mathcal{T}}_{\mu\nu} = \frac{\partial\tilde{x}^\rho}{\partial x^\rho}\frac{\partial\tilde{x}^\rho}{\partial x^\rho}\mathcal{T}_{\mu\nu}\,. \tag{6.48}$$

Instead, under a conformal transformation of the form

$$\begin{cases} c\tilde{t} + \tilde{x} = g(ct + x)\,, \\ c\tilde{t} - \tilde{x} = f(ct - x)\,, \end{cases} \tag{6.49}$$

the chiral components of the momentum-energy tensor

$$\begin{cases} \mathcal{T}_{++} = \frac{1}{4}\left(\mathcal{T}_{00} + \mathcal{T}_{xx} + 2\mathcal{T}_{0x}\right)\,, \\ \mathcal{T}_{--} = \frac{1}{4}\left(\mathcal{T}_{00} + \mathcal{T}_{xx} - 2\mathcal{T}_{0x}\right)\,, \end{cases} \tag{6.50}$$

behave like [76, 226]

$$\begin{cases} \mathcal{T}_{++} \to \tilde{\mathcal{T}}_{++} = \dot{f}^{-2}(ct-x)\left[\mathcal{T}_{++} - \mathcal{C}_+ \frac{\hbar c}{24\pi}\left(\frac{\dddot{f}(ct-x)}{\dot{f}(ct-x)} - \frac{3}{2}\left(\frac{\ddot{f}(ct-x)}{\dot{f}(ct-x)}\right)^2\right)\right]\,, \\ \mathcal{T}_{--} \to \tilde{\mathcal{T}}_{--} = \dot{g}^{-2}(ct+x)\left[\mathcal{T}_{--} - \mathcal{C}_+ \frac{\hbar c}{24\pi}\left(\frac{\dddot{g}(ct+x)}{\dot{g}(ct+x)} - \frac{3}{2}\left(\frac{\ddot{g}(ct+x)}{\dot{g}(ct+x)}\right)^2\right)\right]\,, \end{cases} \tag{6.51}$$

with $\dot{f}(x) = \partial_x f(x)$. Assuming that the system stays at rest in its ground state in the curved space spanned by y and τ, then, at zero temperature, following Casimir [134], the energy density and pressure verify

$$\varepsilon = p = -\frac{\pi\hbar c}{24 l^2} \tag{6.52}$$

Using the transformation rules (6.51), we directly recover, in the original coordinates, the expression of the momentum-energy tensor obtained previously by P. Davies and S. Fulling (6.44).

6.2.3 Conclusion

In conclusion, a time modulation of the parameters of a relativistic system can be taken into account in the equation of motion as a time modulation of the induced spacetime metric. By doing so, it is possible to generate a large variety of dynamical spacetimes. It is, for example, possible to mimic a Friedman-Lemaître-Robertson-walker used to describe the universe expansion. Now, as the space modulation of a metric led to new energy scales in the context of the modified Tolman-Ehrenfest Temperature 3, these time modulations similarly introduce new energy scales. These new energy scales introduce a time modulation of the local energy density and pressure and are captured by the concept of gravitational anomalies. Therefore, it is possible to observe the effects of gravitational anomalies in dynamical systems. While such systems are often related to a historical example of time-modulated systems known as the dynamical Casimir effect, their physics is quite different. Indeed, while G. Moore [222] proved that one could interpret the dynamical Casimir effect as a system with field boundary conditions in a distorted spacetime, the corresponding spacetime is effectively flat. As a consequence, the precise form of its momentum-energy tensor cannot be directly related to the gravitational anomalies.

Chapter 7

The consequences of anomalies for a historical dispute: Does the equilibrium temperature depend on gravity?

In the previous chapters, we analyzed different effects of the gravitational anomalies on thermodynamics quantities and the definition of temperature in a curved spacetime. In this chapter, we will discuss how these modifications shed new light on the historical Loschmidt-Maxwell-Boltzman dispute.

7.1 Loschmidt-Maxwell-Boltzmann dispute and the adiabatic temperature gradient

In this section, we review the historical dispute opposing J. Maxwell, J. Loschmidt, and L. Boltzmann concerning the temperature profile of a column of gas in the presence of a non-zero gravitational potential. This dispute can be traced back to the late 19^{th} century and received a renewed interest at the end of the 20^{th} century following a paper by D. Evans reviewing the origins of the dispute [227] and several papers proposing experimental signatures of these postulates [228–231].

7.1.1 Historical arguments

The historical disputes between J. Maxwell, L. Boltzmann, and J. Loschmidt concern the temperature profile in the presence of gravity. On the one hand, J. Maxwell and L. Boltzmann thought that the temperature in a column of gas should be homogeneous even in the presence of gravity. Their historical argument, relying on the kinetic theory of gases, goes as follows: first, J. Maxwell [232] reminds us that the temperature profile must be identical in every compound,

> "*if two vertical columns of different substances stand on the same perfectly conducting horizontal plate, the temperature of the bottom of each column will be the same; and if each column is in thermal equilibrium of itself, the temperatures at all equal heights must be the same. In fact, if the temperatures of the tops of the two columns were different, we might drive an engine with this difference of temperature, and the refuse heat would pass down the colder column, through the conducting plate, and up the warmer column; and this would go on till all the heat was converted into work, contrary to the second law of thermodynamics.*"

Then, relying on the knowledge of gases, he concludes that the temperature profile must be homogeneous

> "*But we know that if one of the columns is gaseous, its temperature is uniform*[From the kinetic theory of gases]. *Hence that of the other must be uniform, whatever its material.*"

A similar argument, not resorting to the kinetic theory of gases, goes as follows. Assume you have a vertical column of gas in a gravitational field and suppose that, after equilibrium is reached, a vertical temperature gradient is present. If this is true, we can use a wire or some other heat-permeable material to connect the upper and lower parts of the gas container and create, just like in Maxwell's scheme, a heat engine with a single temperature source, using gravity as its fuel.

While the impossibility of creating such an engine is at the heart of J. Maxwell and L. Boltzmann's argument, the possibility of creating such an engine is viewed as an exciting perspective by J. Loschmidt [87]:

> "*Thereby the terroristic nimbus of the second law is destroyed, a nimbus which makes that second law appear as the annihilating principle of all life in the universe, and at the same time we are confronted with the comforting perspective that, as far as the conversion of heat into work is concerned, mankind will not solely be dependent on the intervention of coal or of the sun, but will have available an inexhaustible resource of convertible heat at all times.*"

J. Loschmidt never argued why a temperature gradient did not contradict the second law of thermodynamics but instead proposed an argument based on the first law, which goes as follows. Imagine a vertical column containing gas. At equilibrium, there should be no energy currents. Therefore, this system's energy density is homogeneous. Since the potential energy $\varepsilon_p = \rho g z$ increases with altitude, the kinetic energy has to decrease. Assuming a kinetic distribution of the kinetic energy $\varepsilon_k = \frac{1}{2} k_B T$, this implies that the temperature decreases linearly with height.

Forgotten for a long time, this historical dispute was recently reconsidered experimentally in several papers in liquids, gases, and metals [228–231]. These experiments, directly related to the dispute by the authors, can also be related to more recent discussions of the so-called adiabatic temperature gradient.

7.1.2 The adiabatic temperature gradient

As mentioned previously, this dispute was afterward forgotten. However, the question concerning the presence of a thermal gradient in a fluid submitted to a gravitational potential is an experimental reality known as the adiabatic temperature gradient.

In his book, "Physical Fluid Dynamics" [233], D. Tritton describes the underlying physical process as follows. Let us consider a small fluid bubble. As the fluid rises, the ambient pressure reduces, and the bubble expands, so the fluid cools down; as the bubble falls, it compresses, and the fluid warms up. The corresponding adiabatic temperature gradient can then be computed using adiabatic thermodynamics identities in a perfect fluid. During an adiabatic expansion, there is no heat variation, $\delta Q = 0$. Therefore, following the first rule of thermodynamics,

$$\mathrm{d}U = \delta W \iff n C_v \mathrm{d}T = -P \mathrm{d}V \,. \tag{7.1}$$

From the perfect gases identity

$$PV = nRT\,, \tag{7.2}$$

together with Mayer's relation relating C_p, the molar specific heat at constant pressure, C_v, the molar specific heat at constant volume and R the gas constant,

$$C_p - C_v = R\,, \tag{7.3}$$

these relations simplify to

$$C_p P\mathrm{d}V + C_v V\mathrm{d}P = 0\,. \tag{7.4}$$

Assuming that C_p and C_v are almost constant in the considered system, from this relation, we recover the adiabatic relations

$$\begin{cases} PV^{\gamma} = \mathrm{Cst}\,, \\ TV^{\gamma-1} = \mathrm{Cst}\,, \\ T^{\gamma}P^{1-\gamma} = \mathrm{Cst}\,, \end{cases} \tag{7.5}$$

with $\gamma = C_p/C_v$, the adiabatic index. For perfect monoatomic gases, we have $\gamma \approx 5/3$ while for a diatomic one $\gamma \approx 7/4$. Assuming a mechanical equilibrium, the pressure gradient in the system verifies

$$\nabla P = -\rho g = -m\frac{P}{RT}g\,, \tag{7.6}$$

with m the molar mass of the corresponding gas. Together with the adiabatic relations (7.5), we recover the adiabatic temperature gradient, also known in geophysical usage as the adiabatic lapse rate.

$$\nabla T = \frac{mg}{R}\frac{1-\gamma}{\gamma} = -\frac{mg}{C_p}\,, \tag{7.7}$$

implying a temperature profile of the form

$$T(z) = T_0 - \frac{mg}{C_p}z\,. \tag{7.8}$$

In our readings of the phenomenon, looking back, both points of view are coherent with one another. Indeed, J. Loschmidt focuses on local energy relaxation. On the contrary, the homogeneisation of the temperature in this system is due to large-scale energy relaxation processes such as the Rayleigh-Bénard instability [234, 235]. Since in practice such processes are very slow, such as the global relaxation proposed by L. Boltwman and J. Maxwell is never reached.

Note, however, that in every experimental setup, these temperature profiles, while similar to the Tolmann-Ehrenfest results, have an entirely different origin. Indeed, the speed of light appears explicitly in the classical Tolmann-Ehrenfest's relation, which for a weak gravitational potential reads

$$\frac{\nabla T}{T} = -\frac{g}{c^2} \tag{7.9}$$

and is so weak ($\nabla T \approx 0.88$mK/Km for earth gravity with a mean temperature around 300K) that it is impossible to observe it experimentally in classical systems. In the following section, we will consider relativistic, massless systems and study the interplay between this controversy and Tolmann-Ehrenfest's relation in the presence and absence of gravitational anomalies.

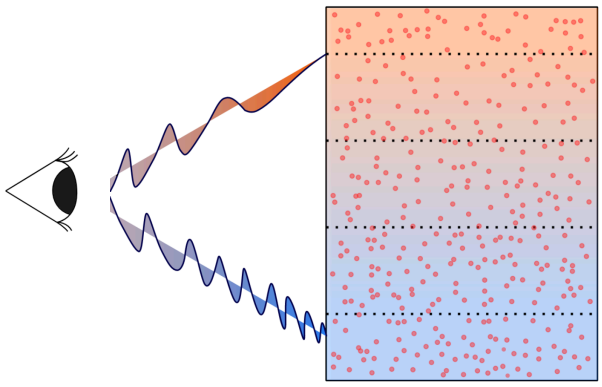

Figure 7.1: **Tolman-Ehrenfest temperature and redshift** Classically, an observer located at some position x_0 perceives the whole system at a homogeneous temperature due to the gravitational blueshifts and redshifts (adapted from [137]).

7.2 Thermodynamic consequences of the anomaly

In the previous section, we considered the historical disputes between J. Maxwell, L. Boltzmann, and J. Loschmidt within classical physics. However, as we have seen in chapter 3, in the presence of curved spacetime, R. Tolmann, and P. Ehrenfest proved that the equilibrium temperature profile is not homogeneous but instead, in a metric of the form

$$\mathrm{d}s^2 = f_1(x)\mathrm{d}t^2 - f_2(x)\mathrm{d}x^2\,, \tag{7.10}$$

it follows

$$T(x) \propto \frac{1}{\sqrt{f_1(x)}}\,. \tag{7.11}$$

We can, therefore, wonder how these results compare to the previously mentioned dispute.

7.2.1 Tolmann-Ehrenfest's temperature and thermal machine

First, let us consider the equilibrium temperature profile of a system in curved spacetime in the absence of gravitational anomalies. In the absence of gravitational anomalies, in a metric of the form

$$\mathrm{d}s^2 = f_1(x)\mathrm{d}t^2 - f_2(x)\mathrm{d}x^2\,, \tag{7.12}$$

we recovered in chapter 3 a temperature profile of the form

$$T(x) \propto \sqrt{\frac{1}{f_1(x)}}\,. \tag{7.13}$$

Following J. Maxwell and L. Boltzmann, such an inhomogeneous temperature profile might seem surprising since it could be used as a perpetual energy source building a thermal machine between two regions with different f_1 values. Such a conclusion would, however, be quite inaccurate. To see this, let us consider a situation in which an observer is located at some position x_0. According to Tolman-Ehrenfest's relation, the local temperature profile at a position x verifies

$$T(x) = T_0\sqrt{\frac{f_1(x_0)}{f_1(x)}}\,. \tag{7.14}$$

However, a photon emitted at some position x_1 towards the observer will be redshifted or blueshifted by a factor $\sqrt{\frac{f_1(x_1)}{f_1(x_0)}}$. Therefore, a photon emitted at a frequency ω will be measured by the observer at a frequency $\omega_r = \omega_1\sqrt{\frac{f_1(x_1)}{f_1(x_0)}}$. Therefore, the emitted photon distribution is given by

$$n_e(\omega) = \frac{1}{e^{\frac{\hbar\omega}{k_B T(x_1)}} - 1}\,. \tag{7.15}$$

The photon distribution received by the observer situated in x_0 is then given by

$$n_r(\omega) = \frac{1}{e^{\frac{\hbar\omega}{k_B T(x_1)}\sqrt{\frac{f_1(x_1)}{f_1(x_0)}}} - 1}\,, \tag{7.16}$$

such that the energy received by this observer is given by

$$\varepsilon = \int c^{-1}\mathrm{d}\omega\,\hbar\omega\, n_r(\omega) = \frac{\pi^2}{6\hbar c}\frac{f_1(x_1)}{f_1(x_0)}k_B^2 T^2(x_1) = \frac{\pi^2}{6\hbar c}k_B^2 T_0^2 \tag{7.17}$$

The perceived temperature at position x_0 is therefore T_0.

In conclusion, the observer perceives the whole system at the same temperature T_0, which is in agreement with the remark from C. Rovelli and M. Smerlak [133] who stated that the Tolman-Ehrenfest temperature profile is passive (no work can be extracted from it). Therefore, the Tolman-Ehrenfest temperature profile is in complete agreement with the argument formulated by J. Maxwell and L. Boltzmann and the second law of thermodynamics. Several authors such as C. Rovelli and M. Smerlak [133] or J. Santiago and M. Visser [137] even consider this agreement with the second law of the thermodynamics as a postulate to redemonstrate the Tolman-Ehrenfest's relations.
However, as we have seen earlier, when one considers the anomalous fluctuations induced by the gravitational anomalies, the temperature profile is corrected, and one can wonder how this new temperature profile compares to Maxwell-Boltmann's arguments.

7.2.2 Anomalous Tolman-Ehrenfest's temperature and thermal machine

As mentioned previously, in the presence of gravitational anomalies, the definition of the equilibrium temperature is altered by the presence of new energy scales. In a metric of the form (7.12), the anomalous Tolman-Ehrenfest temperature reads (3)

$$k_B^2 T_{\mathrm{An}}^2(x) = \frac{k_B^2 T_0^2}{f_1(x)} + \varepsilon_2^{(q)} \tag{7.18}$$

with

$$\varepsilon_2^{(q)} = \frac{\hbar c}{48\pi}\left[\frac{\partial_x^2 f_1}{f_1 f_2} - \frac{\partial_x f_1}{f_1 f_2}\left(\frac{\partial_x f_1}{f_1} + \frac{1}{2}\frac{\partial_x f_2}{f_2}\right)\right]\,. \tag{7.19}$$

Following the same step as above, involving a blueshift or a redshift of the energy current received by an observer situated at position x, the radiation emitted at some position y is perceived at a temperature $T_p(y)$ such that

$$\gamma T_p^2(y) = \gamma T_0^2 + f_1(y)\,\varepsilon_q^{(2)}(y)\,. \tag{7.20}$$

Therefore, it seems possible to harvest the gravitational energy by building a heat engine between the position x and y since they have a non-zero difference of temperature

$$k_B^2 \Delta T^2 = \frac{6\hbar c}{\pi} \left[f_1(y) \varepsilon_q^{(2)}(y) - f_1(x) \varepsilon_q^{(2)}(x) \right] . \tag{7.21}$$

For example, in the case of a Schwarschild black hole, the metric is defined with $f_1 = 1/f_2 = 1 - \frac{r_H}{r}$, such as the anomalous Rolman-Ehrenfest reads

$$T_{\rm An}^2(r) = T_H^2 \left(1 + \frac{r_H}{r} + \frac{r_H^2}{r^2} - 3\frac{r_H^3}{r^3} \right) , \tag{7.22}$$

with $T_H = \frac{\hbar c}{4\pi k_B} \frac{1}{r_H}$, the Hawking temperature. the perceived temperature by an infinite observer is, therefore,

$$T_{\rm P}^2(r) = T_H^2 \left(1 - 4\frac{r_H^3}{r^3} + 3\frac{r_H^4}{r^4} \right) \tag{7.23}$$

and it seems possible for an infinite observer to build a thermal machine using its ambient temperature as a hot source ($T = T_H$) and the black hole horizon as a cold source.

7.3 Conclusion and discussions

In this chapter, after reviewing the historical dispute opposing J. Maxwell and L. Boltzmann to J. Loschmidt concerning the temperature profile of a column of gas in the presence of a non-homogeneous gravitational potential, we generalized our discussion to relativistic gases in generic curved spacetimes. In the absence of gravitational anomalies, the gravitational redshift compensates the gradient of temperature obtained following the work from R. Tolmann and P. Ehrenfest. However, the anomalous corrections induced by the gravitational anomalies induce a non-zero temperature gradient, a conclusion that we examplified in the case of a Schwarzschild black hole in Eq. (7.23).

This conclusion seems to contradict the second principle of thermodynamics since we can build a thermal machine with a single heat source (the black hole). Two reasons might be able to explain such a paradox. First, the system we are considering is not at equilibrium: as proposed by Hawking [2], black holes slowly evaporate, which might explain why we can harvest its energy. Second, another question that naturally arises is whether the strategy applied to the radiating phonon in the previous section can really be applied in this case. Since energy and pressure differ from each other, we can wonder whether the blueshift or redshift can be applied directly to the temperature or if one needs to treat pressure and energy density differently; in other words, what is the phonon distribution associated to the anomalous temperature profile $T_{\rm An}$.

Two things are worth noticing at this point. First, note that while non-zero, the temperature difference observed previously is tiny (around 6.10^{-8}K for the hottest known black hole). Second, note that while we took as an example the situation of a black hole, these ideas can be generalized to any system with an inhomogeneous gravitational potential.

In conclusion, while the classical Tolman-Ehrenfest is in complete agreement with the second law of thermodynamics, inducing only passive temperature gradients, when considering the gravitational anomalies, this conclusion is inaccurate. As a consequence, it then seems possible to harvest free energy from the gravitational anomalies. This conclusion seems to revive the

Maxwell-Boltzmann-Loschidt dispute in relativistic systems. However, it must be considered cautiously since some relativistic systems, such as black holes, are not strictly at equilibrium. A natural perspective of this work would consist in computing the work induced by the metric on its environment, comparing it to the work that one can extract with a heat engine connected to separate points of this system.

Chapter 8

Magnetothermal transport in $ZrTe_5$

Topological semimetals provide a natural playground to study transport properties that can be interpreted as manifestations of anomalies of relativistic field theories [15, 96]. Indeed, the low-energy quasiparticles in these materials are massless pseudo-relativistic quasiparticles that split into two groups with left- and right-handed chirality. The classical conservation laws for the electric and momentum-energy currents preserve quasiparticles of each chirality number and energy. However, a transfer of electrons and energy between chiralities can occur when an electric field E or a temperature gradient ∇T, respectively, are applied parallel to a magnetic field B. Such breaking of the conservation laws are known as the chiral [70, 102, 236] and gravitational anomalies [13, 110, 115, 116, 127, 182] and are predicted to modulate electric (σ_{xx}) and thermal longitudinal conductivities κ_{xx}, respectively.

The possibility of modulating magneto-conductance properties by anomalies motivated an important experimental effort [103, 237–239] to reach the ideal conditions where anomalous transport can be observed [16, 240], as discussed in section 2.2.3. The precise objective was to observe the negative magnetoresistance, recently related to the chiral anomalies in semimetals. However, as discussed in Fig. 2.4, a precise measure of the electrical currents is made difficult by a phenomenon known as the current jetting [241]. This phenomenon, common to metallic samples with low density of carriers whose experimental consequence is illustrated in Fig. 8.1, comes from the fact that in the presence of non-ideal electronic contacts, the inhomogeneous current injection leads, in the presence of a magnetic field, to strongly distorted electronic equipotentials, making a precise measure of the magnetoresistivity challenging. Therefore, reaching the ideal conditions for anomalous transport has proven to be a challenging experimental task. In a remarkable experimental push, $Bi_{1-x}Sb_x$ [240] samples were tuned to such ideal conditions: they lacked current jetting, showed little quantum oscillations (indicating that E_F was near the Weyl nodes). However, the sizable effort required to reach such ideal conditions raises doubts about the fragility of anomaly-induced transport and the carefully tuned conditions in which it can be observed experimentally.

To circumvent this experimental difficulty, it is interesting to study heat conduction instead of electronic conduction, or in other words, to study the magnetothermal conductivity. However, the measurement of such a thermal conductivity presents a major drawback. Indeed, while electronic transport properties can be directly associated to a property of the electrons, the only charge carriers in these materials, heat transport is typically dominated by the phonons, whose contribution must be dominant due to their large density. A challenge in the determination of the electron magnetothermal conductivity then consists in decoupling the contribution of electrons from the one of phonons.

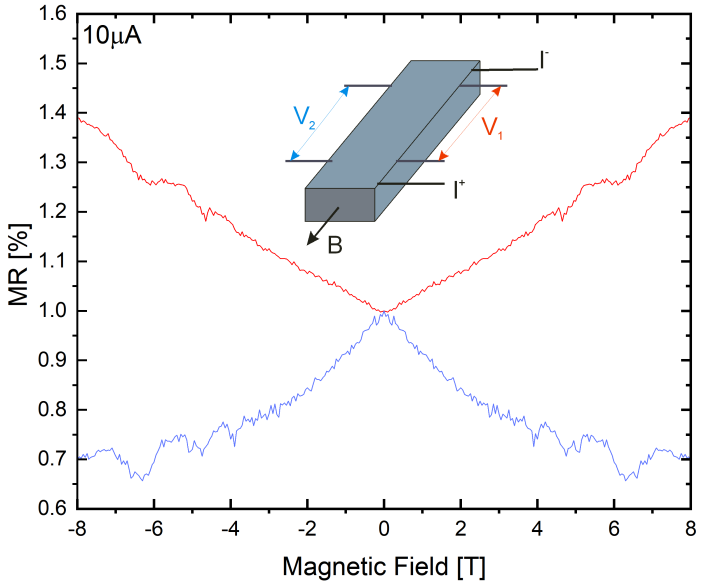

Figure 8.1: **Experimental signatures of current jetting in $ZrTe_5$**: (a) Longitudinal magnetoresistance $MR = V(B)/V(0)$ for different pairs of contacts: The longitudinal magnetoresistance is either negative or positive depending on contact location. The inset depicts the measurement geometry for each measure.

Historically, a strategy used to differentiate the contribution of the electrons from the one of phonons consists in evaluating the electronic contribution , resorting to the proportionality relationship between the contribution of the electrons to the electrical conductivity (σ) and thermal conductivity (κ) known as the Wiedemann-Franz law [242, 243]

$$L_0 = \frac{\kappa}{\sigma T} = \frac{\pi^2 k_B^2}{3e^2}\,. \tag{8.1}$$

However, using such a strategy, we directly come back to the original difficulty of current jetting, discussed in the previous paragraph.

Alternatively, in the presence of a strong magnetic field, as discussed in section 2.2.3, the 3+1 dimensional dynamics is reduced to a finite density of independent 1+1 dimensional conduction channel named Landau levels. When the magnetic field is increased, Landau levels are progressively emptied one by one, leading to an oscillatory behavior of the conductivity induced by the electron, both electronic and thermal. The oscillatory behavior of the electronic conductivity is, for example, captured by the so-called Shubnikov–de Haas effect [244–247]. Since only charged particles couple to a magnetic field, one can expect these oscillations to be of purely electronic origin, allowing to determine the electronic component of the thermal conductivity. Besides, through the Landau-level description of magnetothermal transport, we relate the study of thermal transport in 3+1 dimensional materials to a study of 1+1 dimensional thermal transport, drawing a direct link with the rest of this thesis.

However, in ordinary metals with large Fermi surfaces, such as copper, decoupling the physics of the different Landau levels requires inaccessibly large magnetic fields $B > 10,000T$. Considering semimetals, or in other words, low-density metals, is therefore necessary. Furthermore, even though phonons do not directly couple to the magnetic field, scattering between

phonons and electrons can still induce oscillations in the phonon contribution to the magnetothermal conductivity [248–251]. An experimental strategy to evaluate the magnitude of such a contribution is the measurement of the ultrasound attenuation. Indeed, since interactions of phonons with the electrons would induce a change in the speed of sound, evaluating the attenuation of a sound pulse in the semimetal allows one to evaluate the contribution of the phonon to the fluctuation of the magnetothermal conductivity (See for example Fig. 8.2 for the result of ultrasound attenuation in a $ZrTe_5$ sample).

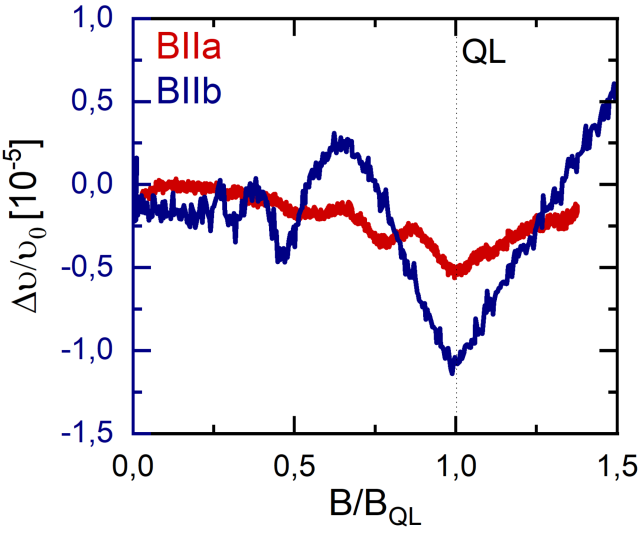

Figure 8.2: **Ultrasound attenuations in $ZrTe_5$**: Sound–velocity variation $\Delta v/v_0$ of a longitudinal sound mode propagating along the a-axis as a function of magnetic field applied along the a-axis (red) and b-axis (blue) at 1.7 K. For clarity the magnetic field in both measurements is scaled with respect to the quantum limit ($B^a_{QL} = 12$T and $B^b_{QL} = 1.2$T). The change of the sound velocity corresponds to the change of the phonon contribution to the thermal conductivity with B.

In this chapter, we will discuss the result of a collaboration with an experimental group from the Max Planck Institute in Dresden dedicated to the study of the magnetothermal transport properties of the Dirac semimetal $ZrTe_5$. First, we will motivate the choice of the Weyl semimetal $ZrTe_5$ to carry out these experiments. Then, we will see that a 1+1 dimensional study of the Landau level conductivity, similar to the one used in section 2.2.3, provides predictions of longitudinal transport properties of $ZrTe_5$ in qualitative agreement with the experimental measurement. However, the orthogonal magnetotransport experiments invalidate these scenarii and point towards a new transport phenomenon resulting from a strong coupling between phonons and electrons.

8.1 Magnetothermal transport in $ZrTe_5$: motivations and measurements

In this section, let us motivate the choice to perform the experiments on the Dirac semimetal $ZrTe_5$.

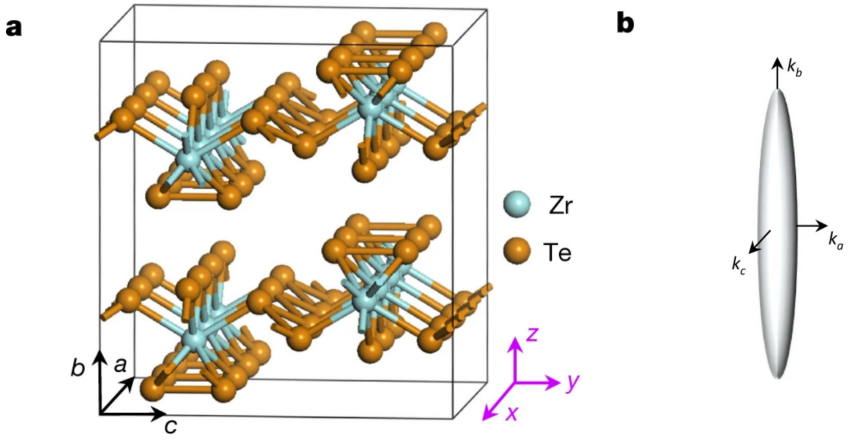

Figure 8.3: **Three-dimensional morphology, and crystalline structure of $ZrTe_5$**: (a) Crystal structure of $ZrTe_5$ and definition of the crystal axis (b) Sketch of the experimentally extracted Fermi surface of $ZrTe_5$ along the momentum vectors k_a, k_b and k_c in a, b, and c directions, respectively (Adapted from [252] and [253]).

$ZrTe_5$ band structure is simple, a single elliptical 3D Fermi surface that comprises less than 1% of the Brillouin zone [103, 252, 253] (see Fig. 8.3(b)). The density of electrons is low, and the quantum limit can be reached in magnetic fields as low as $B^c_{QL} \approx 1.2T$ and $B^a_{QL} \approx 12T$ when B is applied along the c- and a- crystal directions, respectively [252,253]. A measurement highlighting the presence of such a dimensional reduction from a 3+1 dimensional system to 1+1 dimensional subsystems within this Dirac semimetal is the quasi-quantized Hall effect, observed recently in $ZrTe_5$ [253].

To support an electron-dominated magnetothermal conductivity, it is essential to compare the amplitude of electron and phonon magnethothermal oscillations. Two different measurements provide hints pointing towards electron-dominated oscillations. First, below the Bloch-Grüneisen temperature, θ_{BG}, the average phonon wavelength is larger than the Fermi sea's size. Therefore, electrons and phonons are expected to interact weakly. Since phonons interact with the magnetic field only through their interactions with electrons, this implies that the magnetic field effect on magnetothermal conductivity oscillations is very weak. Since the experiment is performed at $1.3K$, smaller than the determined Bloch-Grüneisen temperature, θ_{BG} of $3.1K$, we expect no phonon contribution to the magnetothermal oscillations.

To further quantify the phonon contribution, the experimental group also studied the ultrasound propagation velocity as a function of the magnetic field. Since interactions of acoustic phonons with electrons in Landau bands would lead to a change in the speed of sound, they measured the change in sound velocity Δv_s to study the role of phonons in the thermal magnetotransport experiments. In particular, they measured the change in sound velocity of the longitudinal mode (propagation along the a-axis, polarization vector along the a-axis) as a function of a magnetic field B applied along the a-axis (and along the b-axis) on the same crystal where the heat transport experiments were carried out. As shown in Fig. 8.2, not only the relative change of the sound velocity with the magnetic field at $T = 1.3K$ is five orders of magnitude smaller than the relative change of thermal conductivity with the field, but we also observe a suppression of v_s with increasing field, in contrast to the magneto-thermal conductivity. Hence, the change of the thermal conductivity of phonons with the magnetic field cannot

account for the change of the total longitudinal magneto-thermal conductivity.

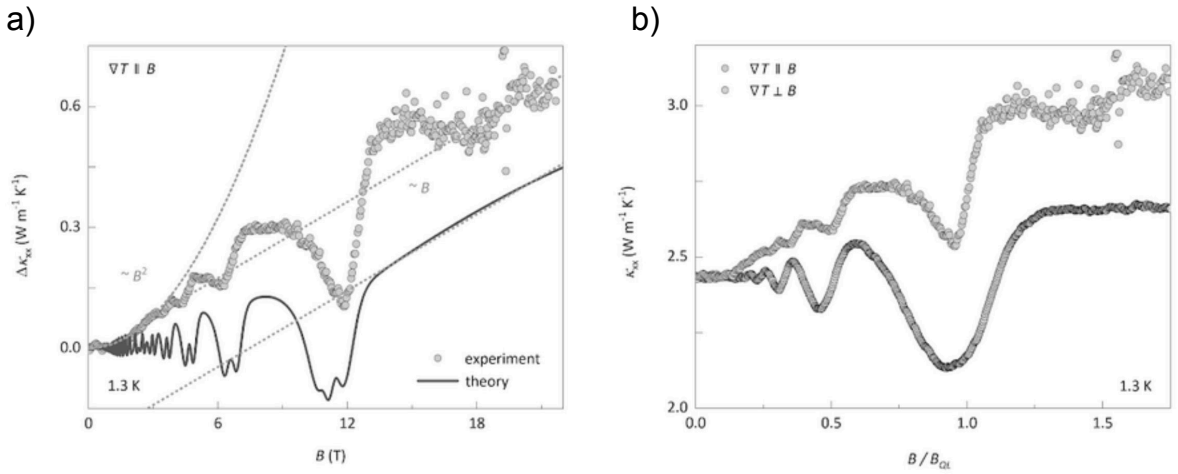

Figure 8.4: **Magnetothermal measurements in $ZrTe_5$** (a) Variation of the thermal conductivity $\kappa_{xx}(B) - \kappa_{xx}(0)$ for B applied parallel to ∇T at $T = 1.3\,K$. At low fields ($B < 3\,T$), the measurement data (large open dots) is well-described by a quadratic fit (dotted line). At $B > 3\,T$, quantum oscillations appear. A transition to the quantum limit identified by a B-linear regime is observed for $B \gtrsim 12T$. The solid red line denotes the results of the theoretical model in the presence of backscattering events, described in section 8.2.3. (b) Thermal conductivity κ_{xx} of $ZrTe_5$ as a function of B with respect to the quantum limit B_{QL} at a temperature of $T = 1.3\,K$ with ∇T applied along the a-axis of the crystal. The red dots denote the measurement data for B applied in parallel to ∇T, and the blue dots for B applied perpendicular to ∇T, along the b-axis of the crystal. Both measurements display quantum oscillations for $B > B_{QL}/4$, for the same magnetic field value.

Therefore, $ZrTe_5$ appears to be a good candidate to probe for the possible signatures of gravitational anomalies in magnetothermal conductivity. $ZrTe_5$ samples display strong electrical current jetting (See Fig. 8.1); the experimental group, therefore, carried out steady-state thermal transport experiments with open electrical contacts. Owing to its low electronic density, we observe clear thermal quantum oscillations.

Fig. 8.4(a) displays the change of the longitudinal magnetothermal conductivity $\Delta\kappa_{xx}(B) = \kappa_{xx}(B) - \kappa_{xx}(B = 0)$ at $1.3K$ for $\nabla T \parallel B$ (both applied along the a-axis of the $ZrTe_5$ crystal). We observe a positive magnetothermal conductivity $\Delta\kappa_{xx}(B) > 0$. At low magnetic field B, in the semiclassical regime, the longitudinal $\Delta\kappa_{xx}(B)$ is well described by a quadratic fit $\Delta\kappa_{xx}(B) \propto B^2$. By increasing B, we observe quantum oscillations in $\Delta\kappa_{xx}(B)$ and a transition to a B-linear behavior $\Delta\kappa_{xx}(B) \propto B$, typical of the quantum limit for $B \gtrsim B^a_{QL} = 12T$. The quantum limit of $B^a_{QL} = 12T$ inferred from these thermal transport measurements (see Fig. 8.4) agrees with the value determined previously in electrical transport experiments [252–254] for a field applied in the a-direction on these samples.

In the following, to analyze the magnetothermal conductivity data and look for possible effects of the 1+1 dimensional gravitational anomaly, we adopt the low energy, linear order $k \cdot P$ model and the parameters experimentally determined in [253] and presented in Eq. (8.2). Based on this model, we compute the longitudinal heat current for a parallel gradient of temperature ∇T and magnetic field B, applied along the a-direction. First, we compare the experimental data to the ballistic results. Then, we resort to a 1+1 dimensional Boltzmann equation

to determine the correction to the magnetothermal heat current induced by the presence of back-scattering. While these calculations reproduce and explain several key features of the experimental data when approaching the quantum limit (for $B > 6T$) and below the Bloch-Grüneisen temperature of $\theta_{BG} = 3.1K$, several features such as the orthogonal conductivity observed in Fig. 8.4(b) cannot be explained by the dimensional reduction. Therefore, in the last section, we will propose another scenario to explain them.

8.2 Thermal transport along the magnetic field as a 1+1 dimensional thermal transport

In this section, using a strategy similar to the one introduced by H. Nielsen and M. Ninomiya to describe electronic transport properties induced by the chiral anomaly in [12] described in section 2.2.3, we analyze the longitudinal magnetothermal measurement. After recalling the low-energy properties of $ZrTe_5$, deriving the corresponding Landau spectrum, we will compute the transport properties of a single Landau level to deduce the transport properties of the whole 3+1 dimensional system. This strategy will first be applied within a ballistic approximation before being refined by considering the effects of backscattering.

8.2.1 From a 3+1 dimensional band structure to 1+1 dimensional Landau levels in $ZrTe_5$

Hamiltonian and coupling to a magnetic field

In order to describe the thermal transport in a $ZrTe_5$ sample based on the above considerations, we will adopt the low energy, linear order $k \cdot P$- model also used for instance in [253] and the values of the parameters determined therein. Let us then consider a massive anisotropic 3+1D Dirac Hamiltonian such as

$$\mathcal{H}_D = m\tau^3\sigma^0 + \hbar\left[v_a k_a \tau^1\sigma^3 + v_b k_b \tau^1\sigma^1 + v_c \tau^2\sigma^0 k_c\right] \tag{8.2}$$

where the τ and σ are the 2×2 Pauli matrices operating on orbital and spin degree of freedom, $m \approx 10$meV is the mass-gap, and $v_a = 116392\, m.s^{-1}$, $v_b = 15340\, m.s^{-1}$ and $v_c = 348875\, m.s^{-1}$ are the Fermi velocity components along the a-, b- and c-direction of the crystal, which correspond to the x, z and y-direction respectively (see Fig. 8.3) A magnetic field will then enter this Hamiltonian via two different contributions:

- The usual minimal coupling procedure $-i\hbar\partial_\mu \rightarrow -i\hbar\partial_\mu + eA_\mu$ with A_μ the vector potential.
- A "Zeeman" coupling term: $H_Z = -\frac{1}{2}g\mu_B\tau^0\vec{\sigma}.\vec{B}$ with μ_B the Bohr magneton and g the orbital-independant Landé g-factor.

Landau level spectrum for $B \parallel x$ (along the a-axis)

In order to describe the longitudinal magneto-thermal conductivity experiment, we first determine the Landau level associated with the model (8.2). Let us consider a situation where the thermal conduction is measured along the x-axis, which is the axis along which the magnetic field is applied ($\vec{B} = B\hat{x}$). Using the translation invariance along the x-axis, the Hamiltonian can, therefore, be expressed in the symmetric gauge where

$$A_\mu = \left(0, 0, \frac{-Bz}{2}, \frac{By}{2}\right) \tag{8.3}$$

as a function of $p_x = -i\hbar\partial_x$, $\Pi_y = -i\hbar\partial_y - \frac{eB}{2}z$ and $\Pi_z = -i\hbar\partial_z + \frac{eB}{2}y$ as

$$H_{Tot} = \begin{pmatrix} m & E_Z & v_a p_x - i v_c \Pi_y & v_b \Pi_z \\ E_Z & m & v_b \Pi_z & -v_a p_x - i v_c \Pi_y \\ v_a p_x + i v_c \Pi_y & v_b \Pi_z & -m & E_Z \\ v_b \Pi_z & -v_a p_x + i v_c \Pi_y & E_Z & -m \end{pmatrix} \tag{8.4}$$

with

$$E_Z = -\frac{1}{2} g \mu_B B \,. \tag{8.5}$$

After a 90° rotation of the spin axis along the $-\hat{y}$ vector $x \to z$ and $z \to -x$, this hamiltonian simplifies to

$$\tilde{H}_{Tot} = \begin{pmatrix} m + E_Z & 0 & E_B \hat{d}^\dagger & -v_a p_x \\ 0 & m - E_Z & -v_a p_x & -E_B \hat{d} \\ E_B \hat{d} & -v_a p_x & -m + E_Z & 0 \\ -v_a p_x & -E_B \hat{d}^\dagger & 0 & -m - E_Z \end{pmatrix} \tag{8.6}$$

with

$$E_B = \sqrt{2e\hbar |B| v_b v_c} \,, \tag{8.7a}$$

and

$$\hat{d} = \frac{1}{E_B} \left[-i\hbar \left(v_b \partial_z + i v_c \partial_y \right) + \frac{eB}{2} \left(v_b y - i v_c z \right) \right] , \tag{8.7b}$$

$$\hat{d}^\dagger = \frac{1}{E_B} \left[-i\hbar \left(v_b \partial_z - i v_c \partial_y \right) + \frac{eB}{2} \left(v_b y + i v_c z \right) \right] , \tag{8.7c}$$

such that

$$\left[\hat{d}, \hat{d}^\dagger \right] = \text{sign}\left(B \right) \,. \tag{8.7d}$$

Using (8.7d), and in analogy with a quantum oscillator, we introduce the ladder operators

$$\left(\hat{a}, \hat{a}^\dagger \right) = \left\{ \left(\hat{d}, \hat{d}^\dagger \right) \text{ if } B > 0 \,, \left(\hat{d}^\dagger, \hat{d} \right) \text{ if } B < 0 \right\} \tag{8.8}$$

such that $\left[\hat{a}, \hat{a}^\dagger \right] = 1$. Introducing $|n\rangle$, $n \in \mathbb{N}$, the eigenvectors of $\hat{N} = \hat{a}^\dagger \hat{a}$, such that

$$\hat{a} \left| 0 \right\rangle = 0 \text{ , and } \hat{a} \left| n \right\rangle = \sqrt{n} \left| n - 1 \right\rangle , \, n \in \mathbb{N}^* \,, \tag{8.9}$$

we can diagonalize the Hamiltonian (8.6) by considering the subspaces spanned by the states ensembles

$$\left\{ \begin{pmatrix} |0\rangle \\ 0 \\ 0 \\ 0 \end{pmatrix} , \begin{pmatrix} 0 \\ 0 \\ 0 \\ |0\rangle \end{pmatrix} \right\} \tag{8.10}$$

and

$$\left\{ \begin{pmatrix} |n\rangle \\ 0 \\ 0 \\ 0 \end{pmatrix} , \begin{pmatrix} 0 \\ 0 \\ 0 \\ |n\rangle \end{pmatrix} , \begin{pmatrix} 0 \\ |n-1\rangle \\ 0 \\ 0 \end{pmatrix} , \begin{pmatrix} 0 \\ 0 \\ |n-1\rangle \\ 0 \end{pmatrix} \right\} , n \in \mathbb{N}^* \tag{8.11}$$

if $B > 0$, and

$$\left\{ \begin{pmatrix} 0 \\ |0\rangle \\ 0 \\ 0 \end{pmatrix} , \begin{pmatrix} 0 \\ 0 \\ |0\rangle \\ 0 \end{pmatrix} \right\} \tag{8.12}$$

and

$$\left\{ \begin{pmatrix} |n-1\rangle \\ 0 \\ 0 \\ 0 \end{pmatrix}, \begin{pmatrix} 0 \\ 0 \\ 0 \\ |n-1\rangle \end{pmatrix}, \begin{pmatrix} 0 \\ |n\rangle \\ 0 \\ 0 \end{pmatrix}, \begin{pmatrix} 0 \\ 0 \\ |n\rangle \\ 0 \end{pmatrix} \right\}, n \in \mathbb{N}^* \tag{8.13}$$

for $B < 0$. The corresponding eigenenergies are

$$E_0^s = s\sqrt{v_a^2 p_x^2 + \left(m - \frac{1}{2} g\mu_B |B|\right)^2}, s \in \{-1, 1\} \tag{8.14a}$$

$$E_n^{s,t} = s\sqrt{v_a^2 p_x^2 + \left(\sqrt{m^2 + 2ne|B|\hbar v_b v_c} - \frac{t}{2} g\mu_B B\right)^2}$$
$$\{s,t\} \in \{-1,1\}^2, n \in \mathbb{N}^* \tag{8.14b}$$

with a density of states $n_B = \frac{1}{2\pi l_B^2} \equiv \frac{e|B|}{2\pi\hbar}$ (see Fig. 8.5(a)).
The 3+1 dimensional conductivity of this system can then be inferred from a 1+1 dimensional reduction through

$$\sigma^{(3+1D)} = A\, n_B \sum_{n,s,t} \sigma_{n,s,t}^{(1+1D)} \tag{8.15}$$

with A the sample cross-section, and $\sigma_{n,s,t}^{(1+1D)}$ the 1+1 dimensional conductivity of the Landau level whose energy is given by $E_n^{s,t}$.

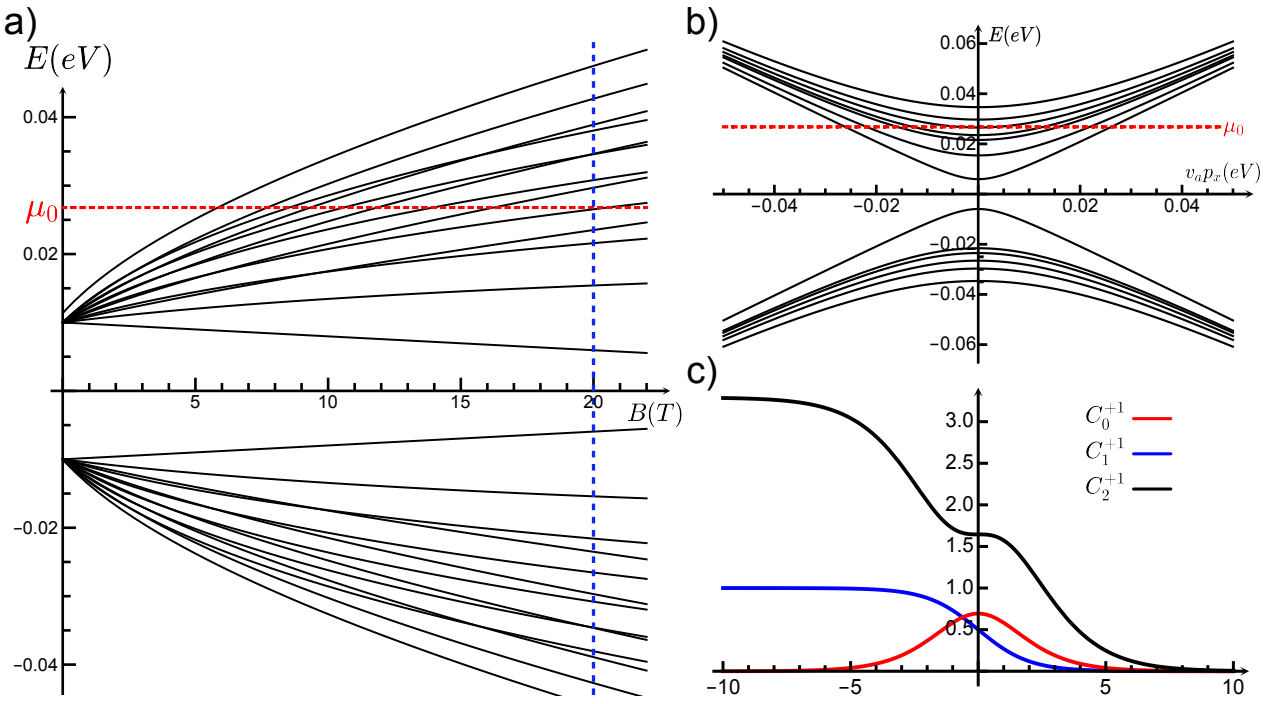

Figure 8.5: **Fan diagram, band dispersion, and anomaly coefficients** (a) Fan diagram in electronvolt for the seven first Landau levels ($n \in [0, 6]$) as a function of the magnetic field expressed in tesla. (b) Dispersion relation of the first four Landau levels (8.14) for a magnetic field of $B = 20T$, corresponding to the dashed blue line in panel (a). The red dashed line in panels (a) and (b) represents the position of the chemical potential μ_0. (c) Anomaly coefficients $\mathcal{C}_i(x)$, given by Eq. (8.26) represented for $i = 1, 2, 3$.

8.2.2 Thermal conduction and Landauer formula in a ballistic sample

Working in a sufficiently high magnetic field, such that the Landau bands deduced in the previous paragraph (8.14) are well separated (see Fig. 8.5(a)), we will compute the current originating from a difference of temperature and of chemical potential between right and left contacts, following a Landauer (ballistic) approach [100, 101, 186, 187]. Here and in the following, in order to describe the experiment and to simplify the following expressions, we will focus on the particle current J and the heat current $J_h = J_\varepsilon - \mu J$ where J_ε is the energy current. Note that one could have alternatively decided, as in [16], to describe the pair of currents (J, J_ε).

Ballistic conductivity in $ZrTe_5$

To calculate the equilibrium currents and the corresponding conductivities, let us consider a situation where right movers are at a temperature T_L and chemical potential μ_L while left movers are respectively at a temperature T_R and a chemical potential μ_R (see Fig. 8.6). Let us then consider a state with energy density $\varepsilon(k)$ and velocity $v(k) = \frac{1}{\hbar}\frac{\partial \varepsilon}{\partial k}$ the temperature and chemical potential of these fermions are then given by (see Fig. 8.6)

$$T(k) = \{T_L \text{ , if } v(k) > 0; T_R \text{ , if } v(k) < 0\} \tag{8.16a}$$
$$\mu(k) = \{\mu_L \text{ , if } v(k) > 0; \mu_R \text{ , if } v(k) < 0\} \tag{8.16b}$$

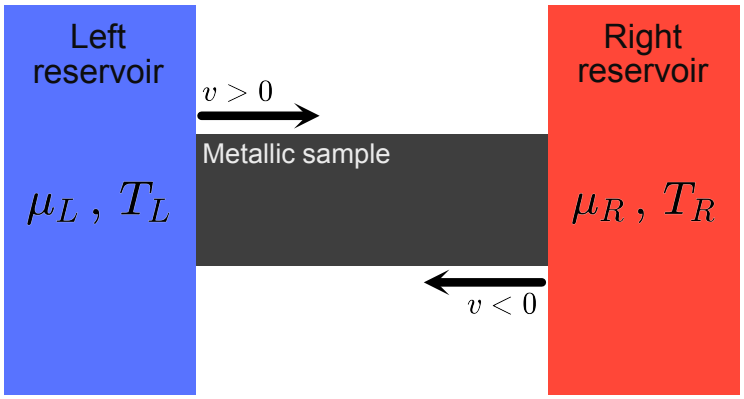

Figure 8.6: **Chiral notations** Right-movers, defined by their positive velocity ($v > 0$), come from the left reservoir and possess a chemical potential μ_L and a temperature T_L. Similarly, left movers, defined by their negative velocity ($v < 0$), come from the right reservoir and possess a chemical potential μ_R and a temperature T_R.

The energy and particle current density for a single channel are defined as

$$J = \mathcal{D}\int \frac{\mathrm{d}k}{2\pi} v(k) \frac{1}{1+\exp\left(\frac{\varepsilon(k)-\mu(k)}{k_B T(k)}\right)} \tag{8.17a}$$
$$J_\varepsilon = \mathcal{D}\int \frac{\mathrm{d}k}{2\pi} v(k) \frac{\varepsilon(k)}{1+\exp\left(\frac{\varepsilon(k)-\mu(k)}{k_B T(k)}\right)} \tag{8.17b}$$

with $\mathcal{D}$ the state degeneracy. For the Landau level energies (8.14), the total currents are given by

$$J = J_R - J_L \,, \tag{8.18a}$$
$$J_\varepsilon = J_{\varepsilon,R} - J_{\varepsilon,L} \,, \tag{8.18b}$$

with the chiral components

$$J_{L/R} = \frac{e|B|k_B T_{R/L}}{4\pi^2\hbar^2}\left[\sum_{s=\pm1} f_0^s\left(\frac{E_0^s(0)-\mu_{R/L}}{k_B T_{R/L}}\right) + \sum_{n=1}^{+\infty}\sum_{s,t=\pm1} f_0^s\left(\frac{E_n^{st}(0)-\mu_{R/L}}{k_B T_{R/L}}\right)\right], \tag{8.19a}$$

$$J_{\varepsilon,L/R} = \frac{e|B|k_B^2 T_{R/L}^2}{4\pi^2\hbar^2}\left[\sum_{s=\pm1} f_1^s\left(\frac{E_0^s(0)-\mu_{R/L}}{k_B T_{R/L}}\right) + \sum_{n=1}^{+\infty}\sum_{s,t=\pm1} f_1^s\left(\frac{E_n^{st}(0)-\mu_{R/L}}{k_B T_{R/L}}\right)\right] + \mu_{R/L} J_{R/L} \,, \tag{8.19b}$$

with,

$$f_i^{+1}(x) = \int_x^{+\infty} \mathrm{d}y \frac{y^i}{1+e^y} \,, \tag{8.20a}$$
$$f_i^{-1}(x) = \int_{-\infty}^{x} \mathrm{d}y \frac{y^i}{1+e^y} \,. \tag{8.20b}$$

The heat current density is then

$$J_h = J_h^R - J_h^L = J_\varepsilon - \bar{\mu} J \,, \tag{8.21}$$

with $\bar{\mu} = \frac{\mu_R+\mu_L}{2}$, or equivalently

$$J_{h,L/R} = \frac{e|B|k_B^2 T_{R/L}^2}{4\pi^2\hbar^2}\left[\sum_{s=\pm1} f_1^s\left(\frac{E_0^s(0)-\mu_{R/L}}{k_B T_{R/L}}\right) + \sum_{n=1}^{+\infty}\sum_{s,t=\pm1} f_1^s\left(\frac{E_n^{st}(0)-\mu_{R/L}}{k_B T_{R/L}}\right)\right] \pm \frac{\mu_R-\mu_L}{2} J_{R/L} \tag{8.22}$$

Under the assumption that the temperature and chemical potential differences are small

$$T_{R/L} = T_0 \mp \frac{1}{2}\Delta T \,, \text{ with } \frac{\Delta T}{T_0} \ll 1 \tag{8.23a}$$
$$\mu_{R/L} = \mu_0 \mp \frac{1}{2}\Delta\mu \,, \text{ with } \frac{\Delta\mu}{\mu_0} \ll 1 \tag{8.23b}$$

these equations simplify at linear order in $\Delta T/T_0$ and $\Delta\mu/\mu_0$ to

$$\begin{pmatrix} J \\ \frac{J_h}{k_B T_0} \end{pmatrix} = \frac{eB}{4\pi^2\hbar^2} . \mathcal{C} \begin{pmatrix} \Delta\mu \\ k_B \Delta T \end{pmatrix} \,, \tag{8.24a}$$

with

$$\mathcal{C} = \begin{pmatrix} \mathcal{C}_0 & \mathcal{C}_1 \\ \mathcal{C}_1 & \mathcal{C}_2 \end{pmatrix} \,, \tag{8.24b}$$

where the $\mathcal{C}_i$ are functions of μ_0, B and T_0,

$$\mathcal{C}_i = \sum_{s=\pm1} C_i^s\left(\frac{E_0^s(0)-\mu_0}{k_B T_0}\right) + \sum_{n=1}^{+\infty}\sum_{s,t=\pm1} C_i^s\left(\frac{E_n^{st}(0)-\mu_0}{k_B T_0}\right) \,, \tag{8.25}$$

with the functions

$$C_i^{+1}(x) = \int_x^{+\infty} \frac{y^i \mathrm{d}y}{(1+e^y)(1+e^{-y})}\,, \tag{8.26a}$$

$$C_i^{-1}(x) = \int_{-\infty}^{x} \frac{y^i \mathrm{d}y}{(1+e^y)(1+e^{-y})}\,, \tag{8.26b}$$

represented in Fig. 8.5(c) for $i = 1, 2, 3$. The longitudinal thermal conductivity is then

$$\kappa_{xx} = A\,l\,\frac{eBk_B^2 T_0}{4\pi^2\hbar^2}\left[\mathcal{C}_2 - \frac{\mathcal{C}_1^2}{\mathcal{C}_0}\right]\,, \tag{8.27}$$

with A the cross-section of the material and l its length. Similarly, the Lorentz number $L = \kappa/\sigma T$ reads

$$L = \left(\frac{k_B}{e}\right)^2 \left[\frac{\mathcal{C}_2}{\mathcal{C}_0} - \frac{\mathcal{C}_1^2}{\mathcal{C}_0^2}\right]\,. \tag{8.28}$$

Following (8.24) and (8.25), we see that each coefficient $\mathcal{C}_i$ can be decomposed as a sum of different terms, each encoding the contribution of a single Landau band[1]. Since, in the relativistic limit, $T_0 \to 0$, the coefficients described by (8.26a) and (8.26b) converge to the coefficients appearing in particle physics in front of the axial and the gravitational anomaly, also used in condensed matter physics such as in [16],

$$C_0^{\pm 1}(x) \underset{x\to\mp\infty}{\to} 1\,, \tag{8.29a}$$

$$C_1^{\pm 1}(x) \underset{x\to\mp\infty}{\to} 0\,, \tag{8.29b}$$

$$C_2^{\pm 1}(x) \underset{x\to\mp\infty}{\to} \frac{\pi^2}{3}\,, \tag{8.29c}$$

the function $C_i^{\pm 1}$ are sometimes referred to as the "anomaly coefficients" [16, 119]. In particular, $C_0(x)$ is the coefficient of the axial anomaly, while C_2 is the coefficient of the gravitational anomaly. However, as observed in [253], close to the band extremum, these coefficients can differ from the values recalled in Eq. (8.29) (see exemplarily Fig. 8.5(c) around $x = 0$).

Magnetic oscillations and Lorentz factor

Plotting the thermal conductivity κ_{xx} for the parameter measured in [253], and for different temperatures (see Fig. 8.7(a)), several things can be noted. First, we observe magnetic oscillations, becoming sharper as the temperature is lowered. These oscillations occur when one Landau level empties, losing one canal of conduction, as expected from the expression of the $\mathcal{C}_i$ (8.25). At a large magnetic field, we observe that the oscillations stop, and the conductivity increases linearly: this behavior characterizes the so-called quantum limit.

It is also interesting to observe the corresponding Lorentz ratio in Fig. 8.7(c). Outside of the band crossings, the Lorentz ratio equals its asymptotic value $L_0 = \frac{\pi^2}{3}\frac{k_B^2}{e^2}$. However, a violation of the Lorentz ratio occurs at each crossing, where the Wiedemann-Franz law ceases to hold. We note that when the temperature is lowered, this violation decreases in amplitude and becomes more and more localized around the level crossing.

[1] Note, that the heat conductivity cannot be decomposed as the sum of the heat conductivity for each Landau level due to the coefficient $\mathcal{C}_1^2/\mathcal{C}_0$

This explanation of the 3+1 dimensional thermal magnetoconductivity of $ZrTe_5$, based on the 1+1 dimensional conductivity of the Landau level in a magnetic field, reproduces well several key features of the experimental measure represented in Fig. 8.4(a), such as the magnetic oscillations and their position. In the following paragraph, we will consider the correction induced by backscattering in this description.

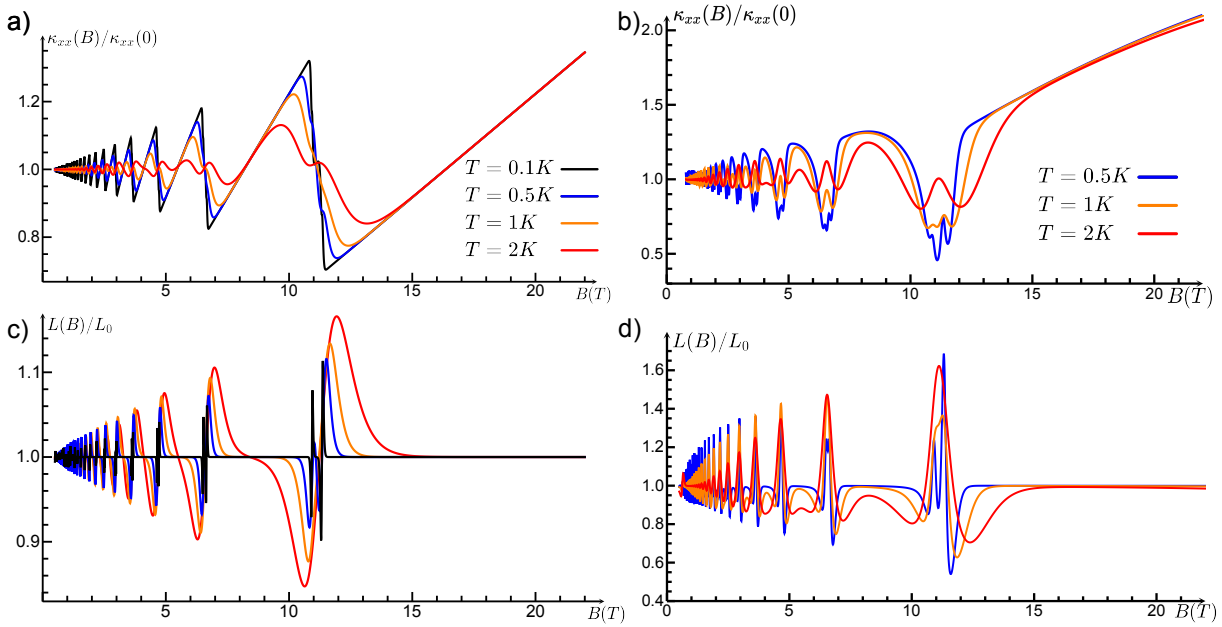

Figure 8.7: **Theoretical evaluation of the magnetothermal conductivity and the Lorentz ratio in $ZrTe_5$** (a) and (c) Numerical evaluation of the longitudinal magnetothermal conductivity κ_{xx} and of the Lorentz ratio L in $ZrTe_5$ based on the ballistic evaluation of Eq. (8.27) and (8.28) respectively, for several temperatures. (b) and (d) provides the same information in the case of the computation led in the presence of backscattering given by Eq. (8.41) and (8.44). The parameters used for the numerical evaluations correspond to the parameters determined in [253].

8.2.3 Scattering corrections to the magnetothermal conductivity properties

We now turn to a 1+1 dimensional Boltzmann equation approach. As described above, a difference between the temperature and the chemical potential of left and right movers can create particle and heat currents in a sample subjected to a magnetic field. In this section, our objective is to complement this study by studying how backscattering effects modify the magnetothermal property discussed in section 8.2.2. To do so, we will see, resort to a 1+1 dimensional Boltzmann somewhat similar to the one used to determine the negative magnetoresisticity in section 2.2.3, but already considered in the study of magnetothermal conductivity in [16] and [119].

Thermal conductivity from a 1+1 dimensional Boltzmann equation approach

Let us suppose that the intra-node scattering is much stronger than the inter-node scattering. Under this assumption, one can suppose that all right and left movers have the same temperature and chemical potential T_L and μ_L or T_R and μ_R, respectively. For the Landau level of quantum numbers (n, s, t, χ) ($\chi = R/L$; $s, t = \pm 1$), let us call $(f_0)_n^{st}$ its equilibrium

distribution function (in the absence of field/temperature gradient, for fixed temperature T_0 and chemical potential μ_0), independent of the chirality χ, and $f_n^{\chi st}$ the non-equilibrium one. Under the assumption that the inter-node scattering time τ_{inter} is a constant, we can relate these distributions, in a Boltzmann equation approach as

$$\frac{\partial f_n^{\chi st}}{\partial t} + \dot{r}\frac{\partial f_n^{\chi st}}{\partial r} + \dot{k}\frac{\partial f_n^{\chi st}}{\partial k} = \frac{f_n^{\chi st} - (f_0)_n^{st}}{\tau_{inter}} . \tag{8.30}$$

Inserting the Hamilton equations of motion[2] for the band labeled (n, s, t)

$$\begin{cases} \dot{r} & = v_n^{st} = \frac{1}{\hbar}\frac{\partial E_n^{st}}{\partial k} \\ \hbar\dot{k} & = -eE \end{cases} \tag{8.31}$$

in the Boltzmann equation (8.30) with E the electric field, we obtain

$$\frac{\partial f_n^{\chi st}}{\partial t} + \frac{1}{\hbar}\frac{\partial E_n^{st}}{\partial k}\frac{\partial f_n^{\chi st}}{\partial r} - \frac{eE}{\hbar}\frac{\partial f_n^{\chi st}}{\partial k} = \frac{f_n^{\chi st} - (f_0)_n^{st}}{\tau_{inter}} \tag{8.32}$$

Considering small electric field and thermal gradient, one can expect the resulting chiral parameters $\delta\mu_{R/L} = \pm\frac{\delta\mu}{2}$ and $\delta T_{R/L} = \pm\frac{\delta T}{2}$ to be small compared to their average value (μ_0 and T_0). Under this assumption, one can write a perturbative expansion in $(\delta\mu, \delta T)$ for $f_n^{\chi st}$,

$$\begin{aligned} f_n^{cst} &\approx (f_0)_n^{st} + \delta\mu_\chi \frac{\partial (f_0)_n^{st}}{\partial \mu} + \delta T_\chi \frac{\partial (f_0)_n^{st}}{\partial T} \\ &\approx (f_0)_n^{st} + \left(\delta\mu_\chi + k_B\delta T_\chi \frac{E_n^{st} - \mu_0}{k_B T_0}\right)\left(-\frac{\partial (f_0)_n^{st}}{\partial E_n^{st}}\right) , \end{aligned} \tag{8.33}$$

and a perturbative expansion for its gradient as

$$\begin{aligned} \frac{\partial f_n^{cst}}{\partial r} &= \nabla\mu \frac{\partial (f_0)_n^{st}}{\partial \mu} + \nabla T \frac{\partial (f_0)_n^{st}}{\partial T} \\ &\approx \left(\nabla\mu + k_B\nabla T \frac{E_n^{st} - \mu_0}{k_B T_0}\right)\left(-\frac{\partial (f_0)_n^{st}}{\partial E_n^{st}}\right) . \end{aligned} \tag{8.34}$$

In the quasi-static limit $\tau_{inter} \ll t, \frac{\partial f_n^{cst}}{\partial t} \approx 0$, we can then combine (8.32), (8.33) and (8.34) as

$$\begin{aligned} &\left[(\nabla\mu + eE) + k_B\nabla T \frac{E_n^{st} - \mu_0}{k_B T_0}\right]\frac{1}{\hbar}\frac{\partial E_n^{st}}{\partial k}\left(-\frac{\partial (f_0)_n^{st}}{\partial E_n^{st}}\right) = \\ &\qquad \frac{1}{\tau_{inter}}\left[\delta\mu_c + k_B\delta T_c \frac{E_n^{st} - \mu_0}{k_B T_0}\right]\left(-\frac{\partial (f_0)_n^{st}}{\partial E_n^{st}}\right) . \end{aligned}$$

Abandoning the suffix "inter" for τ_{inter} and integrating

- (8.35) with respect to k on $[0, +\infty[$ (right chirality sector), summing on the different bands, we finally get

$$k_B\nabla T\mathcal{C}_1 + (\nabla\mu + eE)\mathcal{C}_0 = \frac{\hbar}{2\tau k_B T_0}\left(\delta\mu\mathcal{D}_0 + k_B\delta T\mathcal{D}_1\right) , \tag{8.35}$$

- $\frac{E_n^{st} - \mu_0}{k_B T_0} \times$(8.35) with respect to k on $[0, +\infty[$ (right chirality sector), summing on the different bands we finally get

$$k_B\nabla T\mathcal{C}_2 + (\nabla\mu + eE)\mathcal{C}_1 = \frac{\hbar}{2\tau k_B T_0}\left(\delta\mu\mathcal{D}_1 + k_B\delta T\mathcal{D}_2\right) , \tag{8.36}$$

[2] In 1+1 dimension, Eq. (8.31) are also referred to as the semiclassical equations of motion.

where the anomaly coefficients $\mathcal{C}_i$ are defined in (8.25) while

$$\mathcal{D}_i = \sum_{s=\pm1} \mathcal{D}_i^{0s} + \sum_{n=1}^{+\infty} \sum_{s,t=\pm1} \mathcal{D}_i^{nst}, \tag{8.37a}$$

$$\mathcal{D}_i^{nst} = \int_0^{+\infty} \mathrm{d}k \left(\frac{E_n^{st}(\hbar k) - \mu_0}{k_B T_0} \right)^i \frac{1}{2\left(1 + \cosh\left(\frac{E_n^{st}(\hbar k) - \mu_0}{k_B T_0}\right)\right)}. \tag{8.37b}$$

The chiral differences can then be inferred from the applied fields as

$$\begin{pmatrix} \delta\mu \\ k_B \delta T \end{pmatrix} = 2\frac{k_B T_0}{\hbar} \tau \mathcal{D}^{-1}.\mathcal{C} \begin{pmatrix} eE + \nabla\mu \\ k_B \nabla T \end{pmatrix} \tag{8.38}$$

where $\mathcal{C}$ is defined in (8.24b) and,

$$\mathcal{D} = \begin{pmatrix} \mathcal{D}_0 & \mathcal{D}_1 \\ \mathcal{D}_1 & \mathcal{D}_2 \end{pmatrix}. \tag{8.39}$$

Subsequently, we can calculate the thermal conductivity in $ZrTe_5$. According to (8.38) and (8.24a), the total current density in the sample can be expressed in linear response theory as

$$\begin{pmatrix} J \\ \frac{1}{k_B T_0} J_h \end{pmatrix} = \tau \frac{eBk_B T_0}{2\pi^2\hbar^3} \mathcal{C}.\mathcal{D}^{-1}.\mathcal{C} \begin{pmatrix} eE + \nabla\mu \\ k_B \nabla T \end{pmatrix}. \tag{8.40}$$

The linear magneto-thermal conductivity is then given by

$$\kappa_{xx} = \tau \frac{eBk_B^3 T_0^2}{2\pi^2\hbar^3} \frac{\left(\mathcal{C}_1^2 - \mathcal{C}_0\mathcal{C}_2\right)^2}{\mathcal{C}_1^2\mathcal{D}_0 - 2\mathcal{C}_0\mathcal{C}_1\mathcal{D}_1 + \mathcal{C}_0^2\mathcal{D}_2} \tag{8.41}$$

In practice, however, away from the points where the chemical potential reaches the bottom of a level, $\mathcal{C}_1 \approx 0$ and $\mathcal{D}_1 \ll \mathcal{D}_0, \mathcal{D}_2$. κ_{xx} is then well approximated in such a regime by

$$\kappa_{xx} = \tau \frac{eBk_B^3 T_0^2}{2\pi^2\hbar^3} \frac{\mathcal{C}_2^2}{\mathcal{D}_2}. \tag{8.42}$$

Similarly, the linear magneto-electric conductivity is defined by

$$\sigma_{xx} = \tau \frac{e^3 Bk_B T_0}{2\pi^2\hbar^3} \frac{\mathcal{C}_0^2\mathcal{D}_2 - 2\mathcal{C}_0\mathcal{C}_1\mathcal{D}_1 + \mathcal{C}_1^2\mathcal{D}_0}{\mathcal{D}_0\mathcal{D}_2 - \mathcal{D}_1^2} \approx \tau \frac{e^3 Bk_B T_0}{2\pi^2\hbar^3} \frac{\mathcal{C}_0^2}{\mathcal{D}_0}, \tag{8.43}$$

implying a Lorentz factor of the form

$$L = \frac{k_B^2}{e^2} \frac{\left(\mathcal{C}_1^2 - \mathcal{C}_0\mathcal{C}_2\right)^2 \left(\mathcal{D}_0\mathcal{D}_2 - \mathcal{D}_1^2\right)}{\left(\mathcal{C}_0^2\mathcal{D}_2 - 2\mathcal{C}_0\mathcal{C}_1\mathcal{D}_1 + \mathcal{C}_1^2\mathcal{D}_0\right)^2} \approx \frac{k_B^2}{e^2} \frac{\mathcal{D}_0}{\mathcal{D}_2} \left(\frac{\mathcal{C}_2}{\mathcal{C}_0}\right)^2. \tag{8.44}$$

Discussion

In Fig. 8.7(b), we note that in the scattering-based approach, we recover, as in the ballistic case, oscillations related to the variation of the number of open conduction channels. We also recover, at high magnetic fields, a linear increase of the conductivity characteristic of the quantum limit. We still observe minor discrepancies with the experimental data, such as the non-zero slope of the magnetothermal conductivity observed at low magnetic fields. A comparison of the theoretical predictions evaluated for a mean free path of $l_{mfp} \approx 4 \times 10^{-5} m$ with the experimental data presents a qualitative agreement (see Fig. 8.4(a)).

Therefore, it seems that longitudinal magnetotransport properties of $ZrTe_5$ can be well explained within a 1+1 dimensional approach applied to the Landau level. However, subsequent measurement in $ZrTe_5$ indicates the presence of clean magnetothermal oscillations in the magnetothermal conductivity orthogonal to the magnetic field (see Fig. 8.4(b)). Such measurements still correspond to a linear response relation of the form $\vec{J}_h = \kappa\vec{\nabla}T$. However, we are now considering a situation where the magnetic field is orthogonal to the current direction (along the b-axis). Such measurements question the validity of our study. Indeed, they do not agree with the transport mechanism presented above since these mechanisms implied a transport along the Landau levels in the direction of the magnetic field. In the following, we will describe other transport mechanisms that capture these more recent experimental results.

8.3 From orthogonal energy transport to a new transport phase

While in a strong magnetic field limit, an approach based on independent 1+1 dimensional Landau level provides theoretical prediction in a qualitative agreement with the longitudinal magnetothermal conductivity measurement (see Fig. 8.4(a)), the presence of magnetic oscillations of comparable amplitude when the magnetic field is rotated by 90 degrees and applied along the b-axis question this scenario. Indeed, in the presence of a magnetic field along the b-axis, the Landau levels along the b-axis are orthogonal to the temperature gradient. As a consequence, they cannot account for the magnetothermal conductivity oscillation along the a-axis.

Therefore, the purpose of this section is to propose an alternative mechanism to describe the magnetothermal transport data. We will see that despite the sound attenuation measurements, an explanation of this puzzle might come from the phonon that we neglected until now, which, by coupling strongly to the electrons from the Landau levels, might display oscillations with increasing magnetic field.

8.3.1 Evidence for a phonon-mediated transport

After the experimental observation of magnetothermal conductivity oscillation for a magnetic field applied in a direction orthogonal to the transport direction, we considered several scenarios allowing such oscillations within the Landau level picture. In the presence of a magnetic field along the b-axis, in a finite sample, and similarly to the 2+1 dimensional Hall effect, each occupied Landau level gives rise to an edge state propagating along the edges of the sample [255]. Therefore, we first tried to analyze the contribution of such edge states to the magnetothermal oscillations. In a second trial, we considered the possibility for such oscillation to arise from a transport issued from a scattering-assisted coupling between the Landau levels. However, none of these trials were conclusive, notably due to a failure of these models to capture the proper scaling of the transport properties with the magnetic field. We can then wonder what other scenario might be able to account for the experimental data.

Due to the dominance of the lattice degrees of freedom in thermal transport at zero field, highlighted by the comparison of the zero field thermal conductivity in Fig. 8.8, it is tempting to assume that the huge changes in the amplitude of thermal conductivity in magnetic fields originate from changes of phonon velocity or attenuation due to the interactions with the Fermi liquid. However, and as discussed in section 8.1, further measurements displayed in Fig. 8.2 reveal that changes of attenuation and speed of ultrasound due to magnetoacoustic quantum oscillations do not exceed 1% and thus, at first glance cannot be responsible for the huge field-

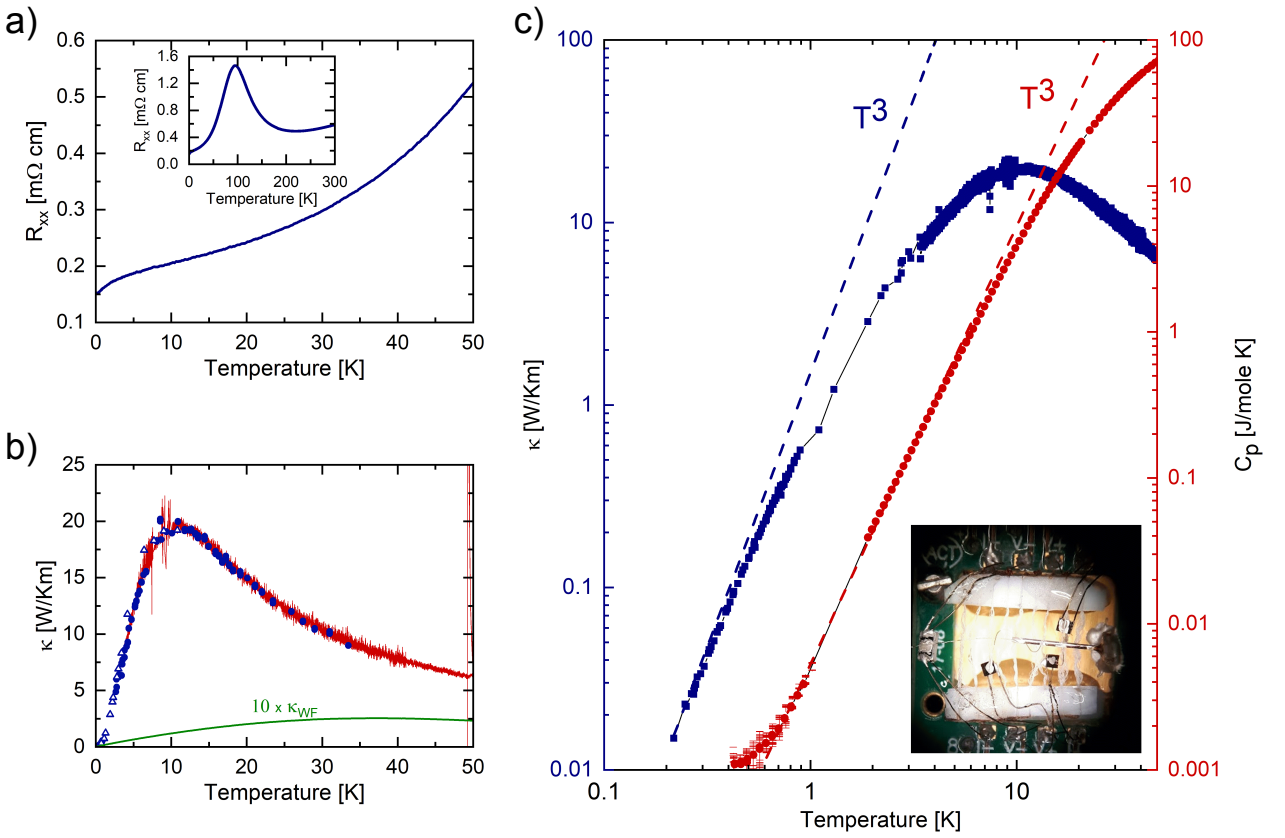

Figure 8.8: **Thermal and electrical transport in $ZrTe_5$.** a) Electrical resistance of $ZrTe_5$ measured with a 10 μA current passed along the crystallographic a-axis. b)Thermal conductivity of $ZrTe_5$ measured with a thermal gradient ($\Delta T < 0.1T_0$)applied along the a-axis. The continuous red line represents measurements where the temperature was slowly changed and the gradient continuously recorded. Full circles and triangles represent measurements performed in two distinct cooldowns with temperature being stabilized for several minutes before taking the measurements. The solid green line represents an estimate of thermal conductivity due to the electrons obtained from the Widemann-Franz law. c) Comparison of thermal conductivity (blue points) and specific heat data (red points) and the expected T^3 dependence (dashed lines). Black hairline acts as a guide to the eye for the data. The Inset displays a microscope photograph of one of the custom-built thermal conductivity setups. Cernox thermometers are attached to the sample using a 200um silver wire. In this setup, used in temperatures T<1K, superconducting TiN wires were used as electrical leads to the thermometers and heater.

induced changes of thermal conductivity.

However, a careful study of the temperature dependence of both the zero field thermal conductivity and the amplitude of the last magnetothermal oscillation (see Fig. 8.9(b)) reveals that both quantities decay as T^3 with cooling. This is in contrast with the canonical temperature dependence of quantum oscillation due to temperature smearing of the Landau levels and described by the so-called Lifshitz-Kosevitsh formula [247]

$$\Delta\chi = \frac{\lambda}{\sinh\lambda} \quad \text{with, } \lambda \propto \frac{T}{B}m^*, \tag{8.45}$$

with the oscillation amplitude $\Delta\chi$ saturating at low temperatures. The suppression of the oscillation amplitude with the same power law as zero field thermal conductivity strongly suggests that the oscillations are indeed related to the phonon subsystem.

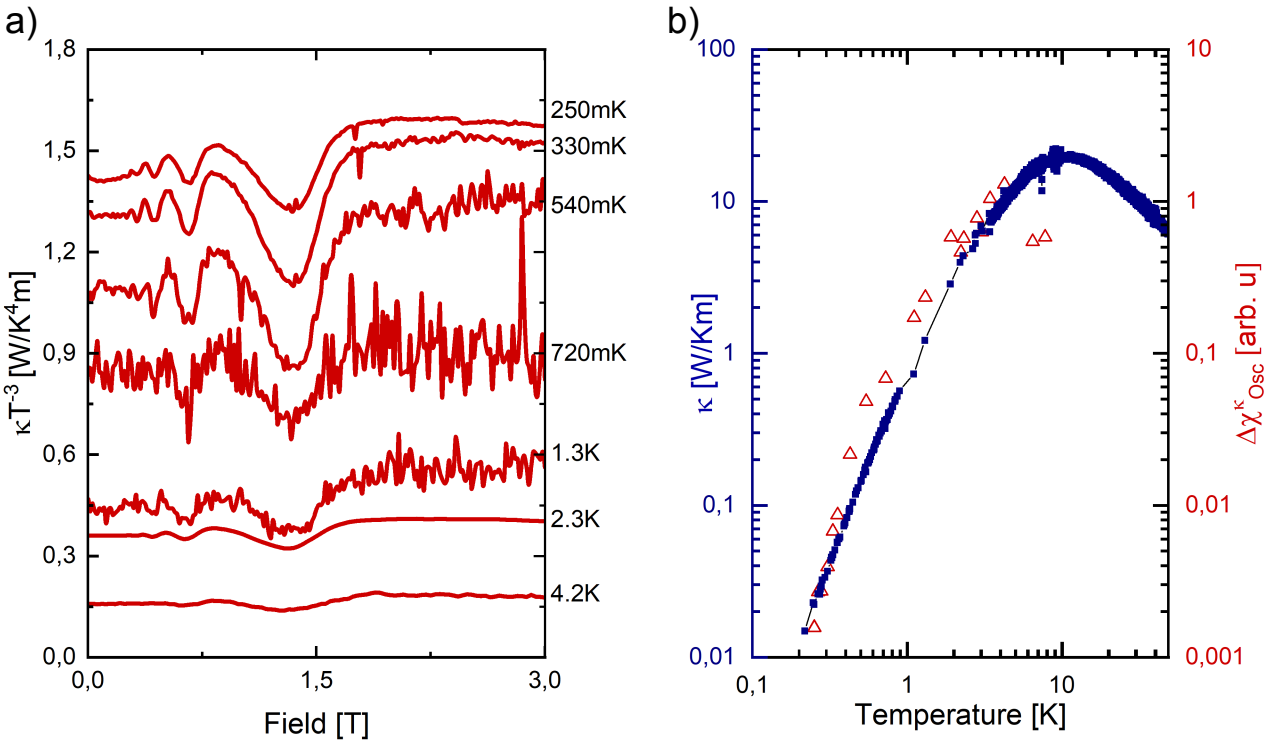

Figure 8.9: **Temperature dependance of the magnetothremal quantum oscillation amplitude in $ZrTe_5$.** a) Example traces of magnetothermal conductivity divided by T^3 for clarity of presentation. b) Comparison of the temperature dependence of zero field thermal conductivity with the temperature dependence of the amplitude of the last oscillation. (red).

This apparent contradiction arises because, at first glance, sound attenuation and thermal conductivity are closely related quantities, both describing energy transport. Thermal conductivity describes the transfer of energy due to a temperature gradient and sound attenuation, the efficiency with which a monochromatic, collimated mechanical wave travels across the crystal. Since attenuation measurements only probe the phononic subsystem, it could be expected that strong quantum oscillations appearing in thermal conductivity due to phonon attenuation by electrons should manifest as a substantial variation of the echo amplitude. Consequently, if quantum oscillations in attenuation are weak, one is directly led to the conclusion that the quantum oscillations observed in thermal conductivity have to be a consequence of an anomalously large contribution of charge carriers to thermal transport.

The difficulty with such an argument lies in the fact that thermal conductivity and sound attenuation measured in typical solid-state experiments probe very different energy scales. In ultrasonic measurements, one typically probes the phonons with frequencies $f \lesssim 1$GHz, whereas thermal conductivity probes thermal phonons whose frequencies, even at 200mK, exceed 25GHz. This distinction becomes crucial in the case of phonon attenuation by the Fermi liquid. At low phonon frequencies, sound attenuation is proportional to both ω^2 and the electron fluid's viscosity. However, at high frequencies, when the phonon wavelength becomes smaller than the electron mean free path, one enters the so-called quantum limit where attenuation is proportional to ω. In the case of $ZrTe_5$, the momentum relaxing electron mean free path is of the order of 1μm, with the sound wavelength at 314MHz being around 10μm, placing our measurements in the hydrodynamic limit. In contrast, the wavelength of thermal phonons is of the order of 10nm. Thus thermal conductivity is expected to probe a very different phonon attenuation

regime, with attenuation due to the electrons more than two orders of magnitude stronger than that probed in the ultrasound experiments, resolving the apparent contradiction.

Since the wavelength of the acoustic phonons is large compared to the size of the Fermi sea, one expects an isotropic thermal conductivity of phonon origins. The oscillations of the thermal conductivity will then be consequences of the density of electrons occupying the Fermi sea, while the dependence of the magnetic field defining the ultraquantum limits comes from the strongly anisotropic Fermi surface.

8.3.2 Discussion

In this chapter, we discussed an experimental collaboration with the Max Planck Institute in Dresden. The original objective of this collaboration was to identify possible signatures of gravitational anomalies in the magnetothermal conductivity of $ZrTe_5$. The weak variations of the sound velocity as a function of the magnetic field originally led us to the conclusion that the magnetic oscillation is of electronic origin. Therefore, in section 8.2, we analyzed the longitudinal variations of the magnetothermal conductivity based on the physics of the electronic Landau levels. However, even though these analyses showed a qualitative agreement with the experimental data (see Fig. 8.4(a)), the observation of oscillations in the presence of a magnetic field orthogonal to the direction of transport led us to reconsider these analyses since they do not account for such oscillations. An analysis of the temperature dependence of the oscillation amplitude unveiled a new heat transport phenomenon resulting from a strong coupling between phonons and electrons and similar to the one described by K. Behnia *et al.* in [256]. The discussion of $ZrTe_5$ magnetothermal conductivity in this chapter indicates that observing the signature of gravitational anomalies in semimetals appears to be trickier than first expected since the study of thermal transport cannot be directly done by applying the Luttinger trick but instead requires considering a bi-fluid model, studying the strongly coupled electron-phonon global system.

Conclusion & future directions

Usually, curved spacetime physics and condensed matter physics are two very distinct domains of physics. Indeed, they deal with physical properties at wildly different length scales. Despite this apparent difference in size, in the middle of the XXth century, scientists realized that quantum field theory proposes a bridge between these two domains of physics. Such a relationship has a two-sided interest. On the one hand, this analogy between curved spacetime physics and condensed matter can be used to design tabletop experiments in quantum fluids probing exotic phenomena such as Hawking radiation, whose cosmological observation surpasses our present observational capabilities: this is the realm of analog gravity. On the other hand, this analogy allowed J. Luttinger to relate the response of a system to a gradient of temperature to the response of the same system to a gradient of gravitational potential. These ideas greatly simplified the computation of thermal transport properties of materials in condensed matter physics.

Despite their similitude in origin, as fields between condensed matter and curved spacetime physics, analog gravity, and thermal transport measurement remain very distinct communities. The main reason for this distance between these two communities is the fact that they consider distinct objects of study, either quantum fluids in analog gravity or solids in thermal response theory. We have shown in this thesis how to relate these two communities, resorting to the notion of anomalous quantum fluctuations. Such fluctuations, captured at the level of quantum field theory by the notion of gravitational anomalies, are indeed a fundamental notion in both analog gravity and thermal transport theory.

In the first part of this thesis, we decided to investigate the effect of the anomalous fluctuations induced in 1+1 dimensional systems by non-zero spacetime curvature. We first identified the physical quantities whose conservation equations are affected by the presence of non-vanishing spacetime curvature. The anomalous non-conservation equations for the momentum-energy transport of the theory ultimately captured the effects of these fluctuations. In 1+1 dimensions, the number of constraints provided by the non-conservation equation is enough to fix the value of the momentum-energy tensor up to a constant. The components of the momentum-energy tensor, together with the Stefan-Boltzmann law, then allowed us to determine the equilibrium temperature profile in curved spacetime. By comparing this derivation in the presence of gravitational anomalies to the historical derivation by R. Tolman and P. Ehrenfest, we identified two energy scales $\varepsilon_q^{(1)}$ and $\varepsilon_q^{(2)}$ controlling the amplitude of the correction induced by the quantum fluctuations. While $\varepsilon_q^{(1)}$ denotes a local bias between the energy and the pressure, $\varepsilon_q^{(2)}$ induces a local modification of the 0 point energy, which induces a modification of the local equilibrium temperature that we denote "anomalous Tolman-Ehrenfest temperature." Since Luttinger's trick can be interpreted as a consequence of the classical Tolman-Ehrenfest temperature, we then analyzed the modification induced by the quantum fluctuation on Lut-

tinger's equivalence between a temperature gradient and a gradient of gravitational potential. We analyzed this relationship both using the non-conservation equations and a perturbative analysis, which revealed the many-body physics nature of the correction.

We then build on this definition of the anomalous Tolman-Ehrenfest temperature to generalize our approach to several physical systems. We reconsidered the example of black holes and showed how the two gravitational anomalies, the trace and the Einstein anomaly, can be used together to redefine the notion of black hole temperature and to determine the value of the Hawking temperature. Then, we generalized these ideas of anomalous Tolman-Ehrenfest temperature to strongly out-of-equilibrium scenarios, considering the physics of temperature quenches and of Floquet thermalization. In the subsequent chapter 5 and 6, we analyzed other platforms on which such anomalies could play a role. We proved that it is possible, within quantum fluids, to realize an analog of the metric used to describe the expansion of our universe and indicate the expected signature of the anomalous fluctuation. Then, we proved that it is possible and essential in some experiments to consider spacetime beyond general relativity, such as a bimetric theory. We considered several examples of physical systems for which such a bimetric theory is essential and computed in each one of them the correction induced by the quantum fluctuations.

We finally described a collaboration with an experimental group dedicated to the study of the magnetothermal response coefficients in the Dirac semimetal $ZrTe_5$. After motivating the choice of this semimetal to analyze the electron contribution to thermal transport, we compared the experimental results with analytical computations realized by considering either a ballistic or a diffusive, electron-dominated thermal transport within a magnetic dimensional reduction strategy. However, the experimental observation of large thermal conductivity oscillations when the magnetic is orthogonal to the direction of propagation led us to reconsider the contribution of the phonons. We finally gave arguments in favor of a phonon origins of the thermal conductivity oscillations originating from a strong coupling between phonon and electrons overlooked until then. This experimental collaboration indicates that in the description of thermal conductivity, it is essential to consider a strongly interacting electron-phonon soup.

To go beyond this work, dedicated to the study of thermal fluctuations engendered by a non-vanishing spacetime curvature and their effects in analog gravity and thermal transport, a first strategy would be to consider other geometrical effects beyond general relativity, such as torsion. One of the main postulates of Einstein's general relativity is that the affine connection is symmetric, implying that the spacetime torsion vanishes. In condensed matter, however, torsion arises naturally at the level of the topological defects known as diclinaisons [257–259] (see appendix A). Moreover, it has been shown by H. Nieh and M. Yan [260, 261] that in the presence of a non-zero torsion tensor, quantum fluctuations induce non-zero contributions to the non-conservation equation in 1+1 dimensional systems. For example, the Nieh-Yan anomaly captures a non-conservation of the chiral current j^μ_A in the presence of a non-vanishing torsion tensor $T^\mu_{\nu\rho}$ expressed as

$$\partial_\mu \left(\sqrt{-g} j^\mu_A\right) = \frac{\mathcal{F}}{4} g_{\mu\nu} \epsilon^{\rho\sigma\alpha\beta} T^\mu_{\rho\sigma} T^\nu_{\alpha\beta}$$

with $\mathcal{F}$ a nonuniversal constant, similar terms correct the trace anomaly and the momentum-energy tensor conservation expression. Therefore, considering the physics of the quantum fluctuations in a system with a non-vanishing torsion tensor appears as a natural extension of this thesis. Such an extension is interesting for condensed matter physics, since such anomalies could give rise to new effects in linear response theory, but also for quantum field theory in curved spacetimes since such condensed matter systems provide an interesting platform to ex-

plore the physics of quantum fields in spacetimes beyond Einstein relativity.

In the future, it would also be interesting to further study the properties of anomalous quantum fluctuations in the presence of non-trivial geometry. First, note that both the Casimir effect and the quantum energy scale $\varepsilon_q^{(2)}$ both redefine the notion of zero point energy locally. Therefore, it is natural to wonder what are the similitudes and differences between these two geometrical effects. Another reason to reconsider the notion of anomalous quantum fluctuation would be to try to solve the puzzle of dimensionality. In chapter 2 of this thesis, we have seen that for symmetry reasons, gravitational anomalies only exist for certain dimensions of spacetime. For example, Einstein anomalies can only appear in dimension $D+1 = 4k+2$, gravitational trace anomalies in any even dimensions, and mixed axial gravitational anomalies in dimensions $D+1 = 4k$. Two questions relevant in condensed matter are thus: First, what are the corrections to the momentum-energy tensor in higher dimensions such as $D = 3+1$, and what are the signatures of these corrections on thermodynamic quantities? Second, as we have seen, in odd spacetime dimensions, there exists no gravitational anomalies. We can, therefore, wonder what properties of the quantum fluctuations lead to such a cancellation and whether, despite the absence of gravitational anomalies, it is possible to observe any signature of the spacetime curvature on the quantum fluctuations in odd dimensions.

Another outlook of this work would be to explore the manifestations of anomalous quantum fluctuations beyond field theory considerations. In this work, most of our computations were done within the formalism of field theory and low-energy physics. However, such a formalism is solely an approximation. In condensed matter physics, the infrared and ultraviolet cut-offs are not free parameters but rather dictated by the underlying energy bands. It would thus be interesting to study the consequences of analog curved spacetime and anomalous fluctuations in real materials. A strategy could be, for example, to consider a numerical simulation of thermal transport or of the out-of-equilibrium processes described in chapter 4. In the same direction, in this work, we mainly considered the effects of anomalous quantum fluctuations on some vacuum averages. However, in most of the analog gravity experiments, the measured quantities are not directly the vacuum properties. Instead, the experiments probe the properties of space and time-resolved wave packets. Therefore, a natural extension of this work would be to analyze the physics of such wave packets to determine if such experiments are sensitive to the underlying vacuum quantum fluctuation, or in other words, if analog gravity experiments of the sort can probe the physics of gravitational anomalies.

Finally, from an experimental point of view, studying the thermal propagation in the picosecond regime would be interesting. As we have seen in chapter 8, in a steady-states thermal transport experiment, it is difficult to isolate the electronic from the phononic contributions. Since anomalous quantum fluctuations mostly affect the electrons, identifying the effect of these fluctuations on thermal transport is difficult. However, as we have seen in chapter 4, the effects of these fluctuations also appear in the out-of-equilibrium response of a system following a thermal quench. In pump-probe experiments [262–266], an intense femtosecond light pulse is shone on a metallic sample. Due to the difference in mass between electrons and phonons, it is reasonable to assume that only the electron gas is heated. If the electron relaxation rate τ_e is short compared to the electron-phonon scattering time τ_{ep}, then it is reasonable to describe the dynamic of the electron gas on a time-scale $\tau \in [\tau_e, \tau_{ep}]$ as the dynamics of heat waves following a temperature quench. Picosecond pump-probe experiments able to heat a metallic sample and study the subsequent energy distribution thus seem to provide a new experimental platform in which it would be interesting to look for signatures of the peculiar quantum fluctuations.

Appendix A

Introduction to curved spacetimes and their coupling with spinor fields

The concept of field theory in curved spacetimes is at the heart of this thesis. Although a funding hypothesis of general relativity is the absence of torsion, it appears in condensed matter physics that this hypothesis is sometimes too restrictive since torsion can be induced in such systems by a crystalline topological defect such as screw-dislocations [257–259, 267] (See Fig. A.1). In this section, we will review some notions of differential geometry useful for this thesis, both in the presence and absence of torsion, before studying how these geometric fields couple to particles.

A.1 Introduction to Riemann-Cartan spaces

One of the postulates of Einstein's general relativity is that the affine connection is symmetric, implying that there is no torsion. In 1922, E. Cartan considered the extension to asymmetric affine connections such that curvature and torsion are non-zero [268]. The associated spaces are called Riemann-Cartan spaces. Even though it is possible to study the properties of these spaces using the metric as the fundamental object, as one usually does in general relativity, for our purposes, it is worth introducing the tetrad(or viebein) formalism[1].

Tetrads, cotetrads, and metrics

On a flat manifold, finding a general basis of coordinates is possible such that the metric is diagonal. On curved spacetimes, this is no longer possible. Nevertheless, we can define a local basis for which the metric is diagonal at each point of the manifold. One then rewrites the metric as

$$g_{\mu\nu} = e^a_\mu \eta_{ab} e^b_\nu, \tag{A.1}$$

where η is the Minkowski metric whose signature in $D+1$ dimension is equal to $D-1$. Or in other words

$$\eta_{\mu\nu} = \begin{pmatrix} 1 & 0 \\ 0 & -\mathbb{1}_D \end{pmatrix}. \tag{A.2}$$

The transformation matrices e^a_μ are known as co-tetrads, and their inverse e^ν_b as tetrads, such that

$$\begin{aligned} e^a_\mu e^\nu_a &= \delta^\nu_\mu, \\ e^a_\mu e^\mu_b &= \delta^a_b, \end{aligned} \tag{A.3}$$

[1] For a detailed discussion of this formalism in general relativity (in the absence of torsion), see [269]

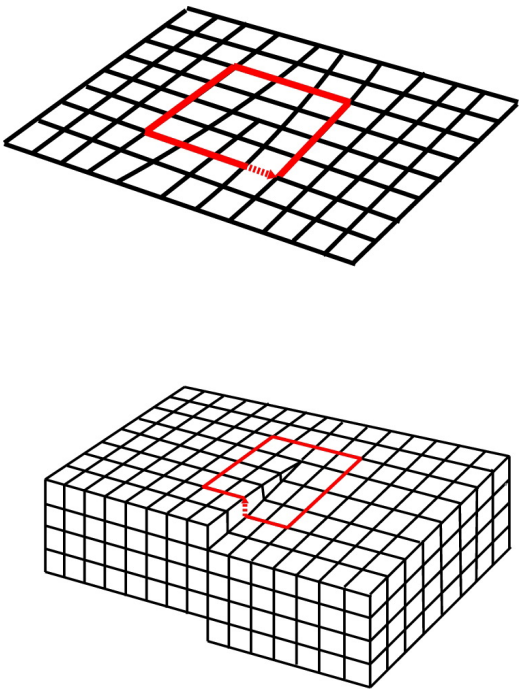

Figure A.1: **Dislocation and torsion on a lattice** Upper: Edge dislocation in a square two-dimensional lattice. The Burgers vector is parallel to the displacement. Lower: Screw dislocation in a three-dimensional cubic lattice. The Burgers vector is perpendicular to the displacement, where the Burgers' vector b^i corresponding to a surface S is defined with respect to the torsion $T^\rho_{\mu\nu}$ by $b^i = \iint_S \mathrm{d}x^\mu \wedge \mathrm{d}x^\nu \, T^i_{\mu\nu}$ (Taken from [257])

where the Einstein notations (summation on repeated indices) are assumed.
Here and in the following, Greek indices will refer to the spacetime, while the Latin ones will refer to the tangent space. The Greek indices will be lowered or raised with the metric g and the Latin one with the Minkowski metric η.

Covariant derivatives, affine connections, and spin connections

Besides the tetrad field, which defines the local coordinate systems, we introduce a Lorentz or spin connection $\omega^a{}_{b\mu}$ which encodes the parallel transport between the tangent spaces and an affine connection described by the Christoffel symbols $\Gamma^\lambda_{\mu\nu}$, such that the parallel transport of both tangent space vector (V^j) and "real" tangent space vector (V^μ) are defined as

$$\begin{aligned} \tilde{V}^j(x+\Delta x) &= V^j(x) + \Delta x^\rho \omega^j{}_{i\rho} V^i(x), \\ \tilde{V}^\mu(x+\Delta x) &= V^\mu(x) + \Delta x^\rho \Gamma^\mu_{\nu\rho} V^\nu(x). \end{aligned} \tag{A.4}$$

These definitions allow one to define the covariant derivatives

$$\begin{aligned} \nabla_\mu X^a_\nu &= \partial_\mu X^a_\nu + \omega^a{}_{b\mu} X^b_\nu - \Gamma^\lambda_{\nu\mu} X^a_\lambda, \\ \nabla_\mu X^\nu_a &= \partial_\mu X^\nu_a - \omega^b{}_{a\mu} X^\nu_b + \Gamma^\nu_{\lambda\mu} X^\lambda_a. \end{aligned} \tag{A.5}$$

The first constraint we impose is that the magnitude of vectors is preserved under parallel transport

$$\nabla_\mu e^\mu_a = 0, \text{and } \nabla_\mu \eta_{ab} = 0\,, \tag{A.6}$$

a condition also known as metricity. These conditions imply a relationship between spin and affine connections

$$\Gamma^\mu_{\rho\nu} = e^\mu_a \left(\partial_\nu e^a_\rho + \omega^a{}_{b\nu} e^b_\rho \right), \tag{A.7}$$

and the antisymmetry of $\omega_{ab\mu}$ with respect to the tangent space indices:

$$\omega_{ab\mu} + \omega_{ba\mu} = 0\,. \tag{A.8}$$

At this level, in general relativity, one imposes that the affine connexion is symmetric ($\Gamma^{\mu}_{\nu\rho} = \Gamma^{\mu}_{\rho\nu}$). Together with equation (A.6), this entirely fixes the value of the affine connection, known as the Levi-Civita connection $\left\{ \begin{matrix} \mu \\ \nu\rho \end{matrix} \right\}$, defined as a function of the metric as

$$\left\{ \begin{matrix} \mu \\ \nu\rho \end{matrix} \right\} = \frac{1}{2} g^{\mu\lambda} \left(\partial_\nu g_{\lambda\rho} + \partial_\rho g_{\nu\lambda} - \partial_\lambda g_{\nu\rho} \right) . \tag{A.9}$$

which can equally be expressed in terms of the tetrad itself using equation (A.1) (see [269]).

In Riemann-Cartan spacetime, since we relaxed the symmetry condition of the affine connection, (A.6) is no longer sufficient to fix the affine connection's value entirely. They, therefore, imply that, in this theory, there are two independent tensors. Generally, using the tetrad formalism, one chooses to consider that these two independent quantities are $\omega^{a}{}_{b\mu}$ and e^{μ}_{a} but we could, for example, also choose $\Gamma^{\mu}_{\nu\rho}$ and e^{μ}_{a}.

Torsion and curvature

From these definitions, it is then possible to define a notion of torsion and curvature.
The spacetime curvature is defined as

$$R^{\mu}_{\nu\rho\sigma} = \partial_\rho \Gamma^{\mu}_{\sigma\nu} - \partial_\sigma \Gamma^{\mu}_{\rho\nu} + \Gamma^{\mu}_{\rho\lambda}\Gamma^{\lambda}_{\sigma\nu} - \Gamma^{\mu}_{\sigma\lambda}\Gamma^{\lambda}_{\rho\nu}\,, \tag{A.10}$$

or expressed in terms of the tetrad and the spinor connection,

$$\begin{aligned} \mathcal{R}^{\rho}{}_{\sigma\mu\nu} &= e^{\rho}_{a}\, e^{b}_{\sigma}\, \mathcal{R}^{a}{}_{b\mu\nu} \\ &= e^{\rho}_{a} e^{b}_{\sigma} \left[\omega^{a}{}_{c\mu}\omega^{c}{}_{b\nu} - \omega^{a}{}_{c\nu}\omega^{c}{}_{b\mu} + \partial_\mu \omega^{a}{}_{b\nu} - \partial_\nu \omega^{a}{}_{b\mu} \right] . \end{aligned} \tag{A.11}$$

In Riemann-Cartan theory, and in contrast with general relativity, the affine connection $\Gamma^{\lambda}_{\mu\nu}$ is not always symmetric under the exchange $\mu \leftrightarrow \nu$. One defines the torsion tensor as

$$T^{\lambda}_{\mu\nu} = \Gamma^{\lambda}_{\mu\nu} - \Gamma^{\lambda}_{\nu\mu}\,, \tag{A.12}$$

or expressed in terms of the tetrad and the spinor connection

$$\begin{aligned} T^{\rho}{}_{\mu\nu} &= e^{\rho}_{a}\, T^{a}{}_{\mu\nu} \\ &= e^{\rho}_{a} \left[\partial_\nu e^{a}_{\mu} - \partial_\mu e^{a}_{\nu} + e^{b}_{\mu}\omega^{a}{}_{b\nu} - e^{b}_{\nu}\omega^{a}{}_{b\mu} \right] . \end{aligned} \tag{A.13}$$

These concepts of torsion and curvature have an intuitive geometrical interpretation through parallel transport(see Fig. A.2). The torsion tensor describes the difference between the transport along u of v and the one along v of u (in contrast to the flat and torsionless space case, the parallelogram does not always close). The curvature describes the angle difference between a vector and its image after a parallel transport around a close loop.
Those geometrical interpretations are summarized by the action of the commutator of two covariant derivatives on a vector field P^{ρ}:

$$[\nabla_\mu\,,\, \nabla_\nu] P^{\rho} = T^{\lambda}{}_{\mu\nu} \nabla_\lambda P^{\rho} + R^{\rho}_{\lambda\mu\nu} P^{\lambda}. \tag{A.14}$$

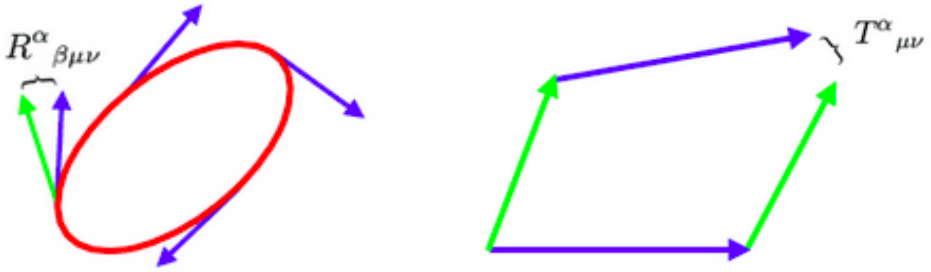

Figure A.2: **Geometrical interpretation of the curvature (left) and the torsion (right) in terms of parallel transport**

A.2 Fermions in curved spacetime with torsion

In the presence of curvature and torsion, the dynamic of relativistic quantum particles is modified due to the modification of the Clifford algebra

$$\{\gamma^{\mu},\gamma^{\nu}\} = 2\eta^{\mu\nu} \rightarrow \{\gamma^{\mu},\gamma^{\nu}\} = 2g^{\mu\nu}. \tag{A.15}$$

In a Riemann-Cartan spacetime, both the tetrad and the spinor connection are fixed background variables (in contrast to the notion of dynamical spacetime obtained when studying general relativity)[2].

Dirac field action and tetrads

The generalization of the flat space Dirac action

$$S_{flat} = \int \mathrm{d}^{D+1}\boldsymbol{x}\, \frac{i\hbar}{2}\left(\bar{\Psi}\gamma^{\mu}\partial_{\mu}(\Psi) - \partial_{\mu}(\bar{\Psi})\gamma^{\mu}\Psi\right), \tag{A.16}$$

to a Riemann-Cartan space with curvature and torsion can be introduced using a minimal coupling procedure [269]. Such a minimal coupling procedure requires three steps:

1. Generalizing the measure of integration covariantly: $\mathrm{d}^{D+1}\boldsymbol{x} \rightarrow \mathrm{d}^{D+1}\boldsymbol{x}\ \det(e^{b}_{\mu})$
2. Modifying the gamma matrices to satisfy the curved spacetime Clifford algebra (A.15): $\gamma^{\mu} = \delta^{\mu}_{a}\gamma^{a} \rightarrow \gamma^{\mu} = e^{\mu}_{a}\gamma^{a}$, with γ^{a} the usual flat spacetime gamma matrices;
3. Replacing the partial derivative by a covariant spinor derivative: $\partial_{\mu} \rightarrow D_{\mu} = \partial_{\mu} - \frac{i}{4}\omega_{ab\mu}\sigma^{ab}$, with σ^{ab} the generator of Lorentz algebra, $\sigma^{ab} = \frac{i}{2}\left[\gamma^{a}\ ,\ \gamma^{b}\right]$. This last step can be understood from two points of view; one can deduce this expression by consistency with the covariant derivative of the vector $\bar{\Psi}\gamma^{\mu}\Psi$(see [270]) or from a gauge field point of view, requiring that under a local Lorentz transformation, $D_{\mu}\Psi$ behaves as a spinor (see [269]).

The full spinor action in Riemann-Cartan space is therefore given by

$$S = \int \mathrm{d}^{D+1}\boldsymbol{x}\ \det\left(e^{a}_{\mu}\right)\frac{i\hbar}{2}\left[\bar{\Psi}\gamma^{a}e^{\mu}_{a}D_{\mu}\Psi - \overline{D_{\mu}\Psi}\gamma^{a}e^{\mu}_{a}\Psi\right]. \tag{A.17}$$

[2]For a more detailed study of the behavior of particles in Riemann-Cartan spaces the reader is referred to [270].

Connection decomposition and simplified action

As we have seen in section A.1, the definition of the affine connection is modified in the presence of torsion. It is, however, possible to decompose it into torsionless and torsion-full components

$$\Gamma^{\lambda}_{\mu\nu} = \begin{Bmatrix} \lambda \\ \mu\nu \end{Bmatrix} + \frac{1}{2} g^{\lambda\rho} \left(T_{\rho\mu\nu} - T_{\mu\rho\nu} - T_{\nu\rho\mu} \right) . \tag{A.18}$$

The torsionless component (first term) corresponds to the Levi-Civita connection(see equation (A.9)), while the torsion-full part (last three terms) is called the contorsion tensor.
Using this decomposition in the covariant derivative and integrating it by part, we simplify the action (A.17) into

$$S = i\hbar \int \mathrm{d}^{D+1}\boldsymbol{x} \, \det\left(e^{b}_{\nu}\right) \bar{\Psi} \left[\gamma^{a} e^{\mu}_{a} \tilde{D}_{\mu} - \frac{i}{8} \gamma^{5} \gamma^{a} e^{\mu}_{a} S_{\mu} \right] \Psi \tag{A.19}$$

with

- $\tilde{D}_{\mu}$ the torsionless covariant derivative or Levi-Civita covariant derivative

$$\tilde{D}_{\mu} = \partial_{\mu} + \frac{1}{8} \underbrace{e_{a\nu} \left(\partial_{\mu} e^{\nu}_{b} + \begin{Bmatrix} \nu \\ \rho\mu \end{Bmatrix} e^{\rho}_{b} \right)}_{\text{Torsionless spin connection } \tilde{\omega}_{ab\mu}} \left[\gamma^{a}, \gamma^{b} \right] \tag{A.20}$$

- S^{μ} is the totally antisymmetric part of the torsion, also called the pseudo-trace of the torsion tensor

$$S^{\mu} = \epsilon^{\alpha\beta\gamma\mu} T_{\alpha\beta\gamma} \tag{A.21}$$

This formulation of the action proves that free fermions only couple to the antisymmetric part of the torsion.
Moreover, we can also write this action with the usual spinor covariant derivative as

$$S = i\hbar \int \mathrm{d}^{D+1}\boldsymbol{x} \det\left(e^{b}_{\nu}\right) \bar{\Psi} \left[\gamma^{a} e^{\mu}_{a} D_{\mu} - \frac{1}{2} \gamma^{a} e^{\mu}_{a} T_{\mu} \right] \Psi \tag{A.22}$$

with T_{μ} the trace of the torsion tensor

$$T_{\mu} = T^{\lambda}_{\mu\lambda}. \tag{A.23}$$

Appendix B

Continuity and metric quenches

B.1 Continuity equations during a metric quench

In this appendix, we study the continuity equation of the covariantly conserved momentum-energy tensor (2.92,2.91) during a quench of metric. For the sake of simplicity and sticking to the protocols detailed in the main text, we consider a metric of the form

$$\mathrm{d}s^2 = f(x,t)v_F^2\mathrm{d}t^2 - \mathrm{d}x^2 \tag{B.1}$$

which is changed abruptly at some time $t = 0$, such as:

$$f(x,t) = \begin{cases} f_I(x) & \text{for } t < 0, \\ f_{II}(x) & \text{for } t > 0. \end{cases} \tag{B.2}$$

Injecting these expression in the (non-)conservation equations (2.91,3.38) leads to the expressions

$$\begin{aligned} &\partial_0 \mathcal{T}^0_{\ 0} + \frac{1}{\sqrt{f}}\partial_x\left(\mathcal{T}^x_{\ 0}\sqrt{f}\right) + \frac{\hbar v_F}{96\pi}\frac{C_g}{\sqrt{f}}\mathcal{R}\partial_x f = 0, \\ &\partial_0\left(\mathcal{T}^0_{\ x}\sqrt{f}\right) + \frac{1}{\sqrt{f}}\partial_x\left(\mathcal{T}^x_{\ x} f\right) - \frac{\hbar v_F}{96\pi}\frac{C_w}{\sqrt{f}}\mathcal{R}\partial_x f = 0. \end{aligned} \tag{B.3}$$

where we recall that $\mathcal{R}(x) = \frac{\partial_x^2 f}{f} - \frac{1}{2}\left(\frac{\partial_x f}{f}\right)^2$. Integrating these equations between $t = 0^-$ and $t = 0^+$, we deduce that the variables that are continuous across the quench are both the energy density $\varepsilon = \mathcal{T}^0_{\ 0}$ and the momentum density $\Pi = \frac{1}{v_F}\mathcal{T}^0_{\ x}\sqrt{f}$:

$$\mathcal{T}^0_{\ 0}(0^-,x) = \mathcal{T}^0_{\ 0}(0^+,x)\,, \tag{B.4}$$

$$\frac{1}{v_F}\sqrt{f_I(x)}\mathcal{T}^0_{\ x}(0^-,x) = \frac{1}{v_F}\sqrt{f_{II}(x)}\mathcal{T}^0_{\ x}(0^+,x)\,. \tag{B.5}$$

B.2 Time evolution and spacetime quenches

The conservation equations (B.3) for ε and Π, which are continuous at metric quenches, can be explicitly written using the anomalies expressions (2.91,3.38) as:

$$\sqrt{f}\partial_0\varepsilon - v_F\partial_x\left(\Pi f\right) = \frac{\hbar v_F}{48\pi}C_g\left(f\partial_x\mathcal{R} + \frac{1}{2}\mathcal{R}\partial_x f\right) = \frac{\hbar v_F}{48\pi}C_g\partial_x\left(f\left(\mathcal{R} - \overline{\mathcal{R}}\right)\right)\,, \tag{B.6}$$

$$v_F\sqrt{f}\partial_0\Pi - \partial_x\left(\varepsilon f\right) = -\frac{\hbar v_F}{48\pi}C_w\partial_x\left(f\left(\mathcal{R} - \overline{\mathcal{R}}\right)\right)\,. \tag{B.7}$$

Defining the chiral component of the momentum-energy tensor $\mathcal{T}^{\pm} = \varepsilon \pm v_F \Pi$, we get

$$\sqrt{f}\partial_0 \mathcal{T}^{\pm} \mp \partial_x \left[f \left(\mathcal{T}^{\pm} - \frac{\hbar v_F}{48\pi} \mathcal{C}_{\pm} \left(\mathcal{R} - \overline{\mathcal{R}} \right) \right) \right] = 0 \,, \tag{B.8}$$

where

$$\overline{\mathcal{R}}(x) = \frac{1}{2f} \int_0^x \mathcal{R} \partial_x f = \frac{1}{4} \left(\frac{\partial_x f}{f} \right)^2 . \tag{B.9}$$

Hence, the evolution of ε and Π are deduced from two rules:

1. At the quenches, $\mathcal{T}^{\pm}$ is continuous.
2. Between quenches, since $f(x)$ does not depend on time, $\mathcal{T}^{\pm}$ satisfies the following equation of motion

$$(\partial_0 \mp \partial_y) \left[f \left(\mathcal{T}^{\pm} - \frac{\hbar v_F}{48\pi} \mathcal{C}_{\pm} \left(\mathcal{R} - \overline{\mathcal{R}} \right) \right) \right] = 0 \tag{B.10}$$

with a rescaled coordinate

$$y(x) = \int_0^x \frac{1}{\sqrt{f(u)}} \mathrm{d}u. \tag{B.11}$$

B.3 Floquet stroboscopic evolution

We now derive the stroboscopic time evolution of $\mathcal{T}^{\pm}$ in a Floquet system from the previous equations of motion.

We consider a metric (B.1) with

$$f(x,t) = \begin{cases} 1 & \text{for } t \in]nt_p, nt_p + t_1[\,, \\ f(x) & \text{for } t \in]nt_p + t_1, (n+1)t_p[\,. \end{cases} \tag{B.12}$$

where $t_p = t_1 + t_2$ and $n \in \mathbb{Z}$. Calling $\mathcal{T}_n^{\pm}(x) = \mathcal{T}^{\pm}(x, nt_p)$ and applying the previous rules we get

$$\begin{aligned} \mathcal{T}^{\pm}(x, nt_p + t_1) &= \mathcal{T}^{\pm}(x \pm v_F t_1, nt_p) \\ &= \mathcal{T}_n^{\pm}(x \pm v_F t_1) \end{aligned} \tag{B.13}$$

and therefore,

$$\begin{aligned} \mathcal{T}_{n+1}^{\pm}(x) &\equiv T^{\pm}(x, nt_p + t_1 + t_2) \\ &= \frac{f(x^{\pm})}{f(x)} \left[T_n^{\pm}(x^{\pm} \pm v_F t_1) - \frac{\hbar v_F}{48\pi} \mathcal{C}_{\pm} \left(\mathcal{R}(x^{\pm}) - \overline{\mathcal{R}}(x^{\pm}) \right) \right] + \frac{\hbar v_F}{48\pi} \mathcal{C}_{\pm} \left(\mathcal{R}(x) - \overline{\mathcal{R}}(x) \right) \end{aligned} \tag{B.14}$$

with

$$x^{\pm}(x) = y^{-1} \left(y(x) \pm v_F t_2 \right) . \tag{B.15}$$

From this definition of $x^{\pm}(x)$, we can rewrite the equation (B.14) in more compact form:

$$\mathcal{T}_{n+1}^{\pm}(x) = \left(\partial_x x^{\pm} \right)^2 \mathcal{T}_n^{\pm} \left(x^{\pm} \right) - \frac{\hbar v_F}{24\pi} \mathcal{C}_{\pm} \left\{ x^{\pm}, x \right\} \tag{B.16}$$

where $\{x^{\pm}, x\}$ denotes the Schwarzian derivative of $x^{\pm}$ with respect to x,

$$\{f, x\} = \frac{\partial_x^3 f}{\partial_x f} - \frac{3}{2} \left(\frac{\partial_x^2 f}{\partial_x f} \right)^2 \tag{B.17}$$

In the end, by recursion, we can simplify the expression for $\mathcal{T}_n^{\pm}$ as

$$\mathcal{T}_n^{\pm}(x) = \left(\partial_x x_n^{\pm}\right)^2 \mathcal{T}_0^{\pm}(x_n^{\pm}) - \frac{\hbar v_F}{24\pi}\mathcal{C}_{\pm}\left\{x_n^{\pm}, x\right\} \tag{B.18}$$

with $x_n^{\pm}$ a function defined recursively by

$$x_{n+1}^{\pm}(x) = x^{\pm}(x_n^{\pm}(x)) \tag{B.19}$$

which, even though compact and able to separate the classical dynamics from the quantum corrections, is not really helpful for numerical evaluation.

Appendix C

Killing vectors and conserved quantities in general relativity

Conserved quantities in flat spacetime

In a $D+1$ dimensional flat spacetime, according to the Noether theorem, to any continuous symmetry, one can associate a conserved current j^μ such that

$$\partial_\mu j^\mu = 0\,. \tag{C.1}$$

It is then possible to define a conserved charge Q associated to the current j^μ such that $\partial_t Q = 0$, writting

$$Q = \int \mathrm{d}^D x\, j^0 \tag{C.2}$$

For example, in a flat spacetime, the conservation of the momentum-energy tensor $\mathcal{T}^{\mu\nu}$ ‘

$$\partial_\mu \mathcal{T}^{\mu\nu} = 0\,, \tag{C.3}$$

directly lead to the conservation of the energy

$$E = \int \mathrm{d}^D x \mathcal{T}^{00}\,, \tag{C.4}$$

and of the momentum

$$\Pi^a = \int d^D x \mathcal{T}^{a0}\,. \tag{C.5}$$

The problem of curved spacetimes

In a curved spacetime, endowed the metric $g_{\mu\nu}$ and the corresponding affine connection $\left\{ \begin{matrix} \mu \\ \nu\rho \end{matrix} \right\}$, this statement is no longer valid since the covariant conservation equation

$$\nabla_\mu \mathcal{T}^{\mu\nu} = 0 \tag{C.6}$$

is not a true conservation equation. To see this, let us define $\mathcal{J}^\mu = \mathcal{T}^{0\mu}$, based on the covariant conservation equation, we have

$$\begin{aligned} \nabla_\mu \mathcal{J}^\mu &= \partial_\mu \mathcal{J}^\mu + \left\{ \begin{matrix} \mu \\ \mu\rho \end{matrix} \right\} \mathcal{J}^\rho \\ &= \nabla_\mu \mathcal{T}^{0\mu} - \left\{ \begin{matrix} 0 \\ \mu\rho \end{matrix} \right\} \mathcal{T}^{\rho\mu} \\ &= - \left\{ \begin{matrix} 0 \\ \mu\rho \end{matrix} \right\} \mathcal{T}^{\mu\rho} \end{aligned} \tag{C.7}$$

such that

$$\begin{aligned}\partial_t\left[\int \mathrm{d}^d x\sqrt{|\det(g_{\mu\nu})|}\mathcal{J}^0\right] &= \int \mathrm{d}^d x\sqrt{|\det(g_{\mu\nu})|}\nabla_0\mathcal{J}^0\,,\\ &= \int \mathrm{d}^d x\sqrt{|\det(g_{\mu\nu})|}\left(-\nabla_a\mathcal{J}^a - \begin{Bmatrix}0\\ \mu\rho\end{Bmatrix}\mathcal{T}^{\mu\rho}\right)\,,\\ &= -\int \mathrm{d}^d x\partial_a\left(\sqrt{|\det(g_{\mu\nu})|}\mathcal{J}^a\right) - \int \mathrm{d}^d x\sqrt{|\det(g_{\mu\nu})|}\begin{Bmatrix}0\\ \mu\rho\end{Bmatrix}\mathcal{T}^{\mu\rho}\,,\\ &= -\int \mathrm{d}^d x\sqrt{|\det(g_{\mu\nu})|}\begin{Bmatrix}0\\ \mu\rho\end{Bmatrix}\mathcal{T}^{\mu\rho} \neq 0\,.\end{aligned} \tag{C.8}$$

Killing vectors and conserved quantities in curved spacetime

Instead, in curved spacetime, one resorts to the notion of Killing vector fields to define conserved quantities.

By definition, a vector field $\xi^\mu(x)$ is called a Killing vector field if an infinitesimal transformation of the form $x^\mu \to \tilde{x}^\mu = x^\mu + \epsilon\xi^\mu(x)$ with $\epsilon \ll 1$ leave the infinitesimal line element $\mathrm{d}s^2 = g_{\mu\nu}\mathrm{d}x^\mu\mathrm{d}x^\nu$ unchanged ($\mathrm{d}s^2 - \mathrm{d}\tilde{s}^2 = o(\epsilon^2)$).
In other words, a vector field $\xi^\mu(x)$ is called a vector fields if and only if

$$\forall\mu,\nu,\ \ \nabla_\mu\xi_\nu + \nabla_\nu\xi_\mu = 0\,. \tag{C.9}$$

Armed with a Killing vector field ξ^μ, it is then possible to define a conserved current $\mathcal{J}^\mu = \xi_\nu\mathcal{T}^{\nu\mu}$, such that

$$\nabla_\mu\mathcal{J}^\mu = \nabla_\mu(\xi_\nu)\,\mathcal{T}^{\nu\mu} + \xi_\nu\nabla_\mu\mathcal{T}^{\mu\nu} = 0\,, \tag{C.10}$$

using the symmetry of the momentum-energy tensor, its conservation law, and the Killing equation. It is then possible to define the corresponding conserved quantity

$$\mathcal{Q} = \int \mathrm{d}^d x\sqrt{|\det(g_{\mu\nu})|}\mathcal{J}^0\,, \tag{C.11}$$

such that $\partial_t\mathcal{Q} = 0$.

Some important facts about Killing vector fields

• Let χ and ξ two Killing vector fields, then

$$\zeta^\mu = \xi^\nu\nabla_\nu\chi^\mu - \chi^\nu\nabla_\nu\xi^\mu \tag{C.12}$$

is also a Killing vector field.

• In a theory in dimension $D+1$, there is a maximum of $\frac{(D+1)(D+2)}{2}$ independent Killing vector fields.

•In a $3+1$ dimension flat spacetime, the 10 Killing vector fields are

- The 4 space and time translation δ^μ_0, δ^μ_x, δ^μ_y, and δ^μ_z
- The three rotations $J^\mu_x = y\delta^\mu_z - z\delta^\mu_y$, $J^\mu_y = -x\delta^\mu_z + z\delta^\mu_x$, and $J^\mu_z = x\delta^\mu_y - y\delta^\mu_x$
- The three boosts $B^\mu_x = x\delta^\mu_0 + v_F t\delta^\mu_x$, $B^\mu_y = y\delta^\mu_0 + V_F t\delta^\mu_y$, and $B^\mu_z = z\delta^\mu_0 + V_F t\delta^\mu_z$

• By definition, a time-like Killing vector is a killing vector field ξ such that

$$\xi^\mu g_{\mu\nu}\xi_\nu > 0\,. \tag{C.13}$$

Similarly, a light-like Killing vector will verify

$$\xi^\mu g_{\mu\nu}\xi_\nu = 0\,. \tag{C.14}$$

and a space-like Killing vector

$$\xi^\mu g_{\mu\nu}\xi_\nu < 0\,. \tag{C.15}$$

Bibliography

[1] K. Schwarzschild, "Uber das gravitationsfeld eines massenpunktes nach der einstein'schen theorie," *Berlin. Sitzungsberichte*, vol. 18, 1916.

[2] S. W. Hawking, "Black hole explosions?," *Nature*, vol. 248, no. 5443, pp. 30–31, 1974.

[3] W. Gordon, "Zur lichtfortpflanzung nach der relativitätstheorie," *Annalen der Physik*, vol. 377, no. 22, pp. 421–456, 1923.

[4] W. G. Unruh, "Experimental black-hole evaporation?," *Physical Review Letters*, vol. 46, no. 21, p. 1351, 1981.

[5] L. J. Garay, J. Anglin, J. I. Cirac, and P. Zoller, "Sonic analog of gravitational black holes in bose-einstein condensates," *Physical Review Letters*, vol. 85, no. 22, p. 4643, 2000.

[6] L. J. Garay, J. Anglin, J. I. Cirac, and P. Zoller, "Sonic black holes in dilute bose-einstein condensates," *Physical Review A*, vol. 63, no. 2, p. 023611, 2001.

[7] R. C. Tolman and P. Ehrenfest, "Temperature equilibrium in a static gravitational field," *Physical Review*, vol. 36, no. 12, p. 1791, 1930.

[8] R. C. Tolman, "On the weight of heat and thermal equilibrium in general relativity," *Physical Review*, vol. 35, no. 8, p. 904, 1930.

[9] J. Luttinger, "Theory of thermal transport coefficients," *Physical Review*, vol. 135, no. 6A, p. A1505, 1964.

[10] S. M. Christensen and S. A. Fulling, "Trace anomalies and the hawking effect," *Physical Review D*, vol. 15, no. 8, p. 2088, 1977.

[11] S. P. Robinson and F. Wilczek, "Relationship between hawking radiation and gravitational anomalies," *Physical review letters*, vol. 95, no. 1, p. 011303, 2005.

[12] H. B. Nielsen and M. Ninomiya, "The adler-bell-jackiw anomaly and weyl fermions in a crystal," *Physics Letters B*, vol. 130, no. 6, pp. 389–396, 1983.

[13] K. Landsteiner, E. Megias, and F. Pena-Benitez, "Gravitational anomaly and transport phenomena," *Physical review letters*, vol. 107, no. 2, p. 021601, 2011.

[14] K. Landsteiner, "Notes on anomaly induced transport," *arXiv preprint arXiv:1610.04413*, 2016.

[15] M. N. Chernodub, Y. Ferreiros, A. G. Grushin, K. Landsteiner, and M. A. Vozmediano, "Thermal transport, geometry, and anomalies," *Physics Reports*, vol. 977, pp. 1–58, 2022.

[16] J. Gooth, A. C. Niemann, T. Meng, A. G. Grushin, K. Landsteiner, B. Gotsmann, F. Menges, M. Schmidt, C. Shekhar, V. Süß, *et al.*, "Experimental signatures of the mixed axial–gravitational anomaly in the weyl semimetal nbp," *Nature*, vol. 547, no. 7663, pp. 324–327, 2017.

[17] M. A. Vozmediano, F. de Juan, and A. Cortijo, "Gauge fields and curvature in graphene," in *Journal of Physics: Conference Series*, vol. 129, p. 012001, IOP Publishing, 2008.

[18] A. Gallerati, "Negative-curvature spacetime solutions for graphene," *Journal of Physics: Condensed Matter*, vol. 33, no. 13, p. 135501, 2021.

[19] E. Kleinherbers, T. Stegmann, and N. Szpak, "Electronic transport in bent carbon nanotubes," *arXiv preprint arXiv:2302.01395*, 2023.

[20] L. Landau and E. Lifshitz, "The classical theory of fields, course of theoretical physics," *Pergamon Press, Oxford*, 1971.

[21] R. W. White, "Acoustic ray tracing in moving inhomogeneous fluids," *The Journal of the Acoustical Society of America*, vol. 53, no. 6, pp. 1700–1704, 1973.

[22] S. Badulin, K. Pokazayev, and A. Rozenberg, "A laboratory study of the transformation of regular gravity-capillary waves in inhomogeneous flows," *Izv. Atmos. Ocean. Phys*, vol. 19, no. 10, pp. 782–787, 1983.

[23] R. Schützhold and W. G. Unruh, "Gravity wave analogues of black holes," *Physical Review D*, vol. 66, no. 4, p. 044019, 2002.

[24] G. Rousseaux, C. Mathis, P. Maïssa, T. G. Philbin, and U. Leonhardt, "Observation of negative-frequency waves in a water tank: a classical analogue to the hawking effect?," *New Journal of Physics*, vol. 10, no. 5, p. 053015, 2008.

[25] G. Rousseaux, P. Maïssa, C. Mathis, P. Coullet, T. G. Philbin, and U. Leonhardt, "Horizon effects with surface waves on moving water," *New Journal of Physics*, vol. 12, no. 9, p. 095018, 2010.

[26] O. Klein, "Quantentheorie und fünfdimensionale relativitätstheorie," *Zeitschrift für Physik*, vol. 37, no. 12, pp. 895–906, 1926.

[27] W. Gordon, "Der comptoneffekt nach der schrödingerschen theorie," *Zeitschrift für Physik*, vol. 40, no. 1-2, pp. 117–133, 1926.

[28] H. Furuhashi, Y. Nambu, and H. Saida, "Simulation of an acoustic black hole in a laval nozzle," *Classical and Quantum Gravity*, vol. 23, no. 17, p. 5417, 2006.

[29] V. Eltsov, M. Krusius, and G. Volovik, "Superfluid 3he: A laboratory model system of quantum field theory," *arXiv preprint cond-mat/9809125*, 1998.

[30] G. Volovik, "Induced gravity in superfluid 3 he," *Journal of low temperature physics*, vol. 113, pp. 667–680, 1998.

[31] G. Volovik, "Is there analogy between quantized vortex and black hole?," *arXiv preprint gr-qc/9510001*, 1995.

[32] G. E. Volovik, "Superfluid analogies of cosmological phenomena," *Physics Reports*, vol. 351, no. 4, pp. 195–348, 2001.

[33] C. Barcelo, S. Liberati, and M. Visser, "Analogue gravity from bose-einstein condensates," *Classical and Quantum Gravity*, vol. 18, no. 6, p. 1137, 2001.

[34] N. Bogoliubov, "On the theory of superfluidity," *J. Phys*, vol. 11, no. 1, p. 23, 1947.

[35] G. E. Volovik, *The universe in a helium droplet*, vol. 117. OUP Oxford, 2003.

[36] N. Mermin and T.-L. Ho, "Circulation and angular momentum in the a phase of superfluid helium-3," *Physical Review Letters*, vol. 36, no. 11, p. 594, 1976.

[37] S. W. Hawking, "Breakdown of predictability in gravitational collapse," *Physical Review D*, vol. 14, no. 10, p. 2460, 1976.

[38] J. Preskill, "Do black holes destroy information," in *Proceedings of the International Symposium on Black Holes, Membranes, Wormholes and Superstrings, S. Kalara and DV Nanopoulos, eds.(World Scientific, Singapore, 1993) pp*, pp. 22–39, World Scientific, 1992.

[39] A. Gullstrand, *Allgemeine lösung des statischen einkörperproblems in der Einsteinschen gravitationstheorie*. Almqvist & Wiksell, 1922.

[40] P. Painlevé, "La mécanique classique et la théorie de la relativité," *Comptes Rendus Academie des Sciences (serie non specifiee)*, vol. 173, pp. 677–680, 1921.

[41] A. J. Hamilton and J. P. Lisle, "The river model of black holes," *American Journal of Physics*, vol. 76, no. 6, pp. 519–532, 2008.

[42] G. Lemaître, "L'univers en expansion," in *Annales de la Société scientifique de Bruxelles*, vol. 53, p. 51, 1933.

[43] S. J. Robertson, "The theory of hawking radiation in laboratory analogues," *Journal of Physics B: Atomic, Molecular and Optical Physics*, vol. 45, no. 16, p. 163001, 2012.

[44] J. Steinhauer, "Observation of quantum hawking radiation and its entanglement in an analogue black hole," *Nature Physics*, vol. 12, no. 10, pp. 959–965, 2016.

[45] J. R. M. de Nova, K. Golubkov, V. I. Kolobov, and J. Steinhauer, "Observation of thermal hawking radiation at the hawking temperature in an analogue black hole," *arXiv preprint arXiv:1809.00913*, 2018.

[46] T. Giamarchi, *Quantum physics in one dimension*, vol. 121. Clarendon press, 2003.

[47] S.-i. Tomonaga, "Remarks on bloch's method of sound waves applied to many-fermion problems," *Progress of Theoretical Physics*, vol. 5, no. 4, pp. 544–569, 1950.

[48] J. Luttinger, "An exactly soluble model of a many-fermion system," *Journal of mathematical physics*, vol. 4, no. 9, pp. 1154–1162, 1963.

[49] D. Sénéchal, "An introduction to bosonization," *Theoretical Methods for Strongly Correlated Electrons*, pp. 139–186, 2004.

[50] P. A. M. Dirac, "The quantum theory of the electron," *Proceedings of the Royal Society of London. Series A, Containing Papers of a Mathematical and Physical Character*, vol. 117, no. 778, pp. 610–624, 1928.

[51] J. Dubail, J.-M. Stéphan, J. Viti, and P. Calabrese, "Conformal field theory for inhomogeneous one-dimensional quantum systems: the example of non-interacting fermi gases," *SciPost Physics*, vol. 2, no. 1, p. 002, 2017.

[52] J. Dubail, J.-M. Stéphan, and P. Calabrese, "Emergence of curved light-cones in a class of inhomogeneous luttinger liquids," *SciPost Physics*, vol. 3, no. 3, p. 019, 2017.

[53] P. Jordan and E. P. Wigner, "About the pauli exclusion principle," *Z. Phys*, vol. 47, no. 631, pp. 14–75, 1928.

[54] E. Lieb, T. Schultz, and D. Mattis, "Two soluble models of an antiferromagnetic chain," *Annals of Physics*, vol. 16, no. 3, pp. 407–466, 1961.

[55] P. Coleman, *Introduction to many-body physics*. Cambridge University Press, 2015.

[56] Y. Brun and J. Dubail, "One-particle density matrix of trapped one-dimensional impenetrable bosons from conformal invariance," *SciPost Physics*, vol. 2, no. 2, p. 012, 2017.

[57] A. Gendiar, R. Krcmar, and T. Nishino, "Spherical deformation for one-dimensional quantum systems," *Progress of Theoretical Physics*, vol. 122, no. 4, pp. 953–967, 2009.

[58] T. Hikihara and T. Nishino, "Connecting distant ends of one-dimensional critical systems by a sine-square deformation," *Physical Review B*, vol. 83, no. 6, p. 060414, 2011.

[59] H. Katsura, "Exact ground state of the sine-square deformed xy spin chain," *Journal of Physics A: Mathematical and Theoretical*, vol. 44, no. 25, p. 252001, 2011.

[60] H. Katsura, "Sine-square deformation of solvable spin chains and conformal field theories," *Journal of Physics A: Mathematical and Theoretical*, vol. 45, no. 11, p. 115003, 2012.

[61] G. Vitagliano, A. Riera, and J. I. Latorre, "Volume-law scaling for the entanglement entropy in spin-1/2 chains," *New Journal of Physics*, vol. 12, no. 11, p. 113049, 2010.

[62] G. Ramírez, J. Rodríguez-Laguna, and G. Sierra, "From conformal to volume law for the entanglement entropy in exponentially deformed critical spin 1/2 chains," *Journal of Statistical Mechanics: Theory and Experiment*, vol. 2014, no. 10, p. P10004, 2014.

[63] G. Ramírez, J. Rodríguez-Laguna, and G. Sierra, "Entanglement over the rainbow," *Journal of Statistical Mechanics: Theory and Experiment*, vol. 2015, no. 6, p. P06002, 2015.

[64] S. N. Santalla, G. Ramírez, S. S. Roy, G. Sierra, and J. Rodríguez-Laguna, "Entanglement links and the quasiparticle picture," *Physical Review B*, vol. 107, no. 12, p. L121114, 2023.

[65] J. Rodríguez-Laguna, J. Dubail, G. Ramírez, P. Calabrese, and G. Sierra, "More on the rainbow chain: entanglement, space-time geometry and thermal states," *Journal of Physics A: Mathematical and Theoretical*, vol. 50, no. 16, p. 164001, 2017.

[66] A. Bastianello, J. Dubail, and J.-M. Stéphan, "Entanglement entropies of inhomogeneous luttinger liquids," *Journal of Physics A: Mathematical and Theoretical*, vol. 53, no. 15, p. 155001, 2020.

[67] H. B. Callen, "Thermodynamics and an introduction to thermostatistics," *John Wiley & Sons, New York*, 1960.

[68] C. Grenier, C. Kollath, and A. Georges, "Probing thermoelectric transport with cold atoms," *arXiv preprint arXiv:1209.3942*, 2012.

[69] E. Noether, "Invariante variationsprobleme," *Nachrichten von der Gesellschaft der Wissenschaften zu Göttingen, Mathematisch-Physikalische Klasse*, vol. 1918, pp. 235–257, 1918.

[70] R. A. Bertlmann, *Anomalies in quantum field theory*, vol. 91. Oxford university press, 2000.

[71] R. Arouca, A. Cappelli, and H. Hansson, "Quantum field theory anomalies in condensed matter physics," *SciPost Physics Lecture Notes*, p. 062, 2022.

[72] A. Bilal, "Lectures on anomalies," *arXiv preprint arXiv:0802.0634*, 2008.

[73] E. Fradkin, *Quantum field theory: an integrated approach*. Princeton University Press, 2021.

[74] J. A. Harvey, "Tasi 2003 lectures on anomalies," *arXiv preprint hep-th/0509097*, 2005.

[75] M. A. Shifman, "Anomalies in gauge theories," *Physics reports*, vol. 209, no. 6, pp. 341–378, 1991.

[76] D. Tong, "Gauge theory," *Lecture notes, DAMTP Cambridge*, vol. 10, 2018.

[77] M. B. Green and J. H. Schwarz, "Anomaly cancellations in supersymmetric d= 10 gauge theory and superstring theory," *Physics Letters B*, vol. 149, no. 1-3, pp. 117–122, 1984.

[78] D. Tong, "Lectures on string theory," *arXiv preprint arXiv:0908.0333*, 2009.

[79] C. Bouchiat, J. Iliopoulos, and P. Meyer, "An anomaly-free version of weinberg's model," *Physics Letters B*, vol. 38, no. 7, pp. 519–523, 1972.

[80] D. J. Gross and R. Jackiw, "Effect of anomalies on quasi-renormalizable theories," *Physical Review D*, vol. 6, no. 2, p. 477, 1972.

[81] E. Witten, "An su (2) anomaly," *Physics Letters B*, vol. 117, no. 5, pp. 324–328, 1982.

[82] J. Steinberger, "On the use of subtraction fields and the lifetimes of some types of meson decay," *Physical Review*, vol. 76, no. 8, p. 1180, 1949.

[83] H. Fukuda and Y. Miyamoto, "On the γ-decay of neutral meson," *Progress of Theoretical Physics*, vol. 4, no. 3, pp. 347–357, 1949.

[84] D. Sutherland, "Current algebra and some non-strong mesonic decays," *Nuclear Physics B*, vol. 2, no. 4, pp. 433–440, 1967.

[85] S. L. Adler, "Axial-vector vertex in spinor electrodynamics," *Physical Review*, vol. 177, no. 5, p. 2426, 1969.

[86] J. S. Bell and R. W. Jackiw, "A pcac puzzle: $\pi^0 \to \gamma\gamma$ in the σ-model," *Nuovo cimento*, vol. 60, no. CERN-TH-920, pp. 47–61, 1969.

[87] S. L. Adler and W. A. Bardeen, "Absence of higher-order corrections in the anomalous axial-vector divergence equation," *Physical Review*, vol. 182, no. 5, p. 1517, 1969.

[88] K. Fujikawa, "Path-integral measure for gauge-invariant fermion theories," *Phys. Rev. Lett.*, vol. 42, pp. 1195–1198, Apr 1979.

[89] K. Fujikawa and H. Suzuki, *Path integrals and quantum anomalies*. No. 122, International Monographs on Ph, 2004.

[90] H. B. Nielsen and M. Ninomiya, "Absence of neutrinos on a lattice:(i). proof by homotopy theory," *Nuclear Physics B*, vol. 185, no. 1, pp. 20–40, 1981.

[91] H. B. Nielsen and M. Ninomiya, "Absence of neutrinos on a lattice:(ii). intuitive topological proof," *Nuclear Physics B*, vol. 193, no. 1, pp. 173–194, 1981.

[92] H. B. Nielsen and M. Ninomiya, "No-go theorum for regularizing chiral fermions," tech. rep., Science Research Council, 1981.

[93] Z. Liu, B. Zhou, Y. Zhang, Z. Wang, H. Weng, D. Prabhakaran, S.-K. Mo, Z. Shen, Z. Fang, X. Dai, *et al.*, "Discovery of a three-dimensional topological dirac semimetal, na3bi," *Science*, vol. 343, no. 6173, pp. 864–867, 2014.

[94] B. Lv, H. Weng, B. Fu, X. P. Wang, H. Miao, J. Ma, P. Richard, X. Huang, L. Zhao, G. Chen, *et al.*, "Experimental discovery of weyl semimetal taas," *Physical Review X*, vol. 5, no. 3, p. 031013, 2015.

[95] O. Vafek and A. Vishwanath, "Dirac fermions in solids: from high-t c cuprates and graphene to topological insulators and weyl semimetals," *Annu. Rev. Condens. Matter Phys.*, vol. 5, no. 1, pp. 83–112, 2014.

[96] N. Armitage, E. Mele, and A. Vishwanath, "Weyl and dirac semimetals in three-dimensional solids," *Reviews of Modern Physics*, vol. 90, no. 1, p. 015001, 2018.

[97] T. Louvet, *Relativistic Phases in Condensed Matter*. PhD thesis, Université de Lyon, 2018.

[98] E. Brillaux, *Relativistic phases in condensed matter*. PhD thesis, Université de Lyon, 2021.

[99] v. H. Weyl, "Elektron und gravitation. i," *Surveys in High Energy Physics*, vol. 5, no. 3, pp. 261–267, 1986.

[100] R. Landauer, "Spatial variation of currents and fields due to localized scatterers in metalic conduction," *IBM J. Res. Dev*, vol. 1, p. 233, 1957.

[101] R. Landauer, "Electrical transport in open and closed systems," *Zeitschrift für Physik B Condensed Matter*, vol. 68, no. 2-3, pp. 217–228, 1987.

[102] D. Son and B. Spivak, "Chiral anomaly and classical negative magnetoresistance of weyl metals," *Physical Review B*, vol. 88, no. 10, p. 104412, 2013.

[103] Q. Li and D. E. Kharzeev, "Chiral magnetic effect in condensed matter systems," *Nuclear Physics A*, vol. 956, pp. 107–111, 2016.

[104] Q. Li, D. E. Kharzeev, C. Zhang, Y. Huang, I. Pletikosic, A. V. Fedorov, R. D. Zhong, J. A. Schneeloch, G. D. Gu, and T. Valla, "Observation of the chiral magnetic effect in ZrTe5," *Nature Phys.*, vol. 12, pp. 550–554, 2016.

[105] X. Huang, L. Zhao, Y. Long, P. Wang, D. Chen, Z. Yang, H. Liang, M. Xue, H. Weng, Z. Fang, *et al.*, "Observation of the chiral-anomaly-induced negative magnetoresistance in 3d weyl semimetal taas," *Physical Review X*, vol. 5, no. 3, p. 031023, 2015.

[106] F. Arnold, C. Shekhar, S.-C. Wu, Y. Sun, R. D. Dos Reis, N. Kumar, M. Naumann, M. O. Ajeesh, M. Schmidt, A. G. Grushin, *et al.*, "Negative magnetoresistance without well-defined chirality in the weyl semimetal tap," *Nature communications*, vol. 7, no. 1, p. 11615, 2016.

[107] T. Kimura, "Divergence of axial-vector current in the gravitational field," *Progress of Theoretical Physics*, vol. 42, no. 5, pp. 1191–1205, 1969.

[108] R. Delbourgo and A. Salam, "The gravitational correction to pcac," *Physics Letters B*, vol. 40, no. 3, pp. 381–382, 1972.

[109] T. Eguchi and P. G. Freund, "Quantum gravity and world topology," *Physical Review Letters*, vol. 37, no. 19, p. 1251, 1976.

[110] L. Alvarez-Gaume and E. Witten, "Gravitational anomalies," *Nuclear Physics B*, vol. 234, no. 2, pp. 269–330, 1984.

[111] T. Matsuki, "Path-integral derivation of the chiral anomaly in higher dimensions," *Physical Review D*, vol. 28, no. 8, p. 2107, 1983.

[112] B. Zumino, W. Yong-Shi, and A. Zee, "Chiral anomalies, higher dimensions, and differential geometry," *Nuclear Physics B*, vol. 239, no. 2, pp. 477–507, 1984.

[113] J. Gordon, "The gravitational chiral anomaly in any dimension," *Classical and Quantum Gravity*, vol. 1, no. 6, p. 673, 1984.

[114] R. Delbourgo and T. Matsuki, "Chiral and gravitational anomalies in any dimension," *Journal of mathematical physics*, vol. 26, no. 6, pp. 1334–1336, 1985.

[115] K. Landsteiner, E. Megías, and F. Pena-Benitez, "Anomalous transport from kubo formulae," *Strongly Interacting Matter in Magnetic Fields*, pp. 433–468, 2013.

[116] A. Lucas, R. A. Davison, and S. Sachdev, "Hydrodynamic theory of thermoelectric transport and negative magnetoresistance in weyl semimetals," *Proceedings of the National Academy of Sciences*, vol. 113, no. 34, pp. 9463–9468, 2016.

[117] K. Jensen, P. Kovtun, and A. Ritz, "Chiral conductivities and effective field theory," *Journal of High Energy Physics*, vol. 2013, no. 10, pp. 1–51, 2013.

[118] K. Jensen, R. Loganayagam, and A. Yarom, "Thermodynamics, gravitational anomalies and cones," *Journal of High Energy Physics*, vol. 2013, no. 2, pp. 1–35, 2013.

[119] K. Das, S. K. Singh, and A. Agarwal, "Chiral anomalies induced transport in weyl metals in quantizing magnetic field," *Physical Review Research*, vol. 2, no. 3, p. 033511, 2020.

[120] Y. Nakayama, "Scale invariance vs conformal invariance," *Physics Reports*, vol. 569, pp. 1–93, 2015.

[121] D. Capper and M. J. Duff, "The one-loop neutrino contribution to the gravitation propagator," *Nuclear Physics B*, vol. 82, no. 1, pp. 147–154, 1974.

[122] D. M. Capper, M. Duff, and L. Halpern, "Photon corrections to the graviton propagator," *Physical Review D*, vol. 10, no. 2, p. 461, 1974.

[123] M. J. Duff, "Twenty years of the weyl anomaly," *Classical and Quantum Gravity*, vol. 11, no. 6, p. 1387, 1994.

[124] L. Bonora, M. Cvitan, P. D. Prester, A. D. Pereira, S. Giaccari, and T. Štemberga, "Axial gravity, massless fermions and trace anomalies," *The European Physical Journal C*, vol. 77, pp. 1–32, 2017.

[125] L. Bonora, "Elusive anomalies," *Europhysics Letters*, vol. 139, no. 4, p. 44001, 2022.

[126] R. A. Bertlmann and E. Kohlprath, "Two-dimensional gravitational anomalies, schwinger terms, and dispersion relations," *Annals of Physics*, vol. 288, no. 1, pp. 137–163, 2001.

[127] M. Stone, "Gravitational anomalies and thermal hall effect in topological insulators," *Physical Review B*, vol. 85, no. 18, p. 184503, 2012.

[128] W. A. Bardeen and B. Zumino, "Consistent and covariant anomalies in gauge and gravitational theories," *Nuclear Physics B*, vol. 244, no. 2, pp. 421–453, 1984.

[129] Y. Habara, H. B. Nielsen, and M. Ninomiya, "A state description of pair production from dirac sea in gravitational field–physical interpretation of weyl anomaly–," *arXiv preprint arXiv:1503.05340*, 2015.

[130] N. Cooper, B. Halperin, and I. Ruzin, "Thermoelectric response of an interacting two-dimensional electron gas in a quantizing magnetic field," *Physical Review B*, vol. 55, no. 4, p. 2344, 1997.

[131] A. Gromov and A. G. Abanov, "Thermal hall effect and geometry with torsion," *Physical review letters*, vol. 114, no. 1, p. 016802, 2015.

[132] G. Tatara, "Thermal vector potential theory of transport induced by a temperature gradient," *Physical review letters*, vol. 114, no. 19, p. 196601, 2015.

[133] C. Rovelli and M. Smerlak, "Thermal time and tolman–ehrenfest effect:'temperature as the speed of time'," *Classical and Quantum Gravity*, vol. 28, no. 7, p. 075007, 2011.

[134] H. B. Casimir, "On the attraction between two perfectly conducting plates," in *Proc. Kon. Ned. Akad. Wet.*, vol. 51, p. 793, 1948.

[135] H. B. Casimir and D. Polder, "The influence of retardation on the london-van der waals forces," *Physical Review*, vol. 73, no. 4, p. 360, 1948.

[136] B. Bermond, M. Chernodub, A. G. Grushin, and D. Carpentier, "Anomalous luttinger equivalence between temperature and curved spacetime: From black hole's atmosphere to thermal quenches," *arXiv preprint arXiv:2206.08784*, 2022.

[137] J. Santiago and M. Visser, "Tolman temperature gradients in a gravitational field," *European Journal of Physics*, vol. 40, no. 2, p. 025604, 2019.

[138] L. Landau, E. Lifshitz, and L. E. Reichl, "Statistical physics, part 1," *Physics Today*, vol. 34, no. 1, p. 74, 1981.

[139] J. Tyndall, *ON LUMINOUS AND OBSCURE RADIATION*, p. 253–268. Cambridge Library Collection - Physical Sciences, Cambridge University Press, 2014.

[140] J. Stefan, "Über die Beziehung zwischen der Wärmestrahlung und der Temperatur," *Sitzungsber. Kaiserl. Akad. Wiss. Math. Naturwiss. Cl. II. Abth.*, vol. 79, no. 3, pp. 391–428, 1879.

[141] L. Boltzmann, *Ableitung des Stefanschen Gesetzes, 1) betreffend die Abhängigkeit der Wärmestrahlung von der Temperatur aus der elektromagnetischen Lichttheorie*. Springer, 1978.

[142] H. Oji and P. Streda, "Theory of electronic thermal transport: Magnetoquantum corrections to the thermal transport coefficients," *Physical Review B*, vol. 31, no. 11, p. 7291, 1985.

[143] T. Qin, Q. Niu, and J. Shi, "Energy magnetization and the thermal hall effect," *Physical review letters*, vol. 107, no. 23, p. 236601, 2011.

[144] A. Shitade, "Heat transport as torsional responses and keldysh formalism in a curved spacetime," *Progress of Theoretical and Experimental Physics*, vol. 2014, no. 12, 2014.

[145] G. Tatara, "Thermal vector potential theory of magnon-driven magnetization dynamics," *Physical Review B*, vol. 92, no. 6, p. 064405, 2015.

[146] F. Manasse and C. W. Misner, "Fermi normal coordinates and some basic concepts in differential geometry," *Journal of mathematical physics*, vol. 4, no. 6, pp. 735–745, 1963.

[147] H. W. Blöte, J. L. Cardy, and M. P. Nightingale, "Conformal invariance, the central charge, and universal finite-size amplitudes at criticality," *Physical review letters*, vol. 56, no. 7, p. 742, 1986.

[148] I. Affleck, "Universal term in the free energy at a critical point and the conformal anomaly," in *Current Physics–Sources and Comments*, vol. 2, pp. 347–349, Elsevier, 1988.

[149] J. Cardy, "The ubiquitous 'c': from the stefan–boltzmann law to quantum information," *Journal of Statistical Mechanics: Theory and Experiment*, vol. 2010, no. 10, p. P10004, 2010.

[150] D. Bernard and B. Doyon, "Energy flow in non-equilibrium conformal field theory," *Journal of Physics A: Mathematical and Theoretical*, vol. 45, no. 36, p. 362001, 2012.

[151] M. Eune and W. Kim, "Proper temperature of the schwarzschild ads black hole revisited," *Physics Letters B*, vol. 773, pp. 57–61, 2017.

[152] K. Gawędzki, E. Langmann, and P. Moosavi, "Finite-time universality in nonequilibrium cft," *Journal of Statistical Physics*, vol. 172, no. 2, pp. 353–378, 2018.

[153] P. Moosavi, "Inhomogeneous conformal field theory out of equilibrium," *arXiv preprint arXiv:1912.04821*, 2019.

[154] E. Langmann, J. L. Lebowitz, V. Mastropietro, and P. Moosavi, "Time evolution of the luttinger model with nonuniform temperature profile," *Physical Review B*, vol. 95, no. 23, p. 235142, 2017.

[155] C. Karrasch, R. Ilan, and J. Moore, "Nonequilibrium thermal transport and its relation to linear response," *Physical Review B*, vol. 88, no. 19, p. 195129, 2013.

[156] X. Wen and J.-Q. Wu, "Floquet conformal field theory," *arXiv preprint arXiv:1805.00031*, 2018.

[157] X. Wen and J.-Q. Wu, "Quantum dynamics in sine-square deformed conformal field theory: Quench from uniform to nonuniform conformal field theory," *Physical Review B*, vol. 97, no. 18, p. 184309, 2018.

[158] R. Fan, Y. Gu, A. Vishwanath, and X. Wen, "Emergent spatial structure and entanglement localization in Floquet conformal field theory," *Physical Review X*, vol. 10, no. 3, p. 031036, 2020.

[159] B. Lapierre, K. Choo, C. Tauber, A. Tiwari, T. Neupert, and R. Chitra, "Emergent black hole dynamics in critical floquet systems," *Physical Review Research*, vol. 2, no. 2, p. 023085, 2020.

[160] B. Lapierre and P. Moosavi, "Geometric approach to inhomogeneous floquet systems," *Physical Review B*, vol. 103, no. 22, p. 224303, 2021.

[161] R. Fan, Y. Gu, A. Vishwanath, and X. Wen, "Floquet conformal field theories with generally deformed Hamiltonians," *SciPost Physics*, vol. 10, no. 2, p. 049, 2021.

[162] K. Choo, B. Lapierre, C. Kuhlenkamp, A. Tiwari, T. Neupert, and R. Chitra, "Thermal and dissipative effects on the heating transition in a driven critical system," *arXiv preprint arXiv:2205.02869*, 2022.

[163] C. G. Callan Jr, S. B. Giddings, J. A. Harvey, and A. Strominger, "Evanescent black holes," *Physical Review D*, vol. 45, no. 4, p. R1005, 1992.

[164] E. Witten, "String theory and black holes," *Physical Review D*, vol. 44, no. 2, p. 314, 1991.

[165] A. Fabbri and J. Navarro-Salas, *Modeling black hole evaporation*. World Scientific, 2005.

[166] S. A. Fulling and P. C. Davies, "Radiation from a moving mirror in two dimensional spacetime: conformal anomaly," *Proceedings of the Royal Society of London. A. Mathematical and Physical Sciences*, vol. 348, no. 1654, pp. 393–414, 1976.

[167] M. C. LoPresto, "Some simple black hole thermodynamics," *The physics teacher*, vol. 41, no. 5, pp. 299–301, 2003.

[168] W. G. Unruh, "Notes on black-hole evaporation," *Physical Review D*, vol. 14, no. 4, p. 870, 1976.

[169] S. B. Giddings, "Hawking radiation, the stefan–boltzmann law, and unitarization," *Physics Letters B*, vol. 754, pp. 39–42, 2016.

[170] S. Weinfurtner, "Quantum simulation of black-hole radiation," 2019.

[171] R. Banerjee and S. Kulkarni, "Hawking radiation and covariant anomalies," *Physical Review D*, vol. 77, no. 2, p. 024018, 2008.

[172] R. Banerjee and S. Kulkarni, "Hawking radiation, covariant boundary conditions, and vacuum states," *Physical Review D*, vol. 79, no. 8, p. 084035, 2009.

[173] Y. Gim and W. Kim, "A quantal tolman temperature," *The European Physical Journal C*, vol. 75, no. 11, pp. 1–5, 2015.

[174] W. Kim, "Origin of hawking radiation: firewall or atmosphere?," *General Relativity and Gravitation*, vol. 49, no. 2, pp. 1–12, 2017.

[175] A. Polkovnikov, K. Sengupta, A. Silva, and M. Vengalattore, "Colloquium: Nonequilibrium dynamics of closed interacting quantum systems," *Reviews of Modern Physics*, vol. 83, no. 3, p. 863, 2011.

[176] W. E. Thirring, "A soluble relativistic field theory," *Annals of Physics*, vol. 3, no. 1, pp. 91–112, 1958.

[177] F. Haldane, "'luttinger liquid theory'of one-dimensional quantum fluids. i. properties of the luttinger model and their extension to the general 1d interacting spinless fermi gas," *Journal of Physics C: Solid State Physics*, vol. 14, no. 19, p. 2585, 1981.

[178] C. C. Ttira and C. D. Fosco, "Casimir effect at finite temperature in a real scalar field theory," *arXiv preprint arXiv:0809.2589*, 2008.

[179] A. C. Neto, F. Guinea, N. M. Peres, K. S. Novoselov, and A. K. Geim, "The electronic properties of graphene," *Reviews of modern physics*, vol. 81, no. 1, p. 109, 2009.

[180] E. A. Laird, F. Kuemmeth, G. A. Steele, K. Grove-Rasmussen, J. Nygård, K. Flensberg, and L. P. Kouwenhoven, "Quantum transport in carbon nanotubes," *Reviews of Modern Physics*, vol. 87, no. 3, p. 703, 2015.

[181] L. Bruneau, V. Jakšić, and C.-A. Pillet, "Landauer-büttiker formula and schrödinger conjecture," *Communications in Mathematical Physics*, vol. 319, no. 2, pp. 501–513, 2013.

[182] M. Stone and J. Kim, "Mixed anomalies: Chiral vortical effect and the sommerfeld expansion," *Physical Review D*, vol. 98, no. 2, p. 025012, 2018.

[183] A. Einstein and M. Grossmann, *Entwurf einer verallgemeinerten Relativitätstheorie und einer Theorie der Gravitation.* BG Teubner, 1913.

[184] A. Einstein, "Prinzipielles zur verallgemeinerten relativitätstheorie und gravitationstheorie," *Physikalische Zeitschrift*, vol. 15, pp. 176–180, 1914.

[185] A. Einstein, *Die grundlage der allgemeinen relativitätstheorie*, vol. 49. JA Barth, 1922.

[186] H.-L. Engquist and P. Anderson, "Definition and measurement of the electrical and thermal resistances," *Physical Review B*, vol. 24, no. 2, p. 1151, 1981.

[187] U. Sivan and Y. Imry, "Multichannel landauer formula for thermoelectric transport with application to thermopower near the mobility edge," *Physical review b*, vol. 33, no. 1, p. 551, 1986.

[188] J. P. McKelvey, R. L. Longini, and T. P. Brody, "Alternative approach to the solution of added carrier transport problems in semiconductors," *Phys. Rev.*, vol. 123, pp. 51–57, Jul 1961.

[189] W. Shockley, "Diffusion and drift of minority carriers in semiconductors for comparable capture and scattering mean free paths," *Phys. Rev.*, vol. 125, pp. 1570–1576, Mar 1962.

[190] J. Maassen and M. Lundstrom, "Steady-state heat transport: Ballistic-to-diffusive with fourier's law," *Journal of Applied Physics*, vol. 117, no. 3, p. 035104, 2015.

[191] Q. Zhu and J. Maassen, "Electron transport with the mckelvey–shockley flux method: The effect of electric field and electron–phonon scattering," *Journal of Applied Physics*, vol. 132, no. 7, p. 075109, 2022.

[192] S. Chadha and H. B. Nielsen, "Lorentz invariance as a low energy phenomenon," *Nuclear Physics B*, vol. 217, no. 1, pp. 125–144, 1983.

[193] S. G. Nibbelink and M. Peloso, "Chiral gravity as a covariant formulation of massive gravity," *Classical and Quantum Gravity*, vol. 22, no. 7, p. 1313, 2005.

[194] L. Bernard and L. Blanchet, "Phenomenology of dark matter via a bimetric extension of general relativity," *Physical Review D*, vol. 91, no. 10, p. 103536, 2015.

[195] L. Bonora, M. Cvitan, P. D. Prester, S. Giaccari, M. Paulišić, and T. Štemberga, "Axial gravity: a non-perturbative approach to split anomalies," *The European Physical Journal C*, vol. 78, pp. 1–23, 2018.

[196] P. Li, Y. Wen, X. He, Q. Zhang, C. Xia, Z.-M. Yu, S. A. Yang, Z. Zhu, H. N. Alshareef, and X.-X. Zhang, "Evidence for topological type-ii weyl semimetal wte2," *Nature communications*, vol. 8, no. 1, p. 2150, 2017.

[197] B. Jiang, J. Zhao, J. Qian, S. Zhang, X. Qiang, L. Wang, R. Bi, J. Fan, H.-Z. Lu, E. Liu, *et al.*, "Antisymmetric seebeck effect in a tilted weyl semimetal," *Physical Review Letters*, vol. 129, no. 5, p. 056601, 2022.

[198] A. R. Karmakar, S. Nandy, A. Taraphder, and G. Das, "Giant anomalous thermal hall effect in tilted type-i magnetic weyl semimetal co 3 sn 2 s 2," *Physical Review B*, vol. 106, no. 24, p. 245133, 2022.

[199] N. Tajima, S. Sugawara, M. Tamura, R. Kato, Y. Nishio, and K. Kajita, "Transport properties of massless dirac fermions in an organic conductor α-(bedt-ttf) 2i3 under pressure," *Europhysics Letters*, vol. 80, no. 4, p. 47002, 2007.

[200] M. Goerbig, J.-N. Fuchs, G. Montambaux, and F. Piéchon, "Tilted anisotropic dirac cones in quinoid-type graphene and α-(bedt-ttf) 2 i 3," *Physical Review B*, vol. 78, no. 4, p. 045415, 2008.

[201] P. P. Ferreira, A. L. Manesco, T. T. Dorini, L. E. Correa, G. Weber, A. J. Machado, and L. T. Eleno, "Strain engineering the topological type-ii dirac semimetal nite 2," *Physical Review B*, vol. 103, no. 12, p. 125134, 2021.

[202] Y. Yekta, H. Hadipour, and S. A. Jafari, "Tunning the tilt of the dirac cone by atomic manipulations in 8pmmn borophene," *Communications Physics*, vol. 6, no. 1, p. 46, 2023.

[203] D. Sabsovich, P. Wunderlich, V. Fleurov, D. I. Pikulin, R. Ilan, and T. Meng, "Hawking fragmentation and hawking attenuation in weyl semimetals," *Physical Review Research*, vol. 4, no. 1, p. 013055, 2022.

[204] J. Nissinen and G. Volovik, "Tetrads in solids: from elasticity theory to topological quantum hall systems and weyl fermions," *Journal of Experimental and Theoretical Physics*, vol. 127, pp. 948–957, 2018.

[205] A. Friedman, "Über die krümmung des raumes," *Zeitschrift für Physik*, vol. 10, no. 1, pp. 377–386, 1922.

[206] A. Friedmann, "Über die möglichkeit einer welt mit konstanter negativer krümmung des raumes," *Zeitschrift für Physik*, vol. 21, no. 1, pp. 326–332, 1924.

[207] G. Lemaître, "L'univers en expansion," *Publications du Laboratoire d'Astronomie et de Geodesie de l'Universite de Louvain, vol. 10, pp. 1-19*, vol. 10, pp. 1–19, 1937.

[208] G. Lemaitre, "A homogeneous universe of constant mass and increasing radius accounting for the radial velocity of extra-galactic nebulae," in *A Source Book in Astronomy and Astrophysics, 1900–1975*, pp. 844–848, Harvard University Press, 1979.

[209] H. P. Robertson, "Kinematics and world-structure," *The Astrophysical Journal*, vol. 82, p. 284, 1935.

[210] H. P. Robertson, "Kinematics and world-structure ii.," *The Astrophysical Journal*, vol. 83, p. 187, 1936.

[211] H. P. Robertson, "Kinematics and world-structure iii.," *The Astrophysical Journal*, vol. 83, p. 257, 1936.

[212] A. G. Walker, "On milne's theory of world-structure," *Proceedings of the London Mathematical Society*, vol. 2, no. 1, pp. 90–127, 1937.

[213] S. Eckel, A. Kumar, T. Jacobson, I. B. Spielman, and G. K. Campbell, "A rapidly expanding bose-einstein condensate: an expanding universe in the lab," *Physical Review X*, vol. 8, no. 2, p. 021021, 2018.

[214] P. Jain, S. Weinfurtner, M. Visser, and C. Gardiner, "Analog model of a friedmann-robertson-walker universe in bose-einstein condensates: Application of the classical field method," *Physical Review A*, vol. 76, no. 3, p. 033616, 2007.

[215] J. Vogels, C. Tsai, R. Freeland, S. Kokkelmans, B. Verhaar, and D. Heinzen, "Prediction of feshbach resonances in collisions of ultracold rubidium atoms," *Physical Review A*, vol. 56, no. 2, p. R1067, 1997.

[216] S. Inouye, M. Andrews, J. Stenger, H.-J. Miesner, D. M. Stamper-Kurn, and W. Ketterle, "Observation of feshbach resonances in a bose–einstein condensate," *Nature*, vol. 392, no. 6672, pp. 151–154, 1998.

[217] I. Martin, "Floquet dynamics of classical and quantum cavity fields," *Annals of Physics*, vol. 405, pp. 101–129, 2019.

[218] S. A. Fulling, "Nonuniqueness of canonical field quantization in riemannian space-time," *Physical Review D*, vol. 7, no. 10, p. 2850, 1973.

[219] P. C. Davies, "Scalar production in schwarzschild and rindler metrics," *Journal of Physics A: Mathematical and General*, vol. 8, no. 4, p. 609, 1975.

[220] Y. Nambu and M. Hotta, "Analog de sitter universe in quantum hall systems with an expanding edge," *Physical Review D*, vol. 107, no. 8, p. 085002, 2023.

[221] E. Nicolai, "On transverse vibrations of a portion of a string of uniformly variable length," *Annals Petrograd Polytechn. Inst*, vol. 28, p. 273, 1921.

[222] G. T. Moore, "Quantum theory of the electromagnetic field in a variable-length one-dimensional cavity," *Journal of Mathematical Physics*, vol. 11, no. 9, pp. 2679–2691, 1970.

[223] J.-C. Jaskula, G. B. Partridge, M. Bonneau, R. Lopes, J. Ruaudel, D. Boiron, and C. I. Westbrook, "Acoustic analog to the dynamical casimir effect in a bose-einstein condensate," *Physical Review Letters*, vol. 109, no. 22, p. 220401, 2012.

[224] P. Lähteenmäki, G. Paraoanu, J. Hassel, and P. J. Hakonen, "Dynamical casimir effect in a josephson metamaterial," *Proceedings of the National Academy of Sciences*, vol. 110, no. 11, pp. 4234–4238, 2013.

[225] J. Johansson, G. Johansson, C. Wilson, and F. Nori, "Dynamical casimir effect in superconducting microwave circuits," *Physical Review A*, vol. 82, no. 5, p. 052509, 2010.

[226] L. S. Brown and J. P. Cassidy, "Stress tensors and their trace anomalies in conformally flat space-time," *Physical Review D*, vol. 16, no. 6, p. 1712, 1977.

[227] D. J. Evans, E. G. D. Cohen, and G. P. Morriss, "Probability of second law violations in shearing steady states," *Physical review letters*, vol. 71, no. 15, p. 2401, 1993.

[228] R. W. Graeff, "Measuring the temperature distribution in gas columns," in *AIP Conference Proceedings*, vol. 643, pp. 225–230, American Institute of Physics, 2002.

[229] R. W. Graeff, "Viewing the controversy loschmidt–boltzmann/maxwell through macroscopic measurements of the temperature gradients in vertical columns of water," *Preprint*, 2007.

[230] C. Liao, "Temperature gradient caused by gravitation.," *International Journal of Modern Physics B: Condensed Matter Physics; Statistical Physics; Applied Physics*, vol. 23, no. 22, 2009.

[231] H. M. Jeong and S. Park, "Temperature gradient of vertical air column in gravitational field," *Scientific Reports*, vol. 12, no. 1, p. 6756, 2022.

[232] J. Maxwell, "1902, theory of heat," 1871.

[233] D. J. Tritton, *Physical fluid dynamics*. Springer Science & Business Media, 2012.

[234] H. Bénard, *Les tourbillons cellulaires dans une nappe liquide propageant de la chaleur par convection: en régime permanent*. Gauthier-Villars, 1901.

[235] L. Rayleigh, "Lix. on convection currents in a horizontal layer of fluid, when the higher temperature is on the under side," *The London, Edinburgh, and Dublin Philosophical Magazine and Journal of Science*, vol. 32, no. 192, pp. 529–546, 1916.

[236] J. Xiong, S. K. Kushwaha, T. Liang, J. W. Krizan, M. Hirschberger, W. Wang, R. J. Cava, and N. P. Ong, "Evidence for the chiral anomaly in the dirac semimetal na3bi," *Science*, vol. 350, no. 6259, pp. 413–416, 2015.

[237] M. Hirschberger, S. Kushwaha, Z. Wang, Q. Gibson, S. Liang, C. A. Belvin, B. A. Bernevig, R. J. Cava, and N. P. Ong, "The chiral anomaly and thermopower of weyl fermions in the half-heusler gdptbi," *Nature materials*, vol. 15, no. 11, pp. 1161–1165, 2016.

[238] C. Schindler, S. Galeski, W. Schnelle, R. Wawrzyńczak, W. Abdel-Haq, S. N. Guin, J. Kroder, N. Kumar, C. Fu, H. Borrmann, *et al.*, "Anisotropic electrical and thermal magnetotransport in the magnetic semimetal gdptbi," *Physical Review B*, vol. 101, no. 12, p. 125119, 2020.

[239] Z. Jia, C. Li, X. Li, J. Shi, Z. Liao, D. Yu, and X. Wu, "Thermoelectric signature of the chiral anomaly in cd3as2," *Nature communications*, vol. 7, no. 1, pp. 1–6, 2016.

[240] D. Vu, W. Zhang, C. Şahin, M. E. Flatté, N. Trivedi, and J. P. Heremans, "Thermal chiral anomaly in the magnetic-field-induced ideal weyl phase of bi1- xsbx," *Nature Materials*, vol. 20, no. 11, pp. 1525–1531, 2021.

[241] A. B. Pippard, *Magnetoresistance in metals*, vol. 2. Cambridge university press, 1989.

[242] R. Franz and G. Wiedemann, "Ueber die wärme-leitungsfähigkeit der metalle," *Annalen der Physik*, vol. 165, no. 8, pp. 497–531, 1853.

[243] J. Xiang, S. Hu, Z. Song, M. Lv, J. Zhang, L. Zhao, W. Li, Z. Chen, S. Zhang, J.-T. Wang, *et al.*, "Giant magnetic quantum oscillations in the thermal conductivity of taas: indications of chiral zero sound," *Physical Review X*, vol. 9, no. 3, p. 031036, 2019.

[244] L. Schubnikow and W. J. de Haas, "Magnetische widerstandsvergrösserung in einkristallen von wismut bei tiefen temperaturen," *Leiden Commun*, vol. 207, p. 3, 1930.

[245] L. Schubnikow and W. De Haas, "Neue erscheinungen bei der widerstandsänderung von wismuthkristallen im magnetfeld bei der temperatur von flüssigem wasserstoff," *Proc. Royal Netherlands Acad. Arts and Science*, vol. 33, pp. 363–378, 1930.

[246] L. Schubnikov and W. De Haas, "Die widerstandsänderung von wismuteinkristallen im magnetfeld bei der temperatur von flussigem stickstoff," *Proc. Netherlands R. Acad. Sci*, vol. 33, pp. 130–163, 1930.

[247] I. Lifshitz and L. Kosevich, "On the theory of the shubnikov-de haas effect," *Sov. Phys. JETP*, vol. 6, pp. 67–77, 1958.

[248] M. C. Steele and J. Babiskin, "Oscillatory thermomagnetic properties of a bismuth single crystal at liquid helium temperatures," *Phys. Rev.*, vol. 98, pp. 359–367, Apr 1955.

[249] R. C. Young, "Quantum oscillations in the thermal transport properties of tin," *Journal of Physics F: Metal Physics*, vol. 3, no. 4, p. 721, 1973.

[250] C. Ayache and M. Locatelli, *Quantum Oscillations Effect on the Lattice Thermal Conductivity of Graphite under Very High Magnetic Fields*, pp. 465–467. Boston, MA: Springer US, 1980.

[251] J. P. Eisenstein, A. C. Gossard, and V. Narayanamurti, "Quantum oscillations in the thermal conductance of gaas/algaas heterostructures," *Phys. Rev. Lett.*, vol. 59, pp. 1341–1344, Sep 1987.

[252] F. Tang, Y. Ren, P. Wang, R. Zhong, J. Schneeloch, S. A. Yang, K. Yang, P. A. Lee, G. Gu, Z. Qiao, *et al.*, "Three-dimensional quantum hall effect and metal–insulator transition in zrte5," *Nature*, vol. 569, no. 7757, pp. 537–541, 2019.

[253] S. Galeski, T. Ehmcke, R. Wawrzyńczak, P. M. Lozano, K. Cho, A. Sharma, S. Das, F. Küster, P. Sessi, M. Brando, *et al.*, "Origin of the quasi-quantized hall effect in zrte5," *Nature communications*, vol. 12, no. 1, pp. 1–8, 2021.

[254] S. Galeski, X. Zhao, R. Wawrzyńczak, T. Meng, T. Förster, P. Lozano, S. Honnali, N. Lamba, T. Ehmcke, A. Markou, *et al.*, "Unconventional hall response in the quantum limit of hfte5," *Nature communications*, vol. 11, no. 1, pp. 1–8, 2020.

[255] C. Kane and M. P. Fisher, "Edge-state transport," *Perspectives in Quantum Hall Effects: Novel Quantum Liquids in Low-Dimensional Semiconductor Structures*, pp. 109–159, 1996.

[256] A. Jaoui, A. Gourgout, G. Seyfarth, A. Subedi, T. Lorenz, B. Fauqué, and K. Behnia, "Formation of an electron-phonon bifluid in bulk antimony," *Physical Review X*, vol. 12, no. 3, p. 031023, 2022.

[257] F. de Juan, A. Cortijo, and M. A. Vozmediano, "Dislocations and torsion in graphene and related systems," *Nuclear physics B*, vol. 828, no. 3, pp. 625–637, 2010.

[258] A. A. Lima, C. Filgueiras, and F. Moraes, "Torsion effects on condensed matter: like a magnetic field but not so much," *The European Physical Journal B*, vol. 90, pp. 1–8, 2017.

[259] J. May-Mann, M. R. Hirsbrunner, X. Cao, and T. L. Hughes, "Topological field theories of three-dimensional rotation symmetric insulators: Coupling curvature and electromagnetism," *arXiv preprint arXiv:2209.00026*, 2022.

[260] H. Nieh and M. Yan, "Quantized dirac field in curved riemann-cartan background. i. symmetry properties, green's function," *Annals of Physics*, vol. 138, no. 2, pp. 237–259, 1982.

[261] Z.-M. Huang, B. Han, and M. Stone, "Hamiltonian approach to the torsional anomalies and its dimensional ladder," *Physical Review B*, vol. 101, no. 16, p. 165201, 2020.

[262] T. Qiu and C. Tien, "Heat transfer mechanisms during short-pulse laser heating of metals," 1993.

[263] J. Hohlfeld, S.-S. Wellershoff, J. Güdde, U. Conrad, V. Jähnke, and E. Matthias, "Electron and lattice dynamics following optical excitation of metals," *Chemical physics*, vol. 251, no. 1-3, pp. 237–258, 2000.

[264] E. M. Grumstrup, M. M. Gabriel, E. E. Cating, E. M. Van Goethem, and J. M. Papanikolas, "Pump–probe microscopy: Visualization and spectroscopy of ultrafast dynamics at the nanoscale," *Chemical Physics*, vol. 458, pp. 30–40, 2015.

[265] A. Block, M. Liebel, R. Yu, M. Spector, Y. Sivan, F. García de Abajo, and N. F. van Hulst, "Tracking ultrafast hot-electron diffusion in space and time by ultrafast thermomodulation microscopy," *Science advances*, vol. 5, no. 5, p. eaav8965, 2019.

[266] M. Na, F. Boschini, A. K. Mills, M. Michiardi, R. P. Day, B. Zwartsenberg, G. Levy, S. Zhdanovich, A. F. Kemper, D. J. Jones, *et al.*, "Establishing nonthermal regimes in pump-probe electron relaxation dynamics," *Physical Review B*, vol. 102, no. 18, p. 184307, 2020.

[267] S. Imaki and A. Yamamoto, "Lattice field theory with torsion," *Physical Review D*, vol. 100, no. 5, p. 054509, 2019.

[268] É. Cartan, "Sur les variétés à connexion affine et la théorie de la relativité généralisée (première partie)," in *Annales scientifiques de l'École normale supérieure*, vol. 40, pp. 325–412, 1923.

[269] M. Gasperini and M. Gasperini, "Vierbeins and lorentz connection," *Theory of Gravitational Interactions*, pp. 243–259, 2017.

[270] I. L. Shapiro, "Physical aspects of the space–time torsion," *Physics Reports*, vol. 357, no. 2, pp. 113–213, 2002.

Abstract:
Symmetries are a cornerstone of the physical description of the world. In some exotic situations, the symmetries of the classical description are violated by quantum fluctuations. Such symmetries are denoted anomalous. Of particular interest, the gravitational anomalies describe how momentum and energy conservation laws are not satisfied by quantum fluctuations in a curved spacetime, typically of gravitational origin.
This thesis explores the consequences of these gravitational anomalies in the context of condensed matter. Historically, R. Tolman and P. Ehrenfest studied in the 30s the black body radiation at equilibrium in a curved spacetime. They realized that the curvature of spacetime induces inhomogeneities of the equilibrium temperature. Later on, J.Luttinger, while studying thermal transport in solids, built on their study to replace an inhomogeneous temperature by a curvature of spacetime or equivalently by a gravitational potential. In this thesis, I revisit these historical works. I show how anomalous quantum fluctuations, captured by the gravitational anomalies, modify the Tolman-Ehrenfest equivalence between a curved spacetime and an inhomogeneous temperature. Then I identify several condensed matter situations in which this modified Tolman and Ehrenfest equivalence leads to measurable consequences. In particular, I consider strongly out-of-equilibrium quantum dynamics induced by a thermal quench or a periodic modulation of couplings. Finally, I discuss the magnetothermal transport properties of a Weyl semimetal, ZrTe5, as part of a collaboration with an experimental group. While initially aiming at identifying signatures of the gravitational anomalies, we realized that these measurements were the signature of a new phenomenon resulting from a strong coupling between electrons and phonons in this material, leading to remarkable quantum oscillations of the magnetothermal conductivity.

Résumé :
Les symétries constituent la pierre angulaire de la description physique du monde. Dans certaines situations exotiques, les symétries de la description classique sont violées par des fluctuations quantiques. De telles symétries sont appelées anormales. En particulier, les anomalies gravitationnelles décrivent comment les lois de conservation de la quantité de mouvement et de l'énergie sont violées par les fluctuations quantiques dans un espace-temps courbe, typiquement d'origine gravitationnelle.
Cette thèse explore les conséquences de ces anomalies gravitationnelles dans le contexte de la matière condensée. Historiquement, R. Tolman et P. Ehrenfest étudiaient dans les années 30 le rayonnement d'équilibre d'un corps noir dans un espace-temps courbe. Ils ont réalisé que la courbure de l'espace-temps induit des inhomogénéités de la température d'équilibre. J.Luttinger, étudiant le transport thermique dans les solides, s'appuya sur leur étude pour montrer qu'une température inhomogène peut être commodément troquée pour un espace-temps courbe, ou de manière équivalente pour un potentiel gravitationnel. Dans cette thèse, je revisite ces travaux historiques. Je montre comment des fluctuations quantiques anormales, captées par les anomalies gravitationnelles, modifient l'équivalence Tolman-Ehrenfest entre un espace-temps courbe et une température inhomogène. Ensuite, j'identifie plusieurs situations de matière condensée dans lesquelles cette équivalence modifiée de Tolman-Ehrenfest conduit à des conséquences mesurables. En particulier, je considère la dynamique quantique fortement hors d'équilibre, induite par une trempe thermique ou une modulation périodique des couplages. Enfin, je discute des propriétés de transport magnétothermique d'un semi-métal de Weyl, ZrTe5, dans le cadre d'une collaboration avec un groupe expérimental. En visant initialement à identifier les signatures des anomalies gravitationnelles, nous nous sommes rendus compte que les mesures étaient la signature d'un nouveau phénomène résultant d'un fort couplage entre électrons et phonons dans ce matériau, conduisant à de remarquables oscillations quantiques de la conductivité magnétothermique.